FEBITHA KANDAN-KULANGARA

POLY(ADP-RIBOSE) POLYMERASE-1 (PARP-1) AND RNA INTERFERENCE (RNAI) DURING CELL DEATH

Thèse présentée
à la Faculté des études supérieures et postdoctorales de l'Université Laval
dans le cadre du programme de doctorat en biologie cellulaire et moléculaire
pour l'obtention du grade de Philosophiae Doctor (Ph.D.)

DÉPARTEMENT DE MÉDECINE
FACULTÉ DE MÉDECINE
UNIVERSITÉ LAVAL
QUÉBEC

2013

Résumé

L'activation de la poly(ADP-ribose) polymérase-1 (PARP-1) en réponse aux dommages à l'ADN est impliquée dans diverses réponses cellulaires, de la réparation de l'ADN à la mort cellulaire. Dans l'**annexe I**, nous avons décrit différentes techniques indispensables pour détecter le métabolisme de PARP-1 en réponse aux dommages à l'ADN in vitro et in vivo. Les travaux de cette thèse se concentrent sur le rôle de PARP-1 dans la mort cellulaire. PARP-1 est clivée et inactivée par des caspases pendant l'apoptose ; j'ai donc utilisé une PARP-1 non-clivable pour étudier le rôle de l'activation et de la fragmentation de PARP-1 dans la mort cellulaire induite par les UVB. Nous avons observé que, contrairement aux fibroblastes de peau humaine exprimant la PARP-1, les fibroblastes avec un « knockdown » de PARP-1 sont résistants à l'apoptose induite par les UVB, phénotype pouvant être totalement inversé par ré-expression de PARP-1 sauvage mais pas de PARP-1 non-clivable par les caspases, suggérant un rôle significatif du clivage de PARP-1 en réponse à la mort cellulaire induite par les UVB (**chapitre 2**). Dans ce contexte, nous avons récemment passé en revue comment les substrats non clivables par des caspases peuvent être utilisés comme outil important pour démystifier le rôle de ce clivage pour la mort comme pour la vie, avec l'exemple spécifique de PARP-1 non-clivable par les caspases (**chapitre 3**). Curieusement, en utilisant l'ARNi comme outil d'étude du rôle de PARP-1 dans la mort cellulaire, nous avons observé que l'ARNi stable (shRNA) de nombreux gènes, incluant PARP-1, échoue lors de l'apoptose, en raison de l'inactivation catalytique par clivage par une caspase de l'endoribonucléase Dicer-1, indispensable pour la régulation de l'ARNi et des miARN (**chapitre 4**). Cependant, nous avons découvert que l'ARNi transitoire persiste plusieurs jours même après induction de l'apoptose, soulignant des différences entre les ARNi stable et transitoire dans la dynamique de « knockdown » génétique et dans la dépendance de la fonction de Dicer-1 (**chapitre 5**). En résumé, mon travail a permis la découverte des avantages et des limites de l'ARNi durant l'apoptose et le rôle de PARP-1 dans la mort cellulaire induite par les UVB.

Abstract

Poly(ADP-ribose) polymerase-1 (PARP-1) activation in response to DNA damage is involved in various cellular responses ranging from DNA repair to cell death. In **Annex I** we have described different state-of-the-art techniques to detect PARP-1 metabolism in response to DNA damage in models ranging from in vitro to mice and humans. The work in this thesis largely focuses on the role of PARP-1 in cell death. Since PARP-1 is cleaved and inactivated by caspases during apoptosis; I used caspase-uncleavable PARP-1 as a model to study the role of PARP-1 activation and fragmentation in UVB-induced cell death. We observed that as compared to PARP-1-replete human skin fibroblasts, PARP-1-knockdown fibroblasts are resistant to UVB-induced apoptosis, a phenotype which could be rescued fully by expression of wild-type PARP-1, but not caspase-uncleavable PARP-1, suggesting a significant role of PARP-1 cleavage in response to UVB-induced cell death **(Chapter 2)**. In this context, we recently reviewed how caspase-uncleavable substrates could be deployed as important tools to unravel the role of caspase-mediated cleavage of proteins not only in death but also in life, using specific example of caspase-uncleavable PARP-1 **(Chapter 3)**. Interestingly, while employing RNAi as a tool to study the role of PARP-1 in cell death, we made a novel observation that stable DNA vector-based RNAi of many genes, including PARP-1, fails upon induction of apoptosis, due to apoptosis-specific caspase-mediated cleavage and catalytic inactivation of the endoribonuclease Dicer-1, which is critical for the regulation of miRNA and RNAi **(Chapter 4)**. In contrast, we discovered that the transient RNAi persists for several days even after the onset of apoptosis, highlighting the differences between stable and transient RNAi in the dynamics of achieving gene-knockdown and dependency on Dicer-1 function **(Chapter 5)**. In summary, my work discovered the usefulness and the limitations of RNAi in study of apoptosis and the role of PARP-1 in UVB-induced cell death.

Avant-propos

Contribution to the work presented in the thesis

This PhD thesis is divided into four chapters and one annex which have been the collaborative work of students and researchers within and outside our laboratory. The following paragraphs emphasize details of relative contribution of my own and the co-authors in research and in writing publications or in any unpublished data that is presented in this thesis in the form of chapters.

Chapter 2: Role of PARP-1 in UVB-induced cell death in human skin fibroblasts

Our laboratory had already created normal human skin fibroblasts in which PARP-1 was stably knocked down by DNA vector-based RNAi. For this chapter, the first part of my project was construction of RNAi-resistant wild-type and caspase-uncleavable PARP-1 expression vectors, both of which were Flag-tagged at the N-terminus and to establish and characterize stable PARP-1 rescued cell lines expressing these vectors. Using this gene rescue model we have shown that PARP-1 activation and cleavage play an important role in facilitating UVB-induced cell death. This work is unpublished and I have contributed in the execution of all the experiments as well as interpretation of the data and the preparation of all the figures and writing of the manuscript under the guidance of my supervisor.

These vector constructs and stable cell lines created by me for this project have been excellent tools to study the role of PARP-1 in different cellular processes. For example, another graduate student in our laboratory recently used these constructs and cell lines to study the role of PARP-1 in NER; and this work titled "Role of poly(ADP-ribose) polymerase-1 in the removal of UV-induced DNA lesions by nucleotide excision repair" has been published in Proc Natl Acad Sci USA, 110, 1658-63 (2013).

Chapter 3: Caspase-uncleavable substrates: A gateway to understand death as well as life

In this chapter, we have examined the question of why selected proteins, including PARP-1, are cleaved by caspases during apoptosis; and what have we learnt about the physiological and apoptosis-related roles of these substrates in the cell by using the caspase-uncleavable forms of these substrates. The specific example of PARP-1, its cleavage by caspases 3 or 7, and the consequences of expressing its caspase-uncleavable form to reveal its death and non-death related functions have been highlighted. This chapter is written in the form a manuscript, which is due to be submitted to Cell Death & Differentiation. I and a new graduate student (Nupur) have made equal contribution in the collection of data and interpretations required for this work under the guidance of my supervisor. In addition, this work benefitted from an earlier draft on this subject written by a former graduate student (Sabina). This review will help in understanding the significance of cleavage of substrates in a molecular mechanism that ensures the apoptosis and also to reveal the non-death functions of substrates.

Chapter 4: Abrogation of DNA vector-based RNAi during apoptosis in mammalian cells due to caspase-mediated cleavage and inactivation of Dicer-1

This chapter has been published in Cell Death and Differentiation, 16, 858-868 (2009). For this first part of my thesis, the focus was to characterize the integrity of gene-knockdown model by RNAi during apoptosis. This project was conceived by my supervisor and colleague who made an interesting initial observation that stable RNAi of PARP-1 fails upon induction of apoptosis. My contribution to this chapter was to execute the protocols of transfection, treatment of cells with various apoptosis-inducing drugs, immunoblotting for the results presented in fig 1b, 2a, b and c (right panel) and fig. 3b. In addition, I also participated in the interpretation of the above results, preparation of these figures as well as critical reading of the revised manuscript that was written by Medini and Girish. In this co-authored work, we showed that abrogation of DNA vector-based stable RNAi of PARP and other genes in different cell types occurs during apoptosis due to caspase-3-mediated cleavage and inactivation of endonuclease Dicer-1.

Chapter 5: Persistence of Different Forms of Transient RNAi during Apoptosis in mammalian Cells

This chapter has been published in the PLoS One, 5, e12263 (2010). For this chapter, I have contributed in execution of all the experiments as well as interpretation of the data for all the figures, preparation of all the figures and writing of the manuscript with my supervisor. Ms. Shah was very helpful in executing the RT-PCR experiments represented in figure 1B. Dr. Affar provided shGFP plasmids. In continuation with above work in chapter 3, my work proves that transient RNAi of endogenous (PARP-1) or exogenous (GFP) gene achieved by gene-targeting 21mer dsRNA, 27mer dsRNA or shRNA continues to remain functional upon induction of apoptosis in the period during which stable RNAi fails. Additionally, both stable and transient RNAi can be used for examining early and late apoptotic events provided RNAi-status during apoptosis and accounting for the possible impact of its failure while interpreting the results.

Annex 1: Approaches to detect PARP-1 activation *in vivo, in situ* and *in vitro*

This has been written as a book chapter and published in Methods in Molecular Biology, 780, 3-34 (2011). This protocol chapter is compiled based on published as well as individual unpublished experimental data from our laboratory on detection of PARP-1 activation and PAR in response to DNA damage. My contribution has been to compile the protocols, to write the text and critical reading of the manuscript that was prepared by Girish, Alicia, Rashmi and I. For readers this chapter will be a great start to understand the biological significance of PARP-1.

Acknowledgement

It would not have been possible to write this doctoral thesis without the help and support of the kind people around me, to only some of whom it is possible to give particular mention here.

First and foremost, I would like to acknowledge the advice and guidance of my esteemed supervisor Dr. Girish Shah for his guidance and valuable advice at every stage. His guidance, encouragement with sincere criticism and attention to details, has helped me to present my work in this form. I thank Rashmi for all the help, encouragement and expertise, I got from her (personal and professional), which turned out to be essential during my PhD. I wish to express my sincere gratitude to all my labmates. Medini, the first person I contacted in this lab and for all the initial help, while I was still learning the ropes here. Marc Decobert Alicia, Veronique, Mihaela, Nancy, Jyotika and Nupur thanks for the fun and support.

I thank Alicia and Veronique, for their valuable time for French translations in my work. It was a great help. I am especially grateful to Alicia for proof reading my thesis, and also helping me through the official channels during my work. Mihaela because of you I could learn whatever little French I know today. Thanks to all the summer interns, Julie, Matthieu, Francis, Melanie. It was wonderful and lively working with them. I would like to thank Nupur, for the timely help with graph pad, on caspase review, with experiments during the last phase of my PhD studies and proof reading my thesis. Wish you the best for your future work. I would like to thank all the academic services that were provided by CHUL. I would especially like to thank France from graphics department for helping me with majority of the figures in this thesis.

I would like to thank Prof. Tapas Kundu from JNCASR, Bangalore for his scientific temperament, which I admire a lot. I would thank my friends Radhika, Swaminathan, Arindam, and Sheetal from JNCASR and IISc Bangalore, India. Also, to my dear friend Mausumi who is no more with us. I would like to thank my parents for their constant encouragement, love, support and blessings, beyond measures through my life. My earnest

thanks to my husband Prasad, without whom, this journey would not have been so beautiful. Thanks to my daughter Roshni, who had to put up with me, during the crazy times of my PhD. She in fact, likes to visit CHUL and its cafeteria for its poutine. Thanks to my brother for his support and encouragement. I would like to thank my in-laws, who were also a constant support.

Once again, thanks to Girish and Rashmi for having me and my family at the memorable fun parties and get together at their house during my stay in Quebec.

Table des matières

Liste des abréviations et des symboles

aa-	Amino acid
3-ABA	3-aminobenzamide
ADH	Alcohol dehydrogenase
ADP	Adenosine diphosphate
ADPr	ADP-ribose
Ago-2	Argonaute 2
AIF	Apoptosis inducing factor
ALC1	Amplified in Liver cancer 1
AMD	Automodification domain
APE	Apurinic/apyrimidinic endonuclease
APLF	Aprataxin PNK-like factor
APS	Ammonium persulfate
ARH	ADP-ribosyl-protein-hydrolase
ARTs	ADP-riboysl transferases
mARTs	Mono(ADP-ribosyl)transferases
ATGs	Autophagy-related genes
ATP	Adenosine-5'-triphosphate
β-ME	2-Mercaptoethanol
BER	Base excision Repair
bp-	base pair
BCECF	2',7'-Bis-(2-Carboxyethyl)-5-(and-6)-Carboxyfluorescein
BRCT	breast cancer susceptibility protein BRCA1, C-terminus
BSA	Bovine serum albumin
CD	Catalytic domain
CHFR	Chekcpoint protein with FHA and RING domains
CHO	Chinese hamster ovarian
cIAP1	Cellular inhibitor of apoptosis 1
CPDs	Cyclobutane pyrimidine dimmers
CS	Cockyane Syndrome
CYLD	Cylindromatosis
DAB	3,3'-Diaminobenzidine
DAPI	4',6-diamidino-2-phenylindole
DBD	DNA binding domain
DFF	DNA fragmentation factor
DGCR8	DiGeorge Critical Region 8
DIABLO	Direct inhibitor of apoptosis binding protein with low pI
DISC	Death-inducing signaling complex
DNA	Deoxyribonucleic acid

DSB	Double strand breaks
dRP	5'-deoxyribose phosphate
dsRNA	Double stranded RNA
Endo G	Endonuclease G
FBS	Fetal bovine serum
FEN 1	Flap endonuclease 1
GFP	Green Fluorescent Protein
GG-NER	Global genome nucleotide excision repair
H2O2	Hydrogen peroxide
HR	Homologous recombination
HMG	High mobilitygroup
Htra2	High-temperature-requirement-protein A2
J/m2	Joules per meter square
ICAD	Inhibitor of caspase activated DNase
ICE	Interleukin-1-beta converting enzyme
IR	Infrared
kDa	Kilodalton
KO	Knockout
LPS	Lipopolysaccharide
MAPK	Mitogen activated protein kinase
MEF	Mouse embryonic fibroblasts
MES	2-(N-morpholino)ethanesulfonic acid
miRNA	Micro RNA
MMR	Mismatch repair
mTOR	Mammalian target of rapamycin
MTT	3-(4,5-Dimethylthiazol-2-yl)-2,5-diphenyltetrazoliumbromide
MNNG	N-Methyl-N'-Nitro-N-Nitrosoguanidine
NAD	Nicotinamide adenine dinucleotide
NER	Nucleotide excision repair
NF-kB	Nuclear factor-kappa B
NHEJ	Non-homologus end joining
NLS	Nuclear localization signal
NOS-2	nitric oxide synthase-2
8-oxoG	8-oxoguanine
PACT	Protein Kinase R Protein Activator
pADPr	(PAR) Poly(ADP-ribose)
PARG	Poly(ADP-ribose) glycohydrolase
PARIS	pADPr formed in situ
PARP	Poly(ADP-ribose) polymerase
PBS	Phosphate buffer saline
PBZ	PAR-binding zinc finger

PCA	Perchloric acid
PCD	Programmed cell death
PCNA	Proliferating cell nuclear antigen
PES	Phenazine ethosulphate
PI	Propidium Iodide
PI3kinase	Phosphatidylinositol 3-kinase
6-4PP	6-4 pyrimidone photoproducts
PP	p-phenulenediamine
Pre-miRNA	Precursor miRNA
Pri-miRNA	Primary miRNA
RISC	RNA-induced silencing complex
RNA	Ribonucleic acid
RNAi	RNA interference
ROS	Reactive oxygen species
RT-PCR	Reverse transcription-Polymerase Chain Reaction
SDS	Sodium dodecyl sulfate
shRNA	Short hairpin RNA
siRNA	Short interfering RNA
Smac	Second mitochondria-derived activator of caspase
SSB	Single strand break
SSBR	Single strand break repair
STS	Staurosporine
STZ	Streptozotocin
TCA	TrichloroaceticAcid
TC-NER	Transcription coupled repair
TEMED	N,N,N',N'-Tetramethylethylenediamine
TNF-α/TNFR1	Tumor necrosis factor-α/TNF Receptor 1
TOP1	Topoisomerase 1
TRADD	TNFR-associated death domain
TRAF2	TNFR-associated factor 2
TRBP	HIV-1 transactivating response RNA-binding protein
TTD	Trichothiodystropy
UV	Ultraviolet
XIAP	X-linked inhibitor of apoptosis protein
XP	Xeroderma pigmentosum
XRCC1	X-ray repair cross-complementing factor-1

Liste des tableaux

Chapter 1

Chapter 3

Liste des Figures

Chapter 1

Chapter 2

Chapter 4

Chapter 5

Annex 1

Chapter 1: General Introduction

INTRODUCTION

The nuclear enzyme, poly(ADP-ribose) polymerase-1 (PARP-1 EC 2.4.2.30) is the most abundant isoform of PARP enzyme family. Among the immediate cellular responses to DNA damage is the catalytic activation of PARP-1. Activated PARP-1 utilizes NAD^+ to poly(ADP-ribosyl)ate several target proteins thereby establishing a molecular link between DNA damage and chromatin modification. This post-translational modification of proteins plays an important role in wide range of molecular and cellular processes. The following sections in my thesis will focus on current knowledge on PARP-1.

1.1 Poly(ADP-ribose) polymerase-1 (PARP-1/PARP)

In the early 60's, Chambon and coworkers first reported the NAD^+ stimulated incorporation of radiolabeled ATP into an acid-insoluble fraction containing polyadenylic acid polymer by a DNA-dependent enzyme (*1*). This polymer was identified as poly(ADP-ribose) and the enzyme responsible for this catalytic activity was labeled as poly(ADP-ribose) synthetase or poly(ADP-ribosyl) transferase and is now commonly known as poly(ADP-ribose) polymerase-1 (PARP-1). Later in the 80's, the gene encoding PARP-1 was isolated (*2*) and PARP-1 protein was purified to homogeneity (*3*). PARP-1 is an abundant (1-2 million molecules per cell), 113-kDa zinc-finger-containing nuclear protein with three distinct functional domains (**Figure 1.1**) (reviewed in(*4*)): a 46-kDa N-terminal DNA-binding domain (DBD), a 22-kDa central auto-modification domain (AMD) and a 54-kDa C-terminal catalytic domain (CD) which is by far the most conserved part of the protein. This enzyme is highly conserved in higher eukaryotes with the exception of yeast, which lacks PARP-1 (reviewed in (*5*)).

PARP-1 is subjected to a variety of covalent post-translational modifications including poly(ADP-ribosyl)ation, phosphorylation, acetylation, ubiquitylation and SUMOylation. The interrelation of these modifications is responsible for the control of diverse PARP-1 regulated signaling pathways (reviewed in (*4*)). The following sections

will be mainly focused on PARP-1, poly(ADP-ribosyl)ation and its role in different cellular processes, which is the principle theme of this thesis.

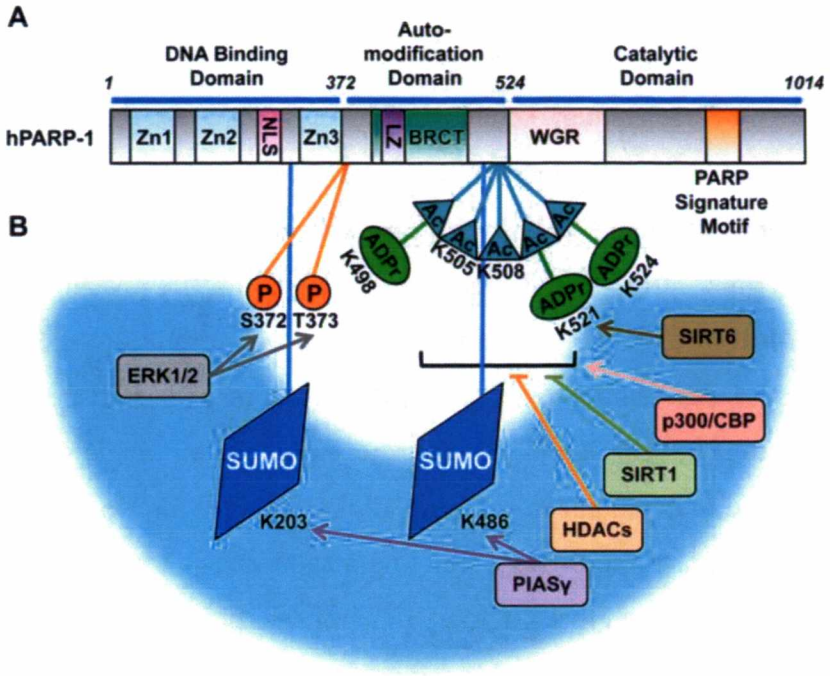

Figure 1.1: Structural and functional organization of PARP and site-specific post-translational modifications. (B) Key post-translational modifications of PARP. Four types of post-translational modifications are shown: phosphorylation (P), SUMOylation (SUMO), acetylation (Ac), and mono(ADPribosyl)ation or poly(ADP-ribosyl)ation (ADPr). The Ser (S), Lys (K), or Thr (T) residues that are the sites of covalent modification are indicated. Enzymes that add (arrows) or remove (blunt lines) the specific post-translational modifications are shown in the blue arc. Taken from Luo *et al.* 2012 (*4*).

1.1.1 DNA binding domain (DBD)

The N-terminal DBD extends from 1-373 amino acid (aa) in human PARP-1 and binds to DNA strand breaks in a zinc-dependent manner. This domain contains three zinc

finger motifs (FI/Zn1, FII/Zn2 and FIII/Zn3), a bipartite nuclear localization signal (NLS) of the form KRK-X(11)-KKKSKK responsible for nuclear localization of PARP-1 (reviewed in (*6*)) and a caspase-3-cleavage site (D214, in the sequence ^{211}DEVD^{214}) (*7*).

The exact mechanism by which PARP-1 binds to DNA damage is still under active investigation. The three zinc fingers PARP-1 are structurally and functionally unique and work independently of each other. Prior to discovery of the third zinc finger (*8*), many earlier studies using biochemical, genetic or structural approaches had shown that Zn1 and Zn2 have more affinity to bind to double or single strand breaks (DSB or SSB) respectively and that 5' or 3' termini at the strand breaks were targets for the possible point of contact with these zinc fingers. Although both zinc fingers facilitate binding of PARP-1 to DNA strand breaks, Zn1 to DSB and Zn2 to SSB (*9*), Zn1 domain is indispensable for DNA-dependent activation of PARP-1 (*10*). However, recent crystallographic studies have shown that Zn1 and Zn2 bind to the exposed or non-hydrogen bonded nucleotide bases rather than 3' or 5' termini of DNA strand breaks mediating a sequence-independent interaction (*10*). While earlier studies speculated that Zn3 may be implicated in homodimerization of PARP-1 molecules that was thought to be required for its catalytic activation (*8, 11*), more recent studies show that Zn3 also mediates the inter-domain contact crucial for DNA-dependent PARP-1 activation thereby coupling the DNA binding and catalytic activity of PARP-1 and also, contributes to the ability of PARP-1 to modulate chromatin structure (*8, 11*).

Apart from DNA strand breaks, in vitro PARP-1 also binds to undamaged DNA structures such as cruciform, curved or hairpin structures with a high affinity and is important for local modulation of chromatin structure (*12*).

1.1.2 Automodification domain (AMD)

The automodification domain (373-524 aa), located in the central region of the PARP-1 was considered as the principle site for auto-poly(ADP-ribosyl)ation by PARP-1. This domain is highly basic and contains glutamic acid, aspartic acid (*13*) and lysine (*14*) residues that were considered as main acceptor site for initiation and binding of polymers of ADP-ribose (reviewed in (*15*)). In addition, the AMD also comprises a 95 residue BRCT

(breast cancer susceptibility protein, BRCA1, C-terminus) motif and a leucine-zipper motif, both of which are known to mediate protein-protein interaction (reviewed in (*4*)). It has been proposed that PARP-1 can homo- and/or heterodimerize to form a catalytic dimer through leucine-zipper motif thus, stimulating the catalytic activity of PARP-1 (*16*). The PARP-1-BRCT allows protein-protein interaction between BRCT-motif-containing proteins involved in DNA repair or in cell-cycle check points such as X-ray repair cross-complementing protein 1 (XRCC1), PARP-2, DNA polymerase β (Pol β) (reviewed in (*5*)). Recently, a specialized role for PARP-1-BRCT in assembling mutagenic DNA repair complexes involved in antibody diversification has been suggested (*17*). However protein partners in this complex remain to be identified.

1.1.3 Catalytic domain (CD)

The C-terminal catalytic/NAD^+-binding domain (525-1014 aa) is composed of an 80-90 amino acid long WGR domain (conserved tryptophane (W), glycine (G), arginine (R) residues), a alpha-helical domain (HD) and ADP-ribosyl transferase (ART) domain required for pADPr synthesis (reviewed in (*18*)).

The in vitro studies have implicated WGR domain in association with DBD and CAT domain in the regulation of double-stranded oligomer dependent PARP-1 activation (*14*) and also in RNA-dependent PARP-1 activation via its ability to bind to ssRNA suggesting a possible role of PARP-1 in regulation of nascent RNA synthesis (*19*). Interestingly, Langelier's recently proposed PARP-1 activation model adds a new function to WGR domain in the formation of DNA-damage recognition surface along with Zn1 and Zn3 (*20*). The ART domain contains a H-Y-E motif encompassing a histidine (H862) and a tyrosine (Y896) residue that are important for NAD^+ binding and a catalytic glutamic residue (E988) essential for the polymerase activity (*21, 22*). The mutation of residues K893, D993, D914 and K953 in this domain completely inactivates human PARP-1, implicating K893 and D993 directly in poly(ADP-ribosyl)ation initiation whereas, D914 and K953 indirectly in pADPr activity (*23*). Residues spanning 859-908 (50 amino acids)

are phylogenetically well conserved and are commonly accepted as the 'PARP signature' motif (reviewed in (*5*).

1.1.4 PARP-1 activation model

Recently based on binding of DBD of human PARP-1 to single strand breaks (SSBs) and double-strand breaks (DSBs), two different models of PARP-1 activation i.e., *cis*-and *trans*-activation (reviewed in (*24*)), respectively have been proposed (*20, 25*)

Langelier *et al.* model explains DNA DSB-dependent PARP-1 activation using a truncated and active PARP-1, consisting of Zn1, Zn3 coupled to the WGR-CAT domains. According to this model, PARP-1 as a monomer binds to exposed nucleotide bases of damaged DNA via Zn1. The Zn1 base stacking loop, the Zn3 extended loop and 5'-terminus of DNA strand provides a binding site for WGR. In this arrangement, on one side WGR provides interaction between Zn1/DNA and CAT domain whereas on other side the extended loop of Zn3 contacts WGR and HD of the CAT domain. This reorganization distorts the hydrophobic core of HD region and alters the stability as well the conformational dynamics of the ART domain thereby activating PARP-1 (*20*). Though AD is absent in this model, the domain reorganization suggests close proximity of AD to the CAT domain, thus explaining the preference for PARP-1 *cis*-automodification (reviewed in (*26*)).

On the contrary, Ali et al provides a *trans* model of PARP-1 automodification. Ali *et al.* uses PARP-1-DBD containing Zn1and Zn2 bound to SSB as a model (*25*). According to their model, PARP-1 dimerizes and the intermolecular Zn1-Zn2 complex forms a functional break-recognition module at the SSB site. This dimerization enables the catalytic domain of one PARP-1 molecule to act on AD of the other PARP-1 molecule thus activating *trans*-automodification.

Both the models have their merits. Studies from Ali's model emphasizes on DNA damage recognition by both Zn1 and Zn2 and both Zn fingers are essential for recruitment

and activation of PARP-1 at the SSB where as Langelier's model completely suggests that Zn2 is dispensable for PARP-1 activation. However, both models display a flexible role of Zn1 in response to different DNA damage and more experiments will be required to determine the relative contributions of *cis* compared to *trans* models of automodification.

1.2 Poly(ADP-ribosyl)ation

PARP-1, carries out poly(ADP-ribosyl)ation, an NAD^+-dependent enzymatic reaction which involves following four reactions (**Figure 1.2**) (reviewed in (*27*)): NAD^+ hydrolysis followed by initiation, elongation and branching of polymer chain (*28, 29*). The first step in this modification is the NAD^+ hydrolysis whereby the glycosidic linkage between nicotinamide and ribose is cleaved to release ADP-ribose, nicotinamide (Nam) and proton (H^+) (reviewed in (*30*). The polymer (pADPr) reaction is initiated by the formation of an ester bond between the first ADP-ribose and carboxyl group of glutamate and to a lesser extent to lysine or aspartate residues of putative acceptor protein. This is followed by polymer elongation involving attachment of additional ADP-ribose moieties to the first covalently bound mono-ADP-ribose and branching of an ADP-ribose moiety at an average of 20 ADP-ribose units along the linear portion of the polymer. For every initiation step catalyzed by PARP-1, there can be more than 200 units of APD-ribose in linear elongation and five to seven branching reaction (reviewed in (*5, 28*)).

This poly(ADP-ribosyl)ation activity of PARP-1 has been detected in organisms ranging from plants to mammals, with an exception of yeast. This covalent post-translational modification alters the activity of target protein through steric and electrostatic effects (reviewed in (*27*)). However, this modification is transient as specific catabolizing enzymes, degrade pADPr and restore the target protein to its native state.

PARP-1 is a major NAD^+-consuming enzyme. Besides poly(ADP-ribosyl)ation reaction, NAD^+ is also utilized as a precursor of ADP-ribose in other ADP-ribosylation reactions including mono(ADP-ribosyl)ation, cyclization of ADP-ribose by ADP-ribosyl cyclases and generation of O-acetyl ADP ribose in deacetylation reaction by sirtuins (*30*).

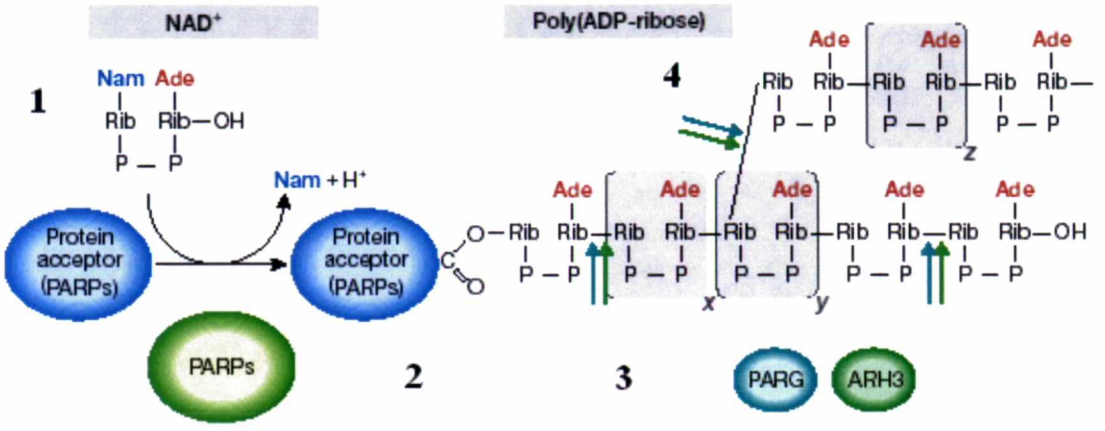

Figure 1.2: Metabolism of poly(ADP-ribose). PAR is heterogeneous in size and complexity, as indicated by the *x*, *y* and *z* labels that represent values from 0 to >200. PARG and ARH3 can both hydrolyse PAR at the indicated positions. Ade, adenine; ARH3, ADP-ribosyl hydrolase-3; Nam, nicotinamide; PAR, poly(ADP-ribose); PARG, poly(ADP-ribose) glycohydrolase; PARP, poly(ADP-ribose) polymerase; Rib, ribose. Taken from Hakme *et al.* 2008 (*27*)

1.3 Poly(ADP-ribose) (pADPr) or PAR

The presence of pADPr was first reported by P. Chambon and co-workers in 1963 and subsequently its structure was solved in three independent laboratories (reviewed in (*29*)).

pADPr is a homopolymer of ADP-ribose units linked by glycosidic (2'→1") adenine-proximal ribose-ribose (A-ribose) bond along the linear and (2"→1'") bonds at branching points occurring between two nicotinamide-proximal ribose (N-ribose) (reviewed in (*31*)). Due to presumed secondary helicoidal structure which is similar to RNA and DNA it is also known as third type of nucleic acid (*32*). Polymers have a high density of negative charge (twice the charge density of DNA), since each monomer

contains two phosphate groups carrying a negative charge each with a high potential for non-covalent reactions and multiple adenine rings capable of both hydrogen bonding and base stacking interactions (reviewed in (*28*)). The constitutive levels of pADPr are usually very low in unstimulated cells (*33*) however, in the presence of DNA strand breaks, the catalytic activity of PARP increases by 10-500x folds, resulting in protein-conjugated long branched pADPr, which can vary from few to more than 200 ADP-ribose units along the length (reviewed in (*5*)).

The target proteins are modified either through a covalent linkage of pADPr chains which were initiated as described above at specified amino acid residues of the protein or through non-covalent binding of free pADPr chains to the target proteins in designated domains (*5, 34-36*). This modification alters the physical and biochemical properties of the modified proteins, ultimately regulating either their enzymatic activities or macromolecular interactions such as protein-protein or protein-DNA interactions. The most prominent target protein/acceptor of this pADPr is PARP-1 itself and this automodification of PARP-1 leads to accumulation of negative charges, thereby abolishing its affinity for DNA strand breaks and its catalytic activity (*20*). Several other DNA-binding nuclear proteins that are involved in metabolism of nucleic acids and in maintenance of chromatin structure such as, histones, topoisomerase I and II, p53, DNA ligases, DNA polymerases, high-mobility-group proteins (HMG), DNA repair protein such as XRCC1 and a variety of transcription factors are modified by pADPR (reviewed in (*35*)).

The non-covalent interaction with pADPr could be highly influenced by pADPr chain length and the binding proteins (*37, 38*). To date, four different types of PAR-binding motifs or domains have been found mediating non-covalent pADPr binding and regulating enzymatic activity (**Figure 1.3**) (reviewed in (*15*)). The first is a short conserved motif with a common feature of basic residue-rich motif interspersed with hydrophobic amino acids found in wide range of proteins involved in DNA-repair and cell cycle check points (*35, 39*); second is PAR-binding zinc finger (PBZ), a short, conserved zinc dependent (C2H2) module, identified in APLF (aprataxin PNK-like factor) and CHFR (checkpoint protein with FHA and RING domains), that are involved in the DNA damage response and

checkpoint regulation (*40, 41*); third is the macrodomain, an ancient and highly conserved structural domain (reviewed in (*42*)) found in histone variant H2A1.1 (*43*) and ALC1 (Amplified in Liver Cancer 1) (*44*), an ATP-dependent nucleosome remodeling enzyme involved in chromatin remodeling; and the fourth is WWE (Trp-Trp-Glu) domain in RNF146 (also known as Iduna), a PAR-binding E3-ligase which mediates a PAR-dependent ubiquitylation (*45*).

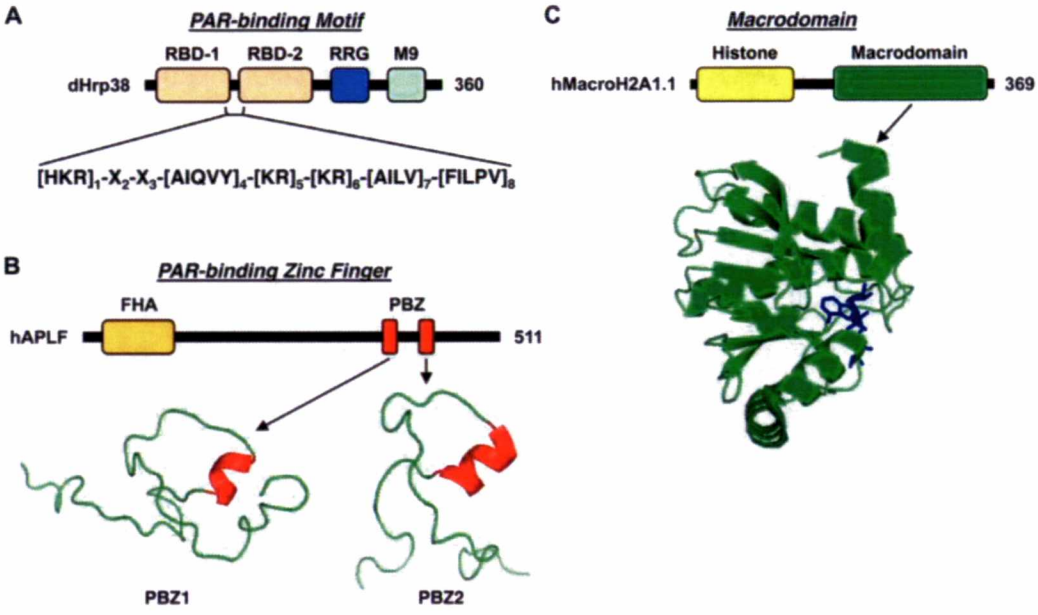

Figure 1.3: PAR-binding motifs. Taken from Krishnakumar *et al.* 2010 (*15*)

Some proteins such as PARP, p53 and histones are modified both covalently or non-covalently by PAR, whereas majority of proteins are modified non-covalently. Recently, Krietsch *et al.* have established a comprehensive repertoire of pADPr-associated proteins and this emphasizes the importance of pADPr in modulating protein activity in a variety of biological processes (**Table 1.1**) (*46*)

Table 1.1: pADPr binding proteins. Taken from Krietsch *et al.* 2012 (*46*)

DNA damage response and checkpoint
Aprataxin
Aprataxin and PNK-like factor (APLF)
Cellular tumor antigen
Cyclin-dependent kinase inhibitor 1 (p21)
DNA ligase 3 PBM + Gagne et al. (2012)
DNA mismatch repair protein MSH6
DNA polymerase epsilon catalytic subunit A (POL ε)
DNA repair protein complementing XP-A cells
DNA repair protein complementing XP-C cells
DNA repair protein XRCC1
DNA topoisomerase 1 (TOP1)
DNA topoisomerase 2-alpha
DNA-dependent protein kinase catalytic subunit (DNA-PK)
Double-strand break repair protein MRE11A
E3 ubiquitin-protein ligase RNF146 (Iduna)
Flap endonuclease 1 (FEN1)
Histone H2A
Histone H2B
Histone H3
Histone H4
Nibrin (NBS1)
Non-POU domain-containing octamer-binding protein (NONO)
RNA-binding motif protein, X chromosome (RBMX)
Serine-protein kinase ATM
X-ray repair cross-complementing protein 6 (XRCC6 / KU70)
Werner syndrome ATP-dependent helicase (WRN)

Chromatin regulation and modification
Core histone macroH2A1.1
O-acetyl-ADP-ribose deacetylase MACROD1
Chromodomain-helicase-DNA-binding protein 1-like (CHD1L/ALC1)
Chromodomain-helicase-DNA-binding protein 4 (CHD4
Chromodomain-helicase-DNA-binding protein Mi-2 homolog (dMi-2)
Condensin complex subunit 1 (hCAP-D2)
DNA methyltransferase 1 (DNMT1)
E3 SUMO-protein ligase CBX4
Metastasis-associated protein MTA1
Polycomb complex protein BMI-1
Protein DEK PBM

Apoptosis
Apoptosis-inducing factor 1, mitochondrial (AIF)
DNA fragmentation factor subunit beta (DFF40/CAD)
E3 ubiquitin-protein ligase RNF146 (Iduna)
Hexokinase domain-containing protein 1 (HKDC1)

Transcription, replication and gene expression
Cellular tumor antigen p53
DNA topoisomerase 1 (TOP1)
DNA topoisomerase 2-alpha (TOP2A)
DNA topoisomerase 2-beta (TOP2B)
E3 SUMO-protein ligase PIAS4 (PIASy)
Heterogeneous nuclear ribonucleoprotein A1 (hnRNP A1)
NF-kappa-B essential modulator (NEMO/IKKγ)
SARS coronavirus non-structural protein nsp3
Nuclear factor NF-kappa-B p100 subunit
Polycomb group RING finger protein 2 (MEL-18/RNF110)
RNA-binding motif protein, X chromosome (RBMX)
Serine/arginine-rich splicing factor 1 (ASF/SF2)
Telomerase reverse transcriptase (TERT)
Transcriptional repressor CTCF
G3BP1

Centromere function and cell cycle checkpoint
Aurora kinase A-interacting protein
E3 ubiquitin-protein ligase CHFR
Histone H3-like centromeric protein A (CENP-A)
Major centromere autoantigen B (CENP-B)
Mitotic checkpoint protein BUB3

Others
Capsid protein viral protein 1 (VP1)
Heat shock factor (HSF-1)
Major vault protein
Myristoylated alanine-rich C-kinase substrate (MARCKS)
Nicotinamide mononucleotide adenylyltransferase 1 (NMNAT-1)
Nitric oxide synthase, inducible (iNOS)

1.4 pADPr Catabolism

In eukaryotic cells, the polymer is rapidly hydrolyzed to free poly(ADP-ribose) by poly(ADP-ribose) glycohydrolase (PARG), a major enzyme responsible for pADPr turnover. Recently, an additional protein ADP-ribose-protein-hydrolase-3 (ARH3) was also shown to possess intrinsic pADPr degradation activity (reviewed in (*29*)). The dynamic turnover of pADPr serve as a molecular signal and can modulate different cellular functions including chromatin remodeling, DNA repair and cell death (reviewed in (*31*).

1.4.1 Poly(ADP-ribose) glycohydrolase (PARG)

Poly(ADP-ribose) glycohydrolase (PARG) (*47*), an enzyme with both exo- and endoglycosidase activities hydrolyses the glycosidic bond between ADP-ribose units of both linear and branched polymer (*48, 49*). In vivo the degradation of PAR by PARG begins immediately after the initiation of PAR synthesis. In addition, branched and short polymers are degraded more slowly than long and linear polymers. Thus, the mode of action of PARG shows biphasic degradation of polymer in vivo clearly indicating the existence of two major types of polymers (linear↔branched) with different structures and distinct half lives (first 40 sec and second 6 min) following DNA damage (*50*). This free pADPr generated by endoglyoaction can bind non-covalently to cellular proteins and structural domains and modulate their function.

In mammals, a single gene codes for four isoforms of PARG which are located in various cellular compartments. The predominant isoform, a 111-kDa nuclear PARG accounts for most of the PARG activity (*51*). Other isoforms are a 60-kDa cytoplasmic/mitochondrial isoform generated by protease cleavage of full length PARG (*52-54*) and 102 and 99 kDa cytoplasmic isoform resulted from alternative splicing of PARG gene transcript (*55*). Complete suppression of PARG gene causes early embryonic lethality (*56*), whereas mice selectively lacking 110 kDa PARG isoform develop normally but are more sensitive to alkylating agents and IR (*57*). This was likely due to dysregulation in PAR catabolism and eventual higher accumulation of polymer. It is also shown that cytoplasmic PARG102 translocates to the nucleus and hydrolyse the PAR, suggesting that other PARGs notably, PARG102 and its activity may also be critical and sufficient for PAR catabolism (*51*). Additionally, in a pADPr- and PCNA-dependent mechanism PARG is recruited at the DNA damage sites thereby regulating the switch between efficient DNA repair and cell death (*58*). Although low in cellular abundance, PARG has a high specific activity, and acts in concert with PARPs to maintain intracellular pADPr at very low concentrations under homeostatic conditions (*59*).

1.4.2 ADP-Ribosyl Protein Lyase and ADP-ribosyl-protein-hydrolase-3 (ARH-3)

ADP-ribosyl protein lyase, cleaves the proximal ADPr residue on the acceptor protein and releases a dehydrated form of ADP-ribose (5'-ADP-3"-deoxypent-2"-enofuranose) (*60, 61*). ADP-ribosyl-protein-hydrolase-3 (ARH3) which is structurally unrelated to PARG shows amino acid identity with the catalytic domain of PARG and generates ADP-ribose from poly(ADP-ribose), albeit at only ~10% of the activity observed for the PARG (*62, 63*).

1.5 The PARP superfamily

PARP-1, the founding member of PARP family, was for a long time considered to be the only enzyme with pADPr activity in mammalian cells. However, with the discovery of residual pADPr activity in PARP-1-deficient (KO) mouse embryonic fibroblasts (MEFs) following treatment with DNA damage gave a clue for the presence of additional PARPs (*64*). Currently, based on high sequence homology with the human PARP-1 catalytic domain 18 PARP homologues have been identified (**Figure 1.4**) and can be grouped into three subfamilies (i) (PARPs 1-5) bonafide members containing a conserved glutamate (Glu 988 in PARP-1) that catalyse poly(ADP-ribosyl)ation activity; (ii) PARPs 6-8, 10-12 and 14-16 lacking the conserved catalytic glutamate and with confirmed or putative mono(ADP-ribosyl)ation activity and (iii) PARPs 9 and 13 which lacks NAD^+-binding histidine in addition to the catalytic glutamate and may therefore be catalytically inactive (*21*). Since some members of PARP family functions as mono(ADP-ribosyl)transferases (mARTs), renaming this family as ADP-ribosyl transferases (ARTs) has been proposed (*65*), however, PARP continues to remain the most frequently used and recognized name for this family.

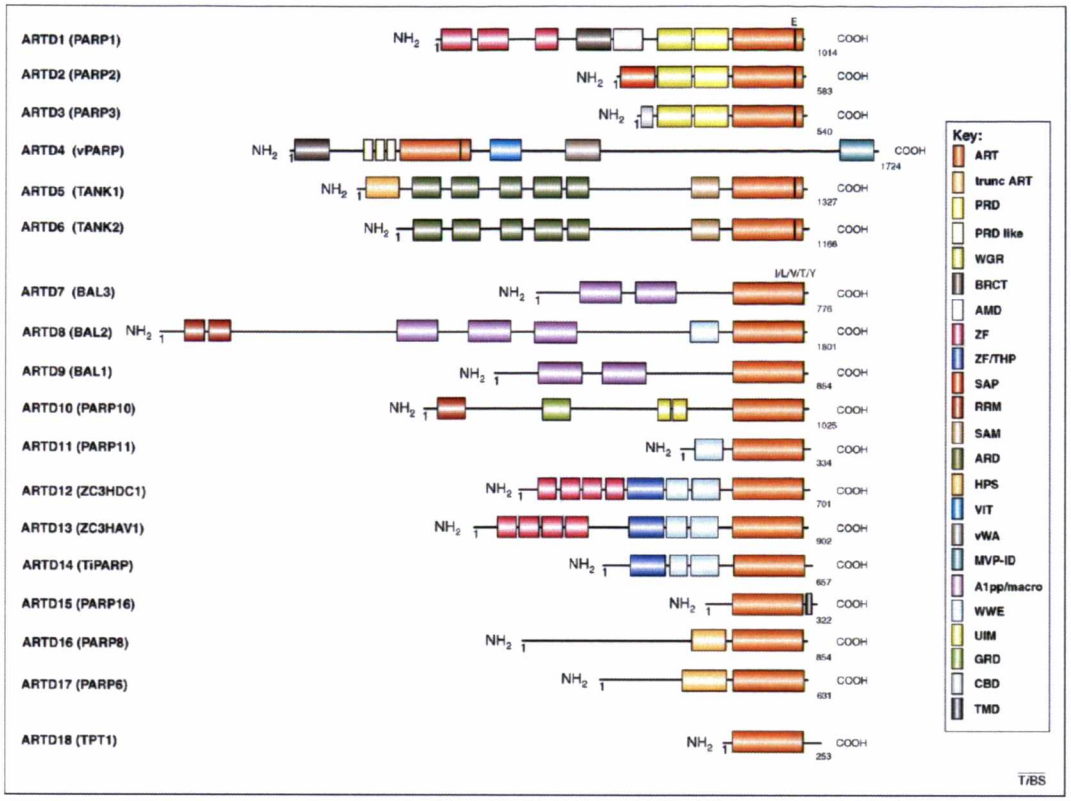

Figure 1.4: Schematic comparison of the domain architecture of the human ARTD (PARP) family. The following domains in ARTD1 (PARP1) are indicated: The ART domain is the catalytic core required for basal ART activity. Within each ART domain, the region that is homologous to the PARP signature (859–908 aa of PARP-1) as well as the equivalent of the PARP-1 catalytic E988 is shaded. The WGR domain named after a conserved central motif (W-G-R). The BRCT domain (BRCA1 carboxy-terminal domain) is found within many DNA damage repair and cell cycle checkpoint proteins. The other known domains are, ARD: ankyrin repeat domains. (W-W-E): WWE domain is a protein–protein interaction motif. PRD: PARP regulatory domain. ZF: zinc finger domains. NLS: nuclear localization signal. Taken from Hottiger *et al*. 2010 (*65*)

Among PARP family members, PARP-2, a 60-kDa protein was discovered as a result of the presence of residual DNA-dependent pADPr activity in PARP-$1^{-/-}$ mouse embryonic fibroblasts (MEFs) (*66*). PARP-2 has a distinct DBD from PARP-1, consisting of only 64 aa and lacking any obvious DNA-binding motif. Unlike PARP-1 which binds to

nicks, PARP-2 has a higher affinity for gaps and flaps, favoring an implication of PARP-2 at later steps of the DNA repair processes (*67, 68*). In the C-terminal catalytic domain it exhibits 69% homology with PARP-1 catalytic domain. Apart from PARP-1, PARP-2 is also activated by DNA-strand interruptions and contributes only 5-10% of total PARP activity (*66, 69*). PARP-2 interacts with PARP-1 and shares common partners such as XRCC1, polymerase β and DNA ligase III that are involved in DNA repair pathways (*69, 70*). Other than in DNA repair, PARP-2 involvement in transcription (*71*) and in metabolic stress (*72, 73*) has also been highlighted. In addition, *PARP-1*$^{-/-}$*/PARP-2*$^{-/-}$ double mutant mice are non-viable and die at the onset of gastrulation, highlighting importance of both PARPs during early embryogenesis (*74*). Nonetheless it needs to be pointed out that PARP-1 knockout phenotypes are not compensated by the presence of PARP-2, and PARP-2 knockout does not display the dramatic DNA damage response-phenotypes indicating that PARP-2 has albeit a minor role at least in DNA damage response.

The other bonafide PARP family proteins include PARP-3 (*75, 76*). PARP-3 a 60 kDa protein with homology to catalytic domain of PARP-1 lacks the N-terminal DNA-binding as well as central automodification domain (*77*). Owing to alternate splicing PARP-3 gene produces two isoforms (62 kDa and 67 kDa) and the long splice variant is the core component of centrosome, preferentially residing in the daughter centriole and regulates cell cycle checkpoints (*78*). Recent data from Caldecott group shows that PARP-3 is stimulated by DNA DSB in vitro (*79*). Nevertheless, PARP-3 has been associated with (i) Polycomb group proteins involved in transcriptional silencing (*80*); (ii) a protein complex containing tankyrase 1 and NuMA, that in turn controls specific mitotic functions (*76*); (iii) components (PARP1, Ku70/80 and DNA-PK) of the DNA repair machinery (*80, 81*) and (iv) with ADP-ribose binding protein APLF ,suggesting an active role in cellular response to DNA damage, DNA repair with special attention to DSB repair via NHEJ (*75*), mitotic progression and maintenance of genomic integrity.

The other PARPs are Vault PARP (VPARP/PARP-4) (*82*) and PARP-5 (Tankyrase) (*83*). Other lesser known PARPs are TCDD-inducible poly(ADP-ribose) polymerase

(TiPARP/PARP-7), PARP-10 and macro PARPs (PARP9, PARP-14 and PARP-15) and these have not been extensively studied (reviewed in (*84*)).

1.6 Function of PARP and pADPr: PARP-1 and its catalytic activity are crucial in mammalian cells to orchestrate vast and diverse cellular functions including DNA damage detection, DNA repair, chromatin remodeling, cell death has been discussed below.

1.6.1 PARP-1 and PAR (pADPr) in DNA damage detection and signaling network

The ultimate cellular response to DNA damage is either to repair the damage and restore the genome to healthy state or trigger cell death to eliminate the damaged genome. However, these responses take place over several hours to days, and are most likely to be strongly influenced by events that occur almost immediately after DNA damage, namely identification or marking of the DNA damaged site among the vast majority of undamaged DNA in the chromatin context and transmission of the signal to downstream effectors to respond with DNA repair or cell death processes. In this early DNA strand break signaling network, PARP-1 plays a dual role as DNA damage sensor and signal transducer to downstream effector pathways (*85*).

In response to low levels of DNA damage induced by oxidation, alkylating agent and UV radiation, PARP-1 binds at DNA damage site and activates its catalytic activity thereby automodifying itself. The modulation of chromatin structure is one of the early events in DNA damage detection and DNA repair. PARP-1 is known to disrupt chromatin structure by destabilizing nucleosomes via poly(ADP-ribosyl)ation of histones. Other proteins such as non-histone chromosomal proteins, chromatin remodeling factors with PAR binding domains such as macro H2A1.1, ALC1 and NuRD promotes chromatin remodeling at the sites of DNA damage. Also, PAR-binding domain-dependent modification of checkpoint proteins such as CHFR and APLF, DNA damage scaffold protein XRCC1 are essential for efficient DNA damage repair. Additionally, Polycomb group (PcG) protein complex 1(PRC1 and PRC2) are also modified by pADPr which are

important in pre-and post-repair remodeling of nucleosome landscape during DNA repair. These PAR-dependent events modulate chromatin structure locally at the sites of DNA breaks in order to facilitate DNA damage signaling and the rapid recruitment of proteins to facilitates DNA repair (**Figure 1.5**) (reviewed in (*31*)).

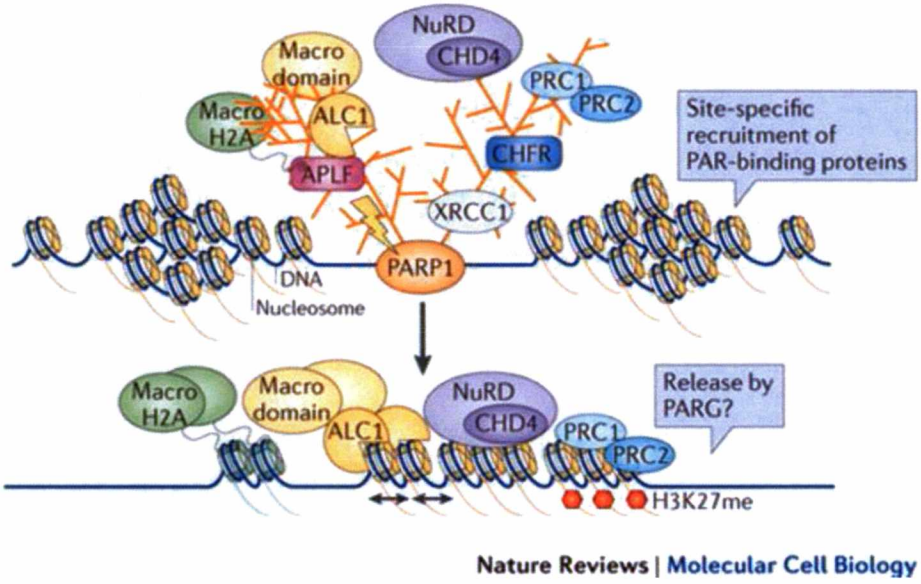

Figure 1.5: PAR-dependent recruitment of factors at the site of DNA damage. Taken from Gibson *et al.* 2012 (*31*)

Additionally, PARP-1$^{-/-}$ mouse models exhibits variety of DNA repair defects and chromosomal aberrations implicating role of PARP-1 in DNA repair (*86*). The following sub-sections will briefly summarize the current understanding of the role of PARP-1 and PAR (or pADPr) in different DNA repair pathways.

1.6.2 PARP-1 in Base Excision repair (BER) or Single Strand Break Repair (SSBR)

Base excision repair (BER) is the primary repair pathway that repairs single-strand breaks (SSBs) and corrects base lesions that arise due to oxidative, alkylation and deamination damage (*87, 88*). BER pathway is initiated by recognition and catalytic removal of damaged base by DNA glycosylases, generating an apurinic/apyrimidinic (AP) site, which is then cleaved by an AP endonuclease (APE) leaving a SSB. This is followed gap filling and ligation by a DNA polymerase β and a DNA ligase III, respectively. Other accessory proteins such as XRCC1, PCNA and PARP-1 are additionally involved and provide a scaffold for the core BER enzymes (**Figure 1.6**) (*89-91*). BER facilitates the repair of damaged DNA via two general pathways-short patch BER (SP-BER) and long patch BER (LP-BER). The SP-BER (responsible for majority of repair) leads to a repair of single nucleotide gap whereas LP-BER produces a repair tract of 2-8 nucleotides by displacing a stretch of old DNA into a flap structure, which is then processed by a flap endonuclease 1 (FEN-1) (*87*).

PARP-1 is denoted as a BER protein (*70, 92*). PARP-1 has been shown to bind at AP site (*93*) and SSBs a BER intermediate (*94*) thereby protecting the DNA damage site. PARP-1 binding to SSBs stimulates PARP-1 catalytic activity and functions to sequester other DNA repair proteins to the sites of strand breaks supporting a "nick protection" model (*95, 96*). PARP-1 is known to interact with BER/SSBR proteins such as APE1 (*97*), XRCC1 (*98*), DNA ligase III (*99*) and pol β (*100, 101*) in both SP-and LP-BER pathway. In pol $\beta^{-/-}$ cell lines PARP-1 is required for efficient repair of 8-oxoG by LP-BER (*102*). XRCC1 preferentially interacts with automodified PARP-1 and is recruited at the site of oxidative and methylated DNA damage (*98, 103*). Similarly, DNA ligase III also associates with modified PARP-1 providing possible mechanism of recruitment of XRCC1-ligaseIIIα complex at site of SSBs (*104*).

In contrast, some studies have challenged the role of PARP-1 in the DNA repair steps involved in BER (*105, 106*). Although none of these studies exclude the possible role of PARP-1 in events that facilitate BER, such as chromatin remodeling or access to the

damaged site, because PARP-inhibition clearly traps PARP-1 to the damaged DNA site that is repaired by BER (*105, 107*) and PARP-inhibitors can potentiate cell killing by DNA damage that is repaired by BER (*108*).

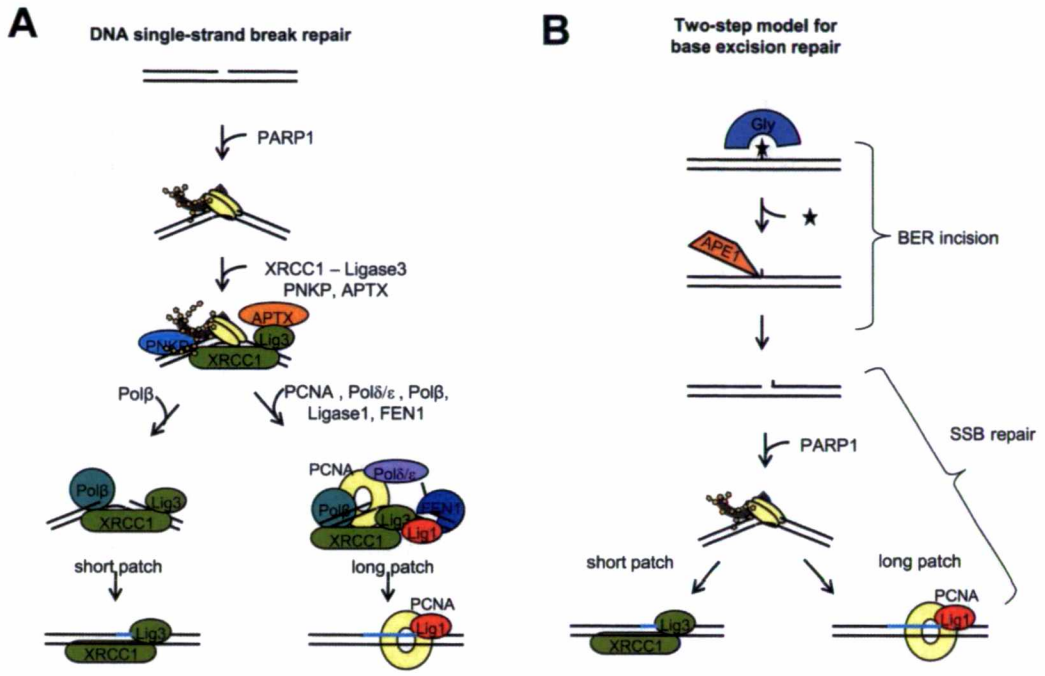

Figure 1.6: Involvement of PARP-1 in SSBR and BER repair pathway. (A) SSB repair: PARP-1 has a high affinity for SSBs and will be amongst the first proteins to bind to the lesion. In turn PARP-1 recruits factors to start end processing and finally ligation, normally through short patch repair and through long patch repair where the lesions are more difficult to repair. (B) Two-step model for BER: Different base lesions are recognised by different glycosylases (Gly), which are excised before SSB incision by the AP-endonuclease (APE). These SSBs are then left unprotected and recognised in a separate process by PARP-1 that will then initiate SSB repair. Taken from Helleday *et al.* (*108*)

Unlike PARP-1, PARP-2 accounts for only 5-10% of total pADPr activity in response to DNA damage and shares PARP-1 DNA repair partners such as XRCC1, polβ, DNA ligase III. However, PARP-2 depletion either has very little impact on repair of SSBR in response to oxidative stress (*109*) or just slows down BER in response to alkylating agent (*69*). In response to laser-induced DNA damage, unlike PARP-1 which is rapidly accumulated at DNA damage site, PARP-2 accumulates with a slower kinetics (*68*) and has a higher affinity for gaps and flaps, favoring an implication of PARP-2 at later steps of the DNA repair processes (*67*). These experimental observations suggest supportive role of PARP-2 in BER along with PAPR-1 which is further strengthened by embryonic lethality of PARP-$1^{-/-}$PARP-$2^{-/-}$double knockout mice (*74*).

1.6.3 PARP-1 in Double strand break repair (DSBR)

In mammalian cells, there are two major pathways for the repair of DSBs: homologous recombination (HR) and non-homologous end joining (NHEJ) (*110*). Members of the PI3 kinase family (ATM, ATR, and DNA-PK) are first recruited to the DNA damage site and phosphorylate histone H2AX, termed γ-H2AX creating a platform for further recruitment of repair factors (*111*). Functional interaction of PARP-1 and pADPr with different NHEJ proteins including Ku70 and DNA-PKcs, has been described suggesting a role of PARP in modulation of DSB signaling and repair by NHEJ (*39, 112-115*). However cells with defects in major NHEJ factors undergo NHEJ at a slower rate implicating an alternative pathway called back-up NHEJ (B-NHEJ) (*116*). This backup pathway depends on PARP-1 and XRCC1/DNA ligase III complex and is more error prone than classical DNA-PK dependent NHEJ (*117, 118*).

PARP-1 has been implicated in HR to promote replication restart at damaged replication fork (*119-121*). In this regard, stalled replication forks formed by hydroxyurea (HU) requires both PARP-1 and PARP-2 to mediate the recruitment and activation of Mre11–Rad50–Nbs1 (MRN) complex to initiate the end processing followed by recruitment of Rad51 (*119*). Further it has been shown that recruitment of Mre11 at DSB is PAR-dependent (*122*). In HR-defective cell lines such as $BRCA^{-/-}$, inhibition of PARP-1

cause an increase in SSBs. Of the known synthetic lethality explanation between $BRCA^{-/-}$ and PARP inhibition, it could be either due to trapping of PARP-1 to the damaged DNA site that is repaired by BER (*108*) or due to conversion of SSBs to DSBs thereby enhanching the error-prone NHEJ (*123*) and contributing to the cytotoxicity.

Additionally, PARP-3 has been associated with PARP-1, Ku70/80 and DNA-PK of the DNA repair machinery (*80, 124*). Recent data from Caldecott group shows PARP-3 is stimulated by DNA DSB in vitro and also associates with ADP-ribose binding protein APLF, suggesting an active role in DSB repair via NHEJ (*75*).

1.6.4 PARP-1 in Nucleotide Excision repair (NER)

Nucleotide excision repair (NER), a highly versatile DNA repair pathway, removes bulky, helix-distorting DNA lesions from genome such as UV-induced photolesions cyclobutane pyrimidine dimers (CPDs), pyrimidine 6-4 pyrimidone photoproducts (6-4PPs) and DNA adducts such as platinum-DNA adducts induced by mutagenic chemicals or chemotherapeutic drugs There are two sub-pathways of NER: transcription coupled repair (TC-NER) and global genome repair (GG-NER). These two pathways differ in their mode of damage/lesion recognition and leads up to damage excision by use of pathway-specific factors (*125, 126*)

TC-NER functions on actively transcribed strands and involves recognition of the lesion through stalled elongating RNA polymerase II at DNA lesion followed by recruitment of CSA, CSB and XAB2 factors to the DNA while, GG-NER removes lesions throughout the genome and is initiated by UV-DDB and XPC-RAD23B protein complex (*126, 127*) After lesion demarcation, the two pathways converge and core NER proteins such as basal transcription factor TFIIH and its helicase component, XPB and XPD unwinds DNA helix in vicinity to DNA lesion; a stable pre-incision complex involving XPA, RPA and XPG stabilizes the open ssDNA structure; endonucleases ERCC1-XPF and XPG incises the damaged strand 5' and 3' to the lesion respectively; DNA pols δ, ε or κ

fills the DNA gap and DNA ligase I or IIIα restores the integrity of DNA backbone (*128, 129*) (**Figure 1.7**)

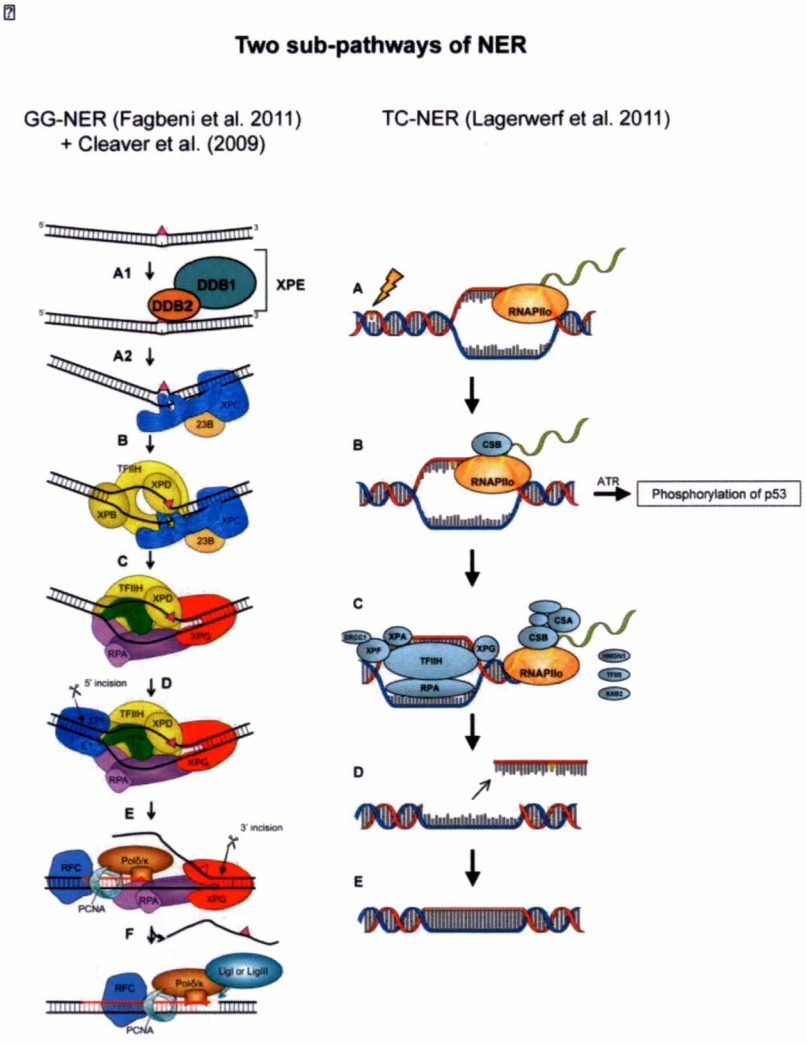

Figure 1.7: The two subpathways of mammalian NER. Taken from Fagbeni et al (*127*), Cleaver et al (*129*) and Lagerwerf et al (*128*)

The possible role of PARP-1 in NER has been elusive; however, experimental data from our laboratory has implicated PARP-1 in lesion recognition step of NER pathway (*130*) and the mechanistic detail of this role is under experimentation. In NER proficient

cells, using Host-Cell Reactivation (HCR) assay, which reflects the DNA repair capacity of the cells, it has been shown that PARP-1 inhibition decreases the DNA lesion repair by both GG-NER and TC-NER to a level closer to NER-deficient XPC and CSB cells after exposure to UVB and UVC (*130*). Additionally, in response to UV-induced DNA direct photolesions CPDs such as T-T dimer, PARP-1 is immediately attached to chromatin DNA containing T-T lesions indicating early lesion recognition role of PARP-1 (*131*). In addition, PARP-1 is also activated in the vicinity of UV-induced DNA damage to form pADPr, indicating its possible role in either chromatin remodeling or transmission of damage signal to downstream NER events. Infact, a recent study strongly supported this notion by showing that DDB2-mediated chromatin decondensation in response to UV irradiation, which is essential for access to the site by NER proteins, is suppressed by PARP inhibition which in turn affects the recruitment of XPC at photolesions indirectly implicating PARP and pADPr in the lesion recognition step of GG-NER (*132*). Additionally, in a genome wide RNAi screening, several potential targets showing sensitivity to PARP-1 inhibition including TC-NER proteins such as DDB1 and XAB2 has been identified, suggesting that PARP-1 activity inhibition could be detrimental to NER pathway (*133*). Thus there is enough evidence to support the role of PARP-1 at early stages in NER such as in the lesion recognition and chromatin remodeling and it will be of interest to see if ongoing efforts from our laboratory and other teams might uncover novel roles of PARP-1 in NER.

The large amount of work done in several labs, have clearly established the role of PARP-1 in different DNA repair pathways. In a recent study, PARP-1 is also implicated in mismatch repair (MMR) and components of mismatch repair such as MutSα and Exo1 have been identified as novel PARP-1 interacting partners in MMR (*134*).

1.6.5 PARP-1 in Cell death

The cell death is defined as an irreversible loss of plasma membrane integrity and represents the final point or 'point-of-no-return' in the cell life. Different forms of cell death have been reported, each with distinct biochemical features and which could also be divided into either of two mutually exclusive groups: the caspase-dependent or caspase-

independent cell death (**Table 1.2**) (reviewed in (*135, 136*)). In contrast to PARP-1's role as a survival factor, it also has been involved as a mediator of cell death. In response to extensive DNA damage, PARP-1 over-activation results in an irreversible NAD^+/ATP depletion thus contributing to cell death implicating PARP-1 as a mediator of cell death by necrosis (*137, 138*). There are different ways in which PARP-1 is implicated in different modes of cell death as described below. The choice of a specific PARP-1 dependent mode of cell death is influenced by the type, strength and duration of stimuli as well as the cell type.

Table 1.2: Functional classification of regulated cell death modes. Taken from Galluzzi *et al.* 2012 (*136*).

	Main biochemical features	Caspase dependence
Anoikis	Downregulation of EGFR Inhibition of ERK1 signaling Lack of β1-integrin engagement Overexpression of BIM Caspase-3 (-6,-7) activation	++
Autophagic cell death	MAP1LC3 lipidation SQSTM1 degradation	– –
Caspase-dependent intrinsic apoptosis	MOMP Irreversible $\Delta\psi_m$ dissipation	++
Caspase-independent intrinsic apoptosis	Release of IMS proteins Respiratory chain inhibition	– –
Cornification	Activation of transglutaminases Caspase-14 activation	+
Entosis	RHO activation ROCK1 activation	– –
Extrinsic apoptosis by death receptors	Death receptor signaling Caspase-8 (-10) activation BID cleavage and MOMP (in type II cells) Caspase-3 (-6,-7) activation	++
Extrinsic apoptosis by dependence receptors	Dependence receptor signaling PP2A activation DAPK1 activation Caspase-9 activation Caspase-3 (-6,-7) activation	++
Mitotic catastrophe	Caspase-2 activation (in some instances) TP53 or TP73 activation (in some instances) Mitotic arrest	– –
Necroptosis	Death receptor signaling Caspase inhibition RIP1 and/or RIP3 activation	– –
Netosis	Caspase inhibition NADPH oxidase activation NET release (in some instances)	– –
Parthanatos	PARP1-mediated PAR accumulation Irreversible $\Delta\psi_m$ dissipation ATP and NADH depletion PAR binding to AIF and AIF nuclear translocation	– –
Pyroptosis	Caspase-1 activation Caspase-7 activation Secretion of IL-1β and IL-18	++

1.6.5.1 PARP-1 in Apoptosis

Apoptosis, a type of caspase-dependent programmed cell death (PCD), is morphologically associated with rounding-up of the cell, reduction of cellular volume, membrane blebbing, chromatin condensation and nuclear fragmentation (reviewed in (*139*)). The two main evolutionarily conserved protein families that are involved in apoptosis are Bcl-2 family of proteins such as Bcl-2, Bcl-xL and Bid which controls mitochondrial integrity and caspases that mediates the execution phase of apoptosis (reviewed in (*140*)). Caspases are the cysteinyl aspartate specific proteases which uses cysteine residue as a catalytic nucleophile to cleave their substrate specifically after aspartic acid residue.

In mammalian cells, depending on the origin of death stimuli, apoptosis is mediated through two pathways, the intrinsic and the extrinsic pathway (**Figure 1.8**) (reviewed in (*139-141*)). The extrinsic pathway is initiated by the stimulation of death receptors of tumor necrosis factor (TNF) receptor family such as CD95 (APO-1/Fas) or TNF-related apoptosis-inducing ligand (TRAIL) receptors (*139*). Binding of death ligands such as FasL to death receptors Fas results in formation of homotrimeric ligand-receptor complex that further recruits cytosolic factors such as FADD and capsape-8 to form an oligomeric death-inducing signaling complex (DISC). This leads to the activation of initiator caspase-8 which in turn cleaves and activates the effector caspase, caspase-3. The intrinsic apoptotic pathway is generated in response to a wide range of death stimuli that are generated from within the cell and are all wired to a mitochondrion-centered control mechanism (reviewed in (*142*)). Some of the well characterized mitochondrial factors are cytochrome-c, apoptosis-inducing factor (AIF), Smac (second mitochondria-derived activator of caspase)/DIABLO (direct inhibitor of apoptosis (IAP)-binding protein with low pI), Endo G (endonuclease G) and OMI/Htra2 (high-temperature-requirement-protein A2). The release of cytochrome-c from mitochondria into the cytosol triggers caspase-3 activation through formation of cyt-c/apaf1/caspase-9-containing apoptosome complex, whereas Smac/DIABLO and Omi/HtrA2 promote caspase activation through neutralizing the inhibitory effects of the IAPs (*141*). The two pathways are interconnected and the

molecular basis for the crosstalk between extrinsic and intrinsic pathway has been established (reviewed in (*143, 144*)). Upon death receptor triggering, caspase-8 can cleave Bid, a Bcl-2 family protein with a BH3 domain only, which in turn translocates to mitochondria to release cyt-c thereby initiating mitochondrial amplification loop.

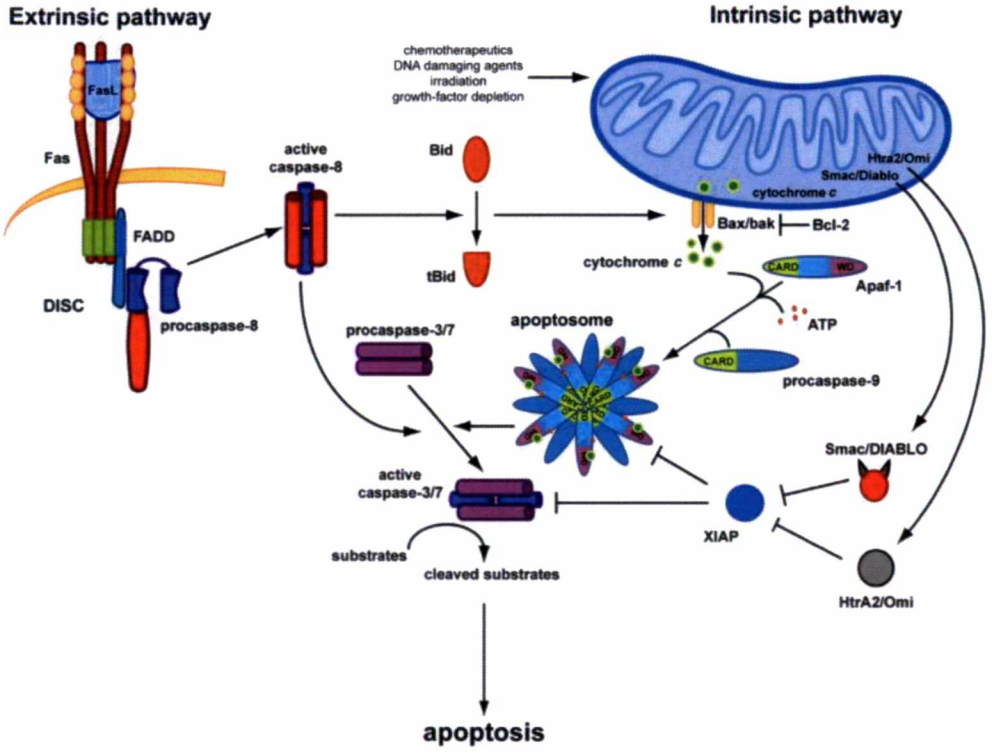

Figure 1.8: Overview of the Extrinsic and Intrinsic Apoptotic Pathways. Taken from Lamkanfi *et al.* 2010 (*141*)

PARP-1 which functions in DNA damage detection and repair, is one of the early substrates to be cleaved during apoptosis by two pro-apoptotic proteases, caspase-3 (*7, 145*) or caspase-7 (*145, 146*) at ^{211}DEVD^{214} site producing a 24-kDa DBD and signature 89-kDa

(previously known as 85-kDa) CD fragment essentially inactivating PARP-1 (*147*). This cleavage is hallmark of apoptosis and prevents additional PARP-1 activation thus ensuring cellular ATP store for the execution of apoptosis (reviewed in (*148, 149*)). The 24-kDa DBD can bind irreversibly to DNA strand breaks (*150*) and acts as a transdominant inhibitor of active PARP-1, thus inhibiting the DNA repair (*151*) or stimulating cell death (*152*). The 89-kDa fragment retains a low basal activity but is not stimulated by DNA strand breaks (*153*) and interacts with intact PARP-1 inhibiting the homodimerization during UV-induced apoptosis (*154*).

Preceding PARP-1 cleavage, in response to different apoptotic stimuli, an early and transient burst of poly(ADP-ribosyl)ation of nuclear proteins including p53, DNA-PK and lamins have been reported in different cell lines (*155*). One of the suggested roles for this modification is that this post-translational modification will be modifying many anti-apoptotic/pro-apoptotic substrates, cell cycle regulatory proteins, protein kinases and structural proteins altering their physical, biochemical and regulatory functions. Additionally, this observation was not found in PARP-1 knockdown or PARP-1 inhibited cell lines suggesting role of PARP-1 and PAR in the course of apoptosis. Subsequently, the degradation of PAR by PARG followed by cleavage of PARP-1 promotes apoptosis (*156*).

Studies using caspase-resistant or uncleavable PARP-1 (^{211}DEVD/A^{214}) retaining its DNA-binding and catalytic activity provided the role of PARP-1 during apoptosis (*157-160*). The introduction of this uncleavable PARP-1 in cells has varied response such as, survival (*157*), enhanced (*160*) or delayed cell death (*158*) or induction of necrosis (*159*) depending on cell type and apoptotic stimulus, supporting the hypotheses for PARP-1 cleavage as inactivation of survival-factor for efficient apoptosis or a switch to necrosis.

In addition to caspase-dependent apoptosis, mammalian cells can also undergo caspase-independent apoptosis that is mediated by the dissipation of inner mitochondrial potential and the release of a mitochondrial oxidoreductase AIF from the mitochondria. Extensive DNA damage provoked by high doses of alkylating agent such as MNNG or NMDA triggers PARP-1 over activation and release of AIF from the mitochondria (*161-163*). The release of AIF from the mitochondria is PAR-dependent. (*164, 165*) and this form of caspase-independent cell death is termed parthanatos (*166, 167*). Following nuclear

translocation, AIF associates with γH2Ax and cyclophilin A and causes nuclear chromatin condensation as well as large scale (~50 kb) DNA fragmentation (*161, 168*).

1.6.5.2 PARP-1 in Autophagy

Diverse experimental evidence has shown that cells can also die through an alternative caspase-independent pathway known as autophagy (reviewed in (*169*)). Autophagy is hallmarked by accumulation of double membrane vesicles that sequester and target cytoplasmic components such as mitochondria for lysosomal degradation in a process dependent on autophagy proteins which are encoded by autophagy-related genes (ATGs) (*170*). This primarily acts as a protective mechanism in normal cells in response to nutrients depletion (*170*) but persistent autophagy with excessive degradation of cell components can lead to cell death and is usually accompanied by inhibition of the phosphatidylinositol 3-kinase/protein kinase mammalian target of rapamycin (PI3kinase/Akt/mTOR) signaling pathway, which is the main regulator of autophagy. (*171*). Autophagy and apoptosis can be triggered by common upstream signals, resulting in combined autophagy and apoptosis or they can be mutually exclusive. There have been recent advances in understanding in the crosstalk between autophagy and apoptosis. Recently, a gene network signaling model has also indicated a central role for Bcl-2 and Beclin 1 in the apoptotic and autophagic responses (*172*) wherein the binding of apoptotic proteins, Bcl-2 and Bcl-xL, to beclin (*173*), or *c*aspase-3-mediated cleavage of Beclin-1 inhibits autophagy (*174*).

Recently few papers have shown role of PARP-1 in autophagy following DNA damage by various stimuli such as doxorubicin and ROS generated by starvation (*175-178*). In starvation-induced autophagy (**Figure 1.9**), the overactivation of PARP-1 in response to ROS-induced DNA damage lead to NAD^+ and ATP depletion, leading to energy collapse and generates a feedback loop to reactivate autophagy. The net consequence of NAD^+/ATP depletion activates the energy sensing LKB1-AMPK pathway and induces autophagic state through inhibition of mammalian target of rapamycin (mTOR) (*176, 178*). However, in the

absence of PARP-1 or PARP-1 inhibition, where ATP depletion is reduced apoptosis is favored over autophagy.

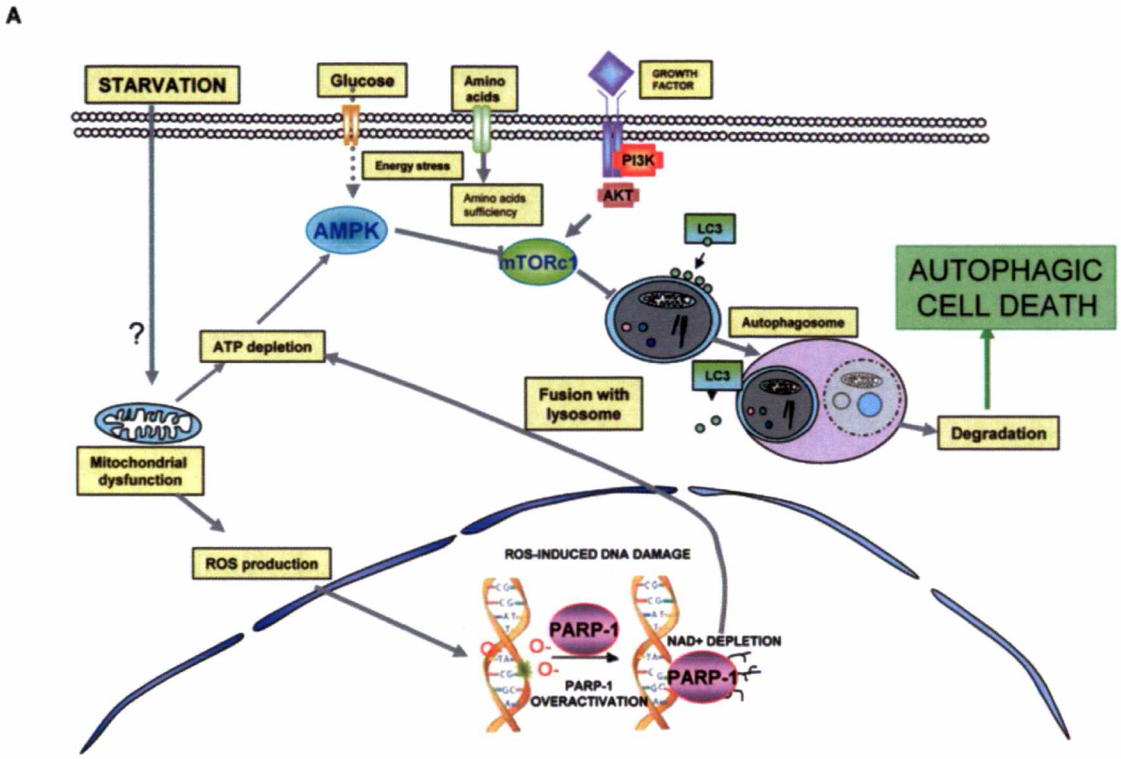

Figure 1.9: PARP-1 in starvation-induced autophagy. Taken from Rodriguez-Vargas *et al.* 2012 (*175*)

1.6.5.3 PARP-1 in Necrosis and Necroptosis

Necrosis is considered as a passive, non-apoptotic and caspase-independent cell death. It is marked by distinct features such as, mitochondrial depolarization, depletion of intracellular ATP, enhanced ROS generation, activation of non-apoptotic proteases such as cathepsins and calpains, loss of cell membrane integrity and release of the cytosolic contents such as high-mobility group box 1 (HMGB1) into the surrounding extracellular space (*179-181*). PARP-1 has been shown to mediate cell death via both apoptosis and

necrosis. The severe DNA damage induced by various DNA damaging agents including, MNNG (*182, 183*), H_2O_2 (*184*), peroxynitrite and NMDA (*185*) causes over-activation of PARP-1 leading to a severe depletion of NAD^+/ATP store, irreversible cellular energy failure and necrotic cell death (*138, 186*). Alternately, rapid depletion of NAD^+/ATP can also lead to rapid intracellular acidification and necrosis due to release of protons from NAD^+ during formation of polymer (*187*). In addition, prevention of acidification shifted mode of cell death from necrosis to apoptosis. PARP-1 inhibition (*188*) or PARP-1 gene deletion (*86*) can inhibit both depletion of NAD^+/ATP and induction of necrosis.

PARP-1 cleavage typical of necrosis is characterized by the appearance of major fragments of 50-kDa and minor fragments of 40- and 35-kDa, caused by lysosomal proteases that are released during necrosis (*189, 190*). Granzyme B, a serine protease (*191*) and cysteine protease calpain (*192*) also has been demonstrated to cleave PARP-1 typical of PARP-1 necrotic cleavage, a 64-kDa and 40-kDa, respectively.

However, necrosis can also occur in a regulated manner by a set of signal transduction pathways and catabolic mechanisms. Necroptosis is such a recently identified programmed necrosis that shares features of necrosis and depends on the serine/threonine kinase activity of receptor-interacting protein 1 (RIP1) (*193, 194*). Among the death receptors-induced necroptosis (reviewed in (*193-195*)), the Tumor necrosis factor-α/TNF Receptor 1 (TNF-α/TNFR1) can mediate NF-kB activation, apoptosis and necroptosis (**Figure 1.10**) (*196*). Stimulation of TNFR1 by TNFα leads to the formation of an intracellular complex at the cytoplasmic membrane (complex I) that includes TNFR-associated death domain (TRADD), TNFR-associated factor 2 (TRAF2), RIP1, and cellular inhibitor of apoptosis 1 (cIAP1). Ubiquitination of RIP1 by cIAP1 recruits NEMO, a regulatory subunit of the IKK complex and acts as a cytoprotective mechanism by NF-κB activation and transcriptional upregulation of pro-survival genes. RIP1 ubiquitination influences the transition from complex I to complex IIa. Upon deubiquitination of RIP1 by cylindromatosis (CYLD), RIP1 is involved in the formation of complex IIa which includes TRADD, Fas-associated protein with a death domain (FADD), RIP1 and caspase-8. This complex IIa activates a caspase cascade to mediate apoptosis. Under apoptosis-deficient conditions or when caspase-8 is inhibited, RIP1 interacts with RIP3 to form complex IIb.

The phosphorylation-driven assembly of RIP1-RIP3 complex (necrosome) activates the necroptosis. However, necroptosis specifically can be inhibited by necrostatin-1 (Nec-1), which inhibits RIP1 kinase activity thereby blocking the assembly of necrosome, (*197*).

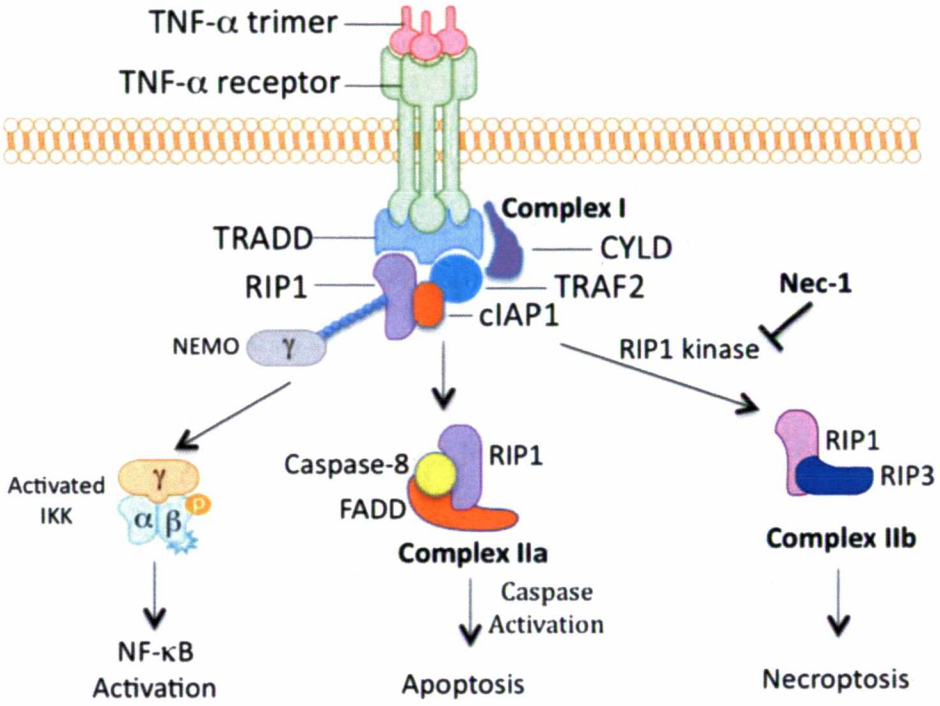

Figure 1.10: The signaling complex of necroptosis. Taken from Yuan et al. 2010 (*196*)

There has been contrasting evidence on role of PARP-1 in necroptosis. It has been shown that PARP-1 activation is potentially not involved in necroptosis in Jurkat and BALB/c 3T3 cells (*197*). However, recently a paper has implicated PARP-1 activation and AIF translocation in glutamate-induced necroptosis in HT-22 cells (*198*). Regulated necrosis can also be induced by alkylating DNA damage possibly by the over-activation of PARP-1. Studies from Susin's group has proposed MNNG-induced AIF-mediated necroptosis (*199*) which is regulated by sequential activation of calpain, Bid and Bax (*200*) Interestingly, in a genome wide screening for genes, Hitomi et al have revealed PARP-2 as one of the core regulators of necroptosis (*195*).

There are different ways in which PARP-1 is implicated in different modes of cell death as described above. **Figure 1.11** shows the involvement of PARP-1 in apoptosis, necrosis, AIF-mediated cell death and autophagy. Nevertheless, there are several other cell death forms such as anoikis, entosis and many others (reviewed in (*136*)) and whether PARP-1 has any role in any of these is not yet known.

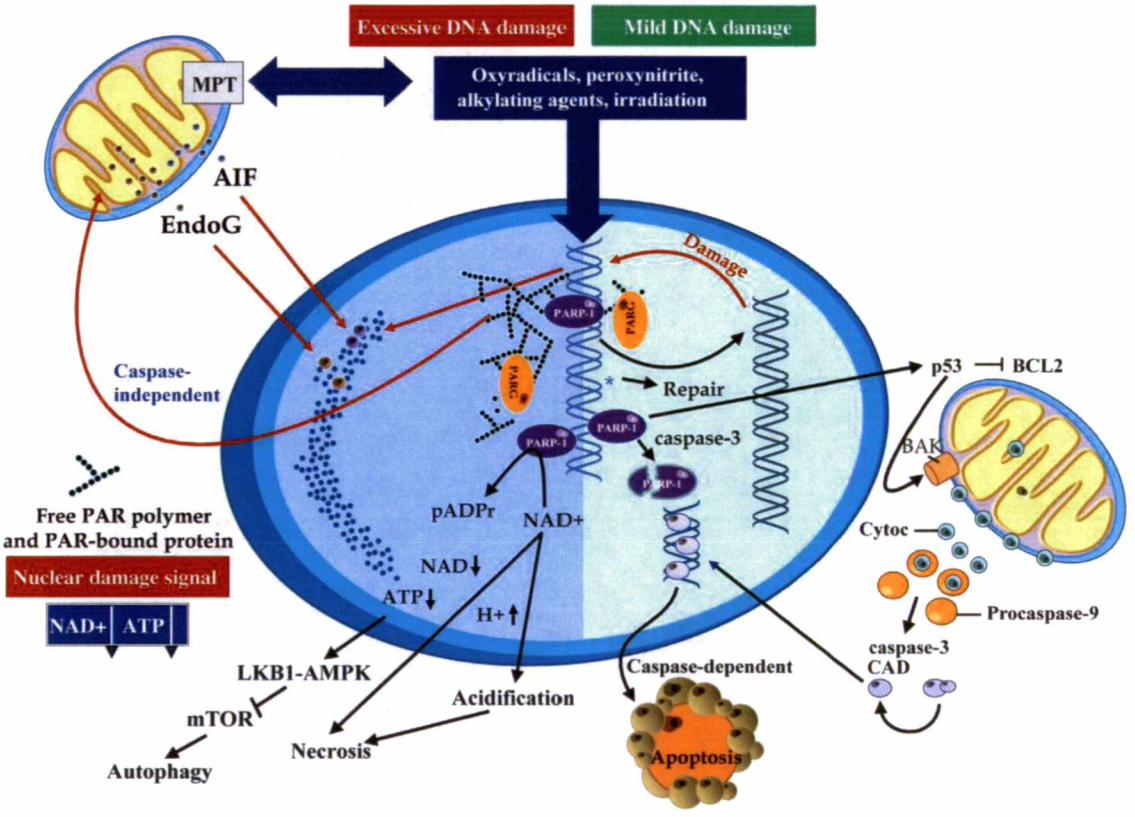

Figure 1.11: PARP-1 in different cell death processes. Modified from Hong *et al.* 2004 (*201*)

1.7 Different approaches to study PARP-1's functions

In any experimental system, targeting both PARP-1 protein and its catalytic activity is important to understand the physiological role of PARP-1. Many approaches such as, in vitro random mutagenesis, PARP-1 antisense oligonucleotides and overexpression of dominant-negative PARP-1 mutants have been used to antagonize PARP-1 activity. Below is the brief summary of other approaches that are currently in use.

1.7.1 PARP-1 knockout mice

The observations from three independently constructed PARP-1 knockout mice, revealed an instrumental role of PARP-1 in survival and cell death (reviewed in (*86*)). Although all three PARP-1 knockouts were viable and fertile, the knockout of PARP-1 gene rendered different phenotypes including genomic instability, defective DNA repair pathway and sensitivity to genotoxic chemicals or radiation. On the contrary, genetic depletion of PARP-1 protected these mice from several DNA-damage dependent pathophysiological conditions such as streptozotocin-induced diabetes, Lipopolysaccharide (LPS)-induced septic shock and cerebral ischemia (**Table 1.3**).

1.7.2 Pharmacological inhibitors of PARP

PARP-1 often referred to as "guardian angel of DNA" has received a much greater attention for potential therapeutic reasons. The chemical inhibitors employed as NAD^+ competitive inhibitors or analogs effectively abolish PARP-1 activity. Of the known DNA-repair inhibitors, PARP-1 inhibitors are furthest in clinical trial for cancer (reviewed in (*202*)). Currently, PARP-1 inhibitors are used as a chemopotentiator with chemo and radiosensitizing agent (TMZ, topoisomerase I inhibitors and ionizing radiations) that could compromise the cancer cell DNA repair mechanisms (reviewed in (*90*)) or as a stand-alone therapy for tumors that are deficient in certain DNA repair mechanisms (BRCA-1/2 deficient cells) (*203*).

1.7.3 PARP-1 RNA-interference

Silencing or ablation of gene expression by RNA-interference (RNAi) is a methodology for the analyses of gene function. Our lab has designed a simple and cost-effective system to achieve stable depletion of PARP-1 by RNAi thus providing a system to study loss of PARP-1 protein and its activity in different cellular processes (*204*). Using this approach, studies from our lab and other labs have confirmed the role of PARP-1 in DNA repair (*130*), chromatin remodeling (*205*), transcription and angiogenesis (*206*). RNAi is discussed in detail in **section 1.9**.

Table 1.3: Phenotypes of the various PARP-1 knockout mice and derived cell lines. Taken from Shall and de Murcia 2000. (*86*)

Constructs	Phenotype
KO 1 (disruption of the 2nd exon)	Mice healthy and fertile. Impaired fibroblast and thymocyte proliferation after gamma-irradiation. Decreased ability to repair DNA damage induced by MNNG Hypersensitivity to whole body gamma-radiation Increased genomic instability (SCE, micronuclei) Telomere length deregulation p53: low basal level, defective post damage induction, normal transactivation Accumulation of DNA breaks following Streptozotocin treatment. Pancreatic islet cells are resistant to the toxicity of NO and ROI Protection against peroxynitrite-induced arthritis Protection against MPTP-induced Parkinsonism Protection against Streptozotocin-induced diabetes. Defective induction of NF-kB Resistance to cerebral ischemia. Resistance to LPS-induced septic shock
KO 2 (disruption of the 4th exon)	Extreme sensitivity and high genomic instability of mice (SCE, chromatid and chromosome breaks) following MNU exposure and gamma-irradiation. Acute radiation toxicity to the small intestine. High sensitivity of splenocytes and bone marrow cells to MNU exposure, G2/M accumulation and apoptosis. p53 accumulation following DNA damage (MNU, MMS). Sensitization to camptothecin Growth retardation, G2/M accumulation, chromosome instability (micronuclei), severe DNA repair defect in the BER pathway in PARP-deficient 3T3 cells exposed to MMS. Normal NER Resistance to VP16 due to decresease expression of Topo IIβ Protection against Streptozotocin-induced diabetes Defective induction of NF-kB Resistance to LPS-induced septic shock
KO 3 (disruption of the 1st exon)	Reduced survival of PARP-deficient ES cells after MMS treatment and gamma-irradiation p53 accumulation following gamma-irradiation Protection against Streptozotocin-induced diabetes

In short, PARP-1 and its catalytic activity play a crucial role in recognition of DNA damage, which on one hand could facilitate DNA repair at lower levels of DNA damage via chromatin remodeling and recruitment of DNA repair factors, and on the other hand, mediate cell death at higher levels of DNA damage. **In the context of PARP-1, the focus of our laboratory is on understanding the roles of PARP-1 in cellular responses to UV radiations, such as, DNA damage, repair, cell death and carcinogenesis using mice and cellular models.** To understand how PARP-1 may be involved in different cellular responses to UV radiations, first it is essential to understand how UV can potentially trigger different signaling pathways at cellular level. In the following section I will briefly describe the different cellular responses to UV and involvement of PARP-1 in response to UV radiations.

1.8 Ultraviolet (UV) spectrum and cellular UV damage responses

The ultraviolet (UV) spectrum of sunlight is conventionally divided into short wavelength UVC (200-280 nm), mid wavelength UVB (290-320 nm), and long wavelength UVA (320-400 nm). Of the three components of solar UV radiation, only UVA and UVB reach the surface of earth. The UVC fraction of sunlight is entirely absorbed by stratospheric oxygen (O_2), which subsequently undergoes decomposition and recombination reactions, giving rise to ozone (O_3). The resulting O_3 molecules can function as a filter and absorb the majority of UVB. Thus, the solar UV wavebands that reaches the surface of the earth, and as such is of relevance for photocarcinogenesis, is UVA and UVB, which comprise 95% and 5% respectively, of the terrestrial sunlight UV (reviewed in (*207*))

The genomic DNA represents the main cellular chromophore with absorption maximum in the UV region (200-290 nm) and thus a direct target for UVB and UVC irradiation, while UVA induces damages mediated by oxidative stress. At the molecular level, UVB radiation causes two types of DNA damages: (i) direct DNA photolesions such as, CPDs and 6,4-PP, which are repaired by NER and (ii) oxidant-induced DNA damage such as SSBs and (8-oxoG), which are repaired by SSBR and BER. The unrepaired DNA

damages induce cell death thereby eliminating harmful mutations and preventing progression of skin cancers (*208*).

Both DNA damage and oxidative damage caused by UV radiations provoke adaptive cellular and defensive responses that involve activation of several signaling cascades which could originate in the nucleus, at the cell membrane or in the cytoplasm (**Figure 1.12**) thus leading to cell cycle arrest, DNA repair or cell death (*209*). The unrepaired DNA damages can induce cell death or in case of repeated exposure or undue delay in DNA repair, can also lead to mutation, pro-inflammatory response leading to photocarcinogenesis (*208*). In response to DNA damage, first response is the cell cycle arrest to allow the repair of DNA lesions. Following UV radiations, a family of phosphoinositol-3-phosphate kinase ATR/Chk1, jun N-terminal kinase and p38 kinase pathways are activated. ATR phosphorylate checkpoint kinases Chk1, as well as p53, which block cell cycle progression by inhibiting cyclin-dependent kinase activity (*210*). p53, a tumor suppressor protein, also plays a very important role in controlling cellular growth, cell cycle arrest and apoptosis. In response to UV, p53 is phosphorylated by kinases such as JNK (*211*), p38 (*212*), and the phosphorylation status of p53 determines the cell cycle arrest or the apoptosis. In response to UVB, p53 induces cell cycle arrest by transactivation of different genes including p21, Gadd45, 14-3-3 (reviewed in (*213, 214*)). The stabilization of p53 is also known to transactivate the pro-apoptotic genes such as Bax, Noxa and Puma (*215*). Additionally, UV radiation also induces AP-1 family of genes (Fos and Jun family), which control growth and differentiation responses which determine carcinogenic response to UV.

Apart from DNA damage, UV can also mediate signaling by activation of MAPK pathway (*216*). MAPK, the serine/threonine kinases can generate both pro-survival or cell death signal. The p38α is a known transducer of survival signals via NF-κB in UV-irradiated cells (*217*) and in human keratinocytes UVB activates the p38α and ERK kinases via reactive oxygen species providing a pro-survival signal (*218*). Similarly, UVB-induced ERK/AKT-dependent PTEN suppression promotes survival of epidermal keratinocytes (*219*). UV radiations can also induce cell death. In keratinocytes in response to UV,

apoptosis can also be mediated by caspase-mediated cleavage and activation of PKC, which potentiates the caspase-activation and disruption of mitochondrial function (*220*). Signaling by clustering of several surface receptors such as TNFR1 or Fas family can cause UV-induced apoptosis which is mediated by activation of caspase-8 (*221*).

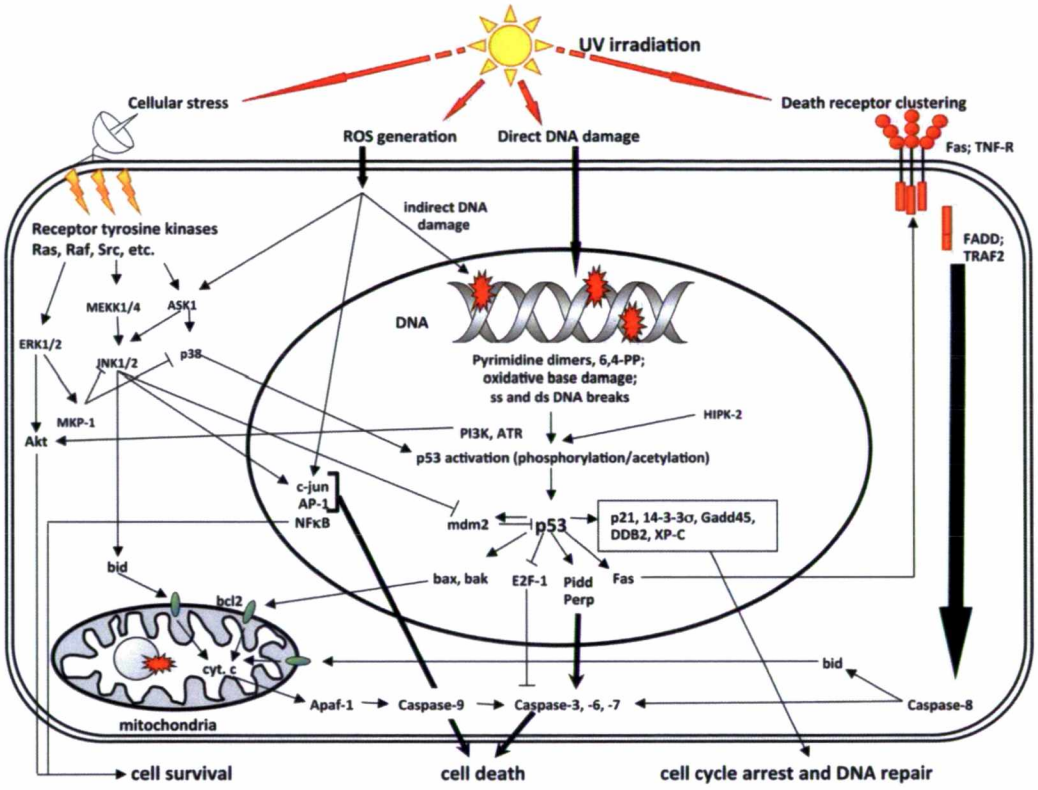

Figure 1.12: Nuclear and non-nuclear signals leading to UV-induced apoptosis. Taken from Vodenicharov, M.D. and Shah, G.M. From DNA photolesions to mutations, skin cancer and cell death, Vol 4, 247-267. New York: Elsevier, 2005 (*209*)

The DNA damage caused by UVB can also contribute significantly to the development of sunlight-induced skin cancers, which is specifically due to compromised NER pathway. However, one of the early responses to DNA damage induced by various

stimuli including UVB is PARP-1 activation as described before in the thesis. In the following section I will focus on role of PARP-1 in different cellular responses to UVB.

1.8.1 Role of PARP-1 in cellular responses to UVB

In response to UV, PARP-1 activation has been shown to participate in DNA repair and cell death.

1.8.1.1 PARP-1 in UVB-induced DNA damage

PARP-1 activation has been implicated in the repair of UVB-induced DNA damage. The inhibition of PARP-1 activation by DPQ or overexpression of PARP-1-DBD delays the DNA repair of UVB-induced CPDs (*222*). Interestingly, Cockayne syndrome B (CSB) deficient cells showed similar repair delay as in PARP-1 inhibited cells implicating, PARP-1 and poly(ADP-ribosyl)ation in a repair pathway dependent on CSB protein (*222*). PARP-1 was shown to interact and poly(ADP-ribosyl)ate CSB protein in response to oxidative stress (*223*). PARP-1 is also known to be activated during BER of UV-induced oxidative DNA damage. In a polβ null cell line, PARP-1 activity is required to remove oxidative DNA damage (*102*). Additionally, in response to UV-induced DNA direct photolesions CPDs such as T-T dimer, PARP-1 is immediately attached to chromatin DNA containing T-T lesions indicating early lesion recognition role of PARP-1 (*131*). Also, PARP-1 is also activated in the vicinity of UV-induced DNA damage to form pADPr, indicating its possible role in either chromatin remodeling or transmission of damage signal to downstream NER events. In NER proficient cells, the PARP knockdown decreases the DNA lesion repair by both GG-NER and TC-NER after exposure to UVB and UVC (*130*).

1.8.1.2 PARP-1 in UVB-induced cell death

PARP-1 activation has been linked to UVB-induced apoptosis in cultured cell or in mouse epidermis (*224, 225*). The UVB-induced apoptosis can be mediated via three ways (i) by UVB-induced DNA damage (ii) activation of death receptors and (iii) by reactive

oxygen species (ROS) within the cell. PARP-1 activation has been linked to UVB-induced apoptosis in cultured cell (*225*). Also in mouse epidermis inhibition of PARP-1 activation by PARP inhibitor (BGP-15M) on a hairless mice model (*224*) and by DHQ on epidermis of SKH-1 mice reduces UVB-induced cell death (*226*) Also, in HeLa cells, the overexpression of N-terminal DBD fragment (24kDa) of PARP-1 has shown to stimulate UV-mediated apoptosis (*152*) and the C-terminal fragment (89-kDa) interacts with intact PARP-1 and inhibits the homodimerization during apoptosis (*154*) suggesting cleavage of PARP-1 and inhibition of PARP-1 activity in maintaining the basal cellular energy required for the completion of UV-induced apoptosis.

In short, PARP-1 could play a role in different signaling pathways generated by UV radiations. Thereby, the first part of my thesis (chapter 2) is focused on the role of PARP-1 in cellular response to UVB in a cellular model in which PARP-1 was knockdown by DNA vector-based RNAi. In the next section, I will briefly describe general guidelines for designing RNAi-inducing molecule such as siRNA and the RNAi mechanism.

1.9 The RNA interference

The phenomenon of RNA interference (RNAi) was first introduced by Fire and Mello to describe the observation that a double-stranded (dsRNA) that was homologous to a specific gene when injected in the *C. elegans* can block gene expression more effectively than either strand (sense or antisense) individually (*227*). However, the molecular trigger or the mechanism of RNAi was not clear. Gene silencing studies in plants and biochemical analysis of RNAi in *Drosophila* lead to discovery of silencing intermediate of 25 nucleotides (nt) and similar 21-23 nt in plants (*228*) and Drosphila cell extracts respectively, suggesting that dsRNA is converted to shorter intermediates, small interfering RNAs (siRNAs) capable of binding to target mRNAs and causing its degradation (*229-231*). Years before the discovery of RNAi and siRNAs, similar endogenous 21-nt non-coding regulatory small RNA *lin-4* (*232*) and *let-7* (*233*), which controlled developmental timing in nematodes by modulating expression of genes at the post-transcriptional level was discovered and were termed as microRNAs (miRNAs) (reviewed in (*234*)). This miRNA

duplex has eventually the same structure as double stranded siRNA (*235*), except that the miRNA duplex is partially paired and regulates expression of its target gene mainly via translational repression whereas siRNA achieves the same end-result by target mRNA cleavage (*236*).

Advancement in research on the generation of mature miRNA from primary and precursor miRNA (pri- and pre-miRNAs) by a series of proteins and enzymes including the endoribonuclease Dicer (*237*) and subsequent implication of RNA-induced silencing complex (RISC) in silencing the target gene of miRNA led to realization that RNAi by exogenously introduced dsRNA or endogenously produced miRNAs shares the same core components, although some specialization do exist (reviewed in (*238*)). Since then, the experimental use of RNAi, based on co-opting miRNA pathway developed into a powerful reverse genetic tool to identify gene function by silencing a specific gene in organism or cell (**Figure 1.13**) (reviewed in (*239*)). Here, in this thesis, I will mainly focus on the biogenesis and function of siRNAs and the purported use of RNAi as a tool to study gene function in different cellular processes including cell death.

1.9.1 Tools of RNAi

The very key trigger of RNAi is the 21-nt siRNA. Currently there are two ways to harness the endogenous RNAi: either by direct delivery of chemically synthesized siRNA (21mer) into the cytoplasm (*235*); or by introducing a 27mer or viral/plasmid vector that directs expression of a short hairpin (shRNA) that would then be processed by endoribonuclease Dicer into siRNA (*240, 241*)

1.9.1.1 21mer/siRNA

In mammalian cells utilization of *in vitro* synthesized siRNA ~21-nt in length is long enough to induce sequence-specific mRNA degradation, but short enough to evade the host interferon response (*235, 242*). The efficiency of siRNA varies and requires strict

sequence specificity with target mRNA. To achieve optimal RNAi efficiency, siRNA duplexes are composed of 21-nt sense and 21-nt antisense siRNAs, selected in order to form a 19-nt perfect base-pairing duplex with 2-nt 3' overhangs. The 2-nt 3' overhang of both strands is composed of 2'-deoxy-thymidine/uridine residues (*235, 243*). The RNA strand whose 5'-end is less stably paired (preferably with more A/U nucleotides) with complementary strand is chosen as the guide (or antisense) strand and the other strand, is known as passenger (or sense) strand homologous in sequence to the mRNA. The 5'-end of the antisense strand contains a phosphate group, which is essential for guide strand uptake into the nuclease complex RISC (*229*) and sets the ruler for target mRNA cleavage (*243*).

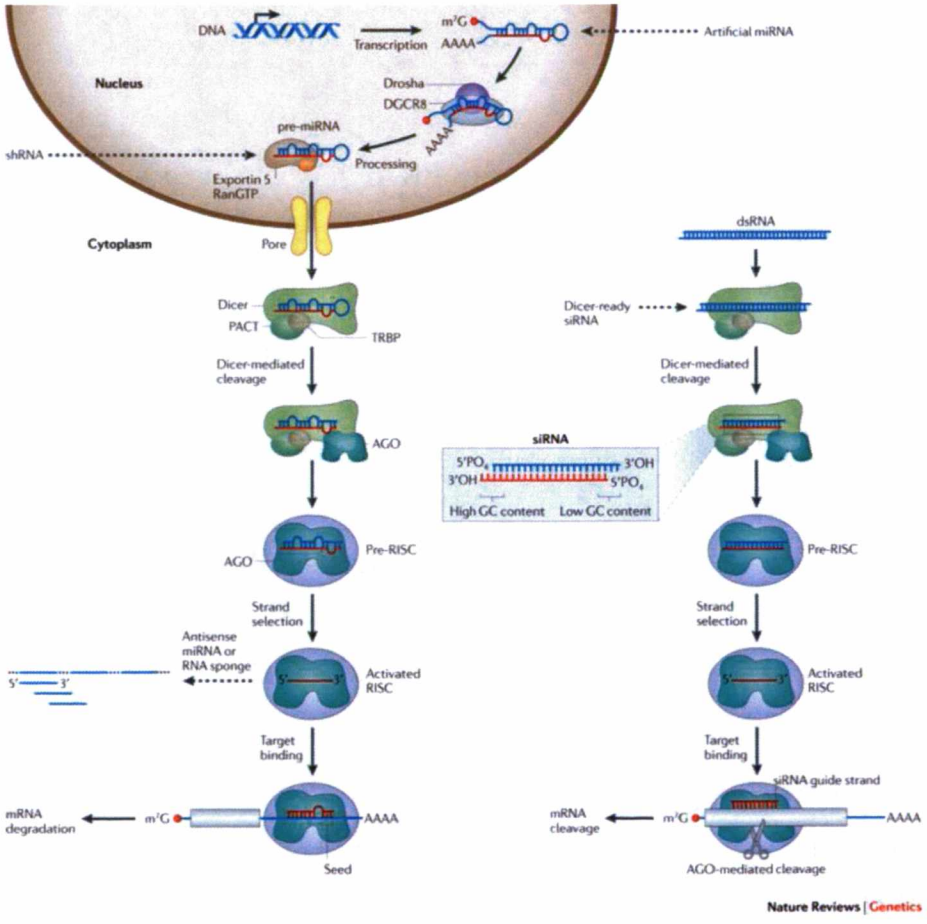

Figure 1.13: The miRNA and siRNA pathways of RNAi in mammals. Taken from Davidson *et al.* (*239*)

1.9.1.2 27mer dsRNA

The chemically synthesized longer dsRNAs duplexes of 27-nt length with 2-nt 3'-overhangs were 100-fold more potent than the corresponding conventional 21mer siRNAs and importantly, were short enough not to activate the interferon response or protein kinase R (PKR) in mammalian cells (*240*). These long dsRNA showed enhanced efficacy and longer duration of RNAi at lower concentrations than 21mer siRNAs and were also suitable to target sites which were refractory to silencing by 21mer siRNAs (*240*). The increased potency of 27mer was attributed to Dicer processing of these long dsRNA duplexes to generate siRNAs thus, conferring functional polarity and incorporation into RISC (*244*).

1.9.1.3 shRNA

Both 21mer and Dicer-substrate 27mer RNAi initiating molecules do not have long half-lives once transfected into cells and thus, the inhibition of target gene is for limited duration (4-6 days) (reviewed in (*245*)). To achieve long-lasting gene silencing, several laboratories created plasmid or viral based vectors in which gene-targeting DNA sequences are linked to specific promoters which permit an accurate transcription from these vectors to form a small defined length RNA that can fold itself into a short hairpin structure (shRNA). This shRNA resembles the pre-miRNA and can be a steady and permanent source for supply of mature siRNA to achieve stable knockdown of the target gene (*246, 247*). These shRNAs modeled conceptually on pre-miRNAs avoid interferon induction (*248, 249*). The first generation of shRNA-vectors carried Pol III promoters (U6 or H1) which are known for accurate initiation of transcription at defined nucleotides (G/A), termination of transcription at 3' end with a stretch of 4-5 thymidines (Ts) and these noncoding transcripts are not capped or polyadenylated at 5' and 3' ends, respectively. Viral/plasmid-based expression vectors encoding short hairpin RNAs contains 19-29-nt stems that match target sequence precisely, 3-9 nt loops and 3' overhangs of 4 or fewer uridines (*241, 250*) . This shRNA are then processed by endoribonuclease Dicer to generate active siRNAs with structural feature required for effective RNAi (*251*). Stable suppression

of gene expression can be achieved using retroviral vectors or by positive selection of integrated plasmids.

1.9.2 Molecular and structural biology of Initiator and Effector machinery of RNAi

Mechanistically RNAi could be divided into two steps: an initiation step involving generation of siRNAs from long dsRNAs (27mer) or shRNAs by Dicer a member of RNase III family (*237*); and an effector step whereby the siRNA becomes part of effector machinery to carry out the nucleolytic destruction of the targeted mRNA (*238*). This is achieved by RISC and a member of Argonaute family (reviewed in (*252*)).

1.9.2.1 Dicer

Dicer, a 1922 amino acid protein is a multidomain endoribonuclease of RNase III family that is responsible for processing of dsRNA or pre-miRNA to characteristic 21-23 nt siRNAs or miRNAs (*237, 253*). Human Dicer has several domains (**Figure 1.14**) that include a Helicase/ATPase domain, Domain of Unknown Function 283 (DUF283), PAZ domain, two neighboring catalytic RNase III domains (RNase IIIa and RNase IIIb) and dsRNA binding domain (dsRBD) (*254*). Dicer functions as a monomer having only one dsRNA processing center, containing two catalytic centers formed through intramolecular dimerization of the two RNase III domains, assisted by dsRBD and PAZ domain. The PAZ domain of Dicer contains a hydrophobic protein fold that specifically recognizes dsRNA containing 2-nt 3'-overhangs (*254*) and dsRBD is assumed to be involved in binding the dsRNA to Dicer. The distance between the PAZ domain and the active sites of both RNase III domains (~65Å) and the distance between two active sites of the RNase III domains (~17.5Å), matches the length of 25 dsRNA base pairs and the distance between the two scissile phosphodiester bonds in the substrate, respectively (*254, 255*). The residues Asp1320 and Glu1564 in RNase IIIa domain and Asp1709 and Glu1813 in RNase IIIb are required to cleave each strand of the long dsRNA to leave the siRNA with 2-nt 3'-overhang (*254*). In mammalian species Dicer has two dsRBD cofactors PACT (protein Kinase R Protein Activator) (*256*) and TRBP (HIV-1 transactivating response RNA-binding protein)

(*257, 258*). TRBP binds and stabilizes Dicer and is known to stimulate the dicing activity of Dicer (*253*).

1.9.2.2 RNA-induced silencing complex (RISC)

RISC is a preformed and fractionable ribonucleoprotein complex containing guide strand of a siRNA as an integral component (*229, 231, 259*). Using size exclusion chromatography a size range of 140-550 kDa was suggested for the RISC, depending on the model system and the presence or absence of protein cofactors (reviewed in (*260*)). Various RISC component proteins have been identified and the first and core component of this complex was Argonaute 2 (Ago-2) and was always present in the various purifications of the RISC from different species (*261*). It has been shown that hAgo2 and siRNA form minimal RISC nuclease (mature or active RISC) that accurately cleaves substrate RNAs (*262, 263*). RISC assembly is a key process in small RNA-mediated silencing and involves two successive steps RISC loading and RISC unwinding/activation of small RNAs (*252*). Once programmed with small RNA, RISC mediates gene silencing by distinct mechanisms, working at (a) the transcript level by sequence-specific degradation of mRNA targets (mechanism used by siRNA), (b) the level of protein synthesis by translational repression which is often used by miRNAs for endogenous gene regulation, or (c) the level of genome itself through the formation of heterochromatin (*260, 264*).

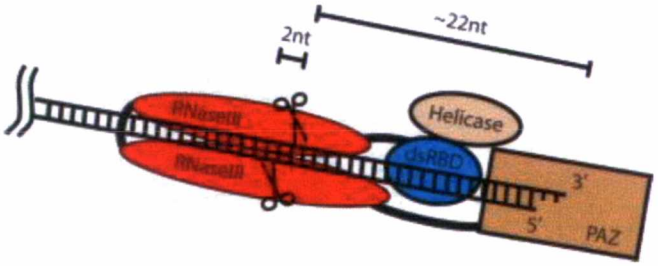

Figure 1.14: Model for Dicer catalysis. Taken from Hammond, S M. (2005) (*238*)

1.9.2.3 Argonaute (Slicer)

Argonaute proteins (~100-kDa) are highly basic proteins and form a large, evolutionarily conserved gene family in eukaryotes (reviewed in (*265*)). The eukaryotic Argonaute family can be classified into three paralogous groups: Argonaute (Ago), Piwi and Group 3 or WAGOs (worm-specific). All Ago proteins possess four distinct domains: the N-terminal, PAZ, MID and PIWI domains. The PAZ domain of argonaute proteins is structurally and functionally similar to the PAZ domain of Dicer (*237*) and is implicated in the binding of 3'-ends of single-stranded RNA (ssRNAs) allowing rest of the siRNA to bind to the target mRNA (*266, 267*). The 5'-end of small RNA is anchored by a divalent cation at the interface between the PIWI and Mid domain (*268, 269*). In case of perfect sequence complementarity between guide (siRNA) and target RNAs, the PIWI domain of catalytically active Ago adopts an RNase H type fold and hydrolyses target RNA using RNase H-like mechanism (*270*). Upon hydrolysis, the RNA is cleaved into two fragments, leaving a 5'-phosphate on one product and a 3'-hydroxyl on the other. This activity has been dubbed 'slicing' of target RNA (*270*). In case of imperfect base-pairing during target recognition by miRNA, mRNA is not cleaved. In mammals, a functional RISC contains four argonautes (Ago1-Ago4) and all four binds to siRNAs and miRNAs at similar levels, but only Ago2 displays a slicer activity (*271, 272*). The cleavage-competent Ago proteins have Apartate-Aspartate-histidine (DDH) motif for catalysis and requires binding of divalent cations for their endonucleolytic/slicer activity (*268, 270, 273*).

1.9.3 Detailed Mechanistic overview of RNAi

The understanding of RNAi mechanism mainly came from *Drosophila* systems and is proving to be very similar in mammalian systems (reviewed in (*274*)). However, the mechanism of RNAi is very complex and constantly under review as new knowledge emerges. In the subsequent sub-sections, the key steps of RNAi have been highlighted (**Figure 1.12**).

1.9.3.1 Processing of dsRNA by Dicer

Dicer is a molecular ruler that measures and processes longer dsRNA to 21-nt effector siRNA in a sequence-independent manner (*237, 255*). The PAZ domain of Dicer recognizes the two nucleotides overhang at the 3'-end and locks the dsRNA into position within Dicer. The dsRNA then lines up along the edges of both RNase III domains (**Figure 1.13**) (*238*). The active sites on each RNase IIIa and IIIb domain contain two magnesium atoms, essential for phosphodiester hydrolysis of the dsRNA and domain cleaves the dsRNA to produce siRNA with 5'-phosphate and 2-nt 3'-overhang with hydroxyl group respectively (*255*).

1.9.3.2 RISC loading: from siRNA formation to inactive RISC

After Dicer processing, in a thermodynamically asymmetric siRNA duplex, the strand whose 5'end lies at the thermodynamically less stable end of the duplex is preferentially loaded onto Ago2 as the guide strand (*275*) bound to the MID domain and 3'end of guide strand bound to PAZ domain (*276*). In mammals, Dicer-TRBP/PACT along with Ago2 comprises the core of RISC-loading complex (RLC) (*277, 278*).

1.9.3.3 RISC unwinding: dissociation of siRNA duplex to form active RISC

The maturation of pre-RISC is very crucial and is achieved by discarding the passenger strand of the duplex by two mechanisms

a. Passenger strand cleavage mechanism: In a pre-RISC loaded with a small RNA duplex, the passenger strand can serve as the guide strand's first RNA target (*279-281*) and is cleaved by Ago2 thus initiating the unwinding and release of mature or active RISC. The nicked passenger strand is degraded by a RISC activator (C3PO in *Drosophila* and QIP in *Neurospora*) that acts as endo/exonuclease respectively (*282, 283*). It has been shown that an active-site mutation in Ago2 cripples the endonuclease activity impeding passenger-strand release (*279*).

b. Bypass mechanism: This is an alternative pathway, which is operational independent of passenger strand cleavage. In this, active RISC is slower to form relying on some helicase that is involved in siRNA unwinding (*279*).

1.9.3.4 Target mRNA recognition and slicing

The N-terminal, MID and PIWI domain of Ago protein together form a unique structure, creating grooves for target mRNA and guide ssRNA interactions (*270, 284*). RISC with ssRNA encounters target mRNA in a diffusion controlled mechanism(reviewed in (*285*)). The key nucleotides (2-8) also known as seed region from the 5'-end of guide strand contributes to mRNA recognition (*286*). The 5'-seed region hybridizes to target mRNA with propagation of duplex formation towards the 3'-end. The phosphate group between the 10^{th} and 11^{th} nucleotide in the duplex is positioned directly in the RNase H type fold of PIWI domain and is cleaved by Ago2 leaving products with a 5'-phosphate and 3'-hydroxyl group (*287, 288*). For miRNA, endogenous miRISC recognizes the 3'UTR of target mRNA and hybridizes in an imperfect manner forming bulge structure due to mismatches. Thus, mRNA cannot be cleaved by Ago2 and, interferes with gene expression by mediating translational repression by sequestering target mRNA in P-bodies (reviewed in (*289*)).

1.9.3.5 Dissociation from target mRNA (recycling)

RISC acts as a multiple-turnover complex and can direct many rounds of site-specific target mRNA cleavage (*277, 290*). For efficient RISC turnover, the degraded mRNA needs to be released and is generally held to be the rate-limiting step. In human cell extracts, ATP hydrolysis is essential to accelerate degraded mRNA release and thus, permitting RISC turnover, but this is not observed in recombinant RISC (*262, 291*).

In short, RNAi, a two-step mechanism has become an important tool for the gene knockdown study in a wide range of organisms. The key players in RNAi are two endoribonucleases Dicer-1 and Ago-2, and a siRNA. The first step involves degradation of

dsRNA into 21 to 25 nucleotides siRNAs by Dicer-1 activity followed by incorporation of siRNAs into an RNase complex, RISC containing Ago-2, which acts on the cognate mRNA and degrades it. At present, RNAi is not only used to analyze gene function but it is also giving a new shape to therapeutic gene silencing.

1.10 Context and Objectives of the Research: PARP-1, RNAi and Cell death

PARP-1, the founding member of PARP-1 family, is a multi-functional and abundant nuclear enzyme known to recognize DNA lesions and promote chromatin remodeling, DNA repair and many other cellular processes, such as transcriptional regulation and cell death (*31*). During apoptosis, caspase-3 mediated cleavage of PARP-1 abolishes the ability of PARP-1 to participate in DNA repair and promotes apoptosis. Studies using caspase-3-uncleavable PARP-1 suggest that PARP-1 cleavage and inactivation prevents energy depletion and facillitates the apoptosis (*157, 158*). Our laboratory has been examining implication of PARP-1 in both DNA repair (*130, 292*) and cell death responses to UV irradiation in mouse and cellular models. In the context of PARP-1 and UV-induced cell death, studies from our laboratory have shown that catalytic inhibition of PARP-1 reduces UVB-induced cell death in epidermis of SKH-1 mice (*226*). Also, it has been shown that PARP-1 fragments acquire dominant negative activity repressing the PARP-1 activity to facilitate UV-mediated apoptosis (*152, 154*); however, the exact molecular mechanism of UVB-induced cell death has not been elucidated. Thus, the first objective of my PhD was to understand the role of PARP-1 in cellular response to UVB in a cellular model in which PARP-1 was knocked down by DNA vector-based RNAi **(chapter 2)**. To delineate the role of PARP-1 cleavage and its catalytic inactivation in UVB-induced cell death, we also planned to use gene rescue models, i.e., reintroduced RNAi-resistant wild-type and caspase-uncleavable PARP-1 in PARP-1 knockdown model. In these PARP-1-depleted or PARP-1-rescued models we examined UVB-induced cell death response and demonstrated that PARP-1 cleavage promotes UVB-induced cell death.

Presently, RNAi is well-exploited as a reverse-genetic tool to silence the expression of genes and analyze their loss-of-function phenotype and gene function in different cellular processes including apoptosis (*293, 294*). Generally, dsRNA duplexes (21mer/27mer) are used for transient RNAi and plasmid/viral shRNA vectors are applied for stable RNAi of a gene. Like RNAi, apoptosis is also an evolutionarily conserved and tightly regulated process involving caspase-mediated cleavage of many key cellular proteins that are involved in different cellular processes such as, cell cycle, DNA replication, DNA repair etc (reviewed in (*295*)). However, it is not known whether RNAi

would continue to function normally during apoptosis. Therefore, it was pertinent to determine whether apoptosis can interfere with the integrity of RNAi core machinery and if yes, how it could affect the cell death studies. Thus, in the context of RNAi and cell death, the objectives were to perform a detailed characterization of stable and transient RNAi during cell death. We employed a DNA vector-based stable RNAi of various genes, including PARP-1 which was earlier established in our lab (*204*) to study the impact of apoptosis on stable RNAi **(Chapter 4)**. Though stable RNAi models are ideal for long term and stable knockdown, they take long to establish. Interestingly, some apoptosis studies use transient RNAi e.g., those using 21mer or 27mer dsRNA (*294*) or shRNA (*296*); thus, we further aimed to study the apoptotic fate of transient RNAi of an exogenous gene GFP and an endogenous gene PARP-1 **(Chapter 5).** In majority of the RNAi studies, knockdown status of protein is rarely verified after the onset of apoptosis. Based on our results, we also defined the limits and usefulness of RNAi as an approach to study functions of a gene during apoptosis.

Furthermore, in the context of PARP-1, we reviewed (i) using specific example of caspase-uncleavable PARP-1, how the caspase-uncleavable substrates, could be deployed as an important cellular biology tool to unravel the role of caspase-mediated cleavage of proteins not only in death but also in non-cell death functions **(Chapter 3)**; (ii) the different approaches to detect PARP-1 activation *in vivo, in vitro and in situ*. In this review, we highlighted on analysis of PAR as the earliest and a useful biological parameter providing direct proof of PARP-1 activation following DNA damage **(Annex I)**.

References:

Please note that cited references for chapter 1 and 6 are pooled at the end of chapter 6 (page no. 179).

Chapter 2: Role of Poly(ADP-ribose) polymerase-1 (PARP-1) in UVB-induced cell death in human skin fibroblasts

2.1 Résumé en français

En réponse aux dommages à l'ADN induits par les UVB, l'enzyme nucléaire poly(ADP-ribose) polymérase-1 (PARP-1) est connue pour jouer un rôle dans la mort cellulaire. Dans la présente étude, nous avons utilisé des fibroblastes humains exprimant PARP-1 ou ayant subi un «knockdown» de PARP-1 (PARP-1-KD) et observé que cette diminution de l'expression de PARP-1 confère aux cellules une résistance à la mort cellulaire induite par les UVB. Pour comprendre si l'activité catalytique de PARP-1 et son clivage par la caspase-3 peuvent altérer la mort cellulaire en réponse aux UVB, nous avons restauré l'expression de PARP-1 avec soit une PARP-1 sauvage soit une PARP-1 non-clivable par les caspases dans les fibroblastes PARP-1-KD. Dans ces cellules exprimant des mutants de PARP-1, nous avons analysé, en réponse aux UVB, la viabilité cellulaire, la clonogénicité et les marqueurs biochimiques de l'apoptose tels que le clivage de PARP-1 et l'activation de la caspase-3. Nos résultats indiquent que la résistance à la mort cellulaire induite par les UVB dans le modèle de PARP-1-KD peut être inversée par la ré-expression de PARP-1 sauvage mais pas de PARP-1 non-clivable par les caspases, suggérant un rôle facilitateur de l'activation ainsi que du clivage de PARP-1 dans la mort cellulaire induite par les UV.

2.2 Article

Role of Poly(ADP-ribose) polymerase-1 (PARP-1) in UVB-induced cell death

Febitha Kandan-Kulangara[1] and Girish M Shah[1*]

[1]Laboratory for Skin Cancer Research, Hospital Research Centre of Laval University (CHUL /CHUQ), Department of Molecular Biology, Medical Biochemistry & Pathology, Faculty of Medicine, Laval University, Quebec (Quebec), Canada.

***Correspondence**: Girish M. Shah, Ph.D.

Tel: (418) 656-4141/Ext. 48259

Fax: (418) 654-2739

E-mail: girish.shah@crchul.ulaval.ca

2.3 Abstract

In response to UV-induced DNA damage, the nuclear enzyme poly(ADP-ribose) polymerase-1 (PARP-1) is known to play a role in cell death. In the present study, we used PARP-1-replete and PARP-1-knockdown human skin fibroblasts to understand the role of PARP-1 in cellular response to UVB. In this model, we observed that PARP-1 knockdown confers resistance to UVB-induced cell death. To address, whether PARP-1 catalytic activity and caspase-3-mediated PARP-1 cleavage could alter the cell death in response to UVB, using a gene rescue method in PARP-1-knockdown fibroblasts, we restored the expression of PARP-1 with either wild-type or caspase-uncleavable PARP-1. In these PARP-1 mutants, we analyzed cell viability, clonogenicity and biochemical markers of apoptosis, such as PARP-1 cleavage and caspase-3-activation in response to UVB. Our results indicate that resistance to UVB-induced cell death in PARP-1 knockdown model could be rescued by wild-type PARP-1 but not by caspase-uncleavable PARP-1, suggesting a positive role of PARP-1 activation as well as PARP-1 cleavage in facilitating UVB-induced cell death.

2.4 Introduction

The ultraviolet (UV) components of sunlight are considered as major environmental factors deleterious to human health. At the molecular level, an UVB radiation causes two types of DNA damages: (i) the direct photolesions such as cyclobutane pyrimidine dimers (CPDs) and 6-4 photoproducts (6-4 PPs) which are repaired by nucleotide excision repair (NER); and (ii) reactive oxygen species (ROS)-induced DNA damage such as single strand breaks (SSBs) and 8-oxoguanine (8-oxoG), which are repaired by single strand break repair (SSBR) and base excision repair (BER) pathways (*1*). Since the catalytic activation of PARP-1 is implicated in DNA repair at lower levels of DNA damage and cell death at higher levels of DNA damage (*2*), our laboratory has been examining implication of PARP-1 in both DNA repair and cell death responses to UVB irradiation in mouse (*3*) and cellular models (*4-6*). The implication of PARP-1 in cellular response to UV radiation has been mainly examined at three levels to address following questions (i) Is PARP-1 activated in response to UV irradiation and if so what is the cause for this activation (ii) Is PARP-1 or its activation implicated in repair of UV-damaged DNA and (iii) Is PARP-1 over-activation after excessive DNA damage implicated in death of irradiated cells? While we have obtained a most definitive affirmative answer for the first question (*5*), the second and third questions have generated sufficient preliminary evidences and need additional work.

As for the activation of PARP-1 in response to UV, previous work from our laboratory has conclusively established the mechanism of activation of PARP-1 by different types of DNA damages induced by UVB (*5*). Additionally, data from our laboratory shows that PARP-inhibition blocks the removal of thymine dimers from UV-irradiated mouse skin or from UV-irradiated human skin fibroblasts (*4*). Overall, it is now increasingly recognized that PARP-1 plays a crucial part in repair of UV-induced damaged DNA by both BER and NER pathways.

However, the unrepaired UVB-induced DNA damages could induce cell death which is known to be mediated by multiple pathways, such as continuous presence of unrepaired UVB-induced DNA damage associated with mutated or deregulated p53 DNA

damage response, mitogen activated protein kinase (MAPK) pathway, activation of death receptors and by ROS generated within the cell (*7*).

PARP-1 activation has been linked to UVB-induced apoptosis in cultured cell as well as in mouse epidermis (*8, 9*). The inhibition of PARP with 3-aminobenzamide (3-ABA) in U937 leukemia cells has been reported to prevent apoptosis from low UVC dose but could not protect the cells from high levels of UVC dose (*8*). Additionally, on hairless mouse skin, the topical PARP inhibitor BGP-15M (O-(3-pyperidino-2-hydroxy-1-propyl) pyrimide-3-carbocylic acid amidoxime monohydrochloride) application prevents PARP-1 activation and protect skin from acute photodamage-induced by moderate UV doses (*9*) suggesting that at low levels of UV-induced DNA damage, PARP-inhibition has protective effect.

During apoptosis, PARP-1 is cleaved by caspase-3 and 7 to 89-kDa catalytic domain (CD) and 24-kDa DNA binding domain (DBD) (*10*). This cleavage eliminates PARP-1 activation in response to DNA damage, inhibiting its pro-survival or pro-DNA repair role, protecting the cells from ATP depletion and contributes to progression of apoptosis (*11*). In this regard, in HeLa cells, the overexpression of 24-kDa DBD of PARP-1 has been shown to stimulate UV-mediated apoptosis (*12*) and the 89-kDa C-terminal fragment interacts with intact PARP-1 and inhibits the homodimerization during apoptosis (*12*) suggesting cleavage of PARP-1 and inhibition of PARP-1 activity in maintaining the basal cellular energy required for the completion of apoptosis. Also, in Jurkat cells, ROS generated by UVB has been shown to be involved in mitochondrial permeabilization and caspase-independent AIF translocation (*13*).

Although the role for PARP-1 in UVB-induced cell death is known, the molecular mechanism by which PARP-1 activation leads to cell death needs more targeted studies. Potentially, the PARP-1 may play critical roles in interconnection between DNA damage mediated, ROS or MAPK pathway in response to UVB. In the present study, in human skin fibroblasts expressing wild type or caspase-uncleavable PARP-1, we have addressed the role of PARP-1 activation and its cleavage in UVB-induced cell death. We report that caspase-mediated PARP-1 cleavage is essential to facilitate UVB-induced cell death.

2.5 Materials and methods:

2.5.1 Plasmids. The p3X-Flag-CMV-7.1, a 4.7 kb expression vector, was provided by Sigma-Aldrich; Tet-Off expression system expressing caspase-uncleavable PARP-1 (pTRE-PARP-D^{214}/A) was obtained as described in (*14*); an eukaryotic expression vector pL15TK carrying the open reading frame of human PARP-1 (pPARP-31) was a kind donation of Jan-Heine Kupper.

2.5.2 Cells. The PARP-1-replete (GMU6) and PARP-1-depleted (GMSiP) cell lines (*15*) derived from human skin fibroblasts (GM637, Coriell Cell Repository) were cultured in a humidified incubator at 37°C in 5% CO_2 in α-MEM (GIBCO) supplemented with 2 mM L-glutamine, 10% fetal bovine serum, 50 Units/mL of penicillin, 50 µg/mL streptomycin (GIBCO); Hygromycin (200 µg/mL) was freshly added during the maintenance of GMU6 and GMSiP cells to keep selection pressure for U6 and SiP plasmid expression.

2.5.3 Construction of different PARP-1 DNA eukaryotic expression vectors.

A) Flag-PARP-1 DNA constructs. Flag-tagged expressing PARP-1 was obtained by cloning a human PARP-1 cDNA (3044bp) into BglII-SmaI site of p3X-FLAG CMV 7.1 containing N-terminal Flag sequence. This Flag-PARP-1-WT construct was used as parent plasmid to create Flag-PARP-1-D/A, the caspase-uncleavable PARP-1. The PARP-1 fragment containing D^{214}→A mutation was isolated from pTRE-PARP-1-D^{214}/A and was subcloned into AscI-EcoRV site of Flag-PARP-1-WT cDNA. The in-frame insertions of wild type and mutant PARP-1 cDNA with FLAG-tag were confirmed by DNA sequencing.

B) RNAi-resistant Flag-PARP-1 DNA constructs. The p3X-Flag-PARP-1-WT and p3X-Flag-PARP-1-D^{214}/A were used to generate PARP-1-siRNA resistant clones. The resistance-conferring silent mutation was introduced in the 21mer RNAi target sequence (5' GGCAAGCACAGTGTCAAAGGT 3') of PARP-1 cDNA with the use of two 21-base complementary oligonucleotides 5' GC AAG TTA CCC AAG GGG AAG CAC TCC GTC AAG GGT TTG GGC AAA AC 3' and 5' GT TTT GCC CAA ACC CTT GAC GGA GTG CTT CCC CTT GGG TAA CTT GC 3'. Mutagenesis was performed by use of a QuikChange XL Site-Directed Mutagenesis Kit (Stratagene) as per manufacturer's protocol. The underlined nucleotide sequences were changed to G, TCC and G

respectively. The resulting plasmid was designated FL-PARPRSiP-WT (or GMRSiP-WT) and FL-PARPRSiP-D^{214}/A (or GMRSiP-D/A) in which RSiP refers to PARP-1 that is resistant to siRNA of PARP-1. The introduction of the mutation was also confirmed by sequencing.

2.5.4 Transfection. To establish stable cell lines expressing RSiP-PARP-1 mutants i.e., wild-type and caspase-uncleavable PARP-1, GMSiP cells were used (*15*). Sub-confluent GMSiP cells were cultured in 10-cm dishes and were transfected with 9 μg of PARP-1 plasmids (GMRSiP-WT or GMRSiP-D/A) by use of Lipofectamine (LPF, Invitrogen) as per instructor's protocol. For positive selection of clones all cells were co-transfected with 1 μg of pcDNA3.1/neo plasmid and clones were selected with 800 μg/mL of geneticin (G418). The PARP-1-mutants expressing clones were maintained in medium containing 200 μg/mL hygromycin and 400 μg/mL geneticin. To minimize clone specific effects, at least 2-3 clones for each PARP-1 phenotype were selected.

2.5.5 Polymer induction and apoptosis. For induction of apoptosis, sub-confluent cells were left untreated or treated with 100 μM of etoposide (VP16) for 16 h. Post treatment cells were harvested and extracts equivalent to 20 μg were resolved on 8% and 12% SDS-PAGE, blotted on nitrocellulose, stained with Ponceau-S and subsequently probed with monoclonal anti-PARP C-2-10 (Aparptosis, 1:10,000) and monoclonal anti-Flag (Sigma, 1:5,000). For polymer (pADPr) induction, briefly, cells were washed with PBS, exposed to 300 μM H_2O_2 in PBS for 7 minutes and harvested for analysis by immunoblot to detect polymer by monoclonal anti-pADPr 10H antibody (1:500).

2.5.6 Viability and Clonogenicity. For viability, cells were plated into 35-mm dishes and were irradiated at 80% confluency with indicated dose of UVB. UVC wavelengths were filtered out using 0.0127 cm film of Kodacel under a layer of dyeless serum-free medium in spectrolinker XL-1500 (*5*). UV flux was measured using UVX digital radiometer equipped with a probe for UVB. Treated cells were incubated at 37°C for indicated time. Then the cells were trypsinized and the viable cells were counted based on their ability to exclude trypan blue dye. Similarly, the cells were treated with UVB for protein extract preparation and analyzed for PARP-1, cleaved caspase-3 and β-actin. For clonogenicity, cells were treated as mentioned above in duplicates and were incubated at 37°C for 3 h. After the

incubation, treated cells were washed with PBS and seeded in triplicate into 6-well cluster (500 cells per well). Cells were then incubated at 37°C and monitored for colony formation. After 10-15 days, cells were rinsed in PBS, fixed in 10% methanol and stained with 0.5% crystal violet. An aggregate of >30 cells was scored as a colony.

2.5.7 Flow cytometry analysis. For FACS analysis, cells were treated with 800 J/m^2 UVB as mentioned above. Following treatment, cells were harvested by trypsinization, and suspended in ice cold PBS at a density of ~1 × 10^6 cells/mL. For every 1mL of suspension, 1 µL YO-PRO-1 stock solution (Vybrant® Apoptosis Assay kit, Molecular probes) was added and the cells were incubated on ice for 30 minutes. Just before the analysis, PI at a concentration of 10 µg/mL was added and cells were analyzed by FACS (BD FACScanto II).

2.5.8 Statistical Analysis:

Cell viability and clonogenicity data were analyzed using GraphPad PRISM software (version 5.01). 2way ANOVA test was performed to determine statistical significance between PARP-1 mutants. Data are presented as mean ± SEM. Results were considered statistically significant when $p < 0.001$; *p-value<0.05, **p-value<0.01 and ***p-value<0.001.

2.6 Results

2.6.1 Characterization of clones expressing RNAi-resistant wild-type and caspase-uncleavable PARP-1

Our lab has established a PARP-1 knockdown cellular model by DNA vector-based RNAi (*15*) which has been used to study the role of PARP-1 in different cellular processes such as DNA repair (*6*), carcinogenesis (*16, 17*), gene expression and cell death (*18*).

To definitively exclude the possibility that the phenotype observed after RNAi-mediated knockdown of any gene is a non-specific or off-target effect, it is important to demonstrate that the phenotype of the wild type can be rescued by introduction of the target gene in a form refractory to RNAi. To achieve this in PARP-1 knockdown model, in an eukaryotic N-terminal FLAG expression vector, we cloned the cDNA of human PARP-1 that was modified in the siRNA-21 bp target sequence (**Fig. 2.1**), such that, while nucleotide sequence is altered to make it refractory to RNAi, the amino acid sequence coded by the altered sequence remained the same as in wild type PARP-1. The mRNA created from the wild type PARP-1 would continue to be cleaved by RNAi, while the mutant mRNA would be spared from destruction by RNAi and cells would be rescued with a fully functional PARP-1, which has the same amino acid sequence as the normal PARP-1. To generate a RNAi-resistant and caspase-3-uncleavable PARP-1, we further carried out appropriate change in the nucleotide sequence by site-directed mutagenesis of the cDNA of RNAi-resistant PARP-1, such that the expressed protein is not only resistant to RNAi but also has an amino acid substitution $D^{214} \rightarrow A$ described earlier (*14*) (**Fig. 2.1**). Both the RNAi-resistant PARP-1 vectors were transfected individually in GMSiP cells, which was depleted of endogenous PARP-1, to obtain stable clones expressing PARP-1 mutants.

To characterize the PARP-1 mutant cell lines, we examined the expression (**Fig. 2.2A)** and the catalytic activity of PARP-1 (**Fig. 2.2B**) in response to DNA damage. In GMSiP (**Fig. 2.2A, lane 3**) where endogenous PARP-1 was knockdown by RNAi, upon introduction of RNAi-resistant PARP-1 vectors, we can observe the expression of wild type PARP-1 (**Fig. 2.2A, lane 5**) and caspase-uncleavable PARP-1 (**Fig. 2.2A, lane 7**) in GMRSiP-WT and GMRSiP-D/A fibroblasts, respectively. We observed that expressed

PARP-1 in these fibroblasts co-migrate with endogenous PARP-1 in GMU6 (**Fig. 2.2A, lane 1**). In GMU6 treated with VP16 (**Fig 2.2A, lane 2**), PARP-1 is cleaved to 89-kDa, which could be detected by PARP-1 antibody that detects both full length PARP-1 (113-kDa) and 89-kDa PARP-1 fragment. We did not observe PARP-1 fragment in VP16-treated GMSiP (**Fig. 2.2A, lane 4**) confirming that PARP-1 knockdown is functional. In GMRSiP-WT since the Flag epitope is tagged at N-terminal, the 24-kDa PARP-1 fragment and the full length PARP-1 can also be probed by a Flag antibody (**Fig. 2.2A, lane 6**, Flag probing). However, in GMRSiP-D/A, PARP-1 remains uncleaved (**Fig. 2.2A, lane 8**) as it can be seen from PARP-1 and Flag probing. These clones were also tested for the catalytic activity of PARP-1 after treatment with DNA damaging agent. In response to H_2O_2 we detected polymers of ADP-ribose (pADPr) as probed by polymer (10H) specific antibody in GMU6 (**Fig. 2.2B, lane 2**) and cells expressing wild type PARP-1 (**Fig. 2.2B, lane 6**) and caspase-uncleavable PARP-1 (**Fig. 2.2B, lane 8**), suggesting that the introduced PARP-1 is enzymatically functional.

2.6.2 PARP-1 cleavage facilitates UVB-induced cell death

To understand whether depletion of PARP-1 affects viability of cells in response to UVB, we exposed PARP-1 mutants, GMU6 and GMSiP from 0 to 800 J/m^2 of UVB for 48 h and assessed the cell viability using trypan blue exclusion assay (**Fig. 2.3A**). At 48 h after exposure to sub-lethal dose of UVB (100 J/m^2), we observed no difference in cell viability between GMU6 and GMSiP. However, with increasing dose of UVB (>200 J/m^2), in GMU6 we observed a rapid loss of cell viability in comparison to GMSiP. Statistical significance was found between GMU6 and GMSiP at 200 J/m^2 ($p<0.001$) and at 800 J/m^2 ($p<0.01$) dose of UVB. The measured IC_{50} values for GMU6 was 380 J/m^2 and for GMSiP it was 700 J/m^2 at 48 h post UVB, suggesting a significant resistance to UVB-induced cell death in the absence of PARP-1.

Next, we examined whether reintroduction of wild-type PARP-1 or uncleavable PARP-1 in GMSiP cells will sensitize these cells to higher dose of UVB (800 J/m^2) to the same level as it was seen for GMU6 (**Fig 2.3B**). As determined by viability at 48 h post UVB (800 J/m^2), GMRSiP-WT showed loss of cell viability ($p<0.01$ between GMU6 and GMRSiP-WT), indicating that restoration of wild type PARP-1 in GMSiP cell lines could

rescue the phenotype to some extent to GMU6 ($p<0.001$ between GMSiP and both GMU6 or GMRSiP-WT); however, cells expressing caspase-uncleavable PARP-1 showed delay in loss of cell viability in comparison to GMU6 ($p<0.001$ between GMU6 and GMRSiP-D/A) suggesting that PARP-1 cleavage facilitates UVB-induced cell death.

2.6.3 Delayed UVB-induced cell death in cells expressing caspase-uncleavable PARP-1

Next, we examined the UVB-induced cell death in PARP-1 mutants by flow cytometry analysis performed by YO-PRO/PI staining. YO-PRO is taken up differently by viable, apoptotic, or necrotic cells due to differences in the permeability of their plasma membrane. Propidium iodide (PI), a nuclear stain does not stain live or early apoptotic cells due to the presence of an intact plasma membrane, whereas in late apoptotic and necrotic cells, the integrity of the plasma and nuclear membranes decreases, allowing PI to pass through the membranes and intercalate into nucleic acids thus, displaying its fluorescence. The percentage of cells in different quadrants are represented as viable ($YO\text{-}PRO^{-}/PI^{-}$), early apoptosis ($YO\text{-}PRO^{+}/PI^{-}$), late apoptosis/early necrosis ($YO\text{-}PRO^{+}/PI^{+}$) and necrosis ($YO\text{-}PRO^{-}/PI^{+}$).

Following treatment with UVB at 800 J/m^2, PARP-1 mutants were analyzed by YO-PRO/PI staining from 12 h to 48 h (**Fig. 2.4A**). In a time dependent manner from 12 h to 48 h, UVB-treated GMU6 cells showed a significant reduction in the number of viable cells from 49% to 18% as compared to GMSiP (75% to 42%), suggesting a delayed cell death in the absence of PARP-1. In GMRSiP-WT, in response to UVB from 12 h to 48 h, the cell viability is lost from 45% to 13%, a YO/PRO staining profile similar to GMU6, suggesting that rescue of wild type PARP-1 restores the cell death phenotype and PARP-1 facilitates UVB-induced cell death. In contrast, in GMRSiP-D/A, viable cells reduced from 80% to only 45% from 12 h to 48 h in response to UVB. At 48 h post-UVB, late apoptotic/early necrotic cells accounted for the majority of the non-viable cell population in GMU6 and GMRSiP-WT (60–67%) while GMSiP and GMRSiP-D/A accounted only for (40-43%) late apoptotic/early necrotic cells, suggesting a delayed apoptotic response in GMSiP and GMRSiP-D/A cells.

To confirm that the doses administered to cells induced apoptosis, we immunoblotted the whole cell extracts of these cell lines before and after UVB (800 J/m^2) irradiation for apoptotic signature fragments of wild-type PARP-1 and cleaved or activated form of caspase-3 (**Fig. 2.4B**). In GMU6 and GMRSiP-WT, the caspase-activation had begun as early as 12 h and wild type PARP-1 was cleaved to 89-kDa fragment by 48 h. While in GMSiP and GMRSiP-D/A, caspase-activation began as late as at 24 h. As expected, despite the activation of caspase-3, the mutant caspase-uncleavable PARP-1 remained intact in GMRSiP-D/A and suggest a delayed induction of apoptosis in GMSiP and GMRSiP-D/A.

2.6.4 Clonogenic survival of PARP-1 mutants in response to UVB

We compared the clonogenic survival of PARP-1 expressing mutants in response to UVB (**Fig. 2.5**). After exposure to a sub-lethal dose of UVB (200 J/m^2) as reported earlier (*6*), GMSiP cells had a lower clonogenic survival (65%) in comparison to GMU6 (91%). Interestingly, at this dose of UVB (200 J/m2), GMRSiP-WT and GMRSiP-D/A showed a significantly improved clonogenicity (80%) in comparison to GMSiP ($p<0.001$). A slight statistically significant difference in clonogenicity between GMU6 and GMRSiP-WT or GMRSiP-D/A was observed ($p<0.05$). However, at higher dose of UVB (600 J/m^2), none of the cells with different PARP-1 phenotypes retained clonogenicity.

In summary, our results show that resistance to UVB-induced cell death phenotype in PARP-1 knockdown cells could be rescued by wild type PARP-1, but not by caspase-uncleavable PARP-1. Also, the cells expressing uncleavable PARP-1 showed a short-term delay in the onset of apoptosis, but conferred long term protection only at low levels of UVB-induced DNA damage.

2.7 Discussion

PARP-1 activation is one of the major responses to UVB-induced DNA damage (*5*). In the present study, using a series of skin fibroblasts with or without wild type or caspase-uncleavable PARP-1, we have addressed whether the PARP-1 activation and cleavage play an active role in regulation of UVB-induced cell death. As compared to PARP-1-replete (GMU6) cells, in our PARP-1 knockdown (GMSiP) model, we saw a delayed induction of apoptosis in response to UVB, as measured by delay in loss of cell viability and late caspase-3-activation. However, this phenotype could be reverted upon introduction of wild type PARP-1 in GMSiP model indicating that PARP-1 does influence apoptosis in response to UVB. The professed role of PARP-1 in UVB-induced apoptosis could be due to an early and transient burst of poly(ADP-ribosyl)ation prior to caspase-3 mediated cleavage of PARP-1 as reported by Simbulan-Rosenthal *et al. (19)*. They showed an early burst of poly(ADP-ribosyl)ation of nuclear proteins during anti Fas or cycloheximide-induced apoptosis in many cells including PARP-$1^{+/+}$ mouse embryonic fibroblasts (MEFs), whereas no induction of apoptosis was observed in PARP-1-depleted 3T3-L1 antisense cells or Jurkat cells and PARP-$1^{-/-}$ MEFs, implicating poly(ADP-ribosyl)ation and subsequent PARP-1 cleavage to prevent depletion of NAD^+/ATP or release of certain nuclear proteins from poly(ADP-ribosyl)ation-induced inhibition, thus, facilitating cell death. The other reason could be the trans-dominant inhibition of PARP-1 activity due to the liberated PARP-1-DBD in response to UVB-induced cell death. It is reported that the overexpression of 24-kDa PARP-1-DBD fragment produces a dominant negative effect as it irreversibly binds to DNA strand breaks and inhibit the activity of intact PARP-1 thereby reducing the PARP-1 mediated NAD^+/ATP depletion and promoting apoptosis (*20*). In addition, in HeLa cells, the overexpression of 24-kDa DBD or 89-kDa CD fragment of PARP-1 has been shown to stimulate UV-mediated apoptosis (*12, 21*) suggesting that cleavage of PARP-1 and catalytic inactivation stimulates apoptosis by maintaining ATP levels.

To understand whether PARP-1 cleavage is important to facilitate cell death, we compared GMU6 with cells expressing caspase-uncleavable PARP-1 (GMRSiP-D/A) in response to UVB. In response to various death-inducing stimuli, including DNA damaging

agent such as N-methyl-N'-nitro-N-nitrosoguanidine (MNNG), Staurosporine (STS) or non-DNA damaging agent like Tumor Necrosis Factor (TNF) family receptors such as CD95 or Fas, TNFα, cells expressing uncleavable PARP-1 showed varied responses such as survival and proliferation (*14*), delayed apoptosis (*22*), or increased apoptosis (*23, 24*) accompanied with increased necrosis (*24*). In our model, GMRSiP-D/A displayed a delayed induction of apoptosis as compared to GMU6. First, the probable reason could be, due to the persistence of PARP-1 activity owing to uncleavable nature of PARP-1, which could allow PARP-1 to participate in DNA repair. In this regard, recently we showed that in response to UV, catalytic activation of PARP-1 is required for the efficient lesion recognition by DDB2 in GG-NER (*4*). Secondly, there could be a possible delay in the progression of apoptosis due to continuous poly(ADP-ribosyl)ation of pro-apoptotic substrates thereby inactivating the pro-apoptotic factors. However this hypothesis needs to be validated with further experiments. Additionally, as seen in clonogenicity data, in GMRSiP-D/A the long term protective effect was seen only at low levels of UVB doses, indicating that in response to high dose of UVB initially there could be an advantage for DNA repair, however, when the DNA damages are beyond repair, the massive depletion of NAD^+/ATP owing to uncleavable nature of PARP-1 will alter the balance to cell death.

In conclusion, in our model, caspase-mediated PARP-1 cleavage facilitates UVB-induced cell death, whereas, the catalytic function of uncleavable PARP-1 could serve a possible advantage for the DNA repair for significant amount of time before commitment to cell death. Altogether, our data from PARP-1 mutants clearly indicates that PARP-1 activation and PARP-1 cleavage are essential for UVB-induced cell death. Nevertheless, the role of catalytic activity of PARP-1 and its cleavage in cell death needs to be analyzed separately using PARP-1 inhibitors, caspase-inhibitors or using catalytically inactive PARP-1 in PARP-1 knockdown model.

2.8 Acknowledgement

This work was supported by the National Cancer Institute of Canada (CCS grant # 016407) with funding from the Canadian Cancer Society. FKK was recipient of the graduate scholarship award from the Natural Sciences & Engineering Research Council of Canada.

2.9 References

1. Vodenicharov, M. D., and Shah, G. M. (2005) Nuclear and non-nuclear signals leading to UV-induced apoptosis, in *From DNA photolesions to mutations, skin cancer and cell death* (Sage, E., Drouin, R., and Rouabhia, M., Eds.), pp 247-267, RSC Elsevier, New York.
2. Le Rhun, Y., Kirkland, J. B., and Shah, G. M. (1998) Cellular responses to DNA damage in the absence of Poly(ADP-ribose) polymerase, *Biochem Biophys Res Commun 245*, 1-10.
3. Brind'Amour, J. (2005) Role of poly(ADP-ribose) polymerase-1 (PARP-1) in cellular response to UVB in SKH-1 mice epidermis, in *Mémoire de maîtrise*, p 125, Université Laval, Québec.
4. Robu, M., Shah, R. G., Petitclerc, N., Brind'amour, J., Kandan-Kulangara, F., and Shah, G. M. (2013) Role of poly(ADP-ribose) polymerase-1 in the removal of UV-induced DNA lesions by nucleotide excision repair, *Proc Natl Acad Sci U S A 110*, 1658-1663.
5. Vodenicharov, M. D., Ghodgaonkar, M. M., Halappanavar, S. S., Shah, R. G., and Shah, G. M. (2005) Mechanism of early biphasic activation of poly(ADP-ribose) polymerase-1 in response to ultraviolet B radiation, *J Cell Sci 118*, 589-599.
6. Ghodgaonkar, M. M., Zacal, N., Kassam, S., Rainbow, A. J., and Shah, G. M. (2008) Depletion of poly(ADP-ribose) polymerase-1 reduces host cell reactivation of a UV-damaged adenovirus-encoded reporter gene in human dermal fibroblasts, *DNA Repair (Amst) 7*, 617-632.
7. Kulms, D., and Schwarz, T. (2002) Independent contribution of three different pathways to ultraviolet-B-induced apoptosis, *Biochem Pharmacol 64*, 837-841.
8. Mi, Y., Thomas, S. D., Xu, X., Casson, L. K., Miller, D. M., and Bates, P. J. (2003) Apoptosis in leukemia cells is accompanied by alterations in the levels and localization of nucleolin, *J Biol Chem 278*, 8572-8579.
9. Farkas, B., Magyarlaki, M., Csete, B., Nemeth, J., Rabloczky, G., Bernath, S., Literati Nagy, P., and Sumegi, B. (2002) Reduction of acute photodamage in skin by topical application of a novel PARP inhibitor, *Biochem Pharmacol 63*, 921-932.
10. Kaufmann, S. H., Desnoyers, S., Ottaviano, Y., Davidson, N. E., and Poirier, G. G. (1993) Specific proteolytic cleavage of poly(ADP-ribose) polymerase: an early marker of chemotherapy-induced apoptosis, *Cancer Res 53*, 3976-3985.
11. Soldani, C., and Scovassi, A. I. (2002) Poly(ADP-ribose) polymerase-1 cleavage during apoptosis: an update, *Apoptosis 7*, 321-328.
12. Kim, J. W., Won, J., Sohn, S., and Joe, C. O. (2000) DNA-binding activity of the N-terminal cleavage product of poly(ADP-ribose) polymerase is required for UV mediated apoptosis, *J Cell Sci 113 (Pt 6)*, 955-961.
13. Murahashi, H., Azuma, H., Zamzami, N., Furuya, K. J., Ikebuchi, K., Yamaguchi, M., Yamada, Y., Sato, N., Fujihara, M., Kroemer, G., and Ikeda, H. (2003) Possible contribution of apoptosis-inducing factor (AIF) and reactive oxygen species (ROS) to UVB-induced caspase-independent cell death in the T cell line Jurkat, *J Leukoc Biol 73*, 399-406.
14. Halappanavar, S. S., Rhun, Y. L., Mounir, S., Martins, L. M., Huot, J., Earnshaw, W. C., and Shah, G. M. (1999) Survival and proliferation of cells expressing caspase-uncleavable Poly(ADP-ribose) polymerase in response to death-inducing DNA damage by an alkylating agent, *J Biol Chem 274*, 37097-37104.
15. Shah, R. G., Ghodgaonkar, M. M., Affar el, B., and Shah, G. M. (2005) DNA vector-based RNAi approach for stable depletion of poly(ADP-ribose) polymerase-1, *Biochem Biophys Res Commun 331*, 167-174.

16. Tentori, L., Muzi, A., Dorio, A. S., Bultrini, S., Mazzon, E., Lacal, P. M., Shah, G. M., Zhang, J., Navarra, P., Nocentini, G., Cuzzocrea, S., and Graziani, G. (2008) Stable depletion of poly (ADP-ribose) polymerase-1 reduces in vivo melanoma growth and increases chemosensitivity, *Eur J Cancer 44*, 1302-1314.
17. Tentori, L., Muzi, A., Dorio, A. S., Scarsella, M., Leonetti, C., Shah, G. M., Xu, W., Camaioni, E., Gold, B., Pellicciari, R., Dantzer, F., Zhang, J., and Graziani, G. (2010) Pharmacological inhibition of poly(ADP-ribose) polymerase (PARP) activity in PARP-1 silenced tumour cells increases chemosensitivity to temozolomide and to a N3-adenine selective methylating agent, *Curr Cancer Drug Targets 10*, 368-383.
18. Nusinow, D. A., Hernandez-Munoz, I., Fazzio, T. G., Shah, G. M., Kraus, W. L., and Panning, B. (2007) Poly(ADP-ribose) polymerase 1 is inhibited by a histone H2A variant, MacroH2A, and contributes to silencing of the inactive X chromosome, *J Biol Chem 282*, 12851-12859.
19. Simbulan-Rosenthal, C. M., Rosenthal, D. S., Iyer, S., Boulares, A. H., and Smulson, M. E. (1998) Transient poly(ADP-ribosyl)ation of nuclear proteins and role of poly(ADP-ribose) polymerase in the early stages of apoptosis, *J Biol Chem 273*, 13703-13712.
20. D'Amours, D., Sallmann, F. R., Dixit, V. M., and Poirier, G. G. (2001) Gain-of-function of poly(ADP-ribose) polymerase-1 upon cleavage by apoptotic proteases: implications for apoptosis, *J Cell Sci 114*, 3771-3778.
21. Kim, J. W., Kim, K., Kang, K., and Joe, C. O. (2000) Inhibition of homodimerization of poly(ADP-ribose) polymerase by its C-terminal cleavage products produced during apoptosis, *J Biol Chem 275*, 8121-8125.
22. Oliver, F. J., de la Rubia, G., Rolli, V., Ruiz-Ruiz, M. C., de Murcia, G., and Murcia, J. M. (1998) Importance of poly(ADP-ribose) polymerase and its cleavage in apoptosis. Lesson from an uncleavable mutant, *J Biol Chem 273*, 33533-33539.
23. Boulares, A. H., Yakovlev, A. G., Ivanova, V., Stoica, B. A., Wang, G., Iyer, S., and Smulson, M. (1999) Role of poly(ADP-ribose) polymerase (PARP) cleavage in apoptosis. Caspase 3-resistant PARP mutant increases rates of apoptosis in transfected cells, *J Biol Chem 274*, 22932-22940.
24. Herceg, Z., and Wang, Z. Q. (1999) Failure of poly(ADP-ribose) polymerase cleavage by caspases leads to induction of necrosis and enhanced apoptosis, *Mol Cell Biol 19*, 5124-5133.

2.10 Legends to Figures

Fig. 2.1: Schematic representation of PARP-1 and RNAi-resistant wild-type and caspase-uncleavable PARP-1 vectors. PARP-1 contains three major domains: a DNA-binding domain containing three zinc fingers and nuclear localization signal (NLS), an automodification domain, and a catalytic domain. Cleavage of wild-type PARP-1 at $DEVD^{214}$ by caspase-3 generates fragments of 24 and 89-kDa. With the use of site-directed mutagenesis, Aspartate (Asp^{214} or D^{214}) was replaced by Alanine (A) to generate a caspase-3-uncleavable PARP-1 mutant. SiP represents the 21 bp RNAi target sequence in PARP-1 cDNA that is targeted for knockdown by 21mer (siRNA) of PARP-1. RSiP represents the resistance-conferring silent mutations (underlined) which were introduced in the 21mer RNAi target sequence of PARP-1 cDNA to make PARP-1 mRNA refractory to siRNA.

Figure 2.2: Characterization of RNAi-resistant PARP-1 mutants. (A) Immunoblot of the cells expressing PARP-1 mutants. Control and VP16 (100 μM/16 h) treated PARP-1 mutant cells were harvested and subjected to immunoblot analyses with antibodies to PARP-1 (top panel) and Flag (middle panel). (B) Catalytic activity of PARP-1 mutants in response to 300 μM H_2O_2. Control and H_2O_2-treated PARP-1 mutants were harvested and subjected to immunoblot analyses with antibodies to polymer (10H) (top panel) and PARP-1 (middle panel). Equal protein loading was verified by Ponceau-S staining (A and B; bottom panel).

Figure 2.3: UVB response of PARP-1 mutants (A) UVB dose response for GMU6 and GMSiP. PARP-1 mutants GMU6, and GMSiP cells were irradiated with different doses of UVB for 48 h and viability by trypan blue exclusion was measured. Data are represented as the mean ± SE obtained from two different experiments; cell counts were made in triplicate for each sample. (n= 6), ***p-value<0.001 and **p-value<0.01. **(B) Time course of UVB-induced cell death in cells expressing PARP-1 mutants.** PARP-1 mutants GMU6, GMSiP, GMRSiP-WT and GMRSiP-D/A cells were irradiated with 800 J/m^2 of UVB for 12-48 h and at each time point viability was measured by trypan blue exclusion assay. Data are represented as the mean ± SE obtained from two different experiments; cell counts were made in triplicates for each sample. (n= 6), ***p-value<0.001 and **p-value<0.01.

Figure 2.4: Cell Death Analysis (A) Flow cytometry analysis of UVB-induced cell death. PARP-1 mutants GMU6, GMSiP, GMRSiP-WT and GMRSiP-D/A were irradiated with 800 J/m^2 of UVB for 12-48 h. At each time point cells were stained with YO-PRO/PI and then processed for flow cytometry analysis. Cell percentages represents viable (YO-PRO$^-$/PI$^-$), early apoptosis (YO-PRO$^+$/PI$^-$), late apoptosis/early necrosis (YO-PRO$^+$/PI$^+$) and necrosis (YO-PRO$^-$/PI$^+$) for UVB-treated PARP-1 mutants. Results shown are one representative of two individual experiments **(B) Time course of PARP-1 cleavage and caspase-3-activation in UVB-treated PARP-1 mutants.** PARP-1 mutants GMU6, GMSiP, GMRSiP-WT and GMRSiP-D/A cells were irradiated with 800 J/m^2 of UVB for the indicated times and whole cell extracts were prepared. Cell extracts were subjected to immunoblot analysis with antibodies to PARP-1 and cleaved caspase-3. Actin was used as loading control. The antibody to PARP-1 (C-2-10) recognizes both the full-length PARP-1 (113-kDa) and 89-kDa PARP-1 fragment. The cleaved caspase-3 antibody recognizes both p19 and p17 subunit of caspase-3.

Figure 2.5: Clonogenicity of cells expressing PARP-1 mutants in response to UVB. PARP-1 mutants GMU6, GMSiP, GMRSiP-WT and GMRSiP-D/A cells were irradiated with indicated dose of UVB. After 3 h incubation at 37°C, UVB-treated cells were seeded in triplicate into 6-well cluster (500 cells per well) and were monitored for colony formation. An aggregate of >30 cells was scored as a colony. Colony forming ability is expressed as percentage of control and was derived from 6 observations obtained in each of the two separate sets of experiments. (n=6), *p-value<0.05, **p-value<0.01 and ***p-value<0.001.

2.11 Figures

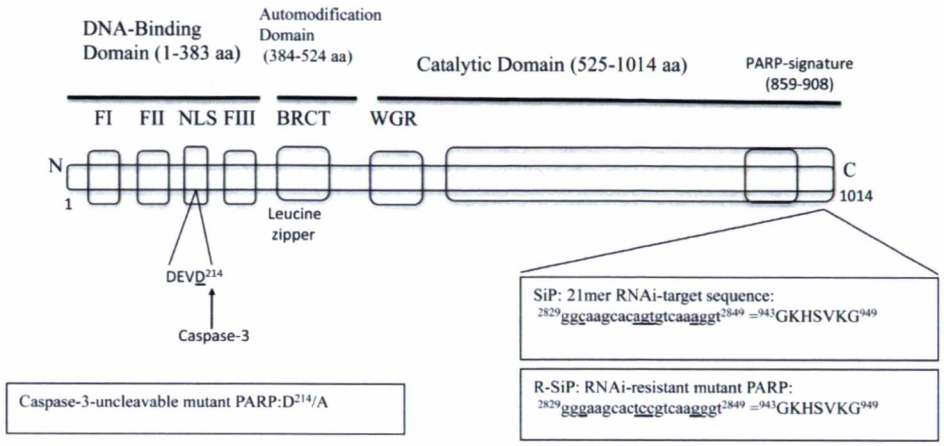

Figure 2.1: Schematic representation of PARP-1 and RNAi-resistant wild type and caspase-uncleavable PARP-1 vectors.

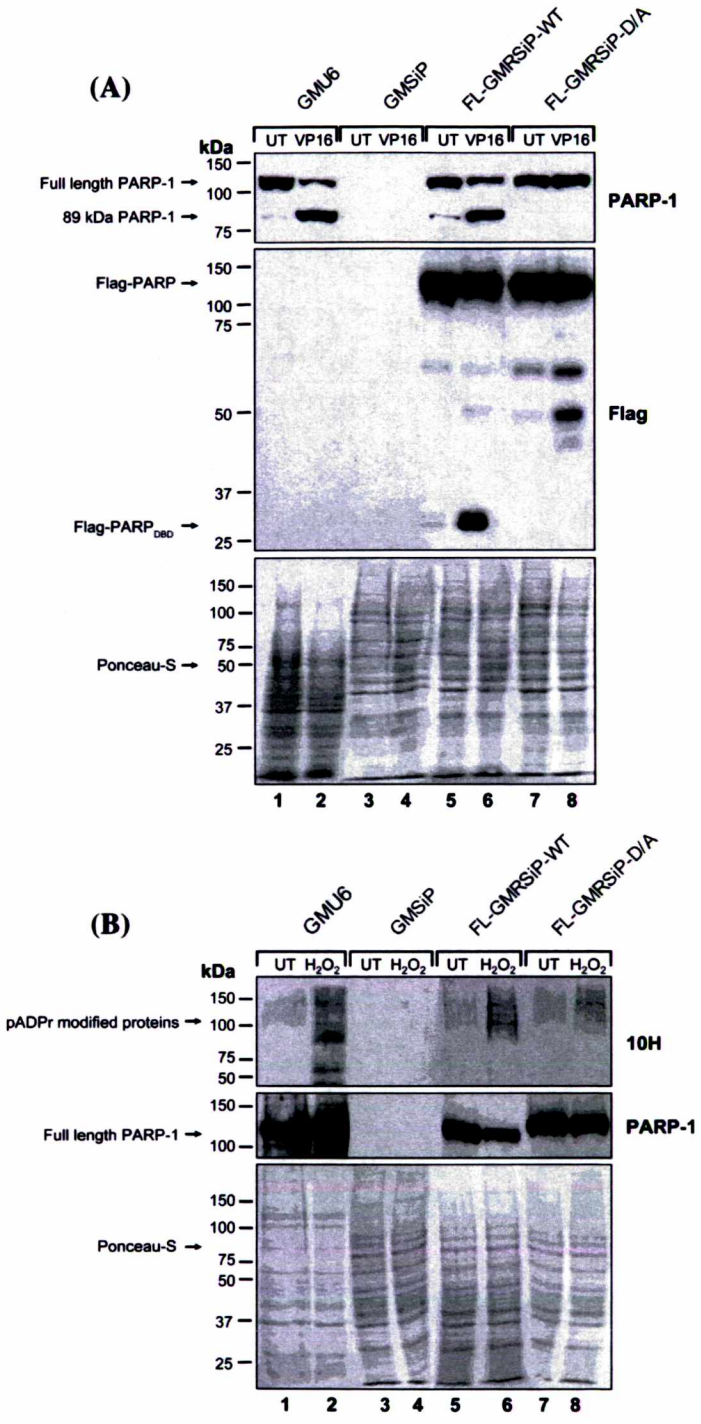

Figure 2.2: Characterization of RNAi-resistant PARP-1 mutants.

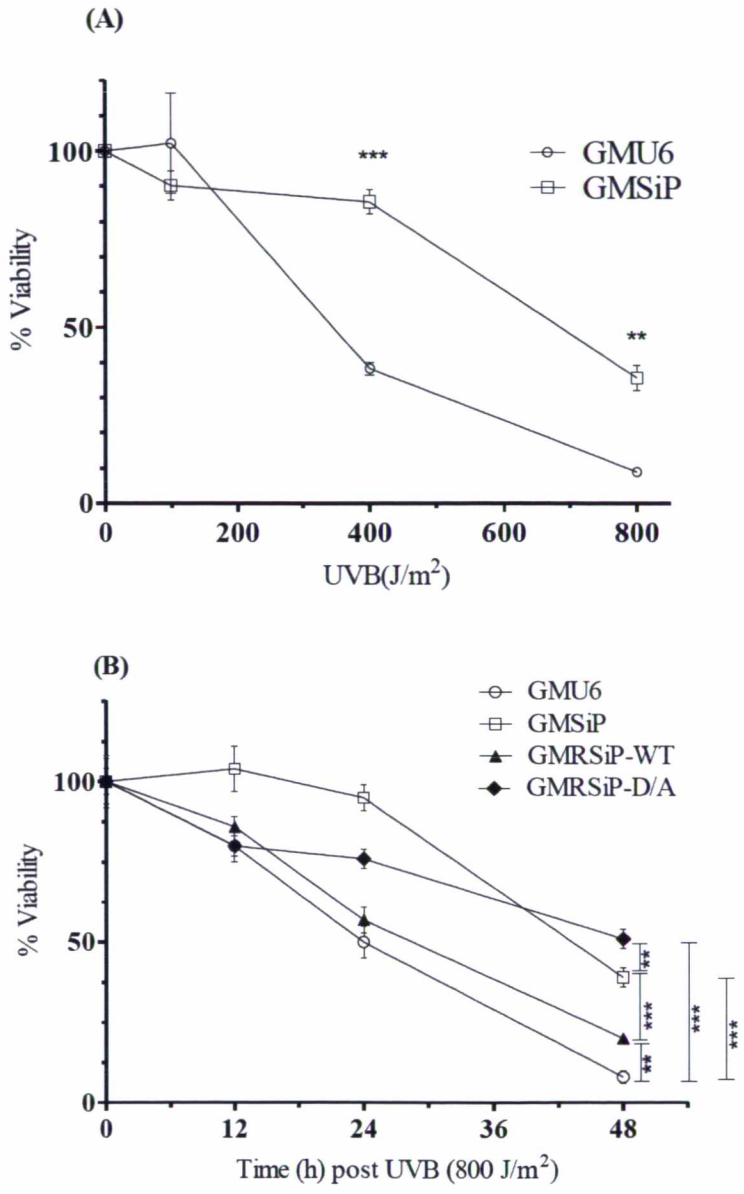

Figure 2.3: UVB response of PARP-1 mutants (A) UVB dose response in GMU6 and GMSiP cells. (B) Time course of UVB-induced cell death in cells expressing PARP-1 mutants.

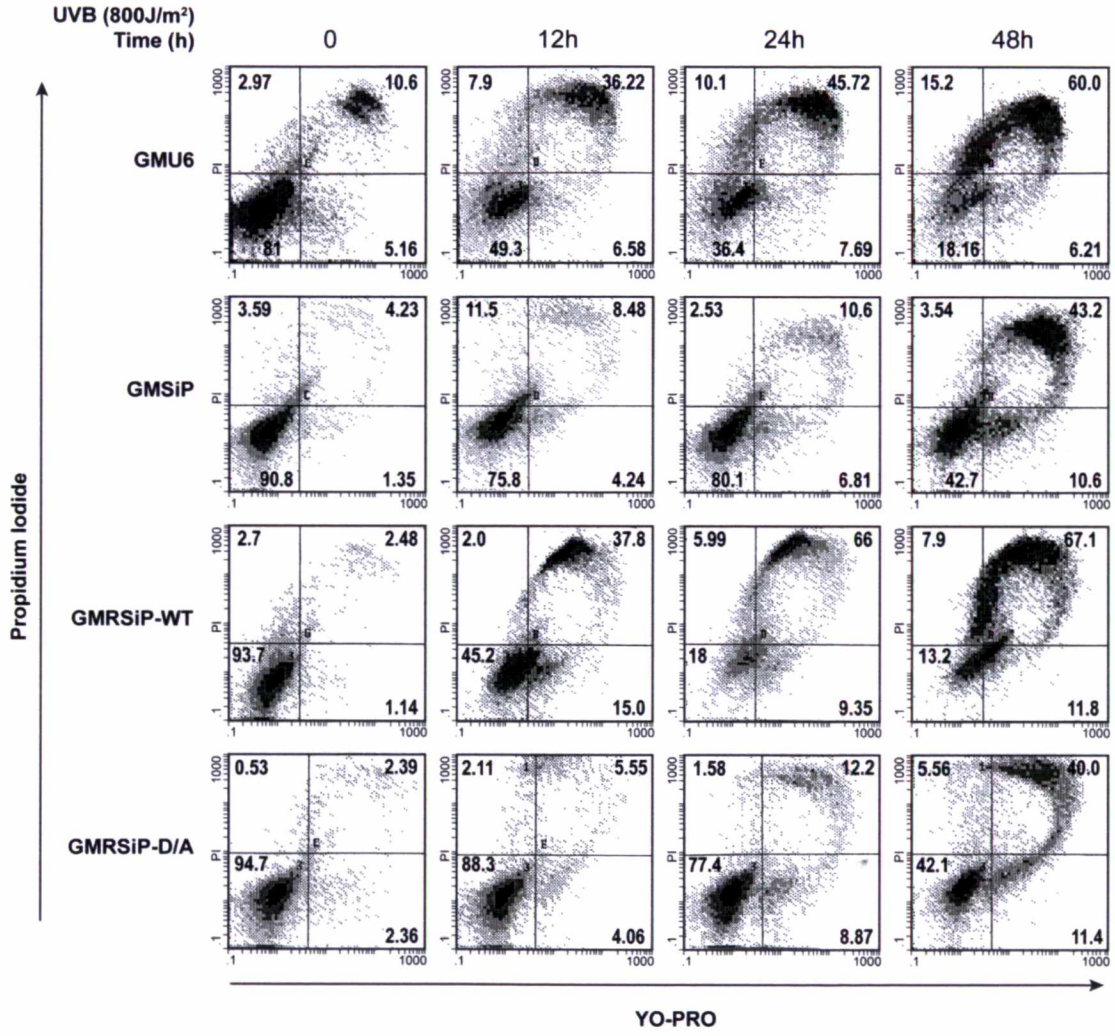

Figure 2.4 Cell Death Analysis (A): Flow cytometry analysis by YO-PRO/PI staining.

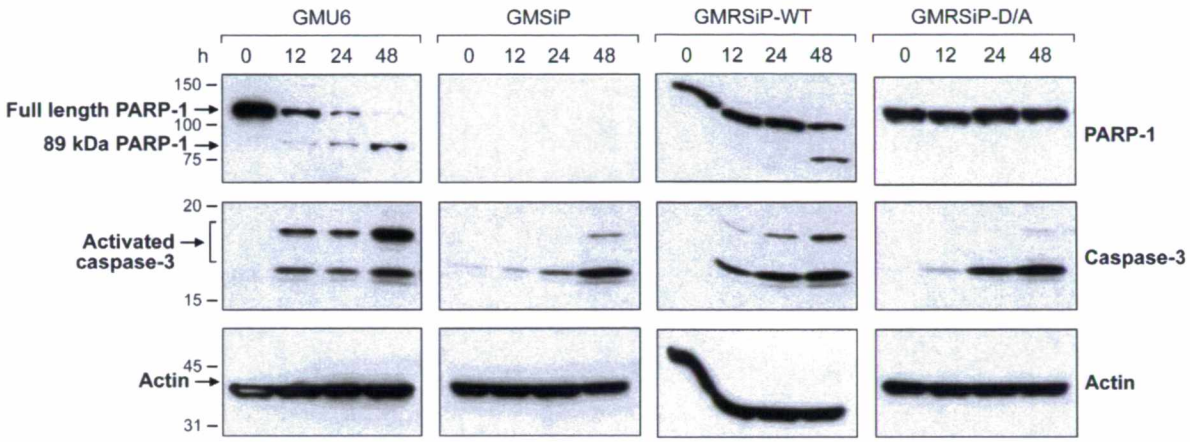

Figure 2.4 (B): Time course of PARP-1 cleavage and caspase-activation in UVB-treated PARP-1 mutants

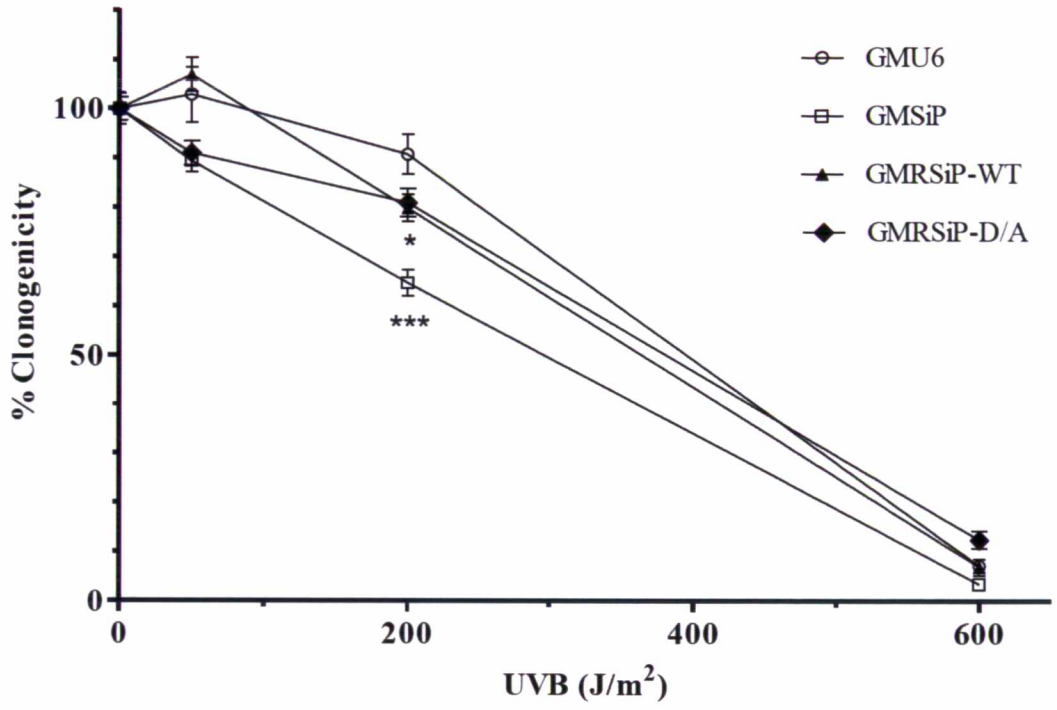

Figure 2.5: Clonogenicity of cells expressing PARP-1 mutants in response to UVB

Chapter 3: Caspase-uncleavable substrates: A gateway to understand death as well as life

(Manuscript in Submission to Cell Death and Differentiation)

3.1 Résumé en français

De nombreuses protéines cellulaires sont spécifiquement clivées par des caspases à différentes étapes de la mort par apoptose. Afin de comprendre leur importance dans l'apoptose, de nombreux mutants non-clivables par les caspases ont été créés afin d'identifier leurs sites de clivage, les caspases responsables et l'impact de ce clivage sur les évènements apoptotiques. Nous décrivons ici différents effets liés à l'apoptose sur environ cinquante substrats non-clivables par les caspases dans des cellules mammaliennes. Nous discutons des défis de l'interprétation des résultats car un seul substrat non-clivable, autre que les caspases elles-mêmes, peut retarder mais peut rarement prévenir la mort par apoptose ou nécrose en raison du chevauchement des voies impliquées dans la mort cellulaire et du clivage de multiples substrats durant l'apoptose des cellules mammaliennes. Depuis peu, de nouvelles voies d'exploration émergent pour ces mutants pour étudier le rôle du clivage par les caspases dans la vie plutôt que dans la mort. Les caspases sont aussi activées de façon localisée et contrôlée pour jouer un rôle non-létale dans une cellule ou un organe, comme la réponse inflammatoire, la différenciation cellulaire ou le remodelage neuronal. Comme les cellules survivent dans ces conditions, elles offrent une opportunité idéale pour analyser les conséquences à long terme de l'absence de clivage de même un seul substrat-cible des caspases. En utilisant l'exemple de la poly(ADP-ribose) polymerase-1 (PARP-1), nous discutons de la façon dont son mutant non clivable par les caspases révèle le rôle du clivage de PARP-1 dans les réponses par la mort cellulaire ou par la continuité de la vie comme le contrôle transcriptionnel durant l'inflammation. Nous recommandons que les centaines de mutants non-clivables par les caspases créés pour l'étude de l'apoptose soient exploités pour découvrir le rôle de leur clivage dans la vie cellulaire.

3.2 Review Article

Caspase-uncleavable substrates: A gateway to understand death as well as life

Running Title: Caspase-uncleavable substrates in death and life

Febitha Kandan-Kulangara[1*], Nupur K. Purohit[1*], Sabina S. Halappanavar[1,2] and Girish M. Shah[1#]

[1]Laboratory for Skin Cancer Research, CHUL (CHUQ) Hospital Research Centre of Laval University, Laval University, Québec (QC) Canada G1V 4G2. [2]Present Address: Health Canada, Healthy Environment and Consumer's Safety Branch, Ottawa (ON) Canada K1A 0K9

*These two authors should be considered as joint first authors due to equal contribution

[#]Corresponding Author: GM Shah, e-mail: girish.shah@crchul.ulaval.ca

Keywords:

Caspases; caspase-uncleavable substrates; apoptosis; necrosis; non-death related limited activation of caspases, different roles for caspase-cleavage of same substrates in apoptosis and in non-death related events;

List of Abbreviations:

PARP-1: Poly(ADP-ribose) polymerase-1

3.3 Abstract

Numerous cellular proteins are specifically cleaved by caspases at different stages of apoptotic death. To address their relevance in apoptosis, many caspase-uncleavable mutants have been created for identification of the cleavage site, the caspases responsible for this action and impact of this cleavage on apoptotic events. Here, we describe different apoptosis-related effects seen with about fifty caspase-uncleavable substrates in mammalian cells, and discuss challenges posed in interpretation of results because a single uncleavable substrate, other than caspases themselves, can delay but rarely prevent eventual death by apoptosis or necrosis because of overlapping nature of the death pathways and cleavage of multiple substrates during apoptosis in mammalian cells. In the meanwhile, newer uses are emerging for these mutants to study the role of their caspase-mediated cleavage in life rather than in death, because caspases are also activated in a localized and controlled manner to achieve non-lethal functions within a cell or an organ, such as inflammatory responses, cellular differentiation and remodeling of neurons. Since cells survive in these responses, they offer an ideal opportunity to examine the long-term consequence of the lack of cleavage of even a single caspase-targeted substrate. Using an example of poly(ADP-ribose) polymerase-1 (PARP-1), we discuss how its caspase-uncleavable mutant revealed the role of cleavage of PARP-1 not only in death but also in non-death response such as transcriptional control during inflammation. We urge that hundreds of other caspase-uncleavable mutants created for study of apoptosis could be readily exploited to discover novel roles of their cleavage in life.

BULLET POINTS:

FACTS:

- Caspase-uncleavable substrates is an useful approach to study relevance of caspase-mediated cleavage of a substrate in apoptosis
- Many caspase-uncleavable substrates can delay but not permanently block eventual death of mammalian cells by apoptosis or necrosis
- Even a partial effect on apoptosis seen with a single caspase-uncleavable substrate should be treated as a positive outcome in mammalian models, due to overlapping nature of caspase actions and cleavage of multiple substrates that ensure death under all circumstances
- Mammalian apoptosis models using caspase-uncleavable substrates could be improved

OPEN QUESTIONS:

- A controlled and localized caspase activation that plays a role in non-death related events, such as inflammation and differentiation allows the cells to survive
- Since some of the same caspases are involved in apoptosis and non-death events, we should expect that at least some of the caspase-target substrates will be cleaved in both apoptosis and non-death related events.
- Using specific examples of caspase-uncleavable PARP-1, we show that while unlimited cleavage of PARP-1 by caspases can play a role in apoptosis, a limited cleavage of PARP-1 by caspase 7, activated by inflammasome /caspase-1, is implicated in transcriptional response during inflammation
- We urge use of previously created caspase-uncleavable mutants of PARP-1 and hundreds of other proteins in study of caspase activation in life as well as in death

3.4 Caspases and their target substrates in apoptosis

Caspases are cysteine-dependent aspartate specific proteases, which after activation from their zymogen forms, cause limited and specific proteolysis of their substrates at Asp (D) residue to facilitate downstream signaling events.[1] Human caspase family has 12 members with a variety of roles ranging from apoptotic death (caspases 2-4, and 6-10) to non-death related functions such as inflammation (caspases 1, 4, 5 and 12) and differentiation (caspases 3, 6-10 and 14).[2] Hence understanding when, where and how different substrates are targeted for cleavage by each of these caspases has the potential to reveal the mechanism by which caspases drive the cells towards their designated end-points. At present, 777 substrates have been listed in the database CASBAH as those cleaved by different caspases in vitro, during apoptosis and inflammation.[3, 4] A vast majority of these substrates are cleaved by apoptotic caspases, because inflammatory caspases are known to cleave very few substrates.[5] Hence in the apoptosis field, the challenge lies in sorting this list to distinguish the substrates whose cleavage is relevant to apoptotic events from those whose cleavage could be termed as "collateral damage". Earlier reviews[2, 6] have summarized following possible outcomes from caspase-mediated cleavage of relevant substrates on apoptosis: (i) gain of function, such as activation of caspases from their inactive zymogen form; (ii) loss of function, e.g. ICAD whose cleavage abolishes its DNase-inhibitory function; (iii) feedback regulation, e.g. caspase 3, which is originally activated by caspase 9, cleaves neo-N-terminal of caspase 9 to make it refractory to inhibition by XIAP; and (iv) change of cellular localization of cleaved fragment:, e.g., cleavage of nuclear export signal sequesters Abl in the nucleus to exert pro-apoptotic function. Interestingly, both gain and loss of different functions have also been reported due to cleavage of some caspase substrates. For example, cleavage of endoribonuclease Dicer-1 at two distinct sites within its RNase IIIa domain by caspase 3 results in loss of its dicing activity that is required to create mature miRNA from their precursors in mammalian cells[7] but the c-terminal caspase-created fragment of Dicer-1 acquires a DNase property that could facilitates apoptotic DNA fragmentation.[8, 9] The use of caspase-uncleavable mutant substrate has been one of the useful approaches to reveal some of these roles for cleavage of a substrate by caspases.

3.5 Lessons from the use of caspase-uncleavable substrates in apoptosis

Taking advantage of the catalytic selectivity of caspases to cleave specifically at one or very few Asp (D) residues in the target, one can create a caspase-uncleavable mutant substrate by replacing the targeted Asp (D) residues with Ala (A), Glu (E) or Asn (N). While a vast majority of the studies used these mutants to confirm the site of cleavage by caspases, fewer studies used them to examine the relevance of their cleavage in apoptosis. In Table I, we review studies with about 50 caspase-uncleavable substrates and discuss the type of results obtained with these mutants during apoptosis in mammalian cells. We have classified these substrates in seven functional groups: (i) structural proteins whose breakdown is required for dismantling the cell; (ii) apoptotic regulatory proteins whose cleavage will facilitate apoptosis, such as conversion of pro-caspases to activated caspases, loss of chaperons or inhibitors of apoptotic DNases and caspases; (iii) cell cycle and proliferation regulatory proteins whose cleavage will abrogate cell cycle arrest that could prevent apoptosis; (iv) DNA repair related proteins, whose cleavage is expected to prevent survival efforts; (v) transcription factors whose cleavage will block expression of pro-survival and pro-growth genes; (vi) proteins kinases and signaling intermediates whose cleavage dampens the survival responses; (vii) proteins involved in neuropathology whose cleavage contributes towards advancing the disease by either blocking immediate death of neurons or causing eventual death of the neurons.

As expected, uncleavable mutants for caspases and other proteins such as DFF45 or Bid which directly regulate key apoptotic events, provided a more direct proof for the role of their cleavage by blocking or delaying apoptosis or the specific apoptotic event. However, for proteins not directly involved in controlling apoptosis, such as those in DNA repair, cell cycle control or cell signaling pathways, it was more challenging to interpret the results with their caspase-uncleavable mutants. As described in Table I, some of these caspase-uncleavable substrates had no effect on apoptosis (e.g., cytokeratin, pGDI2) whereas others changed the mode of cell death from apoptosis to necrosis (e.g., inositol triphosphate receptor, poly(ADP-ribose) polymerase-1 (PARP-1)). A majority of the uncleavable substrates could block or delay apoptosis, whereas others accelerated or even

enhanced apoptosis. Barring rare exceptions of survival (e.g., p21-activated protein kinase-2, PARP-1), a majority of the caspase-uncleavable substrates were not shown to significantly block cell death for a prolonged period of time. The ultimate lack of protection from death by a single caspase-uncleavable substrate, other than the apoptosis-regulatory proteins, could simply mean that we have not yet found "the" critical substrate whose cleavage controls apoptotic events. However, we argue that the ability of a single mutant substrate to show even some degree of influence on apoptosis is an indication that its cleavage plays a role in cell death, which can be sharply defined if we could design better experimental models. Our argument rests on three points: (i) Unlike apoptosis in worms, mammalian apoptosis is controlled by multiple caspases, each of which cuts an overlapping set of substrates under specific circumstances for achieving demise of the cell. Hence the lack of cleavage of one substrate may be important but not sufficient to block the ultimate death of mammalian cells, because other substrates will continue to be cleaved by caspases (see Table I). (ii) Once initiator caspases are activated or mitochondrial outer membrane permeability transition has occurred, it may simply be too late to salvage mammalian cells whether one downstream substrate is cleaved or not, but this scenario does not exclude the possible role for cleavage of a substrate in apoptosis. (iii) Finally, it should not be discounted that cleavage by caspase is likely to be the principle reason why many multifunctional proteins, such as PARP-1 (see below) lose their pro-life functions during apoptosis, hence uncleavable version of such a substrate will ignore ongoing pro-apoptotic clues and continue to work at cross-purposes to save life and impede death processes.

Could we design better experimental models for use of caspase-uncleavable substrates to reveal the true function of their cleavage in mammalian apoptosis? Among the first things to consider is use of these mutant substrates in cells or mice depleted of the endogenous caspase-cleavable substrate. This condition will avoid ill-defined outcomes due to opposing efforts of the endogenous cleavable and exogenous uncleavable mutant with respect to death. As discussed earlier, this stringent condition for testing uncleavable substrates is essential if we are to prove that cleavage of a substrate results in a gain of pro-apoptotic function.[6] The mammalian cells and mice with knockout or knockdown of

endogenous gene are ideal for introduction of the mutant protein. In case of lethality associated with depletion of the endogenous gene, the conditional knockdown or simultaneous knockdown and rescue with RNAi-resistant and caspase-uncleavable form should be considered. Despite the obvious advantage, surprisingly few studies with caspase-uncleavable mutants have been carried out in the absence of endogenous cleavable substrate. The results obtained with seven mutant substrates under this condition could be grouped under three categories (Table I): (i) decreased apoptosis, e.g., integrin β4, inositol triphosphate receptor, DFF45, Bid, cdc42 and PARP-1; (ii) change of mode of death from apoptosis to caspase-independent apoptosis or necrosis, e.g., p21-activated protein kinase-2 or inositol triphosphate receptor; and (iii) increased survival, e.g., PARP-1 and p21-activated protein kinase-2. Due to complete absence of endogenous substrate in these models, different outcomes seen with some of these multifunctional substrates can be unambiguously linked to different known functions of these proteins before or after their cleavage by caspases, as described below for PARP-1.

The second improvement in experimental design for study of apoptosis with these uncleavable mutants is to simultaneously introduce more than one uncleavable substrate belonging to a common functional group, such as structural proteins or apoptosis-regulatory proteins in a background depleted of endogenous versions of these proteins. The newer large-scale gene knockdown and knock-in technologies may be required for these experiments. Final frontier would be to introduce one or more sets of caspase-uncleavable proteins in each of the functional groups to completely block death and allow the cells to resume proliferation despite receiving a death-inducing stimulus. The last scenario will also address the existential question whether a cell that should be killed is worth saving after all.

3.6 Novel use of caspase-uncleavable substrates in study of life rather than death

Although many of the caspase-uncleavable substrates were originally created to study apoptosis, it is important to recognize that they can also be used for studying their caspase-mediated cleavage outside the context of death. While the role of caspase-

activation in inflammation has been known for a long time, there is a steadily growing recognition that a well-controlled and selective activation of caspases occurs in other non-death or life-related events, such as proliferation, terminal differentiation, and neuronal remodelling by axonal or dendritic pruning.[2, 10-12] Since some of the caspases are involved in both apoptosis and differentiation, such as capsases-3 and 6-10,[2] we should expect that substrates that were conventionally known to be cleaved in apoptosis may also be selectively cleaved by caspases during non-death events. This should open up an entirely new frontier for use of caspase-uncleavable mutants in non-death processes. Since cells do survive in non-death responses even after activation of caspase, we argue that these models offer excellent opportunities at identifying the long-term consequence of the lack of cleavage of even a single caspase-targeted substrate.

3.7 Use of caspase-uncleavable PARP-1 in study of both death and life

We review how use of caspase-uncleavable mutant form of the multifunctional protein PARP-1 in PARP-1-deficient cells or mice revealed that caspase-mediated cleavage of PARP-1 plays a key role not only in death but also in life. The cleavage of PARP-1 to its signature 89-kDa ("85 kDa") fragment was among the earliest described examples of specific cleavage of a protein during apoptotic death of mammalian cells.[13, 14] Subsequent studies identified the DEVD[214] as the only PARP-1 sequence that was targeted for cleavage by the "protease resembling ICE",[15] which was identified as Yama/CPP32, currently known as caspase 3 and PARP-1 earned the nickname "the death substrate".[16] Interestingly, four apoptosis-focused studies using caspase-uncleavable mutant PARP-1 expressed in PARP-1$^{-/-}$ cells revealed four different outcomes: (i) delayed apoptosis;[17] (ii) change in mode of cell death from apoptosis to necrosis;[18] (iii) survival of cells instead of death [19]; and (iv) accelerated apoptosis[18, 20] (Table I). These outcomes can be explained by the known roles of PARP-1 in cell survival and cell death. PARP-1 is catalytically activated in response to DNA damage to consume its substrate NAD and form polymers of ADP-ribose, which post-translationally modify target proteins.[21] At lower levels of DNA damage, this metabolism is implicated in survival responses such as DNA base excision repair, whereas at higher levels of DNA damage, an over-activation of PARP-1 causes necrotic death

because of massive depletion of NAD and ATP[22] and increased transient intracellular acidification that suppresses apoptotic death.[23] Therefore, caspase-uncleavable PARP-1 can promote survival through its participation in DNA repair in case of DNA damage-induced apoptosis[19] or it can cause necrosis due to its over-activation in the presence of apoptotically fragmented DNA;[18] and both of these outcomes opposing apoptotic death would be avoided if PARP-1 is cleaved and inactivated by caspases. The delayed[17, 19] or enhanced[18, 20] apoptotic death by caspase-uncleavable PARP-1 have been attributed to role of PARP-1 in DNA repair or possible modification of pro- or anti-apoptotic target proteins by catalytic activity of PARP-1.

Two studies with caspase-uncleavable PARP-1 expressed in PARP-$1^{-/-}$ mice surprisingly revealed non-death related role of caspase-mediated cleavage of PARP-1 in lipopolysaccharide-induced inflammatory response.[24, 25] While mice expressing wild type PARP-1 had normal inflammatory response, mice expressing caspase-uncleavable PARP-1 showed suppressed inflammatory responses.[24] This led to the discovery that wild type PARP-1 occupies the promoter site to suppresses NF-κB regulated target genes under basal conditions. In response to LPS stimulation, a controlled activation of inflammasome containing caspase 1 selectively activates caspase 7, which upon translocation to the nucleus cleaves PARP-1 promoting decondensation of the chromatin and expression of these genes.[25] Thus, use of caspase-uncleavable PARP-1 in inflammation model revealed its novel role in transcriptional regulation of certain genes. We urge that more studies should be conducted with caspase-uncleavable forms of target proteins in the absence of their endogenous counterparts to reveal novel living functions of controlled caspase-mediated cleavage of these substrates in life.

3.8 Acknowledgments:

This work was supported by the grants to GMS from the Natural Sciences and Engineering Research Council of Canada (Discovery Grant # 155257-2011) and the Canadian Institutes of Health Research (Operating Grant #MOP-89964). We acknowledge the scholarship supports from the Natural Sciences and Engineering Research Council of Canada (to FKK) and from Laval University (to SSH). We thank G. Salvesen for helpful discussion on the subject and for critical review of the manuscript.

3.9 References:

1. Pop C, Salvesen GS. Human caspases: activation, specificity, and regulation. *J Biol Chem* 2009; **284**(33): 21777-81.
2. Crawford ED, Wells JA. Caspase substrates and cellular remodeling. *Ann. Review Biochem.* 2011; **80:** 1055-87.
3. Luthi AU, Martin SJ. The CASBAH: a searchable database of caspase substrates. *Cell Death Differ* 2007; **14**(4): 641-50.
4. CASBAH. The CAspase Substrate dataBAse: http://www.casbah.ie In: A. Luthi A and S.J. Martin, 2012.
5. Agard NJ, Maltby D, Wells JA. Inflammatory stimuli regulate caspase substrate profiles. *Mol Cell Proteomics* 2010; **9**(5): 880-93.
6. Timmer JC, Salvesen GS. Caspase substrates. *Cell Death Differ* 2007; **14**(1): 66-72.
7. Ghodgaonkar MM, Shah RG, Kandan-Kulangara F, Affar EB, Qi HH, Wiemer E *et al.* Abrogation of DNA vector-based RNAi during apoptosis in mammalian cells due to caspase-mediated cleavage and inactivation of Dicer-1. *Cell Death Differ* 2009; **16**(6): 858-68.
8. Nakagawa A, Shi Y, Kage-Nakadai E, Mitani S, Xue D. Caspase-dependent conversion of Dicer ribonuclease into a death-promoting deoxyribonuclease. *Science* 2010; **328**(5976): 327-34.
9. Harry BL, Nakagawa A, Xue D. Dicing up chromosomes: the unexpected role of Dicer in apoptosis. *Cell Cycle* 2010; **9**(24): 4772-3.
10. Yang JY, Michod D, Walicki J, Widmann C. Surviving the kiss of death. *Biochem Pharmacol* 2004; **68**(6): 1027-31.
11. Nhan TQ, Liles WC, Schwartz SM. Physiological functions of caspases beyond cell death. *Amer. J. Pathol.* 2006; **169**(3): 729-37.
12. Hyman BT, Yuan J. Apoptotic and non-apoptotic roles of caspases in neuronal physiology and pathophysiology. *Nat Rev Neurosci* 2012; **13**(6): 395-406.
13. Kaufmann SH. Induction of endonucleolytic DNA cleavage in human acute myelogenous leukemia cells by etoposide, camptothecin, and other cytotoxic anticancer drugs: A cautionary note. *Cancer Res.* 1989; **49:** 5870-5878.
14. Kaufmann SH, Desnoyers S, Ottaviano Y, Davidson NE, Poirier GG. Specific proteolytic cleavage of poly(ADP-ribose) polymerase: an early marker of chemotherapy-induced apoptosis. *Cancer Res.* 1993; **53**(17): 3976-3985.
15. Lazebnik YA, Kaufmann SH, Desnoyers S, Poirier GG, Earnshaw WC. Cleavage of poly(ADP-ribose) polymerase by a proteinase with properties like ICE. *Nature* 1994; **371**(6495): 346-347.
16. Tewari M, Quan LT, O'Rourke K, Desnoyers S, Zeng Z, Beidler DR *et al.* Yama/CPP32 beta, a mammalian homolog of CED-3, is a CrmA-inhibitable protease that cleaves the death substrate poly(ADP-ribose) polymerase. *Cell* 1995; **81**(5): 801-809.
17. Oliver FJ, de la Rubia G, Rolli V, Ruiz-Ruiz MC, de Murcia G, Murcia JM. Importance of poly(ADP-ribose) polymerase and its cleavage in apoptosis. Lesson from an uncleavable mutant. *J. Biol. Chem.* 1998; **273**(50): 33533-33539.
18. Herceg Z, Wang ZQ. Failure of Poly(ADP-ribose) polymerase cleavage by caspases leads to induction of necrosis and enhanced apoptosis. *Mol. Cell. Biol.* 1999; **19**(7): 5124-5133.

19. Halappanavar SS, Le Rhun Y, Mounir S, Martins M, Huot J, Earnshaw WC *et al.* Survival and proliferation of cells expressing caspase-uncleavable poly(ADP-ribose) polymerase in response to death-inducing DNA damage by an alkylating agent. *J. Biol. Chem.* 1999; **274**(52): 37097-104.
20. Boulares AH, Yakovlev AG, Ivanova V, Stoica BA, Wang G, Iyer S *et al.* Role of poly(ADP-ribose) polymerase (PARP) cleavage in apoptosis. Caspase 3-resistant PARP mutant increases rates of apoptosis in transfected cells. *J. Biol. Chem.* 1999; **274**(33): 22932-22940.
21. Shah GM, Kandan-Kulangara F, Montoni A, Shah RG, Brind'amour J, Vodenicharov MD *et al.* Approaches to detect PARP-1 activation in vivo, in situ, and in vitro. *Methods Molec Biol* 2011; **780:** 3-34.
22. Berger NA. Poly(ADP-ribose) in the cellular response to DNA damage. *Radiation Res.* 1985; **101:** 4-15.
23. Affar EB, Shah RG, Dallaire A-K, Castonguay V, Shah GM. Role of poly(ADP-ribose) polymerase in rapid intracellular acidification induced by alkylating DNA damage. *Proc. Natl. Acad. Sci. USA* 2002; **99**(1): 245-250.
24. Petrilli V, Herceg Z, Hassa PO, Patel NS, Di Paola R, Cortes U *et al.* Noncleavable poly(ADP-ribose) polymerase-1 regulates the inflammation response in mice. *J Clin invest* 2004; **114**(8): 1072-81.
25. Erener S, Hesse M, Kostadinova R, Hottiger MO. Poly(ADP-Ribose)Polymerase-1 (PARP1) Controls Adipogenic Gene Expression and Adipocyte Function. *Mol Endocrinol* 2012; **26**(1): 79-86.
26. Rao L, Perez D, White E. Lamin proteolysis facilitates nuclear events during apoptosis. *J. Cell. Biol.* 1996; **135**(6 Pt 1): 1441-1455.
27. Caulin C, Salvesen GS, Oshima RG. Caspase cleavage of keratin 18 and reorganization of intermediate filaments during epithelial cell apoptosis. *J Cell Biol* 1997; **138**(6): 1379-94.
28. Byun Y, Chen F, Chang R, Trivedi M, Green KJ, Cryns VL. Caspase cleavage of vimentin disrupts intermediate filaments and promotes apoptosis. *Cell Death Differ* 2001; **8**(5): 443-50.
29. Belichenko I, Morishima N, Separovic D. Caspase-resistant vimentin suppresses apoptosis after photodynamic treatment with a silicon phthalocyanine in Jurkat cells. *Arch Biochem Biophys* 2001; **390**(1): 57-63.
30. Lin HH, Hsu HL, Yeh NH. Apoptotic cleavage of NuMA at the C-terminal end is related to nuclear disruption and death amplification. *J Biomed Sci* 2007; **14**(5): 681-94.
31. Panagopoulou P, Davos CH, Milner DJ, Varela E, Cameron J, Mann DL *et al.* Desmin mediates TNF-alpha-induced aggregate formation and intercalated disk reorganization in heart failure. *J Cell Biol* 2008; **181**(5): 761-75.
32. Chen F, Chang R, Trivedi M, Capetanaki Y, Cryns VL. Caspase proteolysis of desmin produces a dominant-negative inhibitor of intermediate filaments and promotes apoptosis. *J Biol Chem* 2003; **278**(9): 6848-53.
33. Werner ME, Chen F, Moyano JV, Yehiely F, Jones JC, Cryns VL. Caspase proteolysis of the integrin beta4 subunit disrupts hemidesmosome assembly, promotes apoptosis, and inhibits cell migration. *J Biol Chem* 2007; **282**(8): 5560-9.

34. Maag RS, Mancini M, Rosen A, Machamer CE. Caspase-resistant Golgin-160 disrupts apoptosis induced by secretory pathway stress and ligation of death receptors. *Mol Biol Cell* 2005; **16**(6): 3019-27.
35. Mancini M, Machamer CE, Roy S, Nicholson DW, Thornberry NA, Casciola-Rosen LA *et al.* Caspase-2 is localized at the Golgi complex and cleaves golgin-160 during apoptosis. *J Cell Biol* 2000; **149**(3): 603-12.
36. Lane JD, Lucocq J, Pryde J, Barr FA, Woodman PG, Allan VJ *et al.* Caspase-mediated cleavage of the stacking protein GRASP65 is required for Golgi fragmentation during apoptosis. *J Cell Biol* 2002; **156**(3): 495-509.
37. Chiu R, Novikov L, Mukherjee S, Shields D. A caspase cleavage fragment of p115 induces fragmentation of the Golgi apparatus and apoptosis. *J Cell Biol* 2002; **159**(4): 637-48.
38. Nguyen M, Breckenridge DG, Ducret A, Shore GC. Caspase-resistant BAP31 inhibits fas-mediated apoptotic membrane fragmentation and release of cytochrome c from mitochondria. *Mol Cell Biol* 2000; **20**(18): 6731-40.
39. Assefa Z, Bultynck G, Szlufcik K, Nadif Kasri N, Vermassen E, Goris J *et al.* Caspase-3-induced truncation of type 1 inositol trisphosphate receptor accelerates apoptotic cell death and induces inositol trisphosphate-independent calcium release during apoptosis. *J Biol Chem* 2004; **279**(41): 43227-36.
40. Wohrl W, Hacker G. Extent and limitation of the control of nuclear apoptosis by DNA- fragmenting factor. *Biochem. Biophys. Res. Commun.* 1999; **254**(3): 552-558.
41. Huang Y, Nakada S, Ishiko T, Utsugisawa T, Datta R, Kharbanda S *et al.* Role for caspase-mediated cleavage of Rad51 in induction of apoptosis by DNA damage. *Mol Cell Biol* 1999; **19**(4): 2986-97.
42. Zhan Q, Jin S, Ng B, Plisket J, Shangary S, Rathi A *et al.* Caspase-3 mediated cleavage of BRCA1 during UV-induced apoptosis. *Oncogene* 2002; **21**(34): 5335-45.
43. Borges HL, Bird J, Wasson K, Cardiff RD, Varki N, Eckmann L *et al.* Tumor promotion by caspase-resistant retinoblastoma protein. *Proc Natl Acad Sci U S A* 2005; **102**(43): 15587-92.
44. Chau BN, Borges HL, Chen TT, Masselli A, Hunton IC, Wang JY. Signal-dependent protection from apoptosis in mice expressing caspase-resistant Rb. *Nature Cell Biol* 2002; **4**(10): 757-65.
45. Eymin B, Sordet O, Droin N, Munsch B, Haugg M, Van de Craen M *et al.* Caspase-induced proteolysis of the cyclin-dependent kinase inhibitor p27Kip1 mediates its anti-apoptotic activity. *Oncogene* 1999; **18**(34): 4839-47.
46. Pelizon C, d'Adda di Fagagna F, Farrace L, Laskey RA. Human replication protein Cdc6 is selectively cleaved by caspase 3 during apoptosis. *EMBO Rep* 2002; **3**(8): 780-4.
47. Mazumder S, Gong B, Chen Q, Drazba JA, Buchsbaum JC, Almasan A. Proteolytic cleavage of cyclin E leads to inactivation of associated kinase activity and amplification of apoptosis in hematopoietic cells. *Mol Cell Biol* 2002; **22**(7): 2398-409.
48. Lee MW, Hirai I, Wang HG. Caspase-3-mediated cleavage of Rad9 during apoptosis. *Oncogene* 2003; **22**(41): 6340-6.

49. Levkau B, Scatena M, Giachelli CM, Ross R, Raines EW. Apoptosis overrides survival signals through a caspase-mediated dominant-negative NF-kappa B loop. *Nature Cell Biol* 1999; **1**(4)**:** 227-33.
50. Kang KH, Lee KH, Kim MY, Choi KH. Caspase-3-mediated cleavage of the NF-kappa B subunit p65 at the NH2 terminus potentiates naphthoquinone analog-induced apoptosis. *J Biol Chem* 2001; **276**(27)**:** 24638-44.
51. Drewett V, Devitt A, Saxton J, Portman N, Greaney P, Cheong NE *et al.* Serum response factor cleavage by caspases 3 and 7 linked to apoptosis in human BJAB cells. *J Biol Chem* 2001; **276**(36)**:** 33444-51.
52. Zeuner A, Eramo A, Testa U, Felli N, Pelosi E, Mariani G *et al.* Control of erythroid cell production via caspase-mediated cleavage of transcription factor SCL/Tal-1. *Cell Death Differ* 2003; **10**(8)**:** 905-13.
53. Larribere L, Hilmi C, Khaled M, Gaggioli C, Bille K, Auberger P *et al.* The cleavage of microphthalmia-associated transcription factor, MITF, by caspases plays an essential role in melanocyte and melanoma cell apoptosis. *Genes Dev* 2005; **19**(17)**:** 1980-5.
54. De Maria R, Zeuner A, Eramo A, Domenichelli C, Bonci D, Grignani F *et al.* Negative regulation of erythropoiesis by caspase-mediated cleavage of GATA-1. *Nature* 1999; **401**(6752)**:** 489-93.
55. Chen M, Guerrero AD, Huang L, Shabier Z, Pan M, Tan TH *et al.* Caspase-9-induced mitochondrial disruption through cleavage of anti-apoptotic BCL-2 family members. *J Biol Chem* 2007; **282**(46)**:** 33888-95.
56. Levkau B, Garton KJ, Ferri N, Kloke K, Nofer JR, Baba HA *et al.* xIAP induces cell-cycle arrest and activates nuclear factor-kappaB : new survival pathways disabled by caspase-mediated cleavage during apoptosis of human endothelial cells. *Circ Res* 2001; **88**(3)**:** 282-90.
57. Billen LP, Shamas-Din A, Andrews DW. Bid: a Bax-like BH3 protein. *Oncogene* 2008; **27 Suppl 1:** S93-104.
58. Clem RJ, Cheng EH, Karp CL, Kirsch DG, Ueno K, Takahashi A *et al.* Modulation of cell death by Bcl-XL through caspase interaction. *Proc Natl Acad Sci U S A* 1998; **95**(2)**:** 554-9.
59. Rehemtulla A, Hamilton AC, Taneja N, Fridman J, Juan TS, Maybaum J *et al.* A caspase-resistant form of Bcl-X(L), but not wild type Bcl-X(L), promotes clonogenic survival after ionizing radiation. *Neoplasia* 1999; **1**(1)**:** 63-70.
60. Cardone MH, Salvesen GS, Widmann C, Johnson G, Frisch SM. The regulation of anoikis: MEKK-1 activation requires cleavage by caspases. *Cell* 1997; **90**(2)**:** 315-323.
61. Zebrowski DC, Alcendor RR, Kirshenbaum LA, Sadoshima J. Caspase-3 mediated cleavage of MEKK1 promotes p53 transcriptional activity. *J Mol Cell Cardiol* 2006; **40**(5)**:** 605-18.
62. Franke TF, Hornik CP, Segev L, Shostak GA, Sugimoto C. PI3K/Akt and apoptosis: size matters. *Oncogene* 2003; **22**(56)**:** 8983-98.
63. Cardone MH, Roy N, Stennicke HR, Salvesen GS, Franke TF, Stanbridge E *et al.* Regulation of cell death protease caspase-9 by phosphorylation. *Science* 1998; **282**(5392)**:** 1318-21.

64. Lee YJ, Froelich CJ, Fujita N, Tsuruo T, Kim JH. Reconstitution of caspase-3 confers low glucose-enhanced tumor necrosis factor-related apoptosis-inducing ligand cytotoxicity and Akt cleavage. *Clin Cancer Res* 2004; **10**(6): 1894-900.
65. Kruidering M, Schouten T, Evan GI, Vreugdenhil E. Caspase-mediated cleavage of the Ca2+/calmodulin-dependent protein kinase-like kinase facilitates neuronal apoptosis. *J Biol Chem* 2001; **276**(42): 38417-25.
66. Fischer U, Steffens S, Frank S, Rainov NG, Schulze-Osthoff K, Kramm CM. Mechanisms of thymidine kinase/ganciclovir and cytosine deaminase/ 5-fluorocytosine suicide gene therapy-induced cell death in glioma cells. *Oncogene* 2005; **24**(7): 1231-43.
67. Tu S, Cerione RA. Cdc42 is a substrate for caspases and influences Fas-induced apoptosis. *J Biol Chem* 2001; **276**(22): 19656-63.
68. Clarke CA, Bennett LN, Clarke PR. Cleavage of claspin by caspase-7 during apoptosis inhibits the Chk1 pathway. *J Biol Chem* 2005; **280**(42): 35337-45.
69. Semple JI, Smits VA, Fernaud JR, Mamely I, Freire R. Cleavage and degradation of Claspin during apoptosis by caspases and the proteasome. *Cell Death Differ* 2007; **14**(8): 1433-42.
70. Na S, Chuang TH, Cunningham A, Turi TG, Hanke JH, Bokoch GM *et al.* D4-GDI, a substrate of CPP32, is proteolyzed during Fas-induced apoptosis. *J Biol Chem* 1996; **271**(19): 11209-13.
71. Thiede B, Dimmler C, Siejak F, Rudel T. Predominant identification of RNA-binding proteins in Fas-induced apoptosis by proteome analysis. *J Biol Chem* 2001; **276**(28): 26044-50.
72. Thiede B, Treumann A, Kretschmer A, Sohlke J, Rudel T. Shotgun proteome analysis of protein cleavage in apoptotic cells. *Proteomics* 2005; **5**(8): 2123-30.
73. Krieser RJ, Eastman A. Cleavage and nuclear translocation of the caspase 3 substrate Rho GDP-dissociation inhibitor, D4-GDI, during apoptosis. *Cell Death Differ* 1999; **6**(5): 412-9.
74. Bae SS, Choi JH, Oh YS, Perry DK, Ryu SH, Suh PG. Proteolytic cleavage of epidermal growth factor receptor by caspases. *FEBS Lett* 2001; **491**(1-2): 16-20.
75. He YY, Huang JL, Chignell CF. Cleavage of epidermal growth factor receptor by caspase during apoptosis is independent of its internalization. *Oncogene* 2006; **25**(10): 1521-31.
76. Tikhomirov O, Carpenter G. Caspase-dependent cleavage of ErbB-2 by geldanamycin and staurosporin. *J Biol Chem* 2001; **276**(36): 33675-80.
77. Benoit V, Chariot A, Delacroix L, Deregowski V, Jacobs N, Merville MP *et al.* Caspase-8-dependent HER-2 cleavage in response to tumor necrosis factor alpha stimulation is counteracted by nuclear factor kappaB through c-FLIP-L expression. *Cancer Res* 2004; **64**(8): 2684-91.
78. Gervais JL, Seth P, Zhang H. Cleavage of CDK inhibitor p21(Cip1/Waf1) by caspases is an early event during DNA damage-induced apoptosis. *J Biol Chem* 1998; **273**(30): 19207-12.
79. Levkau B, Koyama H, Raines EW, Clurman BE, Herren B, Orth K *et al.* Cleavage of p21Cip1/Waf1 and p27Kip1 mediates apoptosis in endothelial cells through activation of Cdk2: role of a caspase cascade. *Mol. Cell* 1998; **1**(4): 553-563.
80. Marlin JW, Chang YW, Ober M, Handy A, Xu W, Jakobi R. Functional PAK-2 knockout and replacement with a caspase cleavage-deficient mutant in mice reveals

differential requirements of full-length PAK-2 and caspase-activated PAK-2p34. *Mamm Genome*; **22**(5-6): 306-17.

81. Lin Y, Devin A, Rodriguez Y, Liu ZG. Cleavage of the death domain kinase RIP by caspase-8 prompts TNF- induced apoptosis. *Genes Dev* 1999; **13**(19): 2514-26.
82. Miyashita T, Okamura-Oho Y, Mito Y, Nagafuchi S, Yamada M. Dentatorubral pallidoluysian atrophy (DRPLA) protein is cleaved by caspase-3 during apoptosis. *J Biol Chem* 1997; **272**(46): 29238-42.
83. Wellington CL, Ellerby LM, Hackam AS, Margolis RL, Trifiro MA, Singaraja R *et al.* Caspase cleavage of gene products associated with triplet expansion disorders generates truncated fragments containing the polyglutamine tract. *J Biol Chem* 1998; **273**(15): 9158-67.
84. Ellerby LM, Andrusiak RL, Wellington CL, Hackam AS, Propp SS, Wood JD *et al.* Cleavage of atrophin-1 at caspase site aspartic acid 109 modulates cytotoxicity. *J Biol Chem* 1999; **274**(13): 8730-6.
85. Giaime E, Sunyach C, Druon C, Scarzello S, Robert G, Grosso S *et al.* Loss of function of DJ-1 triggered by Parkinson's disease-associated mutation is due to proteolytic resistance to caspase-6. *Cell Death Differ*; **17**(1): 158-69.
86. Giaime E, Sunyach C, Herrant M, Grosso S, Auberger P, McLean PJ *et al.* Caspase-3-derived C-terminal product of synphilin-1 displays antiapoptotic function via modulation of the p53-dependent cell death pathway. *J Biol Chem* 2006; **281**(17): 11515-22.
87. Wellington CL, Singaraja R, Ellerby L, Savill J, Roy S, Leavitt B *et al.* Inhibiting caspase cleavage of huntingtin reduces toxicity and aggregate formation in neuronal and nonneuronal cells. *J Biol Chem* 2000; **275**(26): 19831-8.
88. Young JE, Gouw L, Propp S, Sopher BL, Taylor J, Lin A *et al.* Proteolytic cleavage of ataxin-7 by caspase-7 modulates cellular toxicity and transcriptional dysregulation. *J Biol Chem* 2007; **282**(41): 30150-60.
89. Ellerby LM, Hackam AS, Propp SS, Ellerby HM, Rabizadeh S, Cashman NR *et al.* Kennedy's disease: caspase cleavage of the androgen receptor is a crucial event in cytotoxicity. *J Neurochem* 1999; **72**(1): 185-95.
90. Chaudhry P, Singh M, Parent S, Asselin E. Prostate apoptosis response 4 (Par-4), a novel substrate of caspase-3 during apoptosis activation. *Mol Cell Biol*; **32**(4): 826-39.

Table 3.1 Effect of caspase-uncleavable substrates on apoptosis

Substrates	Caspases	Proposed function of cleavage	Effects of caspase-uncleavable substrates	References
Structural proteins				
Lamin A/C (A-73 and C-63 kDa)	6	nuclear lamina breakdown and facilitates nuclear events	delays the onset of apoptosis	[26]
cytokeratins (Keratin-18: 48 kDa)	3,6 and 7	reorganization of keratin cytoskeleton into discrete nuclear structures in apoptotic cells	no effect on apoptosis	[27]
Vimentin (58 kDa)	3, 6 and 7 (in vitro); also caspase-8 and 9	disrupts cytoplasmic network of intermediate filaments and N-terminal cleaved fragment is pro-apoptotic	mutant exhibit a reduced and delayed apoptosis at low PDT dose; however at high dose there was no difference between wt and mutant	[28, 29]
NuMA	3 and 6	destruction of nuclear matrix, induces DNA fragmentation and micronucleation	prevented nuclear disruption and could attenuate the subsequent death signaling events	[30]
Desmin (55 kDa)	6	disruption of intermediate filament assembly and facilitates apoptosis	protects from apoptosis	[31, 32]

Integrin β4 (~200 kDa)	3 and 7	disruption of hemidesmosome assembly, inhibits epithelial cells migration and sensitizes to apoptosis	less sensitive to TRAIL-mediated apoptosis during early stage (upto 4 h)	[33]
Golgin-160 (runs at 170 kDa)	2,3 and 7	disassembly of golgi complex	less sensitive to apoptosis and delays apoptotic golgi fragmentation	[34, 35]
GRASP-65 (65 kDa)	3	golgi fragmentation	membrane stacking preserved and golgi ribbon fragmentation significantly inhibited.	[36]
p115 (115 kDa)	3 and 8	fragmentation of golgi apparatus and C-terminal pro-apoptotic translocates to the nucleus and contributes to apoptotic signaling independent of golgi fragmentation	delays progression of golgi fragmentation but no difference in kinetics of apoptosis	[37]
BAP31 (28 kDa)	8 and 1	induces apoptosis; p20 fragment induces apoptosis when overexpressed	inhibits Fas-induced apoptotic membrane blebbing	[38]
Inositol Triphosphate Receptor (IP_3R1) (270 kDa)	3	enhances apoptosis due to increase in $(Ca^{2+})i$	rate of apoptosis is slowed and prevents Ca2+ overload and secondary necrosis	[39]
DFF45 (45 kDa)	3	Cleavage leads to release of DFF40, which initiates genomic DNA cleavage	inhibits DNA-degradation and nuclear apoptosis	[40]

DNA-repair related proteins				
PARP-1 (116 kDa)	3 and 7	inhibits catalytic activity	survival, proliferation and change in mode of cell death	[17, 19, 20]
Rad51 (37 kDa)	3	abrogates Rad51 recombinase activity and thereby inhibits the recombinational repair	protection against IR-induced apoptosis and resistance to DNA fragmentation	[41]
BRCA1	3	abrogates its DNA repair activity and proapoptotic c-terminal	reduced cell death	[42]
Cell Cycle and proliferation regulatory proteins				
Rb	3 and 7	N-terminal fragment still binds cyclin D3 but fails to bind MDM2	inhibits endotoxin induced apoptosis and promotes the formation of colonic adenoma	[43, 44]
p27	3	Reduced binding to cyclin cdk2, decreased cdk2 activity and mediates anti apoptotic effect.	increased sensitivity to apoptosis	[45]
cdc6	3	Impaired binding to chromatin	Delays apoptosis	[46]
cyclin E	3	Loss of Cdk2 binding and kinase activity is lost, p18 fragment contributes to apoptosis	inhibits apoptosis	[47]

Rad 9	3	loss of checkpoint complex and N-terminal (BH3 domain) proapoptotic	inhibits apoptosis	[48]
Transcription factor				
NF-kB (p65/Rel A, a subunit of NF-κB)	3	augments cell death	effectively blocks apoptosis.	[49, 50]
Serum response Factor (SRF: 67 kDa)	3 and 7	inactivation of transcriptional events promoting survival and proliferation	reduction in apoptosis	[51]
SCL/Tal-1 (40 kDa)	3, 7 and 8	promotes erythropoietic arrest and apoptosis	helps in survival and differentiation of erythroids	[52]
MITF (55-60 kDa as a doublet)	3	augments melanoma cell apoptosis	more resistant to cell death	[53]
GATA-1	3	Loss of transcriptional activity and impaired erythropoiesis.	Abolishes the expansion, differentiation arrest and erythropoiesis blockage.	[54]
Apoptosis regulatory proteins				
Bcl-2	3	generation of pro-apoptotic fragment	delays apoptosis	[55]
xIAP (53 kDa)	3 and 7	destroys the anti-apoptotic	protects from apoptosis	[56]

		function of xIAP		
Bid	8, 3 and 2	Translocates to mitochondria and induces apoptosis through MOMP	resistant to apoptosis	[57]
Bcl-xl	3	generation of pro-apoptotic fragment and induces apoptosis	delays apoptosis	[58, 59]
Protein kinases and signaling intermediaries				
MEKK-1	3, 7 and 8	increased kinase activity		[60, 61]
AKT	3	Loss of kinase activity and putative loss of survival signaling	prevents apoptosis	[62-64]
CaMKLK	8, 3 and 10	N-terminal fragment is proapoptotic; C-terminal fragment loses kinase activity	reduces apoptosis	[65, 66]
cdc42	3 and 7	allows maximal apoptotic response.	resistance to cell death	[67]
claspin	7 and 3	inhibits Chk1 phosphorylation and checkpoint signaling	degraded by ubiquitin proteasomal complex	[68, 69]
pGDI2	1 and 3	Translocation to nucleus. Loss of Rho GTPase signaling	Does not protect against apoptosis	[70-73]

EGF-R	1, 3 and 7	impaired passing on survival signals	delays apoptosis	74, 75
ErbB2	8	Putative: loss of kinase activity	protects against TNFa mediated cell death.	76, 77
cAbl				
CDK inhibitor 1 p21*WAF1/CIP1*	3	Reduced association with cyclin-cdk2 complexes and increased cdk2 activity.	partially suppress apoptosis	78, 79
PAK-2: p21-activated protein kinase-2	3, less effectively 8 and 10	Increases kinase activity	Reduced levels of spontaneous cell death, consequently increased net cell growth; when treated with cisplatin cell death switch from apoptotic to nonapoptotic, caspase-independent death	80
RIPK1	Caspase 8 (in vivo); 3 and 7 (in vitro)	Inhibits NF-kB Activation	inhibits the apoptosis	66, 81
Proteins involved in human pathology				
Atrophin-1	3, 1, 7 and 8	proapoptotic	complete suppression of apoptotic cell death.	82-84

DJ-1	6	C-terminal fragment has p53-dependent neuroprotective role.	Increases apoptosis	[85]
synphilin-1	3 and 6 (less efficiently)	protects from apoptosis	drastically reduces antiapoptotic phenotype	[86]
Huntingtin	3 and 6	N-terminal fragment is cytotoxic and activates proapoptotic caspases	reduces aggregates formation in parallel with toxicity	[87]
Ataxin-7	7	Proteolytic cleavage products forms aggregates and increased cell death	Attenuates cell death, aggregate formation and transcriptional interference	[88]
Androgen receptor	1, 3 and 8	induces apoptosis	blocks the ability of AR to induce apoptosis	[89]
Par-4	3	promotes apoptosis	Reduction in number of apoptotic cells	[90]

Chapter 4: Abrogation of DNA vector-based RNAi during apoptosis in mammalian cells due to caspase-mediated cleavage and inactivation of Dicer-1

Cell Death and Differentiation (2009) 16, 858–868

4.1 Résumé en français

L'interférence à l'ARN (ARNi) est utilisée comme outil génétique pour analyser les fonctions d'un gène dans différents processus cellulaires incluant l'apoptose. Comme des protéines cellulaires clés sont inactivées durant l'apoptose et comme l'ARNi requière la coopération de ces protéines, nous avons examiné si l'ARNi basée sur un vecteur d'ADN continuait de fonctionner pendant l'apoptose. Le petit ARN en forme d'épingle à cheveux transcrit du vecteur d'ADN est clivé par Dicer-1 afin de former un petit ARN interférant qui sera, par la suite, incorporé dans le complexe *RNA-induced silencing* (RISC) afin de guider la dégradation spécifique *(sequence-specific silencing)* de l'ARNm cible. Nous rapportons içi que l'ARNi basée sur un vecteur d'ADN de trois gènes différents, nommés poly(ADP-ribose) polymérase-1, p14(ARF) et lamine A/C, est supprimée pendant l'apoptose. L'échec de l'ARNi basée sur un vecteur d'ADN n'était pas au niveau de la protéine Ago-2 ou des étapes régulées par RISC, mais due à l'inactivation catalytique de Dicer-1 par un clivage spécifique aux sites STTD(1476) et CGVD(1538) situés dans son domaine RNase IIIa. En utilisant plusieurs approches, la caspase-3 fut identifiée comme la caspase majoritaitement responsable du clivage et de l'inactivation de Dicer-1. Comme Dicer-1 est aussi reconnu comme étant une des endonucléase requise pour la formation des microARN (miARN) dans les cellules de mammifères, nous avons aussi observé une réduction du niveau des formes matures de miR-16, miR-21 et let-7a. Nos résultats suggèrent donc un rôle au clivage apoptotique et à l'inactivation du Dicer-1 dans le contrôle des évènements apoptotiques par l'altération de la disponibilité des miARNs.

4.2 Article

Abrogation of DNA vector-based RNAi during apoptosis in mammalian cells due to caspase-mediated cleavage and inactivation of Dicer-1

Medini M. Ghodgaonkar[1], Rashmi G. Shah[1], Febitha Kandan-Kulangara[1], El-Bachir Affar[2], Hank H. Qi[2], Erik Wiemer[3] and Girish M. Shah[1*]

[1]Laboratory for Skin Cancer Research, CHUL Research Center (CHUQ), Faculty of Medicine, Laval University, Quebec, QC, Canada G1V 4G2, [2]Department of Pathology, Harvard Medical School, Boston, MA 02115, USA and [3]Erasmus Medical Center, Department of Medical Oncology, Josephine Nefkens Institute, GE3000, DR Rotterdam, The Netherlands.

Correspondence: Girish M. Shah, Ph.D.

Tel: (418) 656-4141/Ext. 48259

Fax: (418) 654-2739

E-mail: girish.shah@crchul.ulaval.ca

Running Title: Apoptotic Dicer-1-cleavage and abrogation of shRNA

Note: Present addresses: MMG is at the Institute of Molecular Cancer Research. Zurich, Switzerland, and EBA is at Maisoneuve Rosemont Hospital Research Center, Faculty of Medicine, University of Montreal, Montreal (QC), Canada.

4.3 Abstract

RNA interference (RNAi) is used as a reverse-genetic tool to examine functions of a gene in different cellular processes including apoptosis. Since key cellular proteins are inactivated during apoptosis, and since RNAi requires cooperation of many cellular proteins, we examined whether DNA vector-based RNAi would continue to function during apoptosis. The short hairpin RNA transcribed from the DNA vector is processed by Dicer-1 to form siRNA that is incorporated in the RNA-induced silencing complex (RISC) to guide a sequence-specific silencing of the target mRNA. We report here that DNA vector-based RNAi of three different genes, namely poly(ADP-ribose) polymerase-1, $p14^{ARF}$ and lamin, are abrogated during apoptosis. The failure of DNA vector-based RNAi was not at the level of Ago-2 or RISC-mediated step of RNAi but due to catalytic inactivation of Dicer-1 upon specific cleavage at the $STTD^{1476}$ and $CGVD^{1538}$ sites within its RNase IIIa domain. Using multiple approaches, caspase-3 was identified as the major caspase responsible for the cleavage and inactivation of Dicer-1. Since Dicer-1 is also the common endonuclease required for formation of miRNA in mammalian cells, we observed decreased levels of mature forms of miR-16, miR-21 and let-7a. Our results suggest a role for apoptotic-cleavage and inactivation of Dicer-1 in controlling apoptotic events through altered availability of miRNA.

4.4 Introduction

RNA interference (RNAi) including the miRNA pathway is an evolutionarily conserved mechanism for sequence-specific gene-silencing by small (21-26 nucleotides) guide RNA.[1,2] There are two main types of RNAi-inducing small guide RNA: the endogenously generated microRNA (miRNA) which are derived from long stem-loop structured precursors; and small interfering RNA (siRNA) which may be either exogenously supplied as short or long dsRNA or which may be produced in the cells from a DNA vector-directed short hairpin RNA (shRNA).[2] Regardless of the origin of the small regulatory RNA, the key steps responsible for achieving RNAi are essentially the same and require controlled and coordinated participation of the host-cell machinery. Briefly, different types of precursor RNA, such as the long dsRNA, shRNA transcribed from a DNA vector or pre-processed hairpin pre-miRNA are first converted to small regulatory RNA by the endoribonuclease Dicer-1 in the cytoplasm of mammalian cells. These are then loaded into the RNA effector complexes known as RNA-induced silencing complex (RISC) to guide the machinery to the target mRNA in a sequence-specific manner. Depending on the extent of sequence homology, gene silencing is achieved by cleavage or destabilization of the target cognate mRNA or by inhibition of its translation.[3]

RNAi is increasingly being explored to characterize the roles of miRNA in regulating apoptosis.[3,4] In addition, shRNA based RNAi is also being exploited for understanding the role of a given gene in apoptosis.[5-7] However, since many key cellular proteins are cleaved by caspases during apoptosis,[8] it is pertinent to examine whether apoptotic events compromise the integrity of the core machinery of the RNAi pathway. A recent study reporting specific stimuli-dependent cleavage of Dicer-1 during apoptosis,[9] further warrants a need for characterization of the impact of apoptosis on DNA vector-based RNAi, a process which requires full functionality of Dicer-1-dependent formation of the siRNA from the precursor shRNA and the RISC-dependent silencing of the target mRNA. We used the DNA vector-based RNAi model for three different genes: namely poly(ADP-ribose) polymerase-1 (PARP)[10], a model that has allowed us to reveal its novel

functions in the nucleotide excision repair of UV-damaged DNA,[11] inactivation of X-chromosome[12] and in growth or chemosensitivity of melanoma cells;[13] the mammalian tumor suppressor gene $p14^{ARF}$ and the nuclear protein lamin. We report here that the DNA vector-based RNAi of all three genes is abrogated during apoptosis. We extensively characterized the failure of RNAi and identified its cause to be a specific dual cleavage and catalytic inactivation of Dicer-1. We used multiple approaches to show that caspase-3 is the major caspase responsible for this cleavage and inactivation of Dicer-1. We also show that Dicer-1-cleavage during apoptosis is associated with decreased formation of some of the mature miRNA suggesting a larger role of Dicer-1-cleavage in control of apoptosis.

4.5 Methods

4.5.1 Cells, DNA vector-based RNAi-clones and apoptosis-inducing treatments and Western blotting. Following cell lines were obtained from ATCC (unless specified otherwise) and grown in specified media obtained from GIBCO at 37° C in a humidified incubator with 5% CO_2, supplemented with 10% fetal bovine serum, 50 U/ml penicillin and 50 µg/ml streptomycin: human myeloid leukemic HL-60 (RPMI), human cervical carcinoma HeLa (DMEM-high glucose), monkey kidney COS-1 cells (DMEM-low glucose) and human breast adenoma MCF-7 cells (DMEM-low glucose).

Different stable RNAi-clones were prepared as follows. The PARP-replete (U6) and PARP-depleted (SiP) cell lines derived from human skin fibroblasts (GM637, Coriell Cell Repository, MEM) and Chinese hamster ovary CHO cells (sub-line WT-5, α-MEM) were obtained as described earlier.[10] The human $p14^{ARF}$ expressing cell lines were created by stable transfection of CHO cells with HA tagged $p14^{ARF}$ cloned in pcDNA-3 expression vector (Invitrogen), followed by selection of geneticin (800 µg/ml)-resistant clones. One of the CHO-HA-ARF clones was subsequently transfected with a pBS-U6 vector containing human $p14^{ARF}$-targeting sequence 5'-GAAC ATG GTG CGC AGG TTC TTM-3' along with pTK-Hyg cDNA to isolate stable shARF clones, which were then maintained in medium containing geneticin (400 µg/ml) and hygromycin (200 µg/ml), as described earlier[10.28]. The DNA vector-based RNAi of lamin was achieved in HeLa cells after transfection with pBS-U6 vector containing lamin targeting sequence[29] and pTK-Hyg plasmid to isolate HeLa-shLamin clones that were maintained in medium containing 200 µg/ml hygromycin, as described earlier[10].

Apoptosis was induced by treatment with one of the following reagents: 100 or 300 µM H_2O_2 (Sigma), 1 µM Staurosporin (Sigma), 1,600 J/m^2 UVB (Spectrolinker XL-1000 UV cross-linker), 10 J/m^2 UVC, 10 or 100 µM MNNG (Sigma), 70 or 100 µM etoposide (VP-16) (Sigma), 1200 U/ml TNF□+0.25 µg/ml actinomycin D (Sigma), and 1 or 5 µg/ml

actinomycin D. For in vivo studies with a broad-spectrum caspase-inhibitor, cells were pre-incubated with 50 μM of zVAD-fmk (Calbiochem) at 37°C for 90 min, followed by apoptosis-inducing treatment. Cells were harvested and extracts were analyzed by Western blot.[10]

For the Western blot, the extracts representing 200,000 cells or 20 μg protein were loaded on 6, 8, 12 or 6-15% SDS–PAGE, blotted on nitrocellulose, and probed with following antibodies: PARP (C-2-10, Aparptosis Inc., 1:10,000); 89 kDa-PARP-fragment (Abcam, 1:1,000); human Dicer-1 (Abcam, 1:1,000); human Ago-2 (Wako, 1:200); activated caspases-3 (Cell signaling, 1:1000); activated caspase-7 (Abcam, 1:200); FLAG (Sigma, 1:4,000); HA (Sigma, 1:4,000 or Covance 1:1,000); actin (Sigma, 1:20,000) and GFP (BD Biosciences, 1:5,000).

4.5.2 RNA isolation and RT-PCR. RNA was extracted with RNeasy mini kit (Qiagen). 250 ng of RNA was subjected to RT-PCR using the LightCycler RNA master SyBr green I kit in LightCycler Instrument (Roche) according to manufacturer's protocol. The forward and reverse primers for PARP were: 5'-AGTGACAGGCAAAGGCCAGGA-3' (forward), 5'-CGCACCTGGCCCTTTTCTATC-3' (reverse). The primers of GAPDH were 5'-GAAGGTCGGAGTCACGGATTTGG-3' (forward) and 5'-ACGGTGCCATGGAATTTGCCATGG-3' (reverse). 10μl of the PCR-amplified product was analyzed on 1.5% agarose gel containing ethidium bromide.

4.5.3 Transient knockdown with 21mer siRNA. All transient knockdown experiments were carried out in GM637 cells at 70% confluence in 60 mm dishes. For GFP expression and knockdown studies, a total of 5 μg of pGFP-N1 (Clontech) cDNA (or mock DNA: CMV plasmid) with or without 1 μg of 21mer GFP-targeting siRNA based on the sequence: 5'-GCA AGC UGA CCC UGA AGU UCA U-3' (Qiagen), were transfected by calcium phosphate protocol.[30] At 48h after transfection, cells were treated with 100 μM etoposide for 24h and cells were harvested for Western blotting. For transient knockdown of PARP, GM637 cells were transfected with 600 pmol of 21mer siRNA (IDT)

representing PARP-targeting sequence described for SiP912 vector[10] and 3 μg of pcDNA I/neo using lipofectamine 2000 (Invitrogen). Cells were maintained in 800 μg/ml geneticin for 96h and treated with 100 μM etoposide (VP-16) for 24h, followed by Western blotting.

4.5.4 Wild type and mutant hDicer-1: cloning, expression and immunopurification. The recombinant FLAG-hDicer-1 cDNA was created by in-frame cloning of the cDNA of hDicer-1 in the pCMV-3X-FLAG expression vector (Sigma) just after the 3X-FLAG tag at the 5'-end. The HA tag along with stop codon was inserted in the above cDNA at the 3'-end to create dual tagged FLAG-hDicer-1-HA cDNA. The caspase-uncleavable hDicer-1 D/A mutants were created from dual tagged hDicer-1 cDNA by site-directed mutagenesis (QuikChange-II-XL Site-directed mutagenesis kit, Stratagene). These cDNAs were transiently transfected in COS-1 cells (5-8 μg/10 mm dish) with lipofectamine 2000 (Invitrogen). At 48h after transfection, apoptosis-inducing treatments were carried out as specified for each figure, and cells either harvested for Western blotting or subjected to immunopurification protocol using FLAG or HA-kits (Sigma).

At the end of the immunopurification protocol, the Dicer-1 or its fragments were processed in four different ways for different end-uses. (i) For Western blotting, beads were extracted with SDS-PAGE sample loading buffer and processed for Western blotting. (ii) For the MS-MS analyses, the bead-extracts were prepared as above for Western blotting, resolved on 10% SDS-PAGE and stained with coomassie blue. The bands of interest, identified from a parallel Western blot of the same samples, were excised from the gel and subjected to MS-MS analyses after tryptic digestion at the Taplin Biological Mass Spectrometry Services at the Harvard Medical School. (iii) For some of the in vitro caspase-assays, FLAG-hDicer-1 was eluted from the beads by FLAG-peptide elution protocol (Sigma). (iv) For preparation of the bead-bound Dicer-1 for the in vitro caspase and dicing assays, the beads were washed and suspended at a concentration equivalent of Dicer-1-derived from 0.5×10^6 cells /μl of 50 mM Tris-Cl, pH 7.4 and 150 mM NaCl. The aliquots of bead-bound Dicer-1 were stored frozen at -80°C.

4.5.5 In vitro caspase cleavage assay. For the in vitro cleavage assay with ten caspases, 50 ng of eluted FLAG-hDicer-1 was incubated with 1.5 units of recombinant activated caspase (Biovision) in a 20 µl reaction mixture containing 20 mM PIPES, pH 7.2, 100 mM NaCl, 0.1 % CHAPS, 1 mM EDTA, 10 % sucrose, 10 mM DTT at 37° C for 90 min.[31] An aliquot was analyzed by the Western blot for Dicer-1 and FLAG, as described above.

The in vitro caspase-3-cleavage assay using bead-bound FLAG-hDicer-1 was carried out in a total volume of 5 µl containing above stated caspase-assay buffer[31], 1.5 units of Caspase-3 (Biovision) and 0.5-1 µl of immunobead-bound Dicer-1 that was pre-washed in the caspase-assay buffer. The reaction was carried out at 37° for up to 90 min with intermittent gentle vortexing to resuspend the beads. The reaction was terminated by addition of 5 µl of 2x SDS-PAGE loading buffer and samples were heated at 95°C for 5 min, vortexed and eluted material was loaded on 6% SDS-PAGE, followed by transfer and Western blotting for FLAG or Dicer-1, as described above.

4.5.6 In vitro Dicer-1 activity assays. The catalytic dicing activity of Dicer-1 was measured in an assay derived from Kim et al[19] that examined conversion of 27mer dsRNA substrate to 21mer dsRNA product. The 27mer dsRNA substrate was prepared based on the sequence used in the SiP912 vector for stable knockdown of PARP[10]. The sense oligo: 5'-CAA GCA CAG UGU CAA AGG UUU GGG C-3' and the anti-sense oligo: 3'-CCG UUC GUG UCA CAG UUU CCA AAC CCG-5', obtained from IDT were suspended at 100 µM in RNase-free duplex buffer (100 mM potassium acetate, 30 mM HEPES, pH 7.5), annealed at 94°C for 2 min, followed by gradual cooling at ambient temperature. The 100 µM 27mer dsRNA stocks were stored in aliquots at -30°C. The product 21mer dsRNA duplex was prepared based on PARP-targeting 21mer RNAi sequence[10] using the sense oligo: 5'-CAA GCA CAG UGU CAA AGG UUU-3' and anti-sense oligo: 3'-CCG UUC GUG UCA CAG UUU CCA-5', obtained from IDT and annealed exactly as above for 27mer dsRNA duplex.

For catalytic activity of Dicer-1 without pre-digestion with caspase-3, in a total reaction volume of 5 µl containing 20 mM Tris-Cl, pH 8.0, 200 mM NaCl, 2.5 mM $MgCl_2$ and 1 mM ATP, 25 pmol of 27mer dsRNA was digested with 0.5-1 µl immuno-bead bound

FLAG-hDicer-1, prepared as described above. The reaction was carried out at 37° for up to 16h with intermittent gentle vortexing to resuspend the beads. The samples were mixed with 0.8 µl of 6X DNA gel loading buffer (Fermentas), heated at 95°C for 5 min and electrophoresed on 20% native PAGE in 1X TBE at 280 V for 70 min. The gel was stained in 0.5 µg/ml ethidium bromide for 30 min followed by two five-minute washes with water and visualized on ChemiGenius 2 (SynGene).

For the dicing activity assays after pre-digestion of Dicer-1 with caspase-3, the caspase-3 digestion in vitro was carried out for 90 min exactly as described above for immuno-bead bound Dicer-1, and reagents were washed away by adding 100 µl dicer activity assay buffer (20 mM Tris-Cl, pH 8.0, 200 mM NaCl, 2.5 mM $MgCl_2$ and 1 mM ATP). The supernatant was discarded after centrifugation at 12,000g for 2 min, and the bead-bound digested Dicer-1 was suspended in 5 µl of dicing activity assay buffer to carry out the dicing reaction with 27mer dsRNA substrate, as described above.

For dicing activity assay using cell extracts, the enzymatically active cell extracts were prepared from control or apoptotic GM637cells, based on a modified protocol of Billy et al.[32] Briefly, cells were scraped in the medium, centrifuged at 500*g* for 5 min, washed twice with cold PBS and suspended in 50 mM Tris-Cl, pH 7.5 containing 150 mM NaCl, 2.5 mM $MgCl_2$, 5.5 mM DTT and EDTA-free protease inhibitor cocktail. Cells were lysed on ice by mild sonication using microtip probe for 2x15 sec at 11 setting in Sonic Dismembranator (Fisher Scientific). The supernatant obtained after centrifugation at 16,000*g* for 5min was supplemented with glycerol (10% v/v) and stored in aliquots at -30°C. The Dicer assay in vitro was carried out as described earlier. In brief, the cell extracts were adjusted to 1 mg protein/ml and 25 µl of extract was incubated with 125 pmol of 27mer dsRNA substrate at 37°C. At the end of the specified incubation period, 2.5 µl aliquots were resolved on 3.5-20% non-denaturing PAGE, and RNA was visualized by staining with 0.5 µg/ml ethidium bromide.[19]

4.5.7 miRNA extraction and Northern blot. The total miRNA was extracted from HL-60 cells using the mirVana PARIS kit (Ambion) according to manufacturer's protocol. 2 µg

small RNA was resolved on 15 % PAGE in 6M urea in 1x Tris-borate-EDTA and transferred to charged nylon (Brightstar, Ambion). Two miRNA-specific DNA probes (Invitrogen) were based on sequences derived from http://microrna.sanger.ac.uk: Hsa-let-7a (5' TGAGGTAGTAGGTTGTATAGTTTTTTCCTGTCTC 3') and Hsa-miR-21 (5' TAGCTTATCAGACTGATGTTGATTTTTTTTCCTGTCTC 3'). The RNA probe for Hsa-miR-16 (5'-GGGAGACAGGCGCCAAUAUUUACGUGCUGCUA-3') was obtained from Ambion. The DNA and RNA-probes were end-labeled with KinaseMax 5'-End-Labeling kit (Ambion). The Northern blots of total miRNA were probed with ^{32}P-labelled probes prepared for each of the three miRNA according to manufacturer's instructions. The images were analyzed by Storm 860 with ImageQuant TL software (Amersham Pharmacia Biotech).

4.6 Results

4.6.1 Abrogation of DNA vector-based RNAi of PARP during apoptosis

The effect of apoptotic events on the efficacy of DNA vector-based RNAi was examined first in our earlier reported[10] PARP-replete (GMU6) or PARP-depleted (GMSiP) human skin fibroblasts (**Fig. 4.1a**). The induction of apoptosis by treatment with different agents was accompanied by cleavage/activation of caspase-3 to its large subunit at 17/19 kDa; and cleavage of PARP to its apoptosis-signature 89 kDa fragment in GMU6 cells (**Fig. 4.1a**, lanes 1-4). The GMSiP cells, which were devoid of PARP before apoptosis, surprisingly displayed 89 kDa PARP-fragment during apoptosis (**Fig. 4.1a**, lanes 5-8). The probing with an 89 kDa PARP-fragment-specific antibody confirmed that this major band in apoptotic GMSiP cells co-migrated with the band in the apoptotic HL-60 or GMU6 cells (**Fig. 4.1b** and supplementary **Fig. 4S1a**).

For an 89 kDa PARP-fragment to appear in PARP-depleted GMSiP cells, full length PARP has to be made, which suggests that PARP-mRNA must no longer be subjected to degradation by RNAi. This was verified by analyzing the abundance of PARP-transcripts by RT-PCR (**Fig. 4.1c**). The signal for PARP-mRNA remained almost unchanged in UVB-treated GMU6 cells, but it went from undetectable amounts at 0 h to a significant increase at 48 h in UVB-treated GMSiP cells. The reappearance of mRNA and the presence of caspase-cleaved 89 kDa PARP-fragment confirmed that DNA vector-based RNAi of PARP was abrogated in the apoptotic GMSiP cells.

That apoptosis-associated failure of DNA vector-based RNAi of PARP was not specific for GM-model was confirmed in PARP-depleted CHO-SiP cells[10] (**Fig. 4.1d**). Different apoptosis-inducing treatments resulted in a dose-dependent increase in activated caspase-3 in both the PARP-phenotypes, and cleavage of PARP to its 89 kDa fragment in PARP-replete CHO-U6 cells (**Fig. 4.1d**, PARP lanes 2-5). However, emergence of the 89 kDa fragment of PARP in the PARP-depleted CHO-SiP cells during apoptosis (Fig. 4.1d, PARP lanes 7-10) confirmed a general nature of apoptosis-associated failure of DNA vector-based RNAi of PARP in mammalian cells.

4.6.2 Failure of DNA vector-based RNAi of $p14^{ARF}$ and lamin during apoptosis

We next examined whether apoptosis-associated abrogation of DNA vector-based RNAi would also occur for two other genes, namely human tumor suppressor gene $p14^{ARF}$ and lamin (**Fig. 4.2a-b** and supplementary **Fig. 4S1b-c**). We generated stable CHO-ARF clone which expressed HA-tagged human $p14^{ARF}$ and corresponding stable CHO-ARF-shARF clone in which HA-ARF was significantly knocked-down by DNA vector-based RNAi (**Fig. 4.2a**, HA lanes 1, 2 and 6). Induction of apoptosis in CHO-ARF cells by different agents resulted in formation of activated caspase-3 accompanied by a significant increase in HA-ARF (**Fig. 4.2a**, HA lanes 3-5), which could be reflecting a transcriptional upregulation similar to that reported for its mouse homolog $p19^{ARF}$ during apoptosis[14]. Interestingly, in the apoptotic shARF cells, there was a robust reappearance of the HA-ARF along with activation of caspase-3 (**Fig. 4.2a**, lanes 7-9), which clearly indicated failure of DNA vector-based RNAi permitting formation of full length of HA-$p14^{ARF}$.

The lamins A/C, two alternately spliced ~70 kDa proteins arising from a single gene locus, are cleaved by caspase-3-activated caspase-6 to liberate 45 and 28 kDa fragments.[15] Using DNA vector-based RNAi, we generated a HeLa derived shLamin clone with ~75% lamin-knockdown (**Fig. 4.2b**, lamin lanes 1 and 5). Induction of apoptosis in both the lamin-phenotypes by various agents was associated with activation of caspase-3 and cleavage of PARP to its 89 kDa fragment (**Fig. 4.2b**, caspase-3 and PARP panels). Lamins A/C were also cleaved to their ~28 kDa Δlamin fragment in the apoptotic HeLa cells with a ratio of 0.2-0.5 for Δlamin/intact lamins. In contrast, there was a much stronger presence of Δlamin fragment during apoptosis in the shLamin cells, which was evident from higher (4.3 and 0.9) ratio of Δlamin/intact lamins during stronger apoptosis-inducing treatments with UVB or staurosporin (**Fig. 4.2b**, lamin panel). A significantly larger presence of Δlamin indicated that more lamins were being formed and degraded in apoptotic shLamin cells. The apoptosis-associated abrogation of DNA vector-based RNAi of three different genes in different models of apoptosis indicates a universal nature of this observation.

4.6.3 No impact of apoptosis on RISC-dependent RNAi by 21mer siRNA

The abrogation of DNA vector-based RNAi could be caused by failure of one or both the key steps of RNAi, namely Dicer-1-mediated formation of 21mer siRNA from DNA vector-derived shRNA or the RISC-mediated inactivation of the target mRNA. To distinguish between these two steps, we examined the impact of apoptosis on RISC-dependent and Dicer-independent transient RNAi by 21mer siRNA of GFP and PARP (**Fig. 4.2c**). A high level of GFP-expression achieved in the GFP cDNA-transfected human skin fibroblasts GM637 was significantly suppressed by co-transfection with GFP-targeting 21mer siRNA (**Fig. 4.2c**, GFP lanes 2, 4 and 6). Induction of apoptosis by etoposide resulted in a strong caspase-3 activation, but it was not accompanied by any change in the status of GFP-knockdown (**Fig. 4.2c**, lanes 6-7). Similarly, a significant PARP-knockdown achieved by its corresponding 21mer siRNA was not abrogated during etoposide-induced apoptosis, because the signal for its 89 kDa fragment appeared to be mainly due to partial digestion of the residual PARP in these cells after knockdown (**Fig. 4.2c**, lanes 10-11). Thus, unlike the SiP model in which the emergence of the 89 kDa PARP-fragment during apoptosis was due to the failure of stable shRNA, the feeble appearance of the 89 kDa PARP-fragment in the transient knockdown model was not due to the failure of 21mer siRNA during apoptosis. Although one could not exclude subtle differences in the influence of apoptotic events on the transient knockdown of an exogenous gene GFP versus an endogenous gene PARP, our collective results revealed a general lack of effect of apoptosis on RISC-dependent RNAi by 21mer siRNA. Thus, abrogation of DNA vector-based RNAi must be due to failure of events upstream of the RISC-step.

4.6.4 Selective cleavage of endonuclease Dicer-1 during apoptosis

The caspases strategically cleave a selected number of proteins to facilitate apoptosis,[8] hence we examined integrity of the principal RNases implicated in the two key steps of DNA vector-based RNAi in mammalian cells, namely Dicer-1 and RISC-member Ago-2.[16] In two of the human cell line models described above (GMSiP and HeLa-shLamin), apoptosis had no effect on the integrity of Ago-2, whereas the 230 kDa Dicer-1 was cleaved to a ~180 kDa ΔDicer-1 fragment (**Figs. 4.3a and 4.3b**). Due to lack of

specific antibody, we could not confirm Dicer-1-cleavage in hamster (CHO) model, but we reasoned that this cleavage must be a general phenomenon unrelated to the role of Dicer-1 in RNAi. Hence we examined integrity of Ago-2 and Dicer-1 in two of the well-established models of apoptosis, i.e., HL-60 (**Fig. 4.3c**) or HeLa (**Fig. 4.3d**) cells. The time-course of apoptosis in response to treatment with diverse agents revealed that once caspase-3 was activated, PARP was cleaved to its 89 kDa apoptotic fragment. In these models, Ago-2 remained intact, whereas Dicer-1 was cleaved to its 180 kDa fragment (**Figs. 4.3c and 4.3d**), confirming universal nature of Dicer-1-cleavage to a 180 kDa fragment during apoptosis in human-derived cells.

4.6.5 Identification of caspase responsible for cleavage of Dicer-1 during apoptosis

To examine if any of the caspases were responsible for cleavage of Dicer-1 during apoptosis, we used three independent approaches, namely broad-spectrum caspase-inhibitor, in vitro caspase assays and a caspase-deficient cell line. The broad-spectrum caspase-inhibitor zVAD-fmk could efficiently suppress caspase-3-activation and cleavage of Dicer-1 during staurosporin-induced apoptosis in COS-1 cells (**Fig. 4.4a**).

To identify the specific caspase responsible for Dicer-1-cleavage, an immunopurified N-terminal FLAG-tagged Dicer-1 was cleaved by caspases-1 to 10 in vitro (**Fig. 4.4b**). As a positive control for the in vitro caspase-assay, we confirmed that caspases-3 and 7 could cleave PARP to its signature 89 kDa fragment[17] (**Fig. 4.4b**, top panel). The caspase-cleavage products of N-terminal FLAG-tagged hDicer-1 were identified by probing with anti-Dicer 1 antibody that recognizes an epitope in the N-terminal half of the protein and the anti-FLAG antibody that detects N-terminal FLAG (**Fig. 4.4b**). The probing with anti-Dicer-1 antibody revealed that almost all caspases, notably 1, 3, 5 and 7, could generate some amount of ~180 kDa Dicer-1 fragment (**Fig. 4.4b**: Dicer-1 panel). The FLAG-probing, however, revealed that only caspases-3, 5 and 7 generated major FLAG-positive bands at about 180, 150 and 130 kDa, respectively (**Fig. 4.4b**: FLAG-panel). Thus, only caspase-3-cleavage resulted in a major 180 kDa Dicer-1 fragment with an intact N-terminal FLAG, whereas other caspases had additional cleavages at the N- or C-termini.

To identify which of these cleavage patterns in vitro reflected cellular cleavage of Dicer-1, we examined apoptotic-cleavage of hDicer-1 tagged with N-terminal FLAG and C-terminal HA after its expression in COS-1 cells (**Fig. 4.4c**). The intact hDicer-1, detectable by both FLAG and HA-antibodies in the untreated cells, was degraded to a FLAG-positive 180 kDa and HA-positive major ~42 kDa and minor ~50 kDa fragments during apoptosis (**Fig. 4.4c**, lanes 2 and 4). The formation of a FLAG-positive 180 kDa ΔDicer-1 fragment with an intact N-terminus in apoptotic cells was consistent with caspase-3 digestion of Dicer-1 in vitro.

Finally, we examined if Dicer-1 would be cleaved during apoptosis in caspase-3-deficient[18] MCF-7 cells (**Fig. 4.4d**). During staurosporin or actinomycin-induced apoptosis, there was a caspase-7-activation and cleavage of PARP to its 89 kDa fragment, but Dicer-1 was not cleaved to its 180 kDa fragment. Collectively, these results indicated that caspase-3 is the major, if not the only, caspase responsible for cleavage of Dicer-1 to its 180 kDa N-terminal fragment during cellular apoptosis.

4.6.6 Identification of apoptotic cleavage sites in Dicer-1

To identify the apoptotic cleavage-sites of FLAG-hDicer-1-HA, the N-terminal 180 kDa and C-terminal 42 kDa fragments, immunoprecipitated following experimental conditions similar to that in Fig. 4c, were subjected to mass spectrometry analyses after tryptic digestion. In the 180 kDa fragment, there was a continuous presence of the tryptic fragments from the N-terminus up to STTD^{1476}, whereas ^{1578}AAQL was the first tryptic fragment in the C-terminal 42 kDa fragment, indicating that cleavage occurred between these two sites in RNase IIIa domain of Dicer-1 (Supplementary Fig. 4S2).

There are at least seven putative caspase-cleavage XXXD motifs[8] in this region where a cleavage at D could give rise to 42 or 50 kDa C-terminal fragment (**Fig. 4.5a**). These seven D residues were mutated to A and single mutants were expressed in COS-1 cells which were subjected to apoptosis. Five of these D/A mutations could not prevent

cleavage of Dicer-1 (data not shown), but mutations at D^{1476} and D^{1538} sites altered the cleavage of hDicer-1 (**Fig. 4.5b**). The $STTD^{1476}$/A mutant Dicer-1 was cleaved to generate a FLAG-positive ~180 kDa and HA-positive ~42 kDa fragment, whereas $CGVD^{1538}$/A mutant was cleaved to generate FLAG-positive ~180 kDa and HA-positive ~50 kDa fragments upon induction of apoptosis and activation of caspase-3 (**Fig. 4.5b**, lanes 6 and 8). Therefore, we created and expressed in COS-1 cells, a double mutant D^{1476}/A:D^{1538}/A Dicer-1, which turned out to be completely resistant to cleavage during apoptosis generating neither FLAG nor HA-positive fragments (**Fig. 4.5b**, lanes 9-10). Thus, hDicer-1 is cleaved in the apoptotic COS-1 cells at $STTD^{1476}$ to release 50 kDa C-terminal and 180 kDa N-terminal ΔDicer-1 fragments; and C-terminal 50 kDa fragment is further cleaved at $CGVD^{1538}$ to release 42 kDa fragment **(Fig. 4.5c**).

4.6.7 Inactivation of Dicer-1 and decreased miRNA-formation during apoptosis

As both the cleavage sites of Dicer-1 are located in the catalytically important RNase IIIa domain of hDicer-1, we examined its impact on the catalytic function of Dicer-1 in a dicing assay in vitro to convert a 27mer substrate dsRNA to its product 21mer dsRNA.[19] Due to incompatibility of reagents between caspase and dicing assays, these assays were optimized using FLAG antibody-beads-bound Dicer-1, so as to wash away reagents after each assay. Incubating bead-bound Dicer-1 with caspase-3 resulted in formation of a FLAG and Dicer-1-positive ΔDicer-1, which was also retained on the FLAG-beads (**Fig. 4.6a**). The bead-bound intact Dicer-1 was enzymatically active as it converted 27mer dsRNA to 21mer dsRNA in the dicing assay (**Fig. 4.6b**). That caspase-3-digestion decreased catalytic activity of Dicer-1 was evident from its slower capacity to convert 27mer to 21mer dsRNA from 3-6h, as compared to intact Dicer-1 (**Fig. 4.6c**, lanes 2-3 and 6-7). The caspase-3-digested Dicer-1 preparation could eventually convert all the 27mer substrate by 16h due to the residual intact Dicer-1.

Next, we examined dicing activity in the extracts from control or apoptotic GM637 cells, which had either intact or partially cleaved Dicer-1, respectively (**Fig. 4.6d**, left

panel). While the control cell-extract efficiently converted 27mer to 21mer dsRNA from 1-3 h, the apoptotic cell extract failed to convert the substrate up to 3h (**Fig. 4.6d**, right panel). A more robust inhibition of dicing activity in the apoptotic cell extract, despite the presence of some intact Dicer-1, reflects additional factors that may negatively influence Dicer-1 activity in apoptotic cells, as compared to assays with in vitro partially cleaved Dicer-1 (see discussion). Thus, cleavage of Dicer-1 in apoptotic cells or in vitro by casapse-3 was associated with its catalytic inactivation, which could explain the failure of DNA vector-based RNAi during apoptosis.

Unlike other organisms, mammalian cells have only one Dicer-homolog (Dicer-1) for both the siRNA production and for the conversion of the pre-miRNA into mature miRNA.[16] Hence we examined whether Dicer-1 cleavage and inactivation would also influence maturation of three apoptosis-related miRNAs, namely pro-apoptotic miR-16 that regulates anti-apoptotic bcl-2 gene,[20] anti-apoptotic miR-21[21,22] and let-7a miRNA that is both pro-[23] and anti-apoptotic[24] (**Fig. 4.6e**). In the apoptotic HL-60 cells, there was a decline in the levels of these three mature miRNAs from 6-24h (**Fig. 4.6e**, left panel). The quantification of signal for miRNA from two independent experiments showed nearly 40-60% decrease in the signal for these miRNAs at 18-24h (**Fig. 4.6e**, right panel). Thus, another consequence of Dicer-1 cleavage by caspase-3 during apoptosis was reduced availability of some of the mature miRNA.

4.7 Discussion

We report here that stable knockdown by DNA vector-based RNAi is abrogated during apoptosis in mammalian cells. The data obtained with various cell lines, different apoptosis-inducing treatments and failure of RNAi of three different genes, namely PARP, lamin and $p14^{ARF}$, indicate universal nature of this observation irrespective of the fate or function of the target gene-product during apoptosis. That the transient RNAi achieved with 21mer siRNA was not affected during apoptosis indicated that RISC-dependent part of RNAi pathway does not fail during apoptosis. Our results can not exclude the possibility that RISC complex rapidly loaded with 21mer siRNA immediately after transfection could continue to function during apoptosis; however our observation that Ago-2 remains intact during apoptosis supports the argument that RISC-dependent step of RNAi is not affected during apoptosis.

Using in vitro caspase assays, in vivo apoptotic cleavage of wild type and mutant forms of tagged hDicer-1 and caspase-3-deficient MCF-7 cells, we show that Dicer-1 is specifically cleaved at two sites $STTD^{1476}$ and the $CGVD^{1538}$ within the RNase IIIa domain principally by caspase-3. A recent study has reported cleavage of Dicer-1 during apoptosis at the $DHPD^{1644}$ site.[9] However, our results show that it is unlikely to be the main cleavage site of Dicer-1, because: (a) cleavage at this site would result in a C-terminal fragment of ~278 aa or ~32 kDa, whereas we identified 42 or 50 kDa C-terminal fragments; (b) we show that D/A mutations at $STTD^{1476}$ and $CGVD^{1538}$ sites completely abolish Dicer-1-cleavage during apoptosis, whereas $DHPD^{1644}$/A mutation could not block Dicer-1-cleavage;[9] (c) the MS-MS analyses of C-terminal 42 kDa fragment revealed tryptic fragments starting at ^{1578}AAQL, which is ~80 aa residues upstream of the $DHPD^{1644}$ site. The earlier study also reported that Dicer-1 is cleaved by either caspases-3 or 7,[9] whereas, we provide a reasonable proof using various approaches that cellular cleavage of Dicer-1 is consistent with its cleavage by caspase-3.

For many of the proteins cleaved at specific sites by caspases, the end-result is either a strategic activation or inactivation of their function, which could either facilitate apoptosis or prevent the anti-apoptotic activity of the target protein.[8] Our study provides the first definitive proof of catalytic inactivation of Dicer-1 during apoptosis. We show that

caspase-3 mediated cleavage of Dicer-1 in vitro reduces its catalytic activity, and that apoptotic cell extracts with cleaved ΔDicer-1 have a robust inhibition of catalytic dicing activity despite the presence of some intact Dicer-1. The latter suggests that additional events during apoptosis or presence of the cleaved fragments of Dicer-1 could contribute towards inactivation of catalytic activity of Dicer-1 during apoptosis (see below).

The cleavage of Dicer-1 at two distinct sites STTD^{1476} and CGVD^{1538} within RNase IIIa domain, allows us to propose a model for its catalytic inactivation during apoptosis. The structural studies with Giardia Dicer[25] and human Dicer or bacterial RNase III[26,27] suggest that RNase IIIa and IIIb domains of hDicer-1 form an intramolecular dimer, which with the help of PAZ and dsRBD domains cleave the long dsRNA substrate to the 21mer dsRNA. The catalytic centre of Dicer is composed of two sets of identical motifs located in RNase IIIa and IIIb domains. These motifs with a conserved D or E residues are EXXX<u>D</u>^{1320} and DXX<u>E</u>^{1564} in RNase IIIa domain and EXXX<u>D</u>^{1709} and DXX<u>E</u>^{1813} in RNase IIIb domain. These four motifs allow Dicer to precisely touch the proximal or distal end of the cleavage sites on the long dsRNA substrate; hence mutations at D or E residues in all four or even two of these motifs could abolish or significantly suppress catalytic function of Dicer-1.[27] Therefore, cleavage of Dicer-1 at D^{1476} and D^{1538} by caspase-3 would result in separation of EXXXD^{1320} motif from the DXXE^{1564} motif within the RNase IIIa domain and inactivation of Dicer-1. Our results also suggest that neither the 180 kDa ΔDicer-1 containing one catalytic motif EXXXD^{1320} nor the 42 kDa C-terminal fragment containing the remaining three catalytic motifs can precisely carry out the catalytic function of full Dicer-1. In addition, it is possible that these two enzyme-dead fragments of Dicer-1 can cause trans-dominant inhibition of the residual intact Dicer-1 due to their potential to interact with the dsRNA substrates or other RNAi-proteins including the RISC complex.

Finally, the cleavage and inactivation of Dicer-1 during apoptosis would have two major consequences: (a) abrogation of DNA vector-based RNAi could influence results obtained with stable shRNA models that examine apoptosis; and (b) reduced availability of mature miRNA may be of major consequence for miRNA-mediated control of apoptosis and cancer, since several miRNAs act as positive and negative regulators of cell death.[4]

4.8 Acknowledgments

We are grateful to Véronique Richard for technical help. We are thankful to Martin Simard and Michele Rouleau of Laval University for helpful discussion and G. Sui for shRNA constructs of ARF. We are thankful to Ross Tomaino of Taplin Biological Mass Spectrometry Facility at the Harvard Medical School for MS-MS analyses and interpretation of results. This work was supported by the research grants to GMS from Natural Sciences and Engineering Research Council of Canada (155257-06) and the National Cancer Institute of Canada with the funds from the Canadian Cancer Society (NCIC-16407). HHQ and FKK were supported by a CIHR-post-Doctoral fellowship and an NSERC-Doctoral scholarship awards, respectively. EBA and GMS were supported by a FRSQ-Junior-1 Scientist and FRSQ-Senior Scientist awards, respectively from the Fonds de la Recherche en Santé du Québec.

4.9 References

1. Filipowicz, W, Jaskiewicz, L, Kolb, FA and Pillai, RS, (2005) Post-transcriptional gene silencing by siRNAs and miRNAs. Curr Opin Struct Biol 15: 331-41.

2. Shi, Y, (2003) Mammalian RNAi for the masses. Trends Genet 19: 9-12.

3. Jovanovic, M and Hengartner, MO, (2006) miRNAs and apoptosis: RNAs to die for. Oncogene 25: 6176-87.

4. Wiemer, EA, (2007) The role of microRNAs in cancer: no small matter. Eur J Cancer 43: 1529-44.

5. Yuan, J, Kramer, A, Matthess, Y, Yan, R, Spankuch, B, Gatje, R et al., (2006) Stable gene silencing of cyclin B1 in tumor cells increases susceptibility to taxol and leads to growth arrest in vivo. Oncogene 25: 1753-62.

6. Gonzalez, S, Perez-Perez, MM, Hernando, E, Serrano, M and Cordon-Cardo, C, (2005) p73beta-Mediated apoptosis requires p57kip2 induction and IEX-1 inhibition. Cancer Res 65: 2186-92.

7. Zhang, M, Zhou, Y, Xie, C, Zhou, F, Chen, Y, Han, G et al., (2006) STAT6 specific shRNA inhibits proliferation and induces apoptosis in colon cancer HT-29 cells. Cancer Lett 243: 38-46.

8. Fischer, U, Janicke, RU and Schulze-Osthoff, K, (2003) Many cuts to ruin: a comprehensive update of caspase substrates. Cell Death Differ 10: 76-100.

9. Matskevich, AA and Moelling, K, (2008) Stimuli-dependent cleavage of Dicer during apoptosis. Biochem J 412: 527-534.

10. Shah, RG, Ghodgaonkar, MM, Affar, EB and Shah, GM, (2005) DNA vector-based RNAi approach for stable depletion of poly(ADP-ribose) polymerase-1. Biochem Biophys Res Commun 331: 165-174.

11. Ghodgaonkar, MM, Zacal, NJ, Kassam, SN, Rainbow, AJ and Shah, GM, (2008) Depletion of poly(ADP-ribose)polymerase-1 reduces host cell reactivation for UV-treated adenovirus in human dermal fibroblasts. DNA Repair (Amst) 7: 617-632.

12. Nusinow, DA, Hernandez-Munoz, I, Fazzio, TG, Shah, GM, Kraus, WL and Panning, B, (2007) Poly (ADP-ribose) polymerase 1 is inhibited by a histone H2A variant, MACROH2A, and contributes to silencing of the inactive X chromosome. J. Biol. Chem. 282: 12851-12859.

13. Tentori, L, Muzi, A, Dorio, AS, Bultrini, S, Mazzon, E, Lacal, PM et al., (2008) Stable depletion of poly (ADP-ribose) polymerase-1 reduces in vivo melanoma growth and increases chemosensitivity. Eur J Cancer 44: 1302-1314.

14. Zeini, M, Traves, PG, Lopez-Fontal, R, Pantoja, C, Matheu, A, Serrano, M et al., (2006) Specific contribution of p19(ARF) to nitric oxide-dependent apoptosis. J Immunol 177: 3327-36.

15. Ruchaud, S, Korfali, N, Villa, P, Kottke, TJ, Dingwall, C, Kaufmann, SH et al., (2002) Caspase-6 gene disruption reveals a requirement for lamin A cleavage in apoptotic chromatin condensation. Embo J 21: 1967-77.

16. Cerutti, H and Casas-Mollano, JA, (2006) On the origin and functions of RNA-mediated silencing: from protists to man. Curr Genet 50: 81-99.

17. Germain, M, Affar, EB, D'Amours, D, Dixit, VM, Salvesen, GS and Poirier, GG, (1999) Cleavage of automodified poly(ADP-ribose) polymerase during apoptosis. Evidence for involvement of caspase-7. J Biol Chem 274: 28379-84.

18. Janicke, RU, Sprengart, ML, Wati, MR and Porter, AG, (1998) Caspase-3 is required for DNA fragmentation and morphological changes associated with apoptosis. J Biol Chem 273: 9357-60.

19. Kim, DH, Behlke, MA, Rose, SD, Chang, MS, Choi, S and Rossi, JJ, (2005) Synthetic dsRNA Dicer substrates enhance RNAi potency and efficacy. Nat Biotechnol 23: 222-226.

20. Cimmino, A, Calin, GA, Fabbri, M, Iorio, MV, Ferracin, M, Shimizu, M et al., (2005) miR-15 and miR-16 induce apoptosis by targeting BCL2. Proc Natl Acad Sci U S A 102: 13944-9.

21. Chan, JA, Krichevsky, AM and Kosik, KS, (2005) MicroRNA-21 is an antiapoptotic factor in human glioblastoma cells. Cancer Res 65: 6029-33.

22. Meng, F, Henson, R, Lang, M, Wehbe, H, Maheshwari, S, Mendell, JT et al., (2006) Involvement of human micro-RNA in growth and response to chemotherapy in human cholangiocarcinoma cell lines. Gastroenterology 130: 2113-29.

23. Johnson, SM, Grosshans, H, Shingara, J, Byrom, M, Jarvis, R, Cheng, A et al., (2005) RAS is regulated by the let-7 microRNA family. Cell 120: 635-47.

24. Meng, F, Henson, R, Wehbe-Janek, H, Smith, H, Ueno, Y and Patel, T, (2007) The MicroRNA let-7a modulates interleukin-6-dependent STAT-3 survival signaling in malignant human cholangiocytes. J Biol Chem 282: 8256-64.

25. Macrae, IJ, Zhou, K, Li, F, Repic, A, Brooks, AN, Cande, WZ et al., (2006) Structural basis for double-stranded RNA processing by Dicer. Science 311: 195-8.

26. Gan, J, Tropea, JE, Austin, BP, Court, DL, Waugh, DS and Ji, X, (2006) Structural insight into the mechanism of double-stranded RNA processing by ribonuclease III. Cell 124: 355-66.

27. Zhang, H, Kolb, FA, Jaskiewicz, L, Westhof, E and Filipowicz, W, (2004) Single processing center models for human Dicer and bacterial RNase III. Cell 118: 57-68.

28. Sui, G, Affar el, B, Shi, Y, Brignone, C, Wall, NR, Yin, P et al., (2004) Yin Yang 1 is a negative regulator of p53. Cell 117: 859-72.

29. Sui, G, Soohoo, C, Affar, EB, Gay, F, Shi, Y, Forrester, WC et al., (2002) A DNA vector-based RNAi technology to suppress gene expression in mammalian cells. Proc Natl Acad Sci U S A 99: 5515-5520.

30. Ausubel, FM, Brent, R, Kingston, RE, Moore, DD, Seidonan, JG, Smith, JA et al., (1992) Introduction of DNA into mammalian cells. Ausubel, F. M. et al. eds (John Wiley & Sons, New York).

31. Stennicke, HR and Salvesen, GS, (1997) Biochemical characteristics of caspases-3, -6, -7, and -8. J Biol Chem 272: 25719-23.

32. Billy, E, Brondani, V, Zhang, H, Muller, U and Filipowicz, W, (2001) Specific interference with gene expression induced by long, double-stranded RNA in mouse embryonal teratocarcinoma cell lines. Proc Natl Acad Sci U S A 98: 14428-33.

4.10 Legends to the figures

Fig. 4.1. Abrogation of DNA vector-based RNAi of PARP during apoptosis. (a) Failure of RNAi of PARP in GMSiP cells. In the stable PARP-replete GMU6 and PARP-depleted GMSiP human skin fibroblasts, apoptosis was induced by treatment with 100 μM VP-16 for 18h, 1200 Units/ml TNAF□□+ 0.25 μg/ml actinomycin D for 18h or 1,600 J/m^2 UVB for 48h. Whole cell extracts were immunoblotted with cleaved/activated caspase-3 antibody that detects the larger 19/17 kDa fragment of caspase-3 and with a monoclonal antibody to PARP that detects both the full length PARP and its 89 kDa apoptotic-fragment. Actin immunoprobing served as loading-control and results shown here represent similar results obtained with at least five independent experiments. (b) Identification of 89 kDa PARP-fragment in apoptotic GMSiP cells. The cell extracts from GMU6 and GMSiP cells treated with apoptosis-inducing treatments as described above were probed with antibody specific for the 89 kDa apoptotic fragment of PARP. The Ap lane refers to extract from apoptotic HL-60 cells treated with 70 μM etoposide for 8h. The ponceau-S staining of the blot served as loading control (see supplementary Fig. S1a). The results shown here represent similar results obtained with three independent experiments. (c) Emergence of PARP-mRNA in apoptotic GMSiP cells. GMU6 and GMSiP cells were irradiated with 1,600 J/m^2 UVB and at indicated time-points, RNA was extracted and analyzed by RT-PCR. Upper panels indicate the levels of PARP-mRNA while lower panel indicates the levels of GAPDH-mRNA, which was used as a control. The results shown here represent similar results obtained with two independent experiments. (d) Failure of PARP-RNAi in CHO-SiP cells. PARP-replete CHO-U6 and PARP-depleted CHO-SiP cells were treated with two doses of MNNG or H_2O_2 for 24h and immunoblotted for caspase-3 and PARP. Actin was probed as loading control and Ap refers to apoptotic HL-60 cells, as described above for panel b. The results shown here represent similar results obtained with three independent experiments.

Fig. 4.2. Apoptosis-associated failure of stable shRNA of p14^{ARF} and lamin but not that of transient RNAi of GFP and PARP by 21mer siRNA. (a) Failure of shRNA of HA-p14^{ARF}. The CHO-ARF clone expressing HA-tagged human p14^{ARF} or CHO-ARF-shARF clone in which the HA-ARF expression was knocked down by DNA vector-based RNAi were treated with 1,600 J/m^2 UVB for 32h, 1 μM staurosporin for 18h or 100 μM etoposide (VP-16) for 32h. The cell extracts were immunoblotted for HA and activated caspase-3. Actin immunoprobing served as loading-controls and Ponceau-S membrane-staining is shown in supplementary Fig. S1b. The results shown here represent similar results obtained with three independent experiments. (b) Failure of shRNA of lamin in HeLa-shLamin cells. The lamin-replete HeLa cells and lamin-depleted HeLa-shLamin cells were treated with three apoptosis-inducing treatments, as described above for shARF panel. The immunoprobing was carried out for lamin, activated caspase-3, and PARP. The ratio of ΔLamin/lamins A/C was derived from densitometric measurement of the signals for these bands. Actin immunoprobing served as loading-controls and Ponceau-S membrane-staining is shown in supplementary Fig. S1c. The results shown here represent similar results obtained with three independent experiments. (c) Lack of failure of transient RNAi of GFP and PARP by 21mer siRNA during apoptosis. GM637 cells were transiently transfected with cDNA of GFP ± GFP-targeting 21mer dsRNA (left panel) or with pcDNA I/neo ± PARP-targeting 21mer dsRNA (right panel) for 48 or 96h, respectively, followed by treatment with 100 μM etoposide (VP-16) for 18 or 24h, respectively. The cell extracts were immunoblotted for activated caspase-3 and GFP or PARP. The results shown here represent similar results obtained with at least three independent experiments.

Fig. 4.3. Cleavage of Dicer-1 in human cell lines undergoing apoptosis. (a) GMU6 and GMSiP; (b) HeLa and HeLa-shLamin; (c) HL-60 and (d) HeLa were treated with different apoptosis-inducing conditions as follows. The GMU6/GMSiP and HeLa/HeLa-shLamin cells were treated with etoposide (VP-16), TNF□□+ actinomycin D, staurosporin or UVB as specified in Figs. 1a and 2b. The HL-60 cells were treated with the three conditions as above as well as 100 μM MNNG for the specified time. HeLa cells were treated with 10 J/m^2 UVC and harvested at specified time. The cell extracts were subjected to

immunoblotting for activated caspase-3, PARP, Ago-2 and Dicer-1. Cleaved proteins are indicated as 89 kDa (for cleaved PARP) and ΔDicer-1 (for cleaved Dicer-1). Actin-probing served as loading-controls for panels c and d, whereas loading control for samples in panels a and b were shown in Figs. 1a and 2b. Results shown in all three panels represent similar results obtained with at least 2-3 independent experiments. Ap lane in panels b and c refers to 70 μM etoposide (VP-16, 8h)-treated apoptotic HL-60 cells.

Fig. 4.4. Identification of caspase responsible for cleavage of Dicer-1. (a) Caspase-inhibitor zVAD-fmk blocks cleavage of Dicer-1. COS-1 cells were incubated with 50 μM zVAD-fmk (Calbiochem) at 37°C for 90 min prior to treatment with 1 μM staurosporin (STS) for specified time. The samples were harvested and immunoblotted for activated caspase-3 and Dicer-1. Ap lane refers to 70 μM etoposide (VP-16, 8h)-treated apoptotic HL-60 cells. Actin immunoprobing served as loading-control and results shown here represent similar results obtained with two independent experiments. (b) In vitro cleavage of recombinant hDicer-1 by various caspases. The immunopurified and eluted FLAG-hDicer-1 was digested with ten different recombinant caspases (1 to 10) in an in vitro caspase-digestion assay. The samples were probed by Western blotting for Dicer-1 or FLAG. Ap refers to apoptotic HL-60 cell extract (described in panel a) which served as a positive control for full-length Dicer-1 and its cleaved fragment ΔDicer-1. (c) Identification of apoptotic fragments of FLAG-hDicer-1-HA in apoptotic cells. COS-1 cells transfected with FLAG-hDicer-1-HA cDNA were treated after 48h with 1 μM staurosporin (STS) for 18h to induce apoptosis. Whole cell extracts prepared from the control or apoptotic cells were immunoblotted for FLAG or HA to identify the intact protein or N-terminal FLAG-bound or C-terminal HA-bound fragments. The results shown here represent similar results obtained with four independent experiments. (d) Lack of Dicer-1 cleavage in caspase-3-deficient MCF-7 cells during apoptosis. MCF-7 cells were treated with 5 μM staurosporin or 5 μg/ml actinomycin D for 48h; and immunoblotted for activated caspase-7, PARP and Dicer-1. Ap refers to apoptotic HL-60 cell extract (described in panel a). Actin immunoprobing served as loading-control and results shown here represent similar results obtained with three independent experiments.

Fig. 4.5. Identification of the cleavage site for Dicer-1. (a) The seven putative caspase-target D residues in RNase IIIa domain of hDicer-1. Based on the MS-MS data of apoptotic cleavage fragments of hDicer-1 immunoprecipitated from FLAG-hDicer-1-HA expressing COS-1 cells, seven Asp (D) residues were identified and mutated to caspase-uncleavable D/A. The full Dicer-1 sequence, its functional motifs and D residues of interest are shown in Supplementary Fig. S2. (b) Identification of the cellular apoptotic-cleavage sites in Dicer-1. The cDNA for wild-type Dicer-1, its single mutants $STTD^{1476}/A$ and $CGVD^{1538}/A$ or its double mutant $STTD^{1476}/A$:$CGVD^{1538}/A$ were expressed in COS-1 cells for 48h prior to treatment with 1 μM staurosporin (STS) for 18h to induce apoptosis. The samples were immunoblotted for activated caspase-3 and the N-terminal or C-terminal Dicer-1-fragments were identified by immunoblotting for FLAG or HA. Actin immunoprobing served as loading-control and results shown here represent similar results obtained with three independent experiments. (c) Schematic representation of the full-length hDicer-1 and its apoptotic fragments. The full length recombinant FLAG-hDicer-1-HA (230 kDa) gets cleaved to the N-terminal 180 kDa FLAG-detectable ΔDicer-1 fragment, and two C-terminal HA antibody-detectable fragments of ~50 and ~42 kDa generated by cleavage at $STTD^{1476}$ and $CGVD^{1538}$ sites, respectively.

Fig. 4.6. Consequences of cleavage of Dicer-1 during apoptosis: catalytic inactivation and reduced formation of mature miRNA. (a) In vitro caspase-3-mediated cleavage of immunobead-bound Dicer-1 to its 180 kDa ΔDicer-1 fragment. The immunobead-bound FLAG-hDicer-1 was digested with caspase-3 in an in vitro caspase-digestion assay. The samples were immunoblotted for FLAG and Dicer-1 to identify intact hDicer-1 and N-terminal 180 kDa ΔDicer-1 fragment. The results shown here represent similar results obtained with three independent experiments. (b) In vitro catalytic activity of immunobead bound hDicer-1. The immunobead-bound FLAG-hDicer-1 was incubated with 27mer dsRNA substrate for specified time. The 27mer dsRNA and 21mer dsRNA served as size markers. The samples were resolved on 20% native PAGE and stained with ethidium bromide for visualization of dsRNA bands. The results shown here represent similar results obtained with four independent experiments. (c) Catalytic inactivation of hDicer-1 due to

caspase-3 digestion. The immunobead-bound FLAG-hDicer-1 was digested with caspase-3 for 90 min followed by catalytic Dicer-1 activity assay, as described above for panels a and b. The dicing assay samples were harvested at specified time-points. Mock samples were incubated with boiled caspase-3, and 0h samples were removed at the start of each reaction. The 21mer dsRNA was loaded as size marker. (d) Lack of Dicer-1 catalytic activity in apoptotic cell extract. The enzymatically active cell extracts were prepared from the control or etoposide (VP16-70 μM for 18h)-treated GM637 cells, which contained intact or partially cleaved hDicer-1 as determined by immunoblotting for Dicer-1 (left panel). The cell extracts were used in the in vitro Dicer activity assay for cell extracts. Aliquots of the assay mixture at various time points were resolved on non-denaturing 3.5-20% PAGE and stained with ethidium bromide. Size markers (lanes 1 and 2) were 27 and 21mer dsRNA that were spiked into the assay buffer without the cell-extract. The results shown here represent similar results obtained with at least two independent experiments. (e) Depletion of miR-16, miR-21 and let-7a mature miRNA in the apoptotic HL-60 cells. The HL-60 cells were treated with etoposide for specified time, and small RNA extracted from the cells were loaded on 15 % PAGE with 6M Urea and Northern-blotted. Membranes were probed with ^{32}P-labeled specific probes to examine the levels of three endogenous mature miRNAs (hsa-miR-16, hsa-miR-21 and hsa-let-7a). The staining of membrane with ethidium bromide (EtBr panel) was carried out to reflect equal loading (left panel). The signals from images of two analyses each from two independent experiments were quantified and shown here as mean ±SD values for relative miRNA expression as compared to untreated control cells. (right panel).

Supplementary Fig.4S1: The Ponceau-S staining of blots as loading control. The three ponceau-S stained blots represent the samples loaded in (a) Fig. 1b; (b) Fig. 2a, and (c) Fig. 2b.

Supplementary Fig. 4S2: hDicer-1: functional domains and cleavage sites in RNase IIIa domain. The amino acid sequence of full length hDicer-1 is shown here with its functional domains. In the MS-MS analyses, the highlighted sequence STTD^{1476} was the last identifiable tryptic fragment in the N-terminal FLAG-tagged 180 kDa ΔDicer-1. The highlighted sequence ^{1578}AAQL was the first identifiable tryptic fragment in the HA-tagged

C-terminal 42 kDa fragment of Dicer-1. The seven putative caspase-cleavage Asp (circled D) residues within the RNase IIIa domain were mutated to caspase-uncleavable A and subjected to analyses. The cleavage sites in hDicer-1 were STTD^{1476} CGVD^{1538}.

4.11 Figures

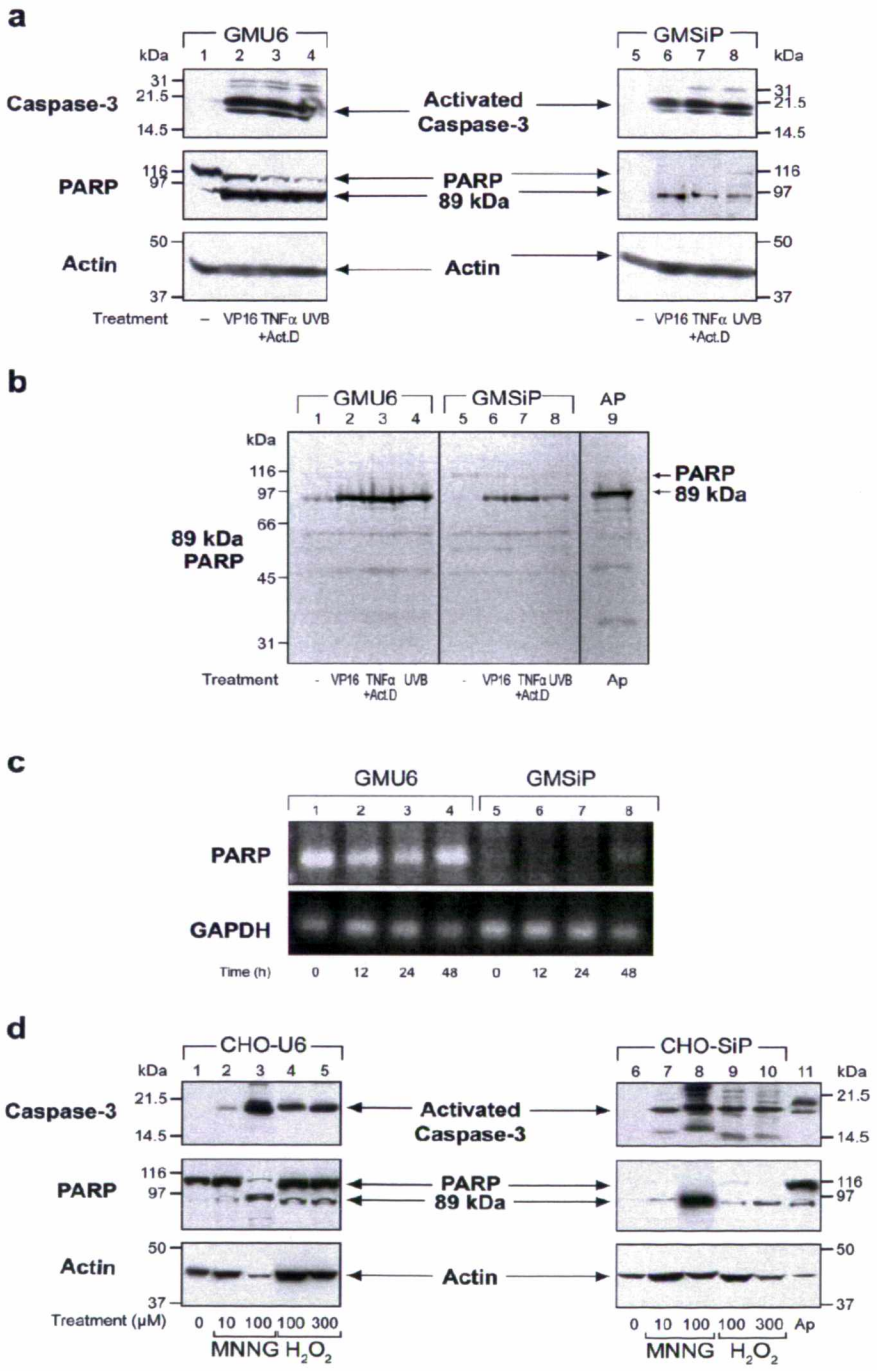

Figure 4.1: Abrogation of DNA vector-based RNAi of PARP during apoptosis

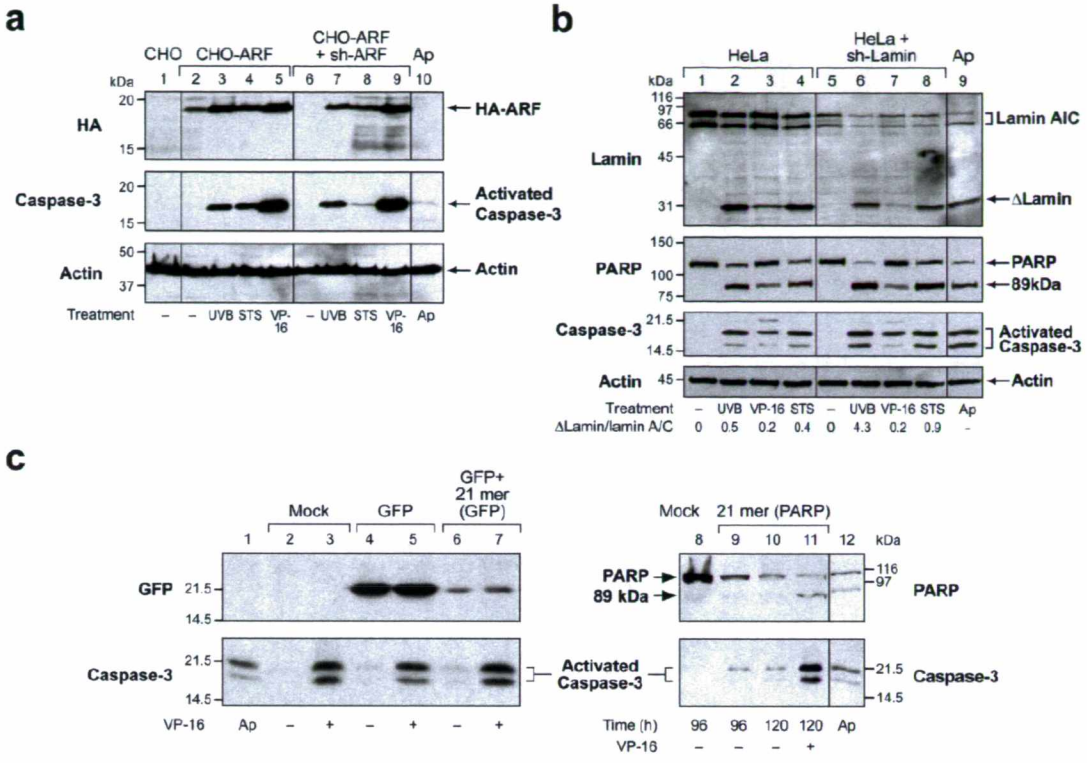

Figure 4.2: Apoptosis-associated failure of stable shRNA of $p14^{ARF}$ and lamin but not that of transient RNAi of GFP and PARP by 21mer siRNA

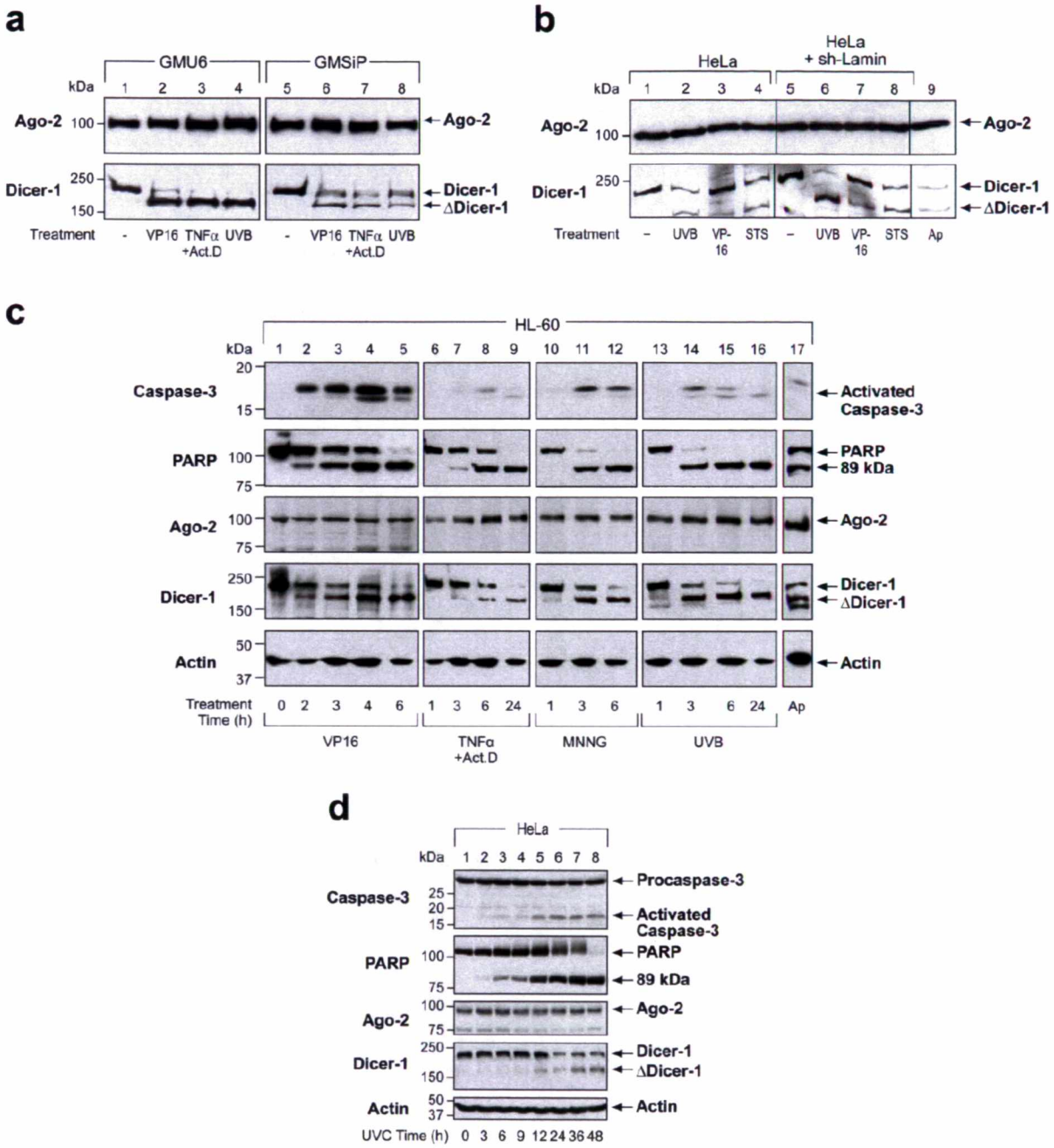

Figure 4.3: Cleavage of Dicer-1 in human cell lines undergoing apoptosis

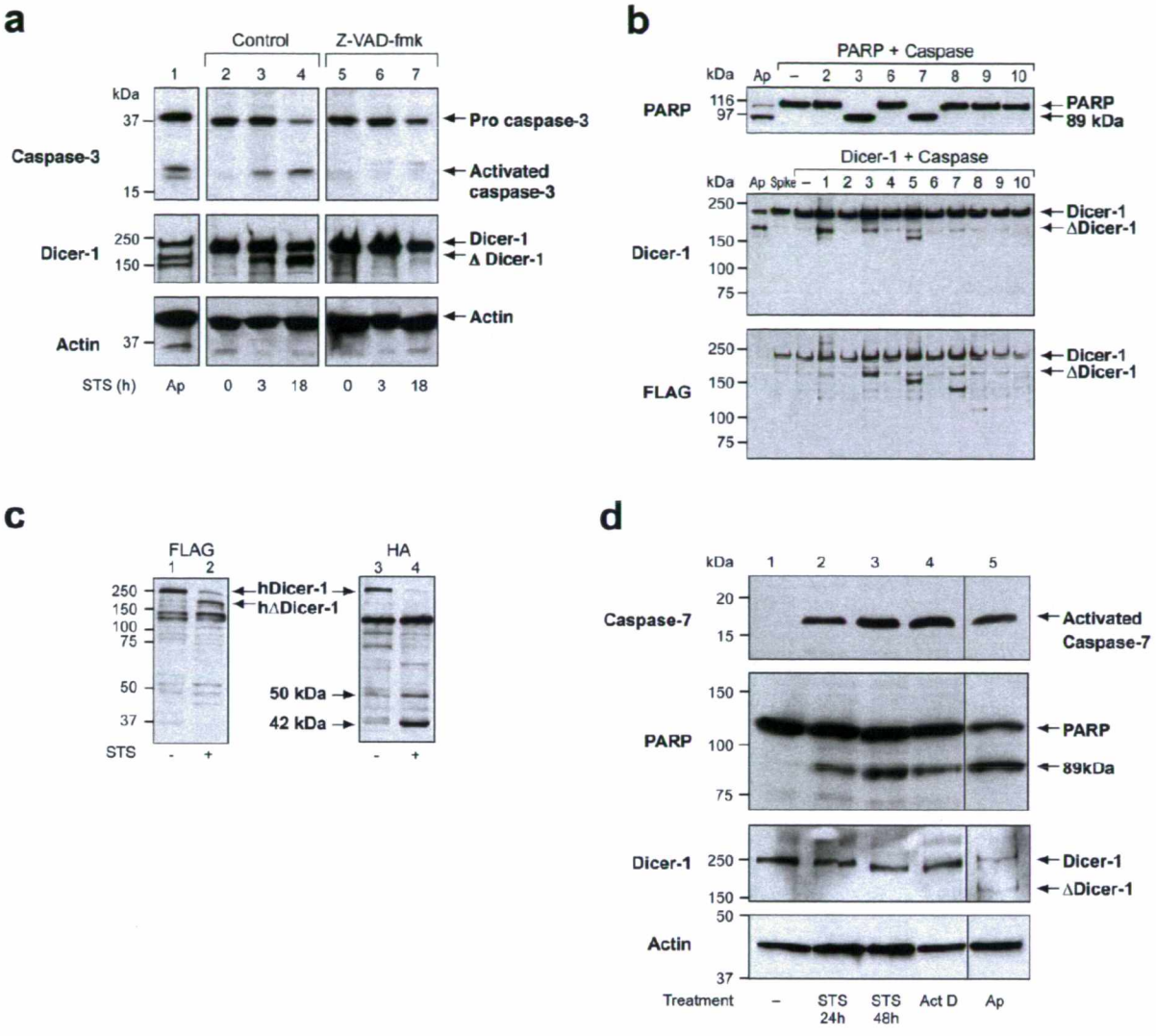

Figure 4.4: Identification of caspase responsible for cleavage of Dicer-1

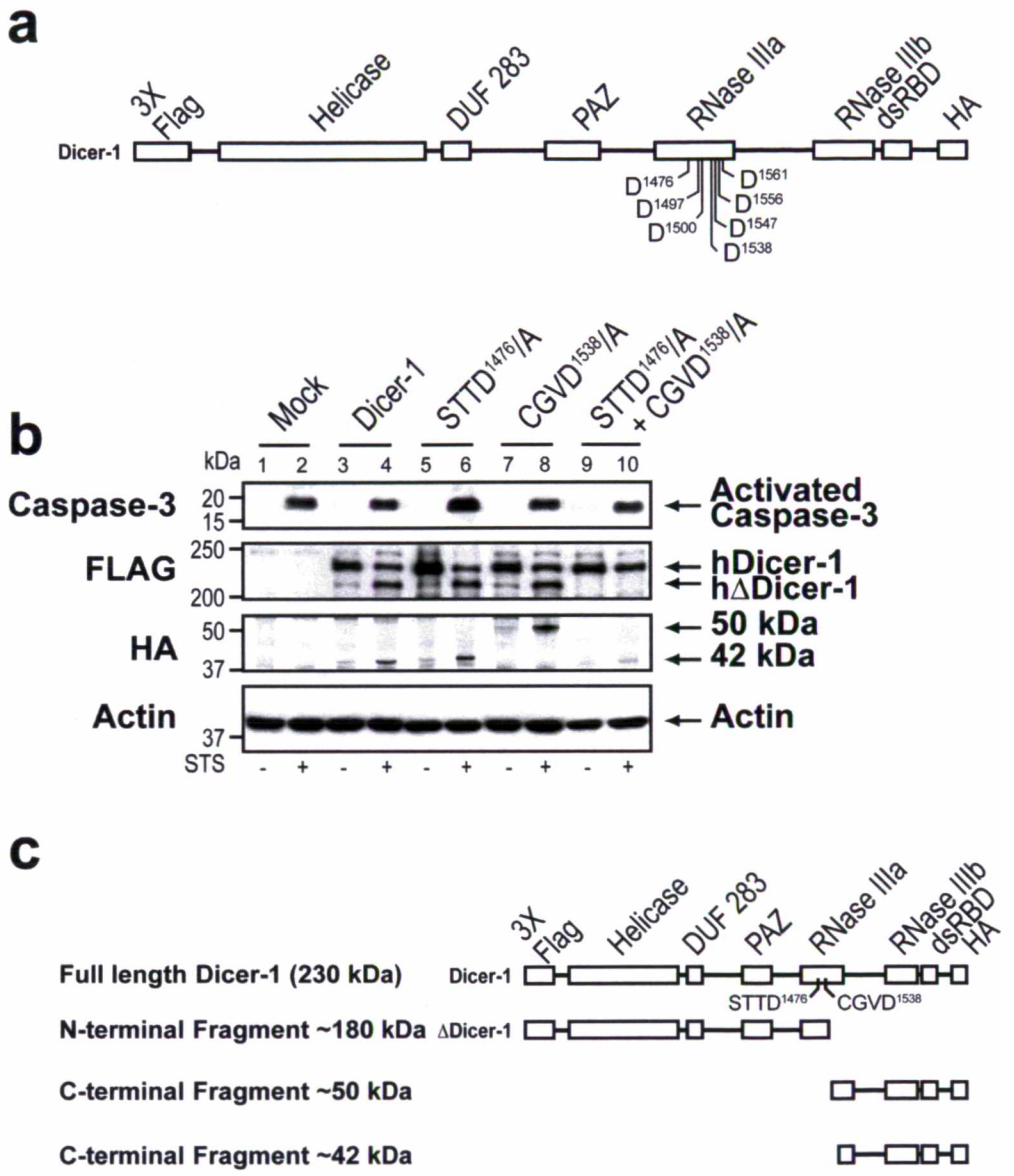

Figure 4.5: Identification of the cleavage site for Dicer-1

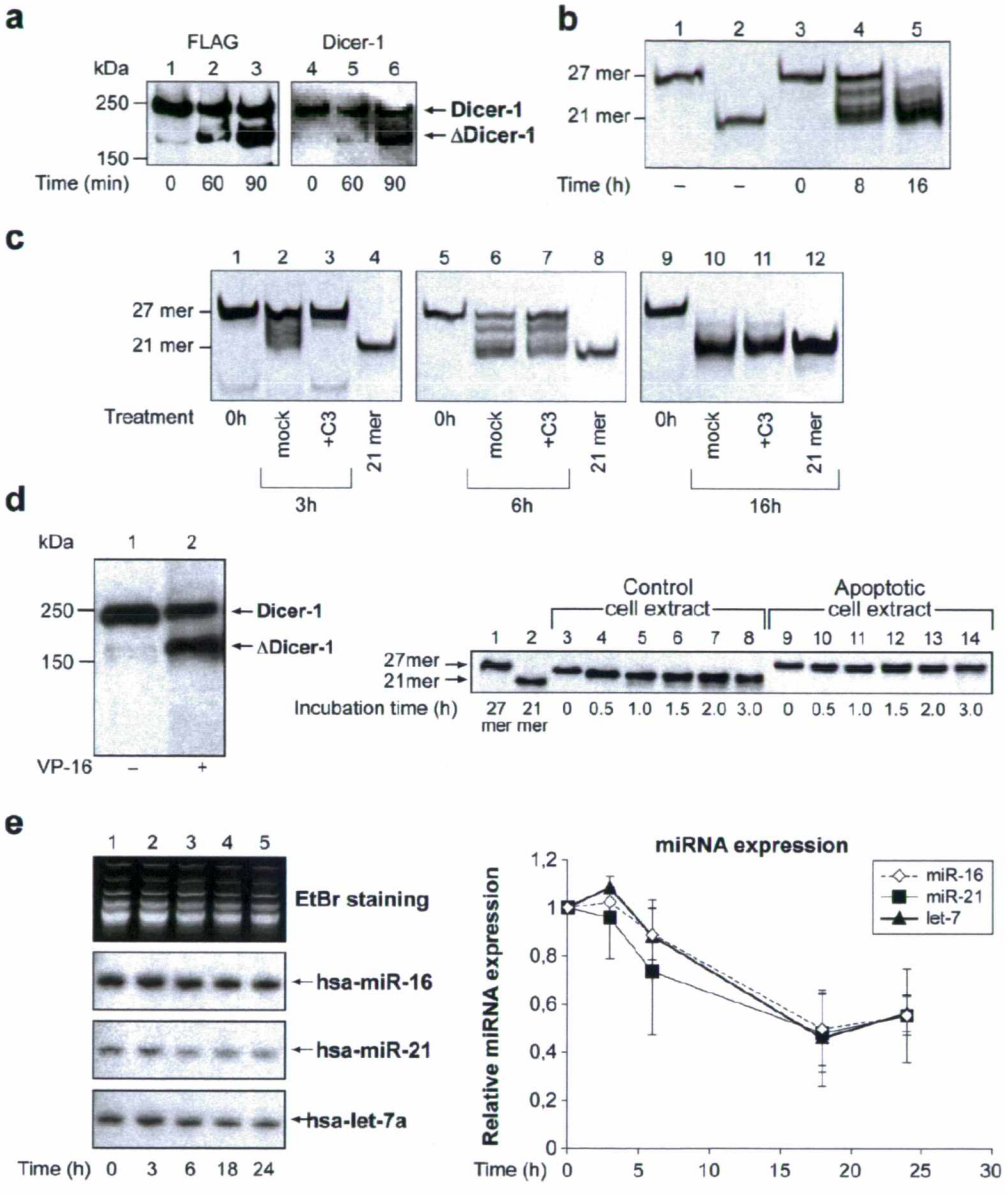

Figure 4.6: Consequences of cleavage of Dicer-1 during apoptosis: catalytic inactivation and reduced formation of mature miRNA

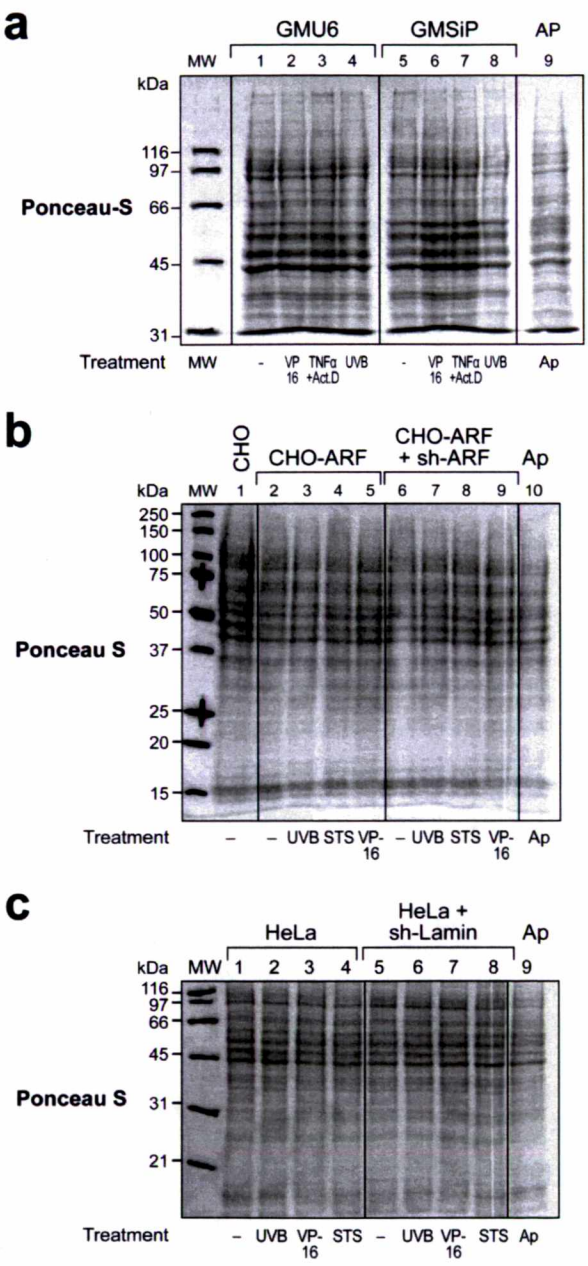

Supplementary Fig. 4S1: The Ponceau-S staining of blots as loading control.

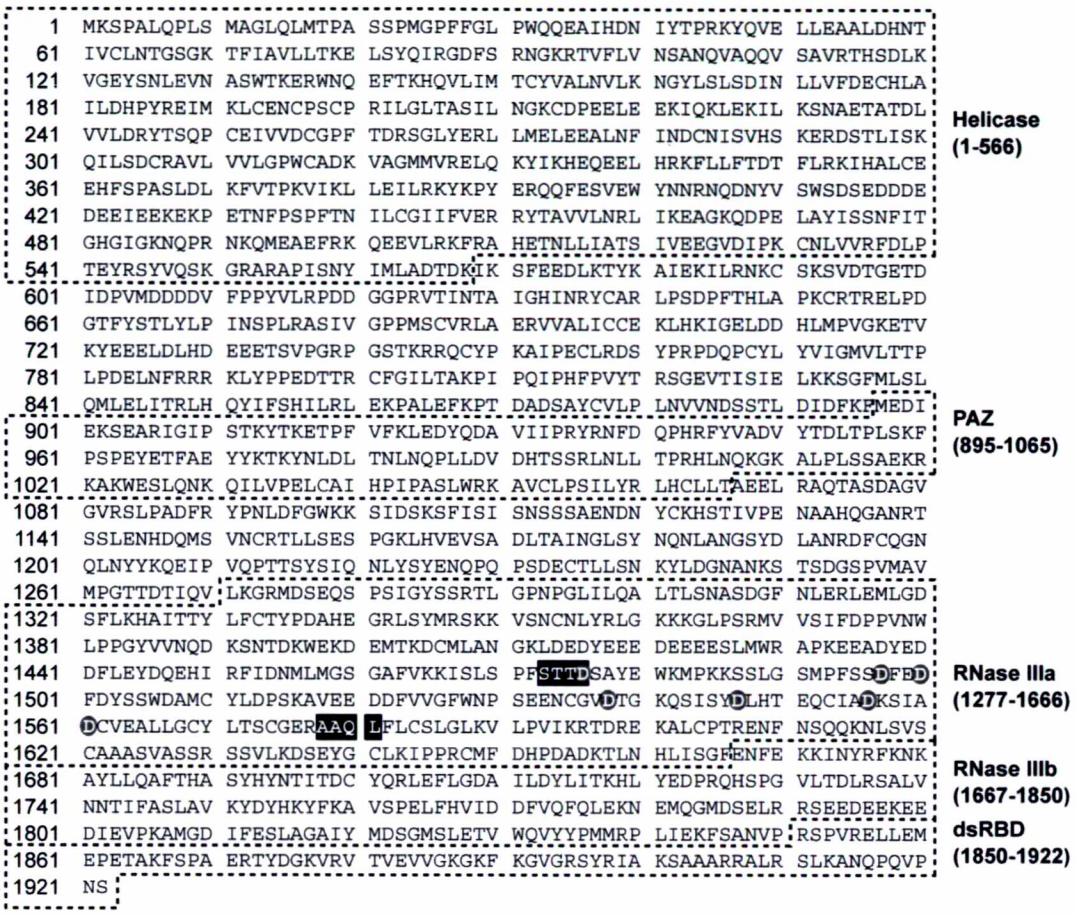

Supplementary Fig. 4S2: hDicer-1: functional domains and cleavage sites in RNase IIIa domain.

Chapter 5: Persistence of different forms of transient RNAi during apoptosis in mammalian cells

(PLoS One. 2010; 5(8): e12263)

5.1 Résumé en français

L'inhibition d'expression de gène (« *gene silencing* ») par interférence à l'ARN (ARNi) transitoire ou stable est utilisée pour étudier l'apoptose en supposant que les évènements apoptotiques n'auront aucune influence sur l'ARNi. Toutefois, nous avons récemment rapporté que l'ARNi stable, *i.e.*, un « *knockdown* » permanent de gène par l'entremise de vecteurs d'ADN, générant des shRNAs intégrés dans le génome, échoue rapidement après l'induction de l'apoptose dû au clivage de la caspase-3 et à l'inactivation de l'endoribonucléase Dicer-1 requise pour la conversion des shRNA en siRNA. Puisque les études sur l'apoptose emploient de plus en plus des modèles d'ARNi transitoire dans lesquels l'apoptose est induite immédiatement après qu'un gène soit temporairement «knocked down» dans un délai de quelques jours suivant la transfection avec un agent induisant l'ARNi, nous avons examiné l'impact de l'apoptose sur une variété de modèles d'ARNi transitoire. Nous rapportons ici que, contrairement à l'ARNi stable, toutes les formes d'ARNi transitoires, autant indépendante de Dicer-1 (à l'aide d'ARN double-brin de 21 mer) que dépendante de Dicer-1 (à l'aide d'ARN double-brin de 27mer ou d'un vecteur d'ADN générant un shRNA), autant pour un gène exogène (GFP) que pour un gène endogène (poly(ADP-ribose) polymérase), n'échouent pas au courant des 2-3 jours suivant le début de l'apoptose. Nos résultats reflètent les différences dans la dynamique servant à maintenir l'ARNi pendant les phases précoces suivant la transfection dans l'ARNi transitoire et la phase stable tardive du «*knock-down*» du gène dans le modèle d'ARNi stable. Nos résultats permettent aussi de faire une recommandation selon laquelle l'état de l'ARNi devrait être validé fréquemment dans les études impliquant l'apoptose et que, même si l'ARNi stable peut être utilisée de façon sure dans les études sur les évènements hâtifs de l'apoptose, l'ARNi transitoire reste plus souhaitable pour les études portant sur les évènements précédant et suivant l'apoptose.

5.2 Article

Persistence of Different Forms of Transient RNAi during Apoptosis in Mammalian Cells

Febitha Kandan-Kulangara[1], Rashmi G Shah[1], El Bachir Affar[2] and Girish M Shah[1*]

[1]Laboratory for Skin Cancer Research, Hospital Research Centre of Laval University (CHUL /CHUQ), Department of Molecular Biology, Medical Biochemistry & Pathology, Faculty of Medicine, Laval University, Quebec (Quebec), Canada, [2]Maisonneuve Rosemont Hospital Research Center, Department of Medicine, Faculty of Medicine, Montreal University, Montreal (Quebec), Canada.

***Correspondence**: Girish M. Shah, Ph.D.

Tel: (418) 656-4141/Ext. 48259

Fax: (418) 654-2739

E-mail: girish.shah@crchul.ulaval.ca

5.3 Abstract

Gene silencing by transient or stable RNA-interference (RNAi) is used for the study of apoptosis with an assumption that apoptotic events will not influence RNAi. However, we recently reported that stable RNAi, i.e., a permanent gene-knockdown mediated by shRNA-generating DNA vectors that are integrated in the genome, fails rapidly after induction of apoptosis due to caspase-3-mediated cleavage and inactivation of the endoribonuclease Dicer-1 that is required for conversion of shRNA to siRNA. Since apoptosis studies also increasingly employ transient RNAi models in which apoptosis is induced immediately after a gene is temporarily knocked down within a few days of transfection with RNAi-inducing agents, we examined the impact of apoptosis on various models of transient RNAi. We report here that unlike the stable RNAi, all forms of transient RNAi, whether Dicer-1-independent (by 21mer dsRNA) or Dicer-1-dependent (by 27mer dsRNA or shRNA-generating DNA vector), whether for an exogenous gene GFP or an endogenous gene poly(ADP-ribose) polymerase-1, do not fail for 2-3 days after onset of apoptosis. Our results reflect the differences in dynamics of achieving and maintaining RNAi during the early phase after transfection in the transient RNAi model and the late steady-state phase of gene-knockdown in stable RNAi model. Our results also sound a cautionary note that RNAi status should be frequently validated in the studies involving apoptosis and that while stable RNAi can be safely used for the study of early apoptotic events, transient RNAi is more suitable for the study of both early and late apoptotic events.

5.4 Introduction

RNA-interference (RNAi) is a mechanism for sequence-specific silencing of a gene by 21-23mer dsRNA, also called small interfering RNA (siRNA) which guides RNA-induced silencing complex (RISC) containing the endoribonuclease of the Argonaut family (Ago) to search and destroy the target mRNA [1,2]. In mammalian cells, transient RNAi, i.e., knockdown of a target gene for a few days can be achieved rapidly after transfection with a synthetic 21mer dsRNA or its precursors, such as 27mer dsRNA [3] or a short hairpin RNA (shRNA)-generating DNA vector [4]. While the transfected 21mer dsRNA/siRNA is directly incorporated in the RISC, the 27mer dsRNA or DNA vector-derived shRNA need to be converted first to siRNA by the endoribonuclease Dicer-1. In transient RNAi models, the gene expression returns to normal once siRNA or its precursors are degraded; and the siRNA-loaded RISC molecules are depleted due to dilution with cell division or metabolic instability in the absence of target mRNA [1]. Stable RNAi, on the other hand, can be achieved when shRNA-generating DNA vector is integrated in the genome under selection pressure, so that its transcription results in a continuous supply of shRNA molecules and stable knockdown of the target gene [4]. Both transient and stable RNAi are being exploited in mammalian cells for examining various cellular processes [2], and more specifically to study apoptosis with an assumption that these RNAi processes would not be affected by apoptosis. However, recently we reported that stable RNAi fails soon after induction of apoptosis because of caspase-mediated cleavage and inactivation of Dicer-1, which is required to form siRNA from DNA vector-derived shRNA [5]. However, the impact of apoptosis on transient RNAi has never been examined although some apoptosis studies use Dicer-1-dependent transient RNAi achieved with 27mer dsRNA [6] or the shRNA-generating DNA vectors [7]. Hence, we characterized apoptotic fate of Dicer-1-dependent and independent forms of transient RNAi of an exogenous and an endogenous gene and compared it with stable RNAi. We report here that while Dicer-1-dependent stable RNAi rapidly fails after onset of apoptosis, the transient RNAi, whether dependent on Dicer-1 or not, continues to knockdown the target genes for several days after onset of apoptosis, reflecting the differences in dynamics of achieving RNAi in transient and stable RNAi.

5.5 Materials and methods

5.5.1 Cells. The human diploid SV-40 transformed skin fibroblast cells GM00637 (Coriell Cell Repository, Camden, NJ) and hamster cell line CHO (sub-line WT-5) were cultured in αMEM (Gibco) supplemented with 10% foetal bovine serum, 50 U/ml penicillin and 50 μg/ml streptomycin at 37 ºC in a humidified incubator with 5% CO_2.

5.5.2 Creation of CHO-derived clones with stable expression of GFP (CHO-GFP) and stable shRNA-mediated RNAi of GFP (CHO-shGFP). The details of creation of CHO-GFP clones and its stable RNAi clones are provided in Methods S1. In brief, CHO cells were transfected with pEGFP-N1 (Clontech) and strong GFP-expressing clones were selected, one of which was used in the present study. For stable RNAi of GFP, CHO-GFP clone was transfected with pBS-U6-based [8] and shRNA-generating DNA vector shGFP-234 along with pTK-Hyg plasmid to isolate stable hygromycin-resistant shGFP clones, two of which were used in the study. The extent of knockdown of GFP was measured relative to the GFP levels expressed in untreated CHO-GFP control cells.

5.5.3 Transient RNAi of GFP or PARP. The details of all transient transfection conditions are provided in Methods S1. In brief, for the transient RNAi of constitutively expressed GFP, CHO-GFP cells were transfected with GFP-targeting DNA vectors shGFP-234, shGFP-477 or 27mer dsRNA for 48-72h prior to induction of apoptosis. For introduction of transient RNAi in the cells with stable RNAi of GFP, the shGFP-234-clone #62 or clone #64 were transfected with GFP-targeting 21mer dsRNA, 27mer dsRNA, shGFP-234 or shGFP-477 DNA vector for 48h prior to induction of apoptosis. The mock control cells were transfected with equivalent amount of blank vector pCMV DNA or unrelated shRNA-generating DNA vector. For transient RNAi of co-expressed GFP, GM637 cells were transfected with pEGFP-N1 (Clontech) cDNA or CMV plasmid (as mock DNA) with or without GFP-targeting 21mer dsRNA, 27mer dsRNA, shGFP-234 or shGFP-477. For transient RNAi of PARP, GM637 cells were transfected with one of the

following PARP-targeting 21mer dsRNA, 27mer dsRNA (IDT) or shRNA-directing SiP912 DNA vector [8].

5.5.4 Apoptosis-inducing treatments and Western blotting. Apoptosis was induced in different models with either 1,600 J/m^2 UVB (Spectrolinker XL-1000 UV cross-linker), 300 μM MNNG or 100 μM etoposide for specified time. The cell extracts were prepared and samples representing 200,000 cells or 10-20 μg protein were resolved on 6, 8 or 12% SDS-PAGE, blotted on nitrocellulose and probed with following antibodies: GFP (Roche, 1:5,000); PARP (C-2-10, Aparptosis Inc., 1:10,000); human Dicer-1 (Abcam, 1:1,000); human Ago-2 (Wako, 1:200); activated caspase-3 (Cell Signaling, 1:1,000) and Actin (Sigma, 1:20,000). The immunoblots were either read directly for chemiluminescence or autoradiographic films were scanned using ChemiGenius 2 Bio Imaging system (SynGene) and quantification of signals was carried out using GeneTools software version 4.00 (SynGene).

5.5.5 Extraction of total RNA and RT-PCR. The details of RNA preparation, RT-PCR primers and cycle conditions as well as data analyses are provided in Methods S1. In brief, total RNA was prepared from 1-3 x 10^6 cells using mirVana^{TM} PARIS^{TM} kit (Ambion). The RT-PCR was carried out using OneStep RT-PCR kit (Qiagen) and the MasterCycler Personal PCR-machine (Eppendorf Life Science). The GFP or GAPDH bands after resolution on 1.5 % agarose gel were quantified using ChemiGenius 2 with GeneTools software (SynGene).

5.6 SUPPLEMENTARY MATERIAL: DETAILED METHODS

5.6.1 Creation of CHO-derived cells with stable expression of GFP (CHO-GFP). The CHO cells with constitutive expression of GFP (CHO-GFP cells) were created by stable transfection of 80% confluent cells in a 60 mm dish with 3 μg pEGFP-N1 (Clontech) using Lipofectamine 2000 (Invitrogen), as per the manufacturer's protocol. The GFP-expressing

clones were selected and maintained in a medium containing 800 and 400 µg/ml geneticin, respectively. One of these CHO-GFP clones was used in the study.

5.6.2 Creation of clones with stable shRNA/DNA vector-based RNAi of GFP (CHO-shGFP). For stable RNAi of GFP, CHO-GFP clone was transfected with pBS-U6-based (Shah et al, 2005) and shRNA-generating DNA vector shGFP-234 containing GFP targeting sequence 5'-GCA TGA AGC AGC ACG ACT TCT T-3' along with pTK-Hyg plasmid to isolate stable hygromycin-resistant shGFP clones, which were maintained in the medium containing 400 µg/ml geneticin and 200 µg/ml hygromycin. Two of these shGFP-234 clones #62 and 64 were used in the study.

5.6.3 Transient RNAi of GFP or PARP. For transient RNAi of constitutively expressed GFP, CHO-GFP cells at 75-80% confluence in 60 mm dishes were transfected with either Lipofectamine-2000 or $CaPO_4$ protocols with specified amounts of shRNA-generating DNA vectors or dsRNA of 27mer or 21mer. After 24h, cells from each dish were trypsinized and distributed in multiple 60 mm dishes to be used for control or apoptotic treatments. At 48 or 72h after transfection, apoptosis-inducing treatments were carried out as described below.

For transient RNAi of GFP in the cells having stable RNAi of GFP, the CHO-shGFP-234 clone was transfected as above with one of the following GFP-RNAi-inducing agents: 120 pmol of 21mer dsRNA based on the sequence 5'-GCA AGC UGA CCC UGA AGU UCA U-3' (Qiagen); 2 or 5 pmol of 27mer dsRNA based on the sequence 5'-ACC CUG AAG UUC AUC UGC ACC ACC G-3' (Qiagen); or 3 µg DNA vectors shGFP-234 or shGFP-477 DNA vector based on the sequence 5'-GAA CGG CAT CAA GGT GAA CTT-3'. After transfection, cells were processed as mentioned above.

For transient RNAi of co-expressed GFP, GM637 cells, under culture and transfection conditions described above, were transfected with 0.2 µg of pEGFP-N1 (Clontech) cDNA or CMV plasmid (as mock DNA) with 120 pmol of 21mer dsRNA, 0.2, 1

and 2 pmol of 27mer dsRNA or 1 μg of shGFP-234 or with shGFP-477. After transfection, cells were processed as mentioned above.

For transient RNAi of PARP, GM637 cells were transfected under conditions described above except that cellular PARP was targeted for knockdown with one of the following PARP-RNAi-inducing agents: 600 pmol of 21mer (IDT); 600 pmol of 27mer dsRNA (IDT) or 5 μg shRNA-directing SiP912 DNA vector (Shah et al, 2005). The PARP-targeting sequence in each of the dsRNA was based on the sequence described earlier for the SiP912 (Shah et al, 2005). After transfection, cells were processed as mentioned above.

5.6.4 Extraction of total RNA and RT-PCR. Total RNA from cells was extracted using the mirVana^{TM} PARIS^{TM} kit (Ambion). In brief, 1-3 x 10^6 cells were trypsinized, washed with PBS and the pellet was extracted using 300-600 μl of disruption buffer provided with the kit. The lysate was mixed with equal volume of 2X denaturation buffer, extracted with acid phenol and the RNA was obtained from the aqueous phase, using the filter cartridge provided in the kit. Elution was performed with 50 μl RNase-free water and RNA was estimated spectrophotometrically. The quality of RNA was confirmed by loading 1 μg on formaldehyde-agarose gel and RNA was stored at -80°C.

The RT-PCR was carried out using the OneStep RT-PCR kit (Qiagen) and the MasterCycler Personal PCR-machine (Eppendorf Life Science). The reaction components were as per the instructions for the one-step PCR, without the use of RNase-inhibitor or the Q solution. The following primer-set for GFP resulted in a DNA product of 530 bp: Forward GFP primer: 5' CAA GCT GAC CCT GAA GTT CAT C 3'; Reverse GFP primer: 5' GAA CTC CAG CAG GAC CAT GTG 3'. The following primer-set for GAPDH resulted in a DNA product of 473 bp: Forward GAPDH primer: 5' CTT CAT TGA CCT CAA CTA CAT GG 3'; Reverse GAPDH primer: 5' GTC TTC TGG GTG GCA GTG ATG 3'. The reaction was performed in a total volume of 25 μl containing 0.6 μM of each of the two primers of the set and 1 μg total RNA. The thermal cycler was set at 50°C before transferring the tubes containing the reaction mixture from ice and the reaction was performed for 25 cycles. At the end of the reaction, 7.5 μl of the GFP or GAPDH mixture was separated on 1.5 % agarose gel in 1X TBE for one hour at 100V. The bands stained

with ethidium bromide were viewed on a transilluminator using ChemiGenius 2 Bio Imaging system (SynGene) and quantification of signals was carried out using GeneTools software version 4.00 (SynGene).

Reference

Shah RG, Ghodgaonkar MM, Affar EB, Shah GM (2005) DNA vector-based RNAi approach for stable depletion of poly(ADP-ribose) polymerase-1. *Biochem Biophys Res Commun* **331**(1)**:** 167-174

5.7 Results

5.7.1 Persistence of transient RNAi whereas failure of stable RNAi of stably expressed GFP

We first compared the apoptotic fate of transient and stable RNAi of GFP which were achieved using the same shRNA-generating DNA vector shGFP-234 in the cells that constitutively express high levels of GFP (CHO-GFP) (**Fig. 5.1**). For stable RNAi, CHO-GFP cells were transfected with shGFP-234 and clones with permanent knockdown of GFP were isolated over several weeks after transfection. A semi-quantitative analyses of GFP signals revealed that two of these shGFP-234 clones #62 and #64 had stable and significant (>90%) knockdown of GFP, when compared to GFP expression in the control CHO-GFP cells (**Fig. 5.1A**, lanes 1, 5 and 9). For transient RNAi, CHO-GFP cells were transfected with shGFP-234 for 48h to obtain ~60% knockdown of GFP (**Fig. 5.1A**, lanes 13 and 16). Apoptosis was induced in both the RNAi models by treatment with ultraviolet B (UVB) and the fate of RNAi was monitored for further 72h. In the CHO-GFP cells, high levels of GFP expression present prior to induction of apoptosis remained unchanged up to 72h after UVB-treatment that caused formation of activated caspase-3 (**Fig. 5.1A**, lanes 1-4). Thus, GFP gene expression or protein stability *per se* is not altered during apoptosis. In the two stable shGFP clones where the expression of GFP was significantly knocked down prior to apoptosis, UVB-induced apoptosis resulted in a failure of RNAi, i.e., an increase in GFP levels by 48-72h concomitant with caspase-3 activation (**Fig. 5.1A**, lanes 5-12). This is in agreement with our earlier demonstration of apoptosis-associated failure of stable RNAi for three other genes, namely poly(ADP-ribose) polymerase-1 (PARP), $p14^{ARF}$ and lamin A/B [5]. Interestingly, transient RNAi by the same shGFP-234, which was achieved prior to induction of apoptosis, did not fail for up to 72h after exposure to UVB, because the GFP signal did not increase in the 120h-UVB-treated cells as compared to 120h-untreated cells (**Fig. 5.1A**, lanes 16-19).

To determine whether changes in GFP protein levels were indeed due to the influence of RNAi on the availability of GFP transcripts, the relative abundance of mRNA for GFP over control gene GAPDH were analyzed in these two models by RT-PCR (**Fig.**

5.1B). In the CHO-GFP cells without any RNAi, the GFP transcript levels before and after induction of apoptosis were not significantly altered confirming that apoptosis does not directly influence transcription of GFP or the stability of its mRNA (**Fig. 5.1B**, lanes 1-4). In two stable RNAi clones, the relative GFP mRNA levels were significantly (4-6x fold) upregulated after induction of apoptosis as compared to the levels seen prior to apoptosis (**Fig. 5.1B,** lanes 5-8 and 9-12), indicating failure of stable RNAi of GFP and the accumulation of its transcripts from 24h onwards. In contrast, in the transient RNAi model, a relatively moderate decrease in GFP transcripts (30%) at 72h after transfection and prior to induction of apoptosis (**Fig. 5.1B,** lanes 13 and 15) was not significantly reversed for up to 72h after UVB-induced apoptosis (**Fig. 5.1B,** lanes 15 and 16), indicating the persistence of transient RNAi during apoptosis. Thus, despite originating from the same shGFP-234 DNA vector, the stable RNAi of GFP rapidly failed by 24-48h, whereas the transient RNAi persisted up to 3 days after onset of apoptosis.

It is plausible that apoptosis-associated failure of RNAi did not become evident in the above described transient RNAi model simply because it started with a much lesser extent of knockdown of GFP (60%) as compared to highly efficient (91-92%) knockdown seen in stable RNAi model. To address this issue, we employed a variety of transient transfection conditions, such as use of a different shRNA-generating DNA vector (shGFP-477), a combination of two shGFP DNA vectors or a 27mer dsRNA to achieve much greater extent of transient GFP knockdown (**Fig. 5.1C**). The DNA vector shGFP-477 or a combination of shGFP-234 and shGFP-477, yielded 67 and 82% GFP-knockdown, respectively at 72h after transfection (**Fig. 5.1C**, lanes 1, 2 and 4). An even greater extent of knockdown (88-89%) was achieved at 72h after transient transfection with 5 or 20 pmol of 27mer dsRNA (**Fig. 5.1C**, lanes 1, 6 and 8). In each of these transient RNAi models, the signal for GFP did not increase for up to 72h after UVB-treatment that caused formation of activated caspase-3 (**Fig. 5.1C**, lanes 2-9: compare lanes +/- UVB in each set), confirming that irrespective of the extent of knockdown from 60-89%, transient RNAi did not fail for up to 3 days after onset of apoptosis.

5.7.2 Persistence of GFP-knockdown during apoptosis in stable RNAi clones supplemented with transient RNAi

As above studies examined transient and stable RNAi in different cellular models, we next examined the apoptotic fate of GFP-knockdown in the cells containing both stable and transient RNAi (**Fig. 5.2**). To the shGFP-234 clone #62 that has a pre-existing (91%) stable RNAi of GFP (**Fig. 5.2A**, lanes 1 and 2), we added transient RNAi by transfection with GFP-targeting 21mer dsRNA, 27mer dsRNA or shGFP-234 DNA vector, which resulted in a total knockdown of 94-97% at 48h after transfection (**Fig. 5.2A**, lanes 1, 2, 3, 5 and 7). When apoptosis was induced by UVB in these cells, it resulted in formation of activated caspase-3, but there was no increase in GFP signal at 72h after UVB treatment (**Fig. 5.2A**, lanes 3-8: paired lanes +/- UVB). Thus, although stable RNAi failed during apoptosis (**Fig. 5.1A**), addition of transient RNAi allowed the same cells to continue to knockdown GFP during apoptosis. To confirm the general nature of above observation, we used another stable clone #64 for shGFP-234 and induced apoptosis with *N*-methyl-*N'*-nitroso-*N*-nitrosoguanidine (MNNG) instead of UVB (**Fig. 5.2B**). In this clone, the original 97% stable GFP-knockdown (**Fig. 5.2B**, lanes 1 and 3) was slightly improved (from <1 to 2%) after addition of transient RNAi with two different combinations of shGFP-234 and shGFP-477 DNA vectors or 27mer dsRNA (**Fig. 5.2B**, lanes 1,3,5,7 and 9). When apoptosis was induced by MNNG in these cells, the GFP signal increased by 3x fold in the cells which had only stable RNAi (**Fig. 5.2B**, lanes 3 and 4), confirming apoptosis-associated abrogation of stable RNAi. However, GFP signal did not increase in the cells which had transient RNAi added to the stable RNAi (**Fig. 5.2B**, lanes 5-10, compare lanes +/- MNNG), confirming that GFP knockdown by transient RNAi continued to remain functional in a background where stable RNAi was failing. We also confirmed in the stable clone #64 with or without added transient RNAi by shGFP-234 that UVB-induced apoptosis caused a failure of RNAi in cells with stable RNAi alone but not in the cells with stable plus transient RNAi (**Supplementary Figure 5S1**). Thus, even in the same cell, while stable RNAi of GFP failed, addition of transient RNAi allowed continued knockdown of GFP during apoptosis, confirming persistence of transient RNAi during UVB or MNNG-induced apoptosis.

5.7.3 Persistence of different forms of transient RNAi of co-expressed GFP during apoptosis

While above studies examined RNAi of target gene GFP that is stably expressed, many transient RNAi studies examine knockdown of a co-transfected target gene; hence we examined apoptotic fate of transient RNAi of a co-transfected GFP. In the human skin fibroblasts, GFP-expression vector was co-transfected with two different shGFP DNA vectors (#234 and 477) or a 21mer dsRNA. The GFP expression at 72h after transfection of the GFP-expression vector alone was significantly suppressed (80-99%) when co-transfected with all three transient RNAi-inducing agents (**Fig. 5.3A**, 72h lanes). At this stage, when apoptosis was induced by treatment with etoposide for 18h, it did not result in any increase in GFP levels at 90 h (i.e., 72h transfection plus 18h etoposide) over its respective 90h non-apoptotic control in each of the RNAi model (**Fig. 5.3A**, paired 90h lanes +/- etoposide), confirming the persistence of Dicer-1-dependent and independent mode of transient RNAi of co-transfected GFP during apoptosis.

Further analyses of these cells revealed that etoposide-treatment caused activation of caspase-3 and cleavage of PARP to its 89 kDa fragment, accompanied by apoptosis-specific cleavage of Dicer-1 to a 180 kDa fragment [5], whereas RISC-associated Ago-2 remained intact (**Fig. 5.3A**, lanes 2, 5, 8, 11, 15 and 18). The presence of intact Ago-2 during apoptosis was in agreement with the persistence of RISC-mediated transient RNAi by 21mer dsRNA. However, despite the cleavage of Dicer-1 to its 180 kDa fragment, which results in its catalytic inactivation [5], pre-existing transient RNAi by the shRNA-generating DNA vector did not fail for at least 18h after induction of apoptosis.

To examine whether the extent of gene knockdown plays a role in the persistence of transient RNAi during cell death, we obtained variable extent of GFP-knockdown with increasing amounts of Dicer-1-substrate 27mer dsRNA. The co-transfection of GFP-expression plasmid with 0.2, 1 or 2 pmol of 27mer dsRNA caused 10, 60 or 90% GFP-knockdown, respectively at 72h (**Fig. 5.3B**, lanes 1, 4, 7 and 10). The induction of apoptosis with etoposide treatment resulted in activation of caspase-3 but caused no significant change in GFP at all three levels of GFP-knockdown (**Fig. 5.3B**, paired 90h

lanes +/- etoposide), indicating that persistence of Dicer-1-dependent transient RNAi during apoptosis was not influenced by the extent of gene-knockdown.

5.7.4 Persistence of different forms of transient RNAi of PARP during apoptosis

Finally, since GFP is an exogenous gene, we examined whether transient RNAi of an endogenous and constitutively expressed gene PARP will also persist during apoptosis (**Fig. 5.4**). In the human skin fibroblasts, transient RNAi of PARP with shRNA-generating DNA vector SiP912 [8], 27mer dsRNA or 21mer dsRNA for 72h resulted in 60-80% PARP-knockdown as compared to PARP-levels seen in the cells without RNAi (**Fig. 5.4**, 72h lanes). Induction of apoptosis by 18h treatment with etoposide at this stage resulted in activation of caspase-3 and cleavage of the residual PARP to its 89 kDa fragment, but no net increase in the total amount of PARP and its 89 kDa fragment after apoptosis in all models of transient RNAi (**Fig. 5.4,** 90h lanes +/- etoposide). Etoposide treatment consistently induced cleavage of Dicer-1 to its 180-kDa fragment (**Fig. 5.4**, 90h lanes), indicating that despite cleavage of Dicer-1, transient RNAi of the endogenous gene PARP by Dicer-1-independent (21mer dsRNA) or Dicer-1-dependent (shRNA and 27mer dsRNA) mechanisms persisted during apoptosis.

5.8 Discussion

We show here that transient RNAi of endogenous or exogenous gene, which has been achieved after short-term transfection with the gene-targeting 21mer dsRNA (siRNA), 27mer dsRNA or shRNA-generating DNA vector, does not fail for 2-3 days after onset of apoptosis. The results with 21mer dsRNA and detection of intact Ago-2 during apoptosis confirm our earlier report that RISC/Ago-2-mediated transient RNAi continues to function normally during apoptosis [5]. However, our results showing the persistence of transient RNAi by Dicer-1-dependent 27mer dsRNA or shRNA for up to 2-3 days during apoptosis is in contrast to the rapid failure of shRNA-mediated stable RNAi, which was reported earlier [5] and confirmed here. Since apoptotic cleavage of Dicer-1 to 180 kDa fragment results in its catalytic inactivation [5], it is evident that the production of new siRNA molecules from its precursors by the action of Dicer-1 would be halted with the onset of apoptosis in both the models of RNAi. However, this seems to interrupt only the stable RNAi and not the transient RNAi, indicating that the dynamics of achieving gene-knockdown and the dependency on Dicer-1 function must be different in stable and transient RNAi.

At least four factors could be responsible for the difference in the response of transient versus stable RNAi during apoptosis: (i) stability of siRNA-loaded RISC molecules; (ii) availability of siRNA in the cells at the time of onset of apoptosis; (iii) the half-life of siRNA; and (iv) the optimum number of siRNA-loaded RISC molecules required for an efficient gene knockdown. It has been suggested that siRNA-loaded RISC may be very stable [1], which could readily explain the persistence of all forms of transient RNAi during apoptosis, because once formed prior to onset of apoptosis, the siRNA-loaded RISC molecules could continue to knockdown the gene for several more days or until the cell dies by apoptosis. However, this does not explain why stable RNAi which also has an efficient (>90%) gene knockdown by siRNA-loaded RISC prior to induction of apoptosis, fails after onset of apoptosis. Our results with stable RNAi strongly indicate that siRNA-loaded RISC cannot be very stable, and that input of siRNA at regular intervals is required for the RISC to continue to knockdown a gene; thus making it potentially susceptible to

interruption in the supply of siRNA due to cleavage/inactivation of Dicer-1. Thus, an RNAi model in which the cells have higher supply of siRNA at the time of onset of apoptosis is likely to persist for a few days during apoptosis, whereas one with a minimal steady-state supply of siRNA is likely to be abrogated rapidly due to rapid exhaustion of its siRNA. In the transient RNAi, since there is a massive influx of siRNA or its precursor (27mer dsRNA or shRNA-generating DNA), a large presence of preformed or Dicer-1-generated siRNA can be expected to remain in the cells for a few more days during which apoptosis is induced in this model. In contrast, the stable RNAi clones are isolated over several weeks after initial transfection; hence these cells would have lost all of the initially transfected free shRNA-generating DNA molecules. Hence, stable RNAi would become totally dependent on the steady-state synthesis of shRNA from the shRNA-generating DNA integrated in the genome.

The second most important issue after availability of siRNA at the onset of apoptosis would be the half-life of the siRNA in cells. In blood, siRNA has been reported to have half-life of few minutes [1], however a recent study showed that siRNA can have a considerably longer half-life of up to 96h in some cells [9]. Our results showing persistence of transient RNAi for several days after failure of Dicer-1 supports the argument that siRNA available at the onset of apoptosis must have sufficiently long half-life to persist for several days and support the RISC-mediated knockdown of the gene. In contrast, the stable RNAi clones appear to be rapidly exhausted of the siRNA, indicating a much lower steady-state levels of siRNA. Our data that additional transient RNAi can be introduced in the clones with stable RNAi (**Fig. 5.3**) supports the argument that stable RNAi clones do not produce saturating amounts of siRNA to load all the available the RISC molecules. In addition, based on microRNA data, it has been estimated that about 1000 siRNA molecules per cell can efficiently silence a gene [1], and this number of siRNA would be readily available for several days after onset of apoptosis in the transient RNAi model as stated above. In contrast, since siRNA and miRNA share the same RISC machinery in mammalian cells, a thriving stable RNAi clone would make just the sufficient quantity of shRNA to efficiently silence the gene while leaving the remaining RISC molecules available for important cellular functions by miRNA. Thus stable RNAi, operating with just the minimally required number of siRNA-loaded RISC molecules, would be more prone

than transient RNAi to the apoptotic inactivation of Dicer-1 and interruption in the supply of fresh siRNA.

In conclusion, our results sound a cautionary note that while using RNAi in the study of apoptosis, one must monitor and account for a possible failure of RNAi after onset of apoptosis. Our results validate the use of stable RNAi mainly for the study of early apoptotic events and transient RNAi for study of both early and late apoptotic events. Our results indicate that siRNA loaded RISC is not very stable because it needs frequent input of fresh siRNA and cellular siRNA formed or introduced in the cells during transient RNAi is more stable than in blood. Thus 21mer and 27mer siRNA have a good therapeutic potential provided their stability could be increased in blood, because once inside the cells, they can achieve knockdown of the target gene for a long period of time.

5.9 Acknowledgement

This study was supported by the research grant to G.M.S. from the Natural Sciences and Engineering Research Council of Canada (155257-06). F.K.K. was a recipient of the NSERC-Doctoral scholarship award. E.B.A. and G.M.S. were recipients of the FRSQ-Junior-1 and FRSQ-Senior Scholarship awards, respectively, from the Fonds de la recherche en Santé du Québec.

5.10 References

1. Dykxhoorn DM, Lieberman J (2006) Knocking down disease with siRNAs. Cell 126: 231-235.

2. Kurreck J (2009) RNA interference: from basic research to therapeutic applications. Angew Chem Int Ed Engl 48: 1378-1398.

3. Kim DH, Behlke MA, Rose SD, Chang MS, Choi S, et al. (2005) Synthetic dsRNA Dicer substrates enhance RNAi potency and efficacy. Nat Biotechnol 23: 222-226.

4. Shi Y (2003) Mammalian RNAi for the masses. Trends Genet 19: 9-12.

5. Ghodgaonkar MM, Shah RG, Kandan-Kulangara F, Affar EB, Qi HH, et al. (2009) Abrogation of DNA vector-based RNAi during apoptosis in mammalian cells due to caspase-mediated cleavage and inactivation of Dicer-1. Cell Death Differ 16: 858-868.

6. Oikawa Y, Matsuda E, Nishii T, Ishida Y, Kawaichi M (2008) Down-regulation of CIBZ, a novel substrate of caspase-3, induces apoptosis. J Biol Chem 283: 14242-14247.

7. Zhang M, Zhou Y, Xie C, Zhou F, Chen Y, et al. (2006) STAT6 specific shRNA inhibits proliferation and induces apoptosis in colon cancer HT-29 cells. Cancer Lett 243: 38-46.

8. Shah RG, Ghodgaonkar MM, Affar EB, Shah GM (2005) DNA vector-based RNAi approach for stable depletion of poly(ADP-ribose) polymerase-1. Biochem Biophys Res Commun 331: 167-174.

9. Abe T, Goda K, Futami K, Furuichi Y (2009) Detection of siRNA administered to cells and animals by using a fluorescence intensity distribution analysis polarization system. Nucleic Acids Res 37: e56.

5.11 Legends to the figures

Fig. 5.1. Failure of stable but not transient RNAi of stably expressed GFP during apoptosis in CHO-GFP cells: (A) Comparison of GFP protein knockdown levels during stable versus transient RNAi by shGFP-234. For stable RNAi (left panel), CHO-GFP parental cells and its two stable shGFP-234 clones #62 and 64 were treated with 1,600 J/m^2 UVB and samples were harvested from 24-72h for immunoblotting. For transient RNAi (right panel), CHO-GFP cells were transfected with shGFP-234 (or mock pCMV vector) for 48h, treated with UVB and harvested from 48-72h for immunoblotting. Caspase-3 probing served to confirm apoptosis and actin-probing served as a loading control. GFP-levels are expressed relative to the untreated CHO-GFP controls (lanes 1 and 13). **(B)** Comparison of GFP transcript levels during stable versus transient RNAi by shGFP-234. From the cells treated as above, total RNA was extracted and subjected to RT-PCR determination of mRNA for GFP and GAPDH, the ratio of GFP/GAPDH is expressed as relative to respective untreated control (lanes 1 and 13). For both A and B panels, experiments were repeated 3-4 times with identical results. **(C)** Comparison of GFP protein knockdown levels in cells with variable extent of transient RNAi introduced by shGFP-234, shGFP-477 or 27mer dsRNA. The CHO-GFP cells were transfected with 3 μg shGFP-477 alone or in (1:2) combination with shGFP-234, and with different concentrations of 27mer dsRNA. The control CHO-GFP cells were mock transfected with unrelated shRNA-generating DNA vector. At 72h after transfection, unirradiated cells were harvested (UVB-) and the rest were treated with 1,600 J/m^2 UVB and harvested after 72h (UVB+). The samples were probed for GFP and activated caspase-3, whereas actin probing served as a loading control. GFP-levels are expressed relative to the untreated CHO-GFP controls (lane 1). The experiments were repeated 4 times with identical results.

Fig. 5.2. Persistence of GFP-knockdown during apoptosis in stable RNAi cells co-expressing transient RNAi. (A) Effect of UVB-induced apoptosis on RNAi of GFP in the stable RNAi clone #62 supplemented with transient RNAi. The shGFP-234 clone #62 with a stable RNAi of constitutively expressed GFP was transiently transfected with one of the

three GFP-targeting RNAi-inducing agents: 120 pmol of 21mer dsRNA, 2 pmol of 27mer dsRNA or 3 μg of shGFP-234 or with 3 μg of unrelated shRNA–generating DNA vector as control (mock) for transfection. At 48h after transfection, unirradiated cells were harvested (UVB-) and the rest were treated with 1,600 J/m^2 UVB (UVB+) and harvested after 72h. **(B)** Effect of MNNG-induced apoptosis on RNAi of GFP in the stable RNAi clone #64 supplemented with transient RNAi. The shGFP-234 clone #64 was transiently transfected with 3 μg of shGFP-234 and shGFP-477 DNA vector (2:1 and 1:2) in combination or with 5 pmol of 27mer dsRNA for 48h. Mock control was transfected as mentioned above. At 48h after transfection, untreated cells were harvested (MNNG-), while the rest were treated with 300 μM MNNG (MNNG+) and harvested 24h later. For both the panels, the samples were probed for GFP and activated caspase-3, whereas actin probing served as a loading control. The experiments were repeated 4 times with identical results.

Fig. 5.3. Persistence of transient RNAi of co-transfected GFP during apoptosis in GM637 cells. For examining apoptotic fate of transient RNAi of co-expressed GFP, GM637 cells were co-transfected with a GFP-expression vector and one of the following RNAi-inducing agents: **(A)** shGFP-234, shGFP-477 and 21mer dsRNA or mock pCMV vector; or **(B)** Varying amounts (0, 0.2, 1.0 and 2.0 pmol) of 27mer dsRNA. At 72h of knockdown, apoptosis was induced by treatment with 100 μM etoposide (or mock-control) for 18h. Samples were harvested at 72h (before apoptosis) or 90h (after apoptosis) for immunoblotting for GFP, Dicer-1, Ago-2, activated caspase-3 and PARP, as specified for each panel. The relative GFP values were determined as described in Fig. 1A. For above panels, either Ponceau-S staining or actin immunoprobing served as loading controls and Ap refers to apoptotic cell extract prepared from etoposide-treated HL-60 cells. The experiments were repeated at least four times with identical results.

Fig. 5.4. Persistence of transient RNAi of endogenous gene PARP during apoptosis in GM637 cells. The GM637 cells were transiently transfected with three RNAi-inducing agents: shRNA-generating DNA vector-SiP912, 27mer dsRNA or 21mer dsRNA or mock

pCMV vector as control. At 72h after transfection, cells were treated with 100 μM etoposide or with solvent control for 18h and samples were harvested for immunoblotting for PARP, activated caspase-3, Dicer-1 and Ago-2. The actin probing served as loading controls and Ap refers to apoptotic cell extract prepared from etoposide-treated HL-60 cells. The (PARP+89-kDa) signals from each sample are expressed as relative to untreated control in lane 1. The results shown in all three above panels are representative of 3-5 independent experiments with identical results.

Fig. 5S1. Abrogation of stable RNAi but persistence of transient RNAi in same cells during UVB-induced apoptosis. The shGFP-234 clone #64 was transiently transfected with 3 μg of shGFP-234 DNA vector for 48h. The CHO-GFP parental cells and shGFP-234 cells with or without additional transient RNAi by shGFP-234 or unrelated shRNA-generating DNA vector (control) were treated either with 1,600 J/m^2 UVB or mock-irradiated. The samples were harvested at 72h and probed for GFP and activated caspase-3, whereas actin probing served as a loading control. The experiments were repeated 3 times with identical results. GFP-levels are expressed relative to the untreated CHO-GFP controls (lane1).

5.12 Figures

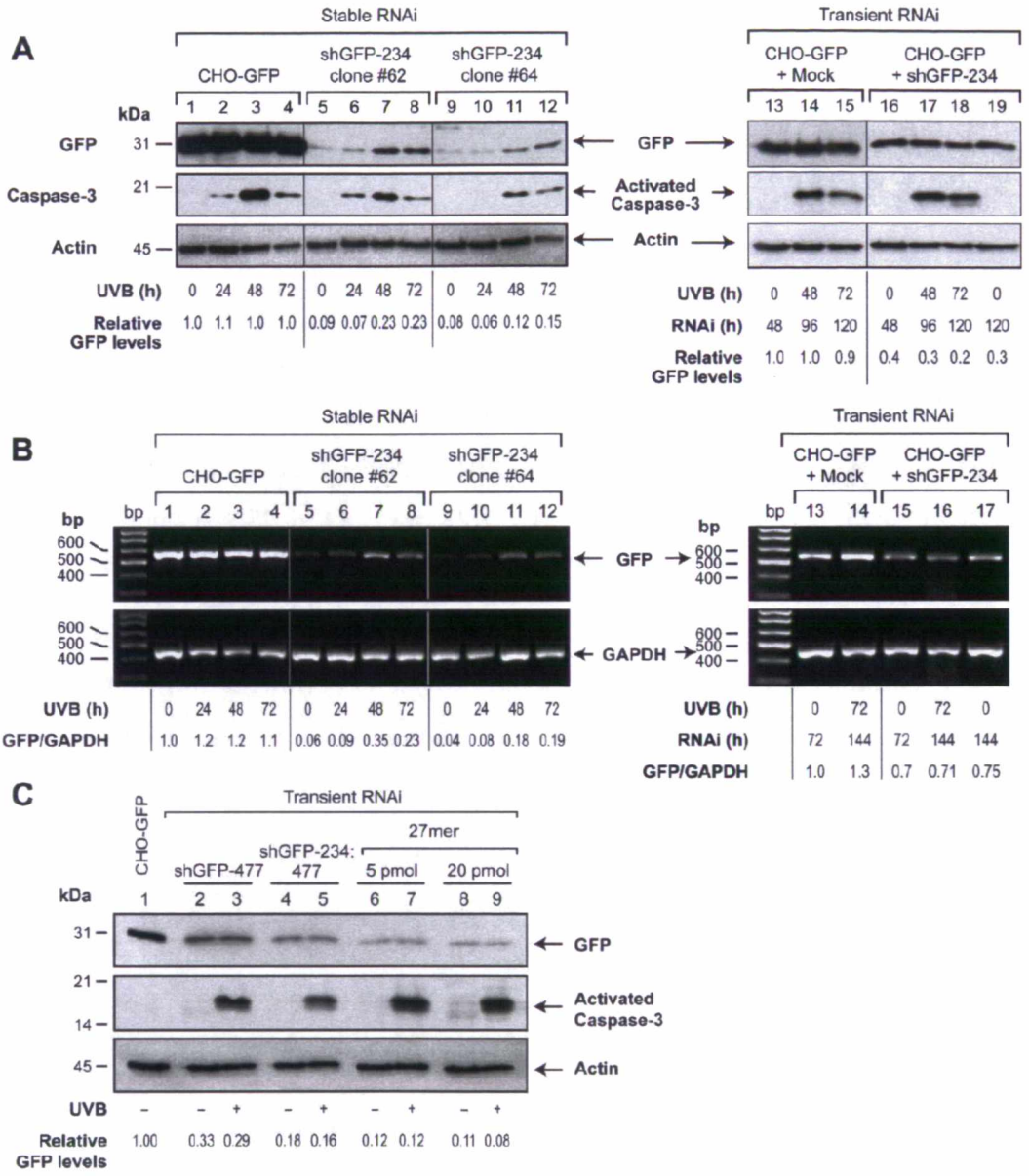

Figure 5.1: Failure of stable but not transient RNAi of stably expressed GFP during apoptosis in CHO-GFP cells

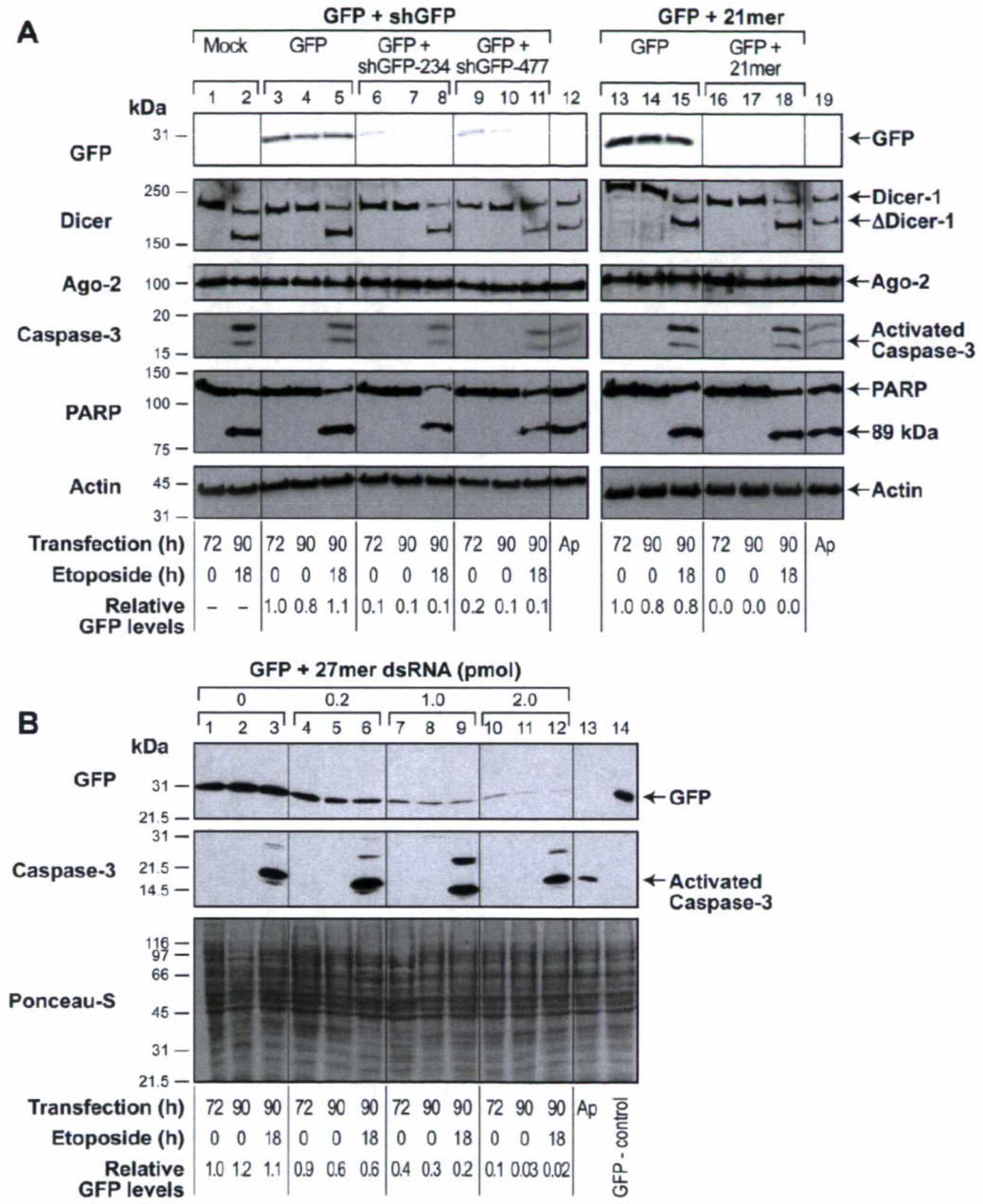

Figure 5.2: Persistence of GFP-knockdown during apoptosis in stable RNAi cells co-expressing transient RNAi

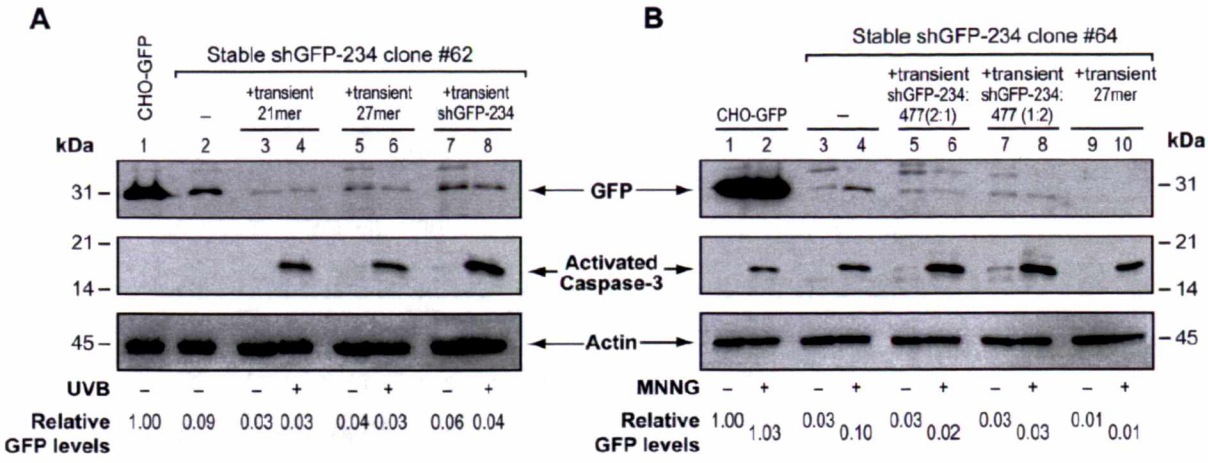

Figure 5.3: Persistence of transient RNAi of co-transfected GFP during apoptosis in GM637 cells

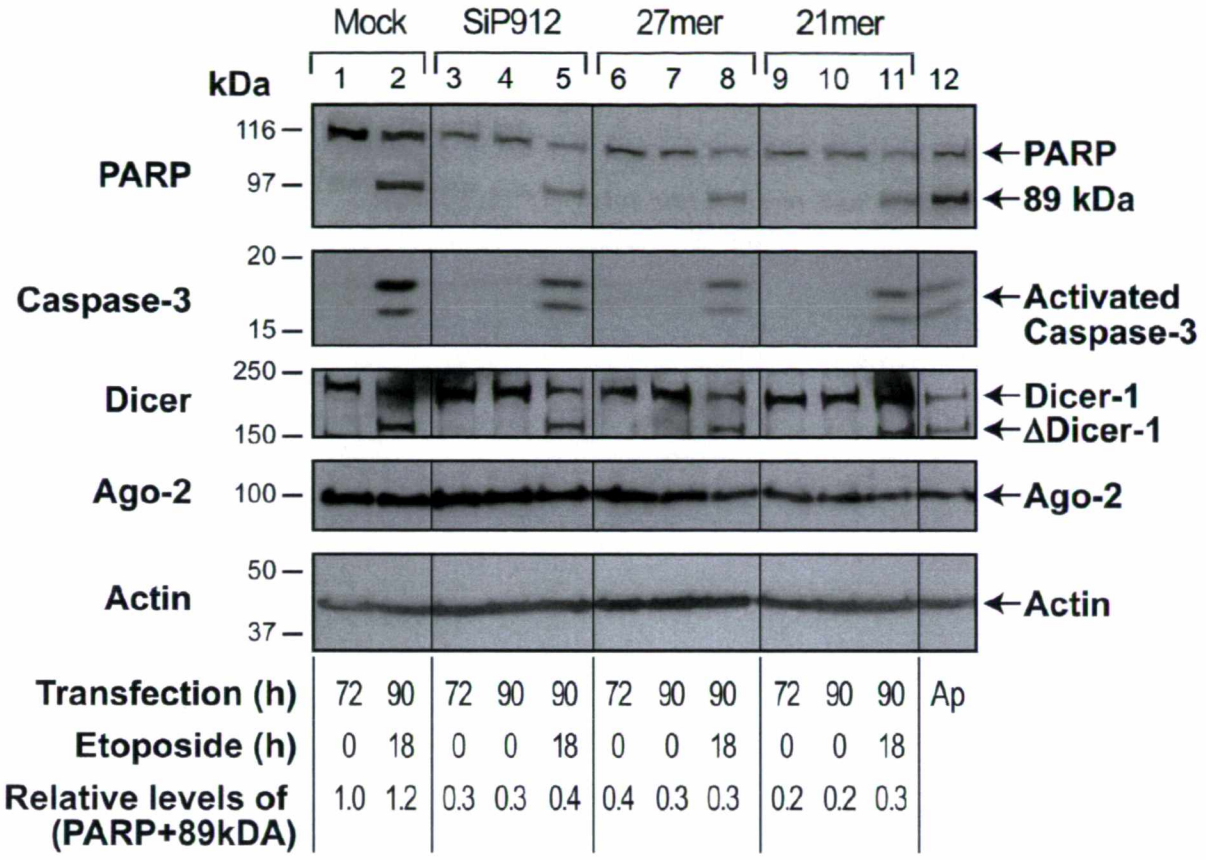

Figure 5.4: Persistence of transient RNAi of endogenous gene PARP during apoptosis in GM637 cells

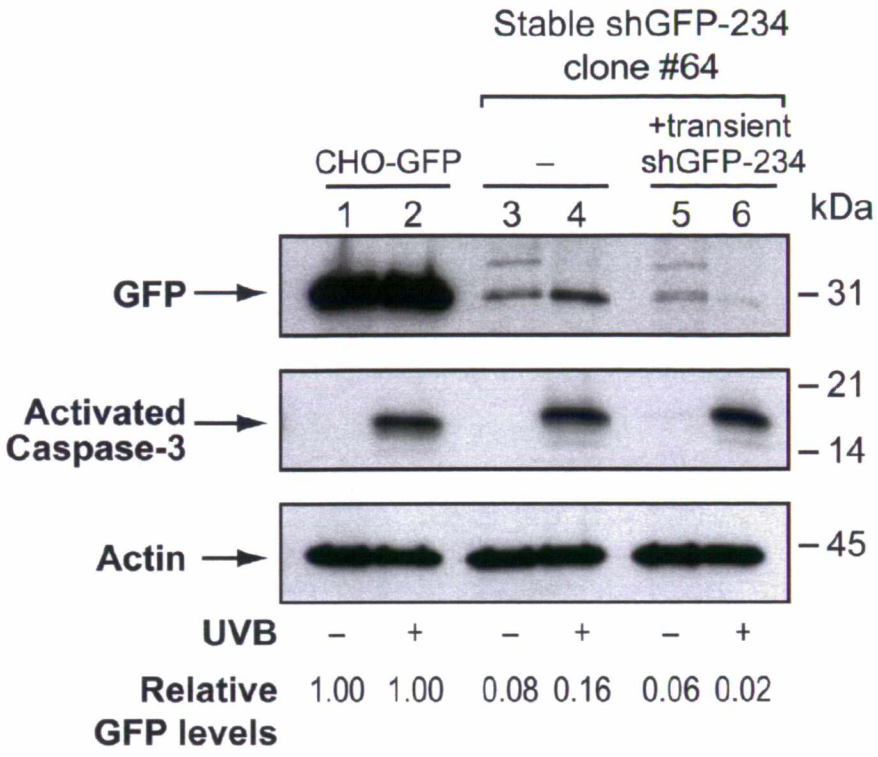

Figure 5S1: Abrogation of stable RNAi but persistence of transient RNAi in same cells during UVB-induced apoptosis

Chapter 6: Discussion and Conclusion

One of the most common signaling cascades involved in apoptosis is the activation of a highly specialized family of cysteine-dependent aspartate specific proteases (caspases) which drive the process of apoptosis through the cleavage of several key proteins required for cellular functioning and survival (*297*). During apoptosis PARP-1 is selectively cleaved by caspase-3 and -7 at the $DEVD^{214}$ generating a 24-kDa DBD and 89-kDa CD fragments (*7, 298*). PARP-1 was among the first identified targets of caspases and until today it remains as the best known targets of caspases because PARP-1 cleavage can be widely observed during apoptosis in many cell types in response to various apoptotic agents (*148*). In addition, PARP-1 cleavage has physiological significance during apoptosis. This cleavage is known to prevent additional PARP-1 activation in response to DNA damage and hence any further depletion of the cellular NAD^+/ATP levels, thereby preventing necrosis (*160*). If PARP-1 was not cleaved, the massive PARP-1 activation due to apoptotic DNA damage would result in depletion of NAD^+/ATP pools and generation of protons which could lead to cell death by necrosis (*138*). In response to UV, PARP-1 activation has been shown to participate in DNA repair and cell death. The initial goal of my PhD was to study the role of PARP-1 in UVB-induced cell death in a cellular model in which DNA vector-based RNAi was used to knockdown PARP-1 and furthermore checked for the integrity of RNAi during cell death.

6.1 PARP-1 and cell death

Our initial interest was to determine the role of PARP-1 in UVB induced cell death **(Chapter 2)**. Towards this, we have used PARP-1 knockdown cellular model in which PARP-1 was knocked-down by DNA vector-based RNAi (*204*). Using a gene rescue method in PARP-1 knockdown model, we also restored the expression of PARP-1 either with wild type or caspase-3-uncleavable PARP-1 (PARP-1-D^{214}/A). In our model, using PARP-1 mutants, we showed that resistance to UVB-induced cell death in PARP-1 knockdown cells could be rescued by wild-type PARP-1, but not by caspase-uncleavable PARP-1. During apoptosis, PARP-1 is cleaved to 24- and 89-kDa fragments. The 89-kDa fragment cannot be stimulated by DNA strand breaks; however, the 24-kDa DBD can bind to DNA and can act as dominant-negative factor. Upon overexpression, the 24-kDa DBD fragment can bind irreversibly to DNA breaks and transdominantly inhibit the full length

PARP-1 binding to residual DNA damage inhibiting polymer formation and thus inhibiting the DNA repair, preventing NAD^+/ATP depletion and thereby promoting apoptosis (*299*). This binding also inhibits polymer formation and the DNA repair related upregulation of transcription (*300*). Additionally, in HeLa cells, the overexpression of 24-kDa has shown to stimulate UV-mediated apoptosis (*152*) and 89-kDa interacts with intact PARP-1 and inhibits the homodimerization (*154*) during apoptosis suggesting that cleavage of PARP-1 and inhibition of PARP-1 activity maintains the basal cellular energy and is required for the completion of apoptosis.

In our model, we observed that the reintroduction of wild type PARP-1 in PARP-1 knockdown model restores the cell death profile suggesting that PARP-1 or its cleaved fragments could facilitate UVB-induced apoptosis. Furthermore, the cells expressing uncleavable PARP-1 showed a short-term delay in the onset of apoptosis and conferred long term protection only at low levels of UVB-induced DNA damage, suggesting that when the DNA damages are beyond repair, the massive depletion of NAD^+/ATP owing to uncleavable nature of PARP-1 will push to cell death. So far, four groups have independently generated and extensively characterized the caspase-3-uncleavable PARP-1 and have gained insight into the consequences of failure to cleave PARP-1 during apoptosis (*157-160*). Three probable consequences of PARP-1-D^{214}/A during apoptosis were reported: (i) survival or delayed apoptosis (ii) accelerated apoptosis and (iii) change in mode of cell death from apoptosis to necrosis. Previous studies from our lab has shown that in PARP-$1^{-/-}$ fibroblasts expressing PARP-1-D^{214}/A the low levels of DNA damage caused by an alkylating agent such as MNNG not only delays apoptosis but also helps in cell survival and proliferation. On the contrary, when challenged by a non-DNA damaging agent, such as TNF-α, PARP-1-D^{214}/A could only delay the progression of apoptosis but could not rescue cells from eventual death (*157*). In another study in response to anti-CD95 treatment, in PARP-$1^{-/-}$ fibroblasts transiently transfected with PARP-1-D^{214}/A reported a significant delay in apoptosis (*158*). This could also be due to two other factors, firstly, the persistence of PARP-1 activity owing to its uncleavable nature which could allow PARP-1 to participate in DNA repair and cell survival. In support of this, our lab has shown the role of PARP-1 in survival through NER of UV-damaged DNA (*130*). Secondly, it could also

inactivate pro-apoptotic factors by continuous poly(ADP-ribosyl)ation of pro-apoptotic substrates thereby delaying the progression of apoptosis which needs to be verified.

However, contrasting results have also been reported. In contrast to the above results, Herceg et al., using TNF-α, a non-DNA damaging agent, showed an accelerated death response and also observed a fraction of the cell population undergoing necrosis in PARP-$1^{-/-}$ fibroblasts carrying PARP-1-D^{214}/A (*159*). Similar results of enhanced apoptosis were also reported in response to staurosporine and TNF-α treatment (*160*). The accelerated death response could be due to rapid PAR synthesis and subsequent NAD^+ depletion clearly indicating that pro-survival function of PARP-1 and its early cleavage during apoptosis is necessary for in-time completion of the apoptotic program consistent with previous PARP inhibition studies (*155*).

Till now, in the context of caspase-uncleavable substrates, the major notion is that uncleavable substrates help only to understand the biological significance of proteins during apoptosis, such as the example of PARP-1. Nevertheless, studies using PARP-1-D^{214}/A in a mice model have revealed the role of PARP-1 and its catalytic activity in a non-death related function (*301, 302*) **(Chapter 3)**. In PARP-$1^{-/-}$ mice expressing a transgenic PARP-1-D^{214}/A mutant, Pétrilli et al. have shown that nitric oxide synthase-2 (NOS-2) gene transcription, which is responsible for the production of pro-inflammatory mediator such as nitric oxide (NO), was down regulated due to impaired NF-kB transcriptional activity (*302*). In this regard, they showed that restoration of wild type PARP-1 or enzymatically dead PARP-1 in PARP-$1^{-/-}$ macrophages restored NF-kB activity. Additionally, caspase inhibition in PARP-$1^{+/+}$ protected mice from renal I/R injury suggesting that it is the PARP-1 cleavage not PARP-1 activity that regulates NF-kB function. Lately Erener et al. showed that in response to LPS-stimulation, the proteolytic activation of caspase-1 within the NLRP3 inflammasome activates downstream caspase-7. The activated caspase-7 then translocates to the nucleus, cleaves the PARP-1, thereby resulting in dissociation of PARP-1 fragments from the promoter of NF-kB target genes.

This allows the decondensation of chromatin at the transcription start site (TSS) and facilitates NF-kB targeted gene expression (*301*).

Altogether, our study suggests that PARP-1 cleavage facilitates UVB-induced cell death and the PARP-1 mutants that we created can be used to study roles of PARP-1 in different cellular responses to DNA damaging agents including UVB and also in non-death related functions.

6.2 Dicer-1 and cell death

Today, RNAi has become an important tool for gene knockdown study in a wide range of organisms. As we discussed before, apoptosis is a process where proteins are cleaved by caspases to facilitate apoptosis, so, it was natural for us to examine whether RNAi which involves multiple proteins will continue to function during apoptosis. To address our curiosity, we characterized the integrity of gene knockdown model by RNAi during apoptosis. We made an initial observation of the failure of DNA vector-based RNAi of three different genes, such as PARP-1, a DNA repair protein; $p14^{ARF}$, a tumor suppressor protein involved in cell cycle regulation; and lamin A/C, a structural protein during apoptosis, assuming that failure of stable RNAi was not gene-specific rather a universal phenomenon. This intrigued us to check the integrity of RNAi at two different steps, involving two major RNases, such as Dicer-1 and Ago-2 during apoptosis. Ago-2, the slicer protein remained intact in the apoptotic RNAi model; interestingly, we found that the Dicer-1 is cleaved by caspase-3 at non canonical cleavage site $STTD^{1476}$ and $CGVD^{1538}$ within the RNaseIIIa domain into two fragments. This cleavage abolishes the dsRNA activity since both the RNaseIII domains of Dicer-1 form the catalytic center. Additionally, in many well-established models of apoptosis such as HL-60 and HeLa, we also showed that Dicer-1 cleavage is a universal feature during apoptosis.

Next, we addressed what is the impact of Dicer-1 cleavage in shRNA-based RNAi model. In our model, this Dicer-1 cleavage completely abolished its dicing activity, thus abrogating DNA vector-based stable RNAi **(Chapter 4)**. Many apoptotic studies utilize transient RNAi models to understand the role of protein during apoptosis, thus, we further

addressed the integrity of transient RNAi during apoptosis **(Chapter 5).** In cultured mammalian cells, transient RNAi can be achieved by introduction of 21mer/siRNAs or 21mer precursors such as 27mer or shRNA which are then dependent on Dicer-1 to process to siRNAs. Contrary to the failure of stable RNAi during apoptosis, the transient RNAi by 27mer dsRNA or shRNA remained functional during apoptosis despite Dicer-1 cleavage. We also showed that additional transient RNAi by 21mer, 27mer or shRNA in a stable RNAi model continued to function in the time frame, in which the stable RNAi failed during apoptosis. This result was interesting because it supported our argument that for stable RNAi to remain functional constant supply of siRNA is required and the cleavage of Dicer-1 compromises the availability of siRNA and so could possibly abrogate the stable RNAi due to non-availability of fresh siRNA. Our results also suggest a difference in dynamics of achieving gene-knockdown and dependency on Dicer-1 integrity between stable and transient RNAi.

One of the immediate effects of Dicer-1 cleavage could be reduced processing and availability of miRNAs. There has been a previous report on Dicer-1 cleavage by protease calpain which removes the helicase domain, but this increases the catalytic activity of Dicer-1 processing of miRNA activity, suggesting an auto-inhibitory role of helicase domain in Dicer-1 (*303*). However, we are the first to report the caspase-3-mediated cleavage of Dicer-1 and this cleavage abrogates the DNA vector-based stable RNAi. However, from our results with *in vitro* caspase assay and caspase-3 deficient MCF-7 cells, it cannot be ruled out that other caspases such as caspase-7 can also cleave Dicer-1 *in vivo*, because even a slight cleavage of Dicer-1 can result in trandominant inhibition of the normal Dicer-1 activity. In our model, Dicer-1 cleavage has resulted in reduction of vital apoptosis-related mature miRNAs. Recently, it is also reported that miRNA processing protein DiGeorge Critical Region 8 (DGCR8) is also a substrate of caspase-3 and its cleavage results in inhibition of pri-miRNA processing (*304*). Our results and recent studies suggest that during apoptosis, the miRNA pathway is compromised by affecting proteins, such as Dicer-1 and DGCR8 involved in RNAi and thereby contributing to cell death. In light of these results, in our model, we should check for the cleavage of DGCR8 and it will be interesting to analyze whether the availability of miRNA is compromised due to cleavage of DGCR8 and thereby contributing to cell death, because DGCR8 along with

Drosha functions upstream of Dicer-1. The other way is to check the accumulation of pre-miRNA transcripts in our experiment; however, the interpretation based on pre-miRNA should be cautiously used since a Dicer-1 independent miRNA biogenesis of miR451 in mice during erythropoiesis has been reported (*305*) suggesting that certain miRNA biogenesis can traverse the Dicer-independent pathway. Another possibility to check is the transcription. In miRNA biogensis, the first step is the transcription of miRNA genes. So, during cell death where there will be lot of DNA fragmentation, can it affect the miRNA transcription making the lesser pre-miRNAs and thereby affecting the availability of miRNA?

Dicer-1 is a highly conserved ribonuclease and the number of genes encoding Dicer homologues varies from 2 (Dcr-1 and Dcr-2) in *Drosophila*, to one (Dicer-1) in *C.elegans* and mammalian species (*285*). In *Drosophila*, Dcr-1 is involved in pre-miRNA cleavage and Dcr-2 in siRNA generation (*306*). Similar to mammalians, in *C.elegans* Dicer-1 is involved in both miRNA and siRNA processing. The Dicer-1 null mutation in mice shows embryonic lethal phenotype at E 7.5 indicating Dicer-1 is important in miRNA pathway which is critical for the mammalian development (*307*) suggesting a pro-survival role of Dicer-1. However, recently, in *C. elegans,* the unexpected gain-of-function for cleaved fragment of Dicer-1 (Dcr-1) has been reported. The C-terminal small fragment with RNaseIIIb domain becomes pro-apoptotic thereby converting Dcr-1 into a death promoting deoxyribonuclease (DNase) which is independent of Dicer-1's action in gene silencing (*308*). Thus, in *C. elegans* Dcr-1 has an RNAi-independent role that is required for internucleosomal degradation during apoptosis suggesting a pro-apoptotic role of Dcr-1. However, such function in mammalian system remains to be identified and will add a new perspective to the decisive role of Dicer-1 cleavage in apoptosis.

6.3 Perspective

During my doctoral work, we have addressed the role of PARP-1 in UVB-induced cell death and the impact of cell death on the integrity of RNAi in cellular models.

In chapter 2, through a series of experiment we have shown that PARP-1 cleavage is important to facilitate UVB-induced cell death. However, in our cell death model, the role of catalytic activity of PARP-1 and its cleavage needs to be analyzed separately. Studies involving PARP inhibitors, caspase-inhibitors or catalytically inactive PARP-1 will help to address the same. Towards this, we have already created the Flag-tagged RNAi-resistant catalytically inactive PARP-1 vectors which need to be expressed in PARP-1-RNAi model. In response to UV radiations, the signaling pathway can originate in the nucleus, at the cell membrane or in the cytoplasm. Thus, we also need to elucidate how PARP-1 activation and its cleavage can interlink the different signaling pathways that could generate at the level of MAPK activation or affect the p53 dependent apoptosis in response to UVB (*209*). Additionally, in response to different apoptotic stimuli, an early and transient burst of poly(ADP-ribosyl)ation of nuclear proteins was shown to be required for apoptosis to proceed in various cell lines (*155*). Based on our results, using PARP-1 mutants we can immunoprecipitate and identify the proteins that may be bound to PARP-1 or its fragment or its polymer in response to apoptosis by UVB.

In chapter 4 and 5, we have identified Dicer-1 as a novel caspase-3 substrate and that caspase-mediated cleavage of Dicer-1 abrogates DNA vector-based stable RNAi in contrast to transient RNAi which persists. Apart from miRNA/siRNA processing, recently in *C. elegans* an unexpected role for RNase Dicer-1 as a DNase in apoptosis has been reported (*308*). It will be interesting to see whether this caspase-cleavage mediated DNase function is conserved in mammalian systems. In our lab we have generated a caspase-uncleavable Dicer-1, using this vector it will be interesting to check the role of Dicer-1 cleavage in apoptosis in mammalian system. Second, using uncleavable Dicer-1 or conditional Dicer-1 knockdown it will be interesting to investigate the role of Dicer-1 in controlling apoptotic events and in cancer through altered availability of miRNA.

REFERENCES: Cited references for chapter 1 and 6

1. Chambon, P., Weill, J. D., and Mandel, P. (1963) Nicotinamide mononucleotide activation of new DNA-dependent polyadenylic acid synthesizing nuclear enzyme, *Biochem Biophys Res Commun 11*, 39-43.
2. Alkhatib, H. M., Chen, D. F., Cherney, B., Bhatia, K., Notario, V., Giri, C., Stein, G., Slattery, E., Roeder, R. G., and Smulson, M. E. (1987) Cloning and expression of cDNA for human poly(ADP-ribose) polymerase, *Proc Natl Acad Sci U S A 84*, 1224-1228.
3. Ushiro, H., Yokoyama, Y., and Shizuta, Y. (1987) Purification and characterization of poly (ADP-ribose) synthetase from human placenta, *J Biol Chem 262*, 2352-2357.
4. Luo, X., and Kraus, W. L. (2012) On PAR with PARP: cellular stress signaling through poly(ADP-ribose) and PARP-1, *Genes Dev 26*, 417-432.
5. D'Amours, D., Desnoyers, S., D'Silva, I., and Poirier, G. G. (1999) Poly(ADP-ribosyl)ation reactions in the regulation of nuclear functions, *Biochem J 342 (Pt 2)*, 249-268.
6. de Murcia, G., Schreiber, V., Molinete, M., Saulier, B., Poch, O., Masson, M., Niedergang, C., and Menissier de Murcia, J. (1994) Structure and function of poly(ADP-ribose) polymerase, *Mol Cell Biochem 138*, 15-24.
7. Kaufmann, S. H., Desnoyers, S., Ottaviano, Y., Davidson, N. E., and Poirier, G. G. (1993) Specific proteolytic cleavage of poly(ADP-ribose) polymerase: an early marker of chemotherapy-induced apoptosis, *Cancer Res 53*, 3976-3985.
8. Langelier, M. F., Servent, K. M., Rogers, E. E., and Pascal, J. M. (2008) A third zinc-binding domain of human poly(ADP-ribose) polymerase-1 coordinates DNA-dependent enzyme activation, *J Biol Chem 283*, 4105-4114.
9. Eustermann, S., Videler, H., Yang, J. C., Cole, P. T., Gruszka, D., Veprintsev, D., and Neuhaus, D. (2011) The DNA-binding domain of human PARP-1 interacts with DNA single-strand breaks as a monomer through its second zinc finger, *J Mol Biol 407*, 149-170.
10. Langelier, M. F., Planck, J. L., Roy, S., and Pascal, J. M. (2011) Crystal structures of poly(ADP-ribose) polymerase-1 (PARP-1) zinc fingers bound to DNA: structural and functional insights into DNA-dependent PARP-1 activity, *J Biol Chem 286*, 10690-10701.
11. Langelier, M. F., Ruhl, D. D., Planck, J. L., Kraus, W. L., and Pascal, J. M. (2010) The Zn3 domain of human poly(ADP-ribose) polymerase-1 (PARP-1) functions in both DNA-dependent poly(ADP-ribose) synthesis activity and chromatin compaction, *J Biol Chem 285*, 18877-18887.
12. Lonskaya, I., Potaman, V. N., Shlyakhtenko, L. S., Oussatcheva, E. A., Lyubchenko, Y. L., and Soldatenkov, V. A. (2005) Regulation of poly(ADP-ribose) polymerase-1 by DNA structure-specific binding, *J Biol Chem 280*, 17076-17083.
13. Tao, Z., Gao, P., and Liu, H. W. (2009) Identification of the ADP-ribosylation sites in the PARP-1 automodification domain: analysis and implications, *J Am Chem Soc 131*, 14258-14260.
14. Altmeyer, M., Messner, S., Hassa, P. O., Fey, M., and Hottiger, M. O. (2009) Molecular mechanism of poly(ADP-ribosyl)ation by PARP1 and identification of lysine residues as ADP-ribose acceptor sites, *Nucleic Acids Res 37*, 3723-3738.

15. Krishnakumar, R., and Kraus, W. L. (2010) The PARP side of the nucleus: molecular actions, physiological outcomes, and clinical targets, *Mol Cell 39*, 8-24.
16. Mendoza-Alvarez, H., and Alvarez-Gonzalez, R. (1993) Poly(ADP-ribose) polymerase is a catalytic dimer and the automodification reaction is intermolecular, *J Biol Chem 268*, 22575-22580.
17. Paddock, M. N., Buelow, B. D., Takeda, S., and Scharenberg, A. M. (2010) The BRCT domain of PARP-1 is required for immunoglobulin gene conversion, *PLoS Biol 8*, e1000428.
18. Langelier, M. F., and Pascal, J. M. (2013) PARP-1 mechanism for coupling DNA damage detection to poly(ADP-ribose) synthesis, *Curr Opin Struct Biol 23*, 1-10.
19. Huambachano, O., Herrera, F., Rancourt, A., and Satoh, M. S. (2011) Double-stranded DNA binding domain of poly(ADP-ribose) polymerase-1 and molecular insight into the regulation of its activity, *J Biol Chem 286*, 7149-7160.
20. Langelier, M. F., Planck, J. L., Roy, S., and Pascal, J. M. (2012) Structural basis for DNA damage-dependent poly(ADP-ribosyl)ation by human PARP-1, *Science 336*, 728-732.
21. Kleine, H., Poreba, E., Lesniewicz, K., Hassa, P. O., Hottiger, M. O., Litchfield, D. W., Shilton, B. H., and Luscher, B. (2008) Substrate-assisted catalysis by PARP10 limits its activity to mono-ADP-ribosylation, *Mol Cell 32*, 57-69.
22. Otto, H., Reche, P. A., Bazan, F., Dittmar, K., Haag, F., and Koch-Nolte, F. (2005) In silico characterization of the family of PARP-like poly(ADP-ribosyl)transferases (pARTs), *BMC Genomics 6*, 139.
23. Simonin, F., Hofferer, L., Panzeter, P. L., Muller, S., de Murcia, G., and Althaus, F. R. (1993) The carboxyl-terminal domain of human poly(ADP-ribose) polymerase. Overproduction in Escherichia coli, large scale purification, and characterization, *J Biol Chem 268*, 13454-13461.
24. Coquelle, N., and Glover, J. N. (2012) PARP pairs up to PARsylate, *Nat Struct Mol Biol 19*, 660-661.
25. Ali, A. A., Timinszky, G., Arribas-Bosacoma, R., Kozlowski, M., Hassa, P. O., Hassler, M., Ladurner, A. G., Pearl, L. H., and Oliver, A. W. (2012) The zinc-finger domains of PARP1 cooperate to recognize DNA strand breaks, *Nat Struct Mol Biol 19*, 685-692.
26. Gagne, J. P., Rouleau, M., and Poirier, G. G. (2012) Structural biology. PARP-1 activation--bringing the pieces together, *Science 336*, 678-679.
27. Hakme, A., Wong, H. K., Dantzer, F., and Schreiber, V. (2008) The expanding field of poly(ADP-ribosyl)ation reactions. 'Protein Modifications: Beyond the Usual Suspects' Review Series, *EMBO Rep 9*, 1094-1100.
28. J. Ame, and, E. J., and Jacobson, M. K. (2000) ADP-ribose polymer metabolism, in *from DNA damage and stress signalling to cell death poly ADP-ribosylation reactions* (deMurcia, G., and Shall, S., Eds.), pp 1-20.
29. Hassa, P. O., Haenni, S. S., Elser, M., and Hottiger, M. O. (2006) Nuclear ADP-ribosylation reactions in mammalian cells: where are we today and where are we going?, *Microbiol Mol Biol Rev 70*, 789-829.
30. Schreiber, V., Dantzer, F., Ame, J. C., and de Murcia, G. (2006) Poly(ADP-ribose): novel functions for an old molecule, *Nat Rev Mol Cell Biol 7*, 517-528.
31. Gibson, B. A., and Kraus, W. L. (2012) New insights into the molecular and cellular functions of poly(ADP-ribose) and PARPs, *Nat Rev Mol Cell Biol 13*, 411-424.

32. Minaga, T., and Kun, E. (1983) Spectral analysis of the conformation of polyadenosine diphosphoribose. Evidence indicating secondary structure, *J Biol Chem 258*, 725-730.
33. Sallmann, F. R., Vodenicharov, M. D., Wang, Z. Q., and Poirier, G. G. (2000) Characterization of sPARP-1. An alternative product of PARP-1 gene with poly(ADP-ribose) polymerase activity independent of DNA strand breaks, *J Biol Chem 275*, 15504-15511.
34. Rouleau, M., Patel, A., Hendzel, M. J., Kaufmann, S. H., and Poirier, G. G. (2010) PARP inhibition: PARP1 and beyond, *Nat Rev Cancer 10*, 293-301.
35. Gagne, J. P., Isabelle, M., Lo, K. S., Bourassa, S., Hendzel, M. J., Dawson, V. L., Dawson, T. M., and Poirier, G. G. (2008) Proteome-wide identification of poly(ADP-ribose) binding proteins and poly(ADP-ribose)-associated protein complexes, *Nucleic Acids Res 36*, 6959-6976.
36. Rouleau, M., Aubin, R. A., and Poirier, G. G. (2004) Poly(ADP-ribosyl)ated chromatin domains: access granted, *J Cell Sci 117*, 815-825.
37. Fahrer, J., Kranaster, R., Altmeyer, M., Marx, A., and Burkle, A. (2007) Quantitative analysis of the binding affinity of poly(ADP-ribose) to specific binding proteins as a function of chain length, *Nucleic Acids Res 35*, e143.
38. Fahrer, J., Popp, O., Malanga, M., Beneke, S., Markovitz, D. M., Ferrando-May, E., Burkle, A., and Kappes, F. (2010) High-affinity interaction of poly(ADP-ribose) and the human DEK oncoprotein depends upon chain length, *Biochemistry 49*, 7119-7130.
39. Pleschke, J. M., Kleczkowska, H. E., Strohm, M., and Althaus, F. R. (2000) Poly(ADP-ribose) binds to specific domains in DNA damage checkpoint proteins, *J Biol Chem 275*, 40974-40980.
40. Ahel, I., Ahel, D., Matsusaka, T., Clark, A. J., Pines, J., Boulton, S. J., and West, S. C. (2008) Poly(ADP-ribose)-binding zinc finger motifs in DNA repair/checkpoint proteins, *Nature 451*, 81-85.
41. Rulten, S. L., Cortes-Ledesma, F., Guo, L., Iles, N. J., and Caldecott, K. W. (2008) APLF (C2orf13) is a novel component of poly(ADP-ribose) signaling in mammalian cells, *Mol Cell Biol 28*, 4620-4628.
42. Kraus, W. L. (2009) New functions for an ancient domain, *Nat Struct Mol Biol 16*, 904-907.
43. Timinszky, G., Till, S., Hassa, P. O., Hothorn, M., Kustatscher, G., Nijmeijer, B., Colombelli, J., Altmeyer, M., Stelzer, E. H., Scheffzek, K., Hottiger, M. O., and Ladurner, A. G. (2009) A macrodomain-containing histone rearranges chromatin upon sensing PARP1 activation, *Nat Struct Mol Biol 16*, 923-929.
44. Ahel, D., Horejsi, Z., Wiechens, N., Polo, S. E., Garcia-Wilson, E., Ahel, I., Flynn, H., Skehel, M., West, S. C., Jackson, S. P., Owen-Hughes, T., and Boulton, S. J. (2009) Poly(ADP-ribose)-dependent regulation of DNA repair by the chromatin remodeling enzyme ALC1, *Science 325*, 1240-1243.
45. Kang, H. C., Lee, Y. I., Shin, J. H., Andrabi, S. A., Chi, Z., Gagne, J. P., Lee, Y., Ko, H. S., Lee, B. D., Poirier, G. G., Dawson, V. L., and Dawson, T. M. (2011) Iduna is a poly(ADP-ribose) (PAR)-dependent E3 ubiquitin ligase that regulates DNA damage, *Proc Natl Acad Sci U S A 108*, 14103-14108.

46. Krietsch, J., Rouleau, M., Pic, E., Ethier, C., Dawson, T. M., Dawson, V. L., Masson, J. Y., Poirier, G. G., and Gagne, J. P. (2012) Reprogramming cellular events by poly(ADP-ribose)-binding proteins, *Mol Aspects Med In Press*.
47. Slade, D., Dunstan, M. S., Barkauskaite, E., Weston, R., Lafite, P., Dixon, N., Ahel, M., Leys, D., and Ahel, I. (2011) The structure and catalytic mechanism of a poly(ADP-ribose) glycohydrolase, *Nature 477*, 616.
48. Brochu, G., Duchaine, C., Thibeault, L., Lagueux, J., Shah, G. M., and Poirier, G. G. (1994) Mode of action of poly(ADP-ribose) glycohydrolase, *Biochim Biophys Acta 1219*, 342-350.
49. Braun, S. A., Panzeter, P. L., Collinge, M. A., and Althaus, F. R. (1994) Endoglycosidic cleavage of branched polymers by poly(ADP-ribose) glycohydrolase, *Eur J Biochem 220*, 369-375.
50. Alvarez-Gonzalez, R., and Althaus, F. R. (1989) Poly(ADP-ribose) catabolism in mammalian cells exposed to DNA-damaging agents, *Mutat Res 218*, 67-74.
51. Haince, J. F., Ouellet, M. E., McDonald, D., Hendzel, M. J., and Poirier, G. G. (2006) Dynamic relocation of poly(ADP-ribose) glycohydrolase isoforms during radiation-induced DNA damage, *Biochim Biophys Acta 1763*, 226-237.
52. Lin, W., Ame, J. C., Aboul-Ela, N., Jacobson, E. L., and Jacobson, M. K. (1997) Isolation and characterization of the cDNA encoding bovine poly(ADP-ribose) glycohydrolase, *J Biol Chem 272*, 11895-11901.
53. Winstall, E., Affar, E. B., Shah, R., Bourassa, S., Scovassi, A. I., and Poirier, G. G. (1999) Poly(ADP-ribose) glycohydrolase is present and active in mammalian cells as a 110-kDa protein, *Exp Cell Res 246*, 395-398.
54. Di Meglio, S., Denegri, M., Vallefuoco, S., Tramontano, F., Scovassi, A. I., and Quesada, P. (2003) Poly(ADPR) polymerase-1 and poly(ADPR) glycohydrolase level and distribution in differentiating rat germinal cells, *Mol Cell Biochem 248*, 85-91.
55. Meyer-Ficca, M. L., Meyer, R. G., Coyle, D. L., Jacobson, E. L., and Jacobson, M. K. (2004) Human poly(ADP-ribose) glycohydrolase is expressed in alternative splice variants yielding isoforms that localize to different cell compartments, *Exp Cell Res 297*, 521-532.
56. Koh, D. W., Lawler, A. M., Poitras, M. F., Sasaki, M., Wattler, S., Nehls, M. C., Stoger, T., Poirier, G. G., Dawson, V. L., and Dawson, T. M. (2004) Failure to degrade poly(ADP-ribose) causes increased sensitivity to cytotoxicity and early embryonic lethality, *Proc Natl Acad Sci U S A 101*, 17699-17704.
57. Cortes, U., Tong, W. M., Coyle, D. L., Meyer-Ficca, M. L., Meyer, R. G., Petrilli, V., Herceg, Z., Jacobson, E. L., Jacobson, M. K., and Wang, Z. Q. (2004) Depletion of the 110-kilodalton isoform of poly(ADP-ribose) glycohydrolase increases sensitivity to genotoxic and endotoxic stress in mice, *Mol Cell Biol 24*, 7163-7178.
58. Mortusewicz, O., Fouquerel, E., Ame, J. C., Leonhardt, H., and Schreiber, V. (2011) PARG is recruited to DNA damage sites through poly(ADP-ribose)- and PCNA-dependent mechanisms, *Nucleic Acids Res 39*, 5045-5056.
59. Davidovic, L., Vodenicharov, M., Affar, E. B., and Poirier, G. G. (2001) Importance of poly(ADP-ribose) glycohydrolase in the control of poly(ADP-ribose) metabolism, *Exp Cell Res 268*, 7-13.
60. Okayama, H., Honda, M., and Hayaishi, O. (1978) Novel enzyme from rat liver that cleaves an ADP-ribosyl histone linkage, *Proc Natl Acad Sci U S A 75*, 2254-2257.

61. Oka, J., Ueda, K., Hayaishi, O., Komura, H., and Nakanishi, K. (1984) ADP-ribosyl protein lyase. Purification, properties, and identification of the product, *J Biol Chem 259*, 986-995.
62. Oka, S., Kato, J., and Moss, J. (2006) Identification and characterization of a mammalian 39-kDa poly(ADP-ribose) glycohydrolase, *J Biol Chem 281*, 705-713.
63. Mueller-Dieckmann, C., Kernstock, S., Lisurek, M., von Kries, J. P., Haag, F., Weiss, M. S., and Koch-Nolte, F. (2006) The structure of human ADP-ribosylhydrolase 3 (ARH3) provides insights into the reversibility of protein ADP-ribosylation, *Proc Natl Acad Sci U S A 103*, 15026-15031.
64. Shieh, W. M., Ame, J. C., Wilson, M. V., Wang, Z. Q., Koh, D. W., Jacobson, M. K., and Jacobson, E. L. (1998) Poly(ADP-ribose) polymerase null mouse cells synthesize ADP-ribose polymers, *J Biol Chem 273*, 30069-30072.
65. Hottiger, M. O., Hassa, P. O., Luscher, B., Schuler, H., and Koch-Nolte, F. (2010) Toward a unified nomenclature for mammalian ADP-ribosyltransferases, *Trends Biochem Sci 35*, 208-219.
66. Ame, J. C., Rolli, V., Schreiber, V., Niedergang, C., Apiou, F., Decker, P., Muller, S., Hoger, T., Menissier-de Murcia, J., and de Murcia, G. (1999) PARP-2, A novel mammalian DNA damage-dependent poly(ADP-ribose) polymerase, *J Biol Chem 274*, 17860-17868.
67. Yelamos, J., Schreiber, V., and Dantzer, F. (2008) Toward specific functions of poly(ADP-ribose) polymerase-2, *Trends Mol Med 14*, 169-178.
68. Mortusewicz, O., Ame, J. C., Schreiber, V., and Leonhardt, H. (2007) Feedback-regulated poly(ADP-ribosyl)ation by PARP-1 is required for rapid response to DNA damage in living cells, *Nucleic Acids Res 35*, 7665-7675.
69. Schreiber, V., Ame, J. C., Dolle, P., Schultz, I., Rinaldi, B., Fraulob, V., Menissier-de Murcia, J., and de Murcia, G. (2002) Poly(ADP-ribose) polymerase-2 (PARP-2) is required for efficient base excision DNA repair in association with PARP-1 and XRCC1, *J Biol Chem 277*, 23028-23036.
70. Dantzer, F., de La Rubia, G., Menissier-De Murcia, J., Hostomsky, Z., de Murcia, G., and Schreiber, V. (2000) Base excision repair is impaired in mammalian cells lacking Poly(ADP-ribose) polymerase-1, *Biochemistry 39*, 7559-7569.
71. Szanto, M., Brunyanszki, A., Kiss, B., Nagy, L., Gergely, P., Virag, L., and Bai, P. (2012) Poly(ADP-ribose) polymerase-2: emerging transcriptional roles of a DNA-repair protein, *Cell Mol Life Sci*, 4079-4092.
72. Bai, P., Canto, C., Brunyanszki, A., Huber, A., Szanto, M., Cen, Y., Yamamoto, H., Houten, S. M., Kiss, B., Oudart, H., Gergely, P., Menissier-de Murcia, J., Schreiber, V., Sauve, A. A., and Auwerx, J. (2011) PARP-2 regulates SIRT1 expression and whole-body energy expenditure, *Cell Metab 13*, 450-460.
73. Luo, X., and Kraus, W. L. (2011) A one and a two ... expanding roles for poly(ADP-ribose) polymerases in metabolism, *Cell Metab 13*, 353-355.
74. Menissier de Murcia, J., Ricoul, M., Tartier, L., Niedergang, C., Huber, A., Dantzer, F., Schreiber, V., Ame, J. C., Dierich, A., LeMeur, M., Sabatier, L., Chambon, P., and de Murcia, G. (2003) Functional interaction between PARP-1 and PARP-2 in chromosome stability and embryonic development in mouse, *EMBO J 22*, 2255-2263.

75. Rulten, S. L., Fisher, A. E., Robert, I., Zuma, M. C., Rouleau, M., Ju, L., Poirier, G., Reina-San-Martin, B., and Caldecott, K. W. (2011) PARP-3 and APLF function together to accelerate nonhomologous end-joining, *Mol Cell 41*, 33-45.
76. Boehler, C., Gauthier, L. R., Mortusewicz, O., Biard, D. S., Saliou, J. M., Bresson, A., Sanglier-Cianferani, S., Smith, S., Schreiber, V., Boussin, F., and Dantzer, F. (2011) Poly(ADP-ribose) polymerase 3 (PARP3), a newcomer in cellular response to DNA damage and mitotic progression, *Proc Natl Acad Sci U S A 108*, 2783-2788.
77. Johansson, M. (1999) A human poly(ADP-ribose) polymerase gene family (ADPRTL): cDNA cloning of two novel poly(ADP-ribose) polymerase homologues, *Genomics 57*, 442-445.
78. Augustin, A., Spenlehauer, C., Dumond, H., Menissier-De Murcia, J., Piel, M., Schmit, A. C., Apiou, F., Vonesch, J. L., Kock, M., Bornens, M., and De Murcia, G. (2003) PARP-3 localizes preferentially to the daughter centriole and interferes with the G1/S cell cycle progression, *J Cell Sci 116*, 1551-1562.
79. Rulten, S. L., Fisher, A. E., Robert, I., Zuma, M. C., Rouleau, M., Ju, L., Poirier, G., Reina-San-Martin, B., and Caldecott, K. W. PARP-3 and APLF function together to accelerate nonhomologous end-joining, *Mol Cell 41*, 33-45.
80. Rouleau, M., McDonald, D., Gagne, P., Ouellet, M. E., Droit, A., Hunter, J. M., Dutertre, S., Prigent, C., Hendzel, M. J., and Poirier, G. G. (2007) PARP-3 associates with polycomb group bodies and with components of the DNA damage repair machinery, *J Cell Biochem 100*, 385-401.
81. Loseva, O., Jemth, A. S., Bryant, H. E., Schuler, H., Lehtio, L., Karlberg, T., and Helleday, T. PARP-3 is a mono-ADP-ribosylase that activates PARP-1 in the absence of DNA, *J Biol Chem 285*, 8054-8060.
82. Raval-Fernandes, S., Kickhoefer, V. A., Kitchen, C., and Rome, L. H. (2005) Increased susceptibility of vault poly(ADP-ribose) polymerase-deficient mice to carcinogen-induced tumorigenesis, *Cancer Res 65*, 8846-8852.
83. Cook, B. D., Dynek, J. N., Chang, W., Shostak, G., and Smith, S. (2002) Role for the related poly(ADP-Ribose) polymerases tankyrase 1 and 2 at human telomeres, *Mol Cell Biol 22*, 332-342.
84. Ame, J. C., Spenlehauer, C., and de Murcia, G. (2004) The PARP superfamily, *Bioessays 26*, 882-893.
85. Althaus, F. R., Kleczkowska, H. E., Malanga, M., Muntener, C. R., Pleschke, J. M., Ebner, M., and Auer, B. (1999) Poly ADP-ribosylation: a DNA break signal mechanism, *Mol Cell Biochem 193*, 5-11.
86. Shall, S., and de Murcia, G. (2000) Poly(ADP-ribose) polymerase-1: what have we learned from the deficient mouse model?, *Mutat Res 460*, 1-15.
87. Robertson, A. B., Klungland, A., Rognes, T., and Leiros, I. (2009) DNA repair in mammalian cells: Base excision repair: the long and short of it, *Cell Mol Life Sci 66*, 981-993.
88. Caldecott, K. W. (2008) Single-strand break repair and genetic disease, *Nat Rev Genet 9*, 619-631.
89. Caldecott, K. W. (2007) Mammalian single-strand break repair: mechanisms and links with chromatin, *DNA Repair (Amst) 6*, 443-453.
90. Miwa, M., and Masutani, M. (2007) PolyADP-ribosylation and cancer, *Cancer Sci 98*, 1528-1535.

91. Zharkov, D. O. (2008) Base excision DNA repair, *Cell Mol Life Sci 65*, 1544-1565.
92. Allinson, S. L., Dianova, II, and Dianov, G. L. (2003) Poly(ADP-ribose) polymerase in base excision repair: always engaged, but not essential for DNA damage processing, *Acta Biochim Pol 50*, 169-179.
93. Khodyreva, S. N., Prasad, R., Ilina, E. S., Sukhanova, M. V., Kutuzov, M. M., Liu, Y., Hou, E. W., Wilson, S. H., and Lavrik, O. I. (2010) Apurinic/apyrimidinic (AP) site recognition by the 5'-dRP/AP lyase in poly(ADP-ribose) polymerase-1 (PARP-1), *Proc Natl Acad Sci U S A 107*, 22090-22095.
94. Lavrik, O. I., Prasad, R., Sobol, R. W., Horton, J. K., Ackerman, E. J., and Wilson, S. H. (2001) Photoaffinity labeling of mouse fibroblast enzymes by a base excision repair intermediate. Evidence for the role of poly(ADP-ribose) polymerase-1 in DNA repair, *J Biol Chem 276*, 25541-25548.
95. Satoh, M. S., and Lindahl, T. (1992) Role of poly(ADP-ribose) formation in DNA repair, *Nature 356*, 356-358.
96. Parsons, J. L., Dianova, II, Allinson, S. L., and Dianov, G. L. (2005) Poly(ADP-ribose) polymerase-1 protects excessive DNA strand breaks from deterioration during repair in human cell extracts, *FEBS J 272*, 2012-2021.
97. Sukhanova, M. V., Khodyreva, S. N., Lebedeva, N. A., Prasad, R., Wilson, S. H., and Lavrik, O. I. (2005) Human base excision repair enzymes apurinic/apyrimidinic endonuclease1 (APE1), DNA polymerase beta and poly(ADP-ribose) polymerase 1: interplay between strand-displacement DNA synthesis and proofreading exonuclease activity, *Nucleic Acids Res 33*, 1222-1229.
98. El-Khamisy, S. F., Masutani, M., Suzuki, H., and Caldecott, K. W. (2003) A requirement for PARP-1 for the assembly or stability of XRCC1 nuclear foci at sites of oxidative DNA damage, *Nucleic Acids Res 31*, 5526-5533.
99. Leppard, J. B., Dong, Z., Mackey, Z. B., and Tomkinson, A. E. (2003) Physical and functional interaction between DNA ligase IIIalpha and poly(ADP-Ribose) polymerase 1 in DNA single-strand break repair, *Mol Cell Biol 23*, 5919-5927.
100. Sukhanova, M., Khodyreva, S., and Lavrik, O. (2010) Poly(ADP-ribose) polymerase 1 regulates activity of DNA polymerase beta in long patch base excision repair, *Mutat Res 685*, 80-89.
101. Prasad, R., Lavrik, O. I., Kim, S. J., Kedar, P., Yang, X. P., Vande Berg, B. J., and Wilson, S. H. (2001) DNA polymerase beta -mediated long patch base excision repair. Poly(ADP-ribose)polymerase-1 stimulates strand displacement DNA synthesis, *J Biol Chem 276*, 32411-32414.
102. Le Page, F., Schreiber, V., Dherin, C., De Murcia, G., and Boiteux, S. (2003) Poly(ADP-ribose) polymerase-1 (PARP-1) is required in murine cell lines for base excision repair of oxidative DNA damage in the absence of DNA polymerase beta, *J Biol Chem 278*, 18471-18477.
103. Okano, S., Lan, L., Caldecott, K. W., Mori, T., and Yasui, A. (2003) Spatial and temporal cellular responses to single-strand breaks in human cells, *Mol Cell Biol 23*, 3974-3981.
104. Cappelli, E., Taylor, R., Cevasco, M., Abbondandolo, A., Caldecott, K., and Frosina, G. (1997) Involvement of XRCC1 and DNA ligase III gene products in DNA base excision repair, *J Biol Chem 272*, 23970-23975.
105. Strom, C. E., Johansson, F., Uhlen, M., Szigyarto, C. A., Erixon, K., and Helleday, T. (2011) Poly (ADP-ribose) polymerase (PARP) is not involved in base excision

repair but PARP inhibition traps a single-strand intermediate, *Nucleic Acids Res 39*, 3166-3175.

106. Vodenicharov, M. D., Sallmann, F. R., Satoh, M. S., and Poirier, G. G. (2000) Base excision repair is efficient in cells lacking poly(ADP-ribose) polymerase 1, *Nucleic Acids Res 28*, 3887-3896.
107. Kedar, P. S., Stefanick, D. F., Horton, J. K., and Wilson, S. H. (2012) Increased PARP-1 association with DNA in alkylation damaged, PARP-inhibited mouse fibroblasts, *Mol Cancer Res 10*, 360-368.
108. Helleday, T. (2011) The underlying mechanism for the PARP and BRCA synthetic lethality: clearing up the misunderstandings, *Mol Oncol 5*, 387-393.
109. Fisher, A. E., Hochegger, H., Takeda, S., and Caldecott, K. W. (2007) Poly(ADP-ribose) polymerase 1 accelerates single-strand break repair in concert with poly(ADP-ribose) glycohydrolase, *Mol Cell Biol 27*, 5597-5605.
110. Shrivastav, M., De Haro, L. P., and Nickoloff, J. A. (2008) Regulation of DNA double-strand break repair pathway choice, *Cell Res 18*, 134-147.
111. Summers, K. C., Shen, F., Sierra Potchanant, E. A., Phipps, E. A., Hickey, R. J., and Malkas, L. H. (2011) Phosphorylation: the molecular switch of double-strand break repair, *Int J Proteomics 2011*, 373816.
112. Ariumi, Y., Masutani, M., Copeland, T. D., Mimori, T., Sugimura, T., Shimotohno, K., Ueda, K., Hatanaka, M., and Noda, M. (1999) Suppression of the poly(ADP-ribose) polymerase activity by DNA-dependent protein kinase in vitro, *Oncogene 18*, 4616-4625.
113. Couto, C. A., Wang, H. Y., Green, J. C., Kiely, R., Siddaway, R., Borer, C., Pears, C. J., and Lakin, N. D. PARP regulates nonhomologous end joining through retention of Ku at double-strand breaks, *J Cell Biol 194*, 367-375.
114. Aguilar-Quesada, R., Munoz-Gamez, J. A., Martin-Oliva, D., Peralta, A., Valenzuela, M. T., Matinez-Romero, R., Quiles-Perez, R., Menissier-de Murcia, J., de Murcia, G., Ruiz de Almodovar, M., and Oliver, F. J. (2007) Interaction between ATM and PARP-1 in response to DNA damage and sensitization of ATM deficient cells through PARP inhibition, *BMC Mol Biol 8*, 29.
115. Kedar, P. S., Stefanick, D. F., Horton, J. K., and Wilson, S. H. (2008) Interaction between PARP-1 and ATR in mouse fibroblasts is blocked by PARP inhibition, *DNA Repair (Amst) 7*, 1787-1798.
116. Wang, M., Wu, W., Rosidi, B., Zhang, L., Wang, H., and Iliakis, G. (2006) PARP-1 and Ku compete for repair of DNA double strand breaks by distinct NHEJ pathways, *Nucleic Acids Res 34*, 6170-6182.
117. Audebert, M., Salles, B., and Calsou, P. (2008) Effect of double-strand break DNA sequence on the PARP-1 NHEJ pathway, *Biochem Biophys Res Commun 369*, 982-988.
118. Audebert, M., Salles, B., and Calsou, P. (2004) Involvement of poly(ADP-ribose) polymerase-1 and XRCC1/DNA ligase III in an alternative route for DNA double-strand breaks rejoining, *J Biol Chem 279*, 55117-55126.
119. Bryant, H. E., Petermann, E., Schultz, N., Jemth, A. S., Loseva, O., Issaeva, N., Johansson, F., Fernandez, S., McGlynn, P., and Helleday, T. (2009) PARP is activated at stalled forks to mediate Mre11-dependent replication restart and recombination, *EMBO J 28*, 2601-2615.

120. Helleday, T., Bryant, H. E., and Schultz, N. (2005) Poly(ADP-ribose) polymerase (PARP-1) in homologous recombination and as a target for cancer therapy, *Cell Cycle 4*, 1176-1178.
121. Sugimura, K., Takebayashi, S., Taguchi, H., Takeda, S., and Okumura, K. (2008) PARP-1 ensures regulation of replication fork progression by homologous recombination on damaged DNA, *J Cell Biol 183*, 1203-1212.
122. Haince, J. F., McDonald, D., Rodrigue, A., Dery, U., Masson, J. Y., Hendzel, M. J., and Poirier, G. G. (2008) PARP1-dependent kinetics of recruitment of MRE11 and NBS1 proteins to multiple DNA damage sites, *J Biol Chem 283*, 1197-1208.
123. Patel, A. G., Sarkaria, J. N., and Kaufmann, S. H. (2011) Nonhomologous end joining drives poly(ADP-ribose) polymerase (PARP) inhibitor lethality in homologous recombination-deficient cells, *Proc Natl Acad Sci U S A 108*, 3406-3411.
124. Loseva, O., Jemth, A. S., Bryant, H. E., Schuler, H., Lehtio, L., Karlberg, T., and Helleday, T. (2010) PARP-3 is a mono-ADP-ribosylase that activates PARP-1 in the absence of DNA, *J Biol Chem 285*, 8054-8060.
125. Reed, S. H. (2011) Nucleotide excision repair in chromatin: damage removal at the drop of a HAT, *DNA Repair (Amst) 10*, 734-742.
126. Fousteri, M., and Mullenders, L. H. (2008) Transcription-coupled nucleotide excision repair in mammalian cells: molecular mechanisms and biological effects, *Cell Res 18*, 73-84.
127. Fagbemi, A. F., Orelli, B., and Scharer, O. D. (2011) Regulation of endonuclease activity in human nucleotide excision repair, *DNA Repair (Amst) 10*, 722-729.
128. Lagerwerf, S., Vrouwe, M. G., Overmeer, R. M., Fousteri, M. I., and Mullenders, L. H. (2011) DNA damage response and transcription, *DNA Repair (Amst) 10*, 743-750.
129. Cleaver, J. E., Lam, E. T., and Revet, I. (2009) Disorders of nucleotide excision repair: the genetic and molecular basis of heterogeneity, *Nat Rev Genet 10*, 756-768.
130. Ghodgaonkar, M. M., Zacal, N., Kassam, S., Rainbow, A. J., and Shah, G. M. (2008) Depletion of poly(ADP-ribose) polymerase-1 reduces host cell reactivation of a UV-damaged adenovirus-encoded reporter gene in human dermal fibroblasts, *DNA Repair (Amst) 7*, 617-632.
131. Vodenicharov, M. D., Ghodgaonkar, M. M., Halappanavar, S. S., Shah, R. G., and Shah, G. M. (2005) Mechanism of early biphasic activation of poly(ADP-ribose) polymerase-1 in response to ultraviolet B radiation, *J Cell Sci 118*, 589-599.
132. Luijsterburg, M. S., Lindh, M., Acs, K., Vrouwe, M. G., Pines, A., van Attikum, H., Mullenders, L. H., and Dantuma, N. P. (2012) DDB2 promotes chromatin decondensation at UV-induced DNA damage, *J Cell Biol 197*, 267-281.
133. Lord, C. J., McDonald, S., Swift, S., Turner, N. C., and Ashworth, A. (2008) A high-throughput RNA interference screen for DNA repair determinants of PARP inhibitor sensitivity, *DNA Repair (Amst) 7*, 2010-2019.
134. Liu, Y., Kadyrov, F. A., and Modrich, P. (2011) PARP-1 enhances the mismatch-dependence of 5'-directed excision in human mismatch repair in vitro, *DNA Repair (Amst) 10*, 1145-1153.
135. Duprez, L., Wirawan, E., Vanden Berghe, T., and Vandenabeele, P. (2009) Major cell death pathways at a glance, *Microbes Infect 11*, 1050-1062.

136. Galluzzi, L., Vitale, I., Abrams, J. M., Alnemri, E. S., Baehrecke, E. H., Blagosklonny, M. V., Dawson, T. M., Dawson, V. L., El-Deiry, W. S., Fulda, S., Gottlieb, E., Green, D. R., Hengartner, M. O., Kepp, O., Knight, R. A., Kumar, S., Lipton, S. A., Lu, X., Madeo, F., Malorni, W., Mehlen, P., Nunez, G., Peter, M. E., Piacentini, M., Rubinsztein, D. C., Shi, Y., Simon, H. U., Vandenabeele, P., White, E., Yuan, J., Zhivotovsky, B., Melino, G., and Kroemer, G. (2012) Molecular definitions of cell death subroutines: recommendations of the Nomenclature Committee on Cell Death 2012, *Cell Death Differ 19*, 107-120.
137. El Bachir Affar, Germain, M., and, and Poirier, G. G. (2000) Role of poly (ADP-ribose) polymerase in cell death, in *From DNA damage and stress signalling to cell death poly ADP-ribosylation reactions* (Murcia, G. d., and, and Shall, S., Eds.), pp 125-150.
138. Ha, H. C., and Snyder, S. H. (1999) Poly(ADP-ribose) polymerase is a mediator of necrotic cell death by ATP depletion, *Proc Natl Acad Sci U S A 96*, 13978-13982.
139. Elmore, S. (2007) Apoptosis: a review of programmed cell death, *Toxicol Pathol 35*, 495-516.
140. Ola, M. S., Nawaz, M., and Ahsan, H. (2011) Role of Bcl-2 family proteins and caspases in the regulation of apoptosis, *Mol Cell Biochem 351*, 41-58.
141. Lamkanfi, M., and Dixit, V. M. (2010) Manipulation of host cell death pathways during microbial infections, *Cell Host Microbe 8*, 44-54.
142. Kroemer, G., Galluzzi, L., and Brenner, C. (2007) Mitochondrial membrane permeabilization in cell death, *Physiol Rev 87*, 99-163.
143. Fulda, S., and Debatin, K. M. (2006) Extrinsic versus intrinsic apoptosis pathways in anticancer chemotherapy, *Oncogene 25*, 4798-4811.
144. Roy, S., and Nicholson, D. W. (2000) Cross-talk in cell death signaling, *J Exp Med 192*, 21-26.
145. Lazebnik, Y. A., Kaufmann, S. H., Desnoyers, S., Poirier, G. G., and Earnshaw, W. C. (1994) Cleavage of poly(ADP-ribose) polymerase by a proteinase with properties like ICE, *Nature 371*, 346-347.
146. Boucher, D., Blais, V., and Denault, J. B. (2012) Caspase-7 uses an exosite to promote poly(ADP ribose) polymerase 1 proteolysis, *Proc Natl Acad Sci U S A 109*, 5669-5674.
147. Soldani, C., and Scovassi, A. I. (2002) Poly(ADP-ribose) polymerase-1 cleavage during apoptosis: an update, *Apoptosis 7*, 321-328.
148. Duriez, P. J., and Shah, G. M. (1997) Cleavage of poly(ADP-ribose) polymerase: a sensitive parameter to study cell death, *Biochem Cell Biol 75*, 337-349.
149. Oliver, F. J., Menissier-de Murcia, J., and de Murcia, G. (1999) Poly(ADP-ribose) polymerase in the cellular response to DNA damage, apoptosis, and disease, *Am J Hum Genet 64*, 1282-1288.
150. Smulson, M. E., Pang, D., Jung, M., Dimtchev, A., Chasovskikh, S., Spoonde, A., Simbulan-Rosenthal, C., Rosenthal, D., Yakovlev, A., and Dritschilo, A. (1998) Irreversible binding of poly(ADP)ribose polymerase cleavage product to DNA ends revealed by atomic force microscopy: possible role in apoptosis, *Cancer Res 58*, 3495-3498.
151. Molinete, M., Vermeulen, W., Burkle, A., Menissier-de Murcia, J., Kupper, J. H., Hoeijmakers, J. H., and de Murcia, G. (1993) Overproduction of the poly(ADP-

ribose) polymerase DNA-binding domain blocks alkylation-induced DNA repair synthesis in mammalian cells, *EMBO J 12*, 2109-2117.

152. Kim, J. W., Won, J., Sohn, S., and Joe, C. O. (2000) DNA-binding activity of the N-terminal cleavage product of poly(ADP-ribose) polymerase is required for UV mediated apoptosis, *J Cell Sci 113 (Pt 6)*, 955-961.
153. Shah, G. M., Kaufmann, S. H., and Poirier, G. G. (1995) Detection of poly(ADP-ribose) polymerase and its apoptosis-specific fragment by a nonisotopic activity-western blot technique, *Anal Biochem 232*, 251-254.
154. Kim, J. W., Kim, K., Kang, K., and Joe, C. O. (2000) Inhibition of homodimerization of poly(ADP-ribose) polymerase by its C-terminal cleavage products produced during apoptosis, *J Biol Chem 275*, 8121-8125.
155. Simbulan-Rosenthal, C. M., Rosenthal, D. S., Iyer, S., Boulares, A. H., and Smulson, M. E. (1998) Transient poly(ADP-ribosyl)ation of nuclear proteins and role of poly(ADP-ribose) polymerase in the early stages of apoptosis, *J Biol Chem 273*, 13703-13712.
156. Scovassi, A. I., and Poirier, G. G. (1999) Poly(ADP-ribosylation) and apoptosis, *Mol Cell Biochem 199*, 125-137.
157. Halappanavar, S. S., Rhun, Y. L., Mounir, S., Martins, L. M., Huot, J., Earnshaw, W. C., and Shah, G. M. (1999) Survival and proliferation of cells expressing caspase-uncleavable Poly(ADP-ribose) polymerase in response to death-inducing DNA damage by an alkylating agent, *J Biol Chem 274*, 37097-37104.
158. Oliver, F. J., de la Rubia, G., Rolli, V., Ruiz-Ruiz, M. C., de Murcia, G., and Murcia, J. M. (1998) Importance of poly(ADP-ribose) polymerase and its cleavage in apoptosis. Lesson from an uncleavable mutant, *J Biol Chem 273*, 33533-33539.
159. Herceg, Z., and Wang, Z. Q. (1999) Failure of poly(ADP-ribose) polymerase cleavage by caspases leads to induction of necrosis and enhanced apoptosis, *Mol Cell Biol 19*, 5124-5133.
160. Boulares, A. H., Yakovlev, A. G., Ivanova, V., Stoica, B. A., Wang, G., Iyer, S., and Smulson, M. (1999) Role of poly(ADP-ribose) polymerase (PARP) cleavage in apoptosis. Caspase 3-resistant PARP mutant increases rates of apoptosis in transfected cells, *J Biol Chem 274*, 22932-22940.
161. Yu, S. W., Wang, H., Poitras, M. F., Coombs, C., Bowers, W. J., Federoff, H. J., Poirier, G. G., Dawson, T. M., and Dawson, V. L. (2002) Mediation of poly(ADP-ribose) polymerase-1-dependent cell death by apoptosis-inducing factor, *Science 297*, 259-263.
162. Moubarak, R. S., Yuste, V. J., Artus, C., Bouharrour, A., Greer, P. A., Menissier-de Murcia, J., and Susin, S. A. (2007) Sequential activation of poly(ADP-ribose) polymerase 1, calpains, and Bax is essential in apoptosis-inducing factor-mediated programmed necrosis, *Mol Cell Biol 27*, 4844-4862.
163. Wang, Y., Kim, N. S., Li, X., Greer, P. A., Koehler, R. C., Dawson, V. L., and Dawson, T. M. (2009) Calpain activation is not required for AIF translocation in PARP-1-dependent cell death (parthanatos), *J Neurochem 110*, 687-696.
164. Wang, Y., Kim, N. S., Haince, J. F., Kang, H. C., David, K. K., Andrabi, S. A., Poirier, G. G., Dawson, V. L., and Dawson, T. M. (2011) Poly(ADP-ribose) (PAR) binding to apoptosis-inducing factor is critical for PAR polymerase-1-dependent cell death (parthanatos), *Sci Signal 4*, ra20.

165. Andrabi, S. A., Kim, N. S., Yu, S. W., Wang, H., Koh, D. W., Sasaki, M., Klaus, J. A., Otsuka, T., Zhang, Z., Koehler, R. C., Hurn, P. D., Poirier, G. G., Dawson, V. L., and Dawson, T. M. (2006) Poly(ADP-ribose) (PAR) polymer is a death signal, *Proc Natl Acad Sci U S A 103*, 18308-18313.
166. Andrabi, S. A., Dawson, T. M., and Dawson, V. L. (2008) Mitochondrial and nuclear cross talk in cell death: parthanatos, *Ann N Y Acad Sci 1147*, 233-241.
167. David, K. K., Andrabi, S. A., Dawson, T. M., and Dawson, V. L. (2009) Parthanatos, a messenger of death, *Front Biosci 14*, 1116-1128.
168. Artus, C., Boujrad, H., Bouharrour, A., Brunelle, M. N., Hoos, S., Yuste, V. J., Lenormand, P., Rousselle, J. C., Namane, A., England, P., Lorenzo, H. K., and Susin, S. A. (2010) AIF promotes chromatinolysis and caspase-independent programmed necrosis by interacting with histone H2AX, *EMBO J 29*, 1585-1599.
169. Lockshin, R. A., and Zakeri, Z. (2004) Caspase-independent cell death?, *Oncogene 23*, 2766-2773.
170. Mizushima, N. (2007) Autophagy: process and function, *Genes Dev 21*, 2861-2873.
171. Codogno, P., and Meijer, A. J. (2005) Autophagy and signaling: their role in cell survival and cell death, *Cell Death Differ 12 Suppl 2*, 1509-1518.
172. Esteve, J. M., and Knecht, E. (2011) Mechanisms of autophagy and apoptosis: Recent developments in breast cancer cells, *World J Biol Chem 2*, 232-238.
173. Pattingre, S., Tassa, A., Qu, X., Garuti, R., Liang, X. H., Mizushima, N., Packer, M., Schneider, M. D., and Levine, B. (2005) Bcl-2 antiapoptotic proteins inhibit Beclin 1-dependent autophagy, *Cell 122*, 927-939.
174. Zhu, Y., Zhao, L., Liu, L., Gao, P., Tian, W., Wang, X., Jin, H., Xu, H., and Chen, Q. (2010) Beclin 1 cleavage by caspase-3 inactivates autophagy and promotes apoptosis, *Protein Cell 1*, 468-477.
175. Rodriguez-Vargas, J. M., Ruiz-Magana, M. J., Ruiz-Ruiz, C., Majuelos-Melguizo, J., Peralta-Leal, A., Rodriguez, M. I., Munoz-Gamez, J. A., de Almodovar, M. R., Siles, E., Rivas, A. L., Jaattela, M., and Oliver, F. J. (2012) ROS-induced DNA damage and PARP-1 are required for optimal induction of starvation-induced autophagy, *Cell Res 22*, 1181-1198.
176. Munoz-Gamez, J. A., Rodriguez-Vargas, J. M., Quiles-Perez, R., Aguilar-Quesada, R., Martin-Oliva, D., de Murcia, G., Menissier de Murcia, J., Almendros, A., Ruiz de Almodovar, M., and Oliver, F. J. (2009) PARP-1 is involved in autophagy induced by DNA damage, *Autophagy 5*, 61-74.
177. Zhang, N., Chen, Y., Jiang, R., Li, E., Chen, X., Xi, Z., Guo, Y., Liu, X., Zhou, Y., Che, Y., and Jiang, X. (2011) PARP and RIP 1 are required for autophagy induced by 11'-deoxyverticillin A, which precedes caspase-dependent apoptosis, *Autophagy 7*, 598-612.
178. Huang, Q., Wu, Y. T., Tan, H. L., Ong, C. N., and Shen, H. M. (2009) A novel function of poly(ADP-ribose) polymerase-1 in modulation of autophagy and necrosis under oxidative stress, *Cell Death Differ 16*, 264-277.
179. Zong, W. X., and Thompson, C. B. (2006) Necrotic death as a cell fate, *Genes Dev 20*, 1-15.
180. Golstein, P., and Kroemer, G. (2007) Cell death by necrosis: towards a molecular definition, *Trends Biochem Sci 32*, 37-43.
181. Kroemer, G., Galluzzi, L., Vandenabeele, P., Abrams, J., Alnemri, E. S., Baehrecke, E. H., Blagosklonny, M. V., El-Deiry, W. S., Golstein, P., Green, D. R., Hengartner,

M., Knight, R. A., Kumar, S., Lipton, S. A., Malorni, W., Nunez, G., Peter, M. E., Tschopp, J., Yuan, J., Piacentini, M., Zhivotovsky, B., and Melino, G. (2009) Classification of cell death: recommendations of the Nomenclature Committee on Cell Death 2009, *Cell Death Differ 16*, 3-11.

182. Zong, W. X., Ditsworth, D., Bauer, D. E., Wang, Z. Q., and Thompson, C. B. (2004) Alkylating DNA damage stimulates a regulated form of necrotic cell death, *Genes Dev 18*, 1272-1282.
183. Wsierska-Gadek, J., Gueorguieva, M., and Wojciechowski, J. (2003) MNNG induces dramatic DNA damage and non-apoptotic changes in cervical carcinoma HeLa cells, *Ann N Y Acad Sci 1010*, 278-282.
184. Filipovic, D. M., Meng, X., and Reeves, W. B. (1999) Inhibition of PARP prevents oxidant-induced necrosis but not apoptosis in LLC-PK1 cells, *Am J Physiol 277*, F428-436.
185. Meli, E., Pangallo, M., Picca, R., Baronti, R., Moroni, F., and Pellegrini-Giampietro, D. E. (2004) Differential role of poly(ADP-ribose) polymerase-1in apoptotic and necrotic neuronal death induced by mild or intense NMDA exposure in vitro, *Mol Cell Neurosci 25*, 172-180.
186. Vanlangenakker, N., Vanden Berghe, T., and Vandenabeele, P. (2012) Many stimuli pull the necrotic trigger, an overview, *Cell Death Differ 19*, 75-86.
187. Affar el, B., Shah, R. G., Dallaire, A. K., Castonguay, V., and Shah, G. M. (2002) Role of poly(ADP-ribose) polymerase in rapid intracellular acidification induced by alkylating DNA damage, *Proc Natl Acad Sci U S A 99*, 245-250.
188. Ye, K. (2008) PARP inhibitor tilts cell death from necrosis to apoptosis in cancer cells, *Cancer Biol Ther 7*, 942-944.
189. Shah, G. M., Shah, R. G., and Poirier, G. G. (1996) Different cleavage pattern for poly(ADP-ribose) polymerase during necrosis and apoptosis in HL-60 cells, *Biochem Biophys Res Commun 229*, 838-844.
190. Gobeil, S., Boucher, C. C., Nadeau, D., and Poirier, G. G. (2001) Characterization of the necrotic cleavage of poly(ADP-ribose) polymerase (PARP-1): implication of lysosomal proteases, *Cell Death Differ 8*, 588-594.
191. Froelich, C. J., Hanna, W. L., Poirier, G. G., Duriez, P. J., D'Amours, D., Salvesen, G. S., Alnemri, E. S., Earnshaw, W. C., and Shah, G. M. (1996) Granzyme B/perforin-mediated apoptosis of Jurkat cells results in cleavage of poly(ADP-ribose) polymerase to the 89-kDa apoptotic fragment and less abundant 64-kDa fragment, *Biochem Biophys Res Commun 227*, 658-665.
192. McGinnis, K. M., Gnegy, M. E., Park, Y. H., Mukerjee, N., and Wang, K. K. (1999) Procaspase-3 and poly(ADP)ribose polymerase (PARP) are calpain substrates, *Biochem Biophys Res Commun 263*, 94-99.
193. Vandenabeele, P., Galluzzi, L., Vanden Berghe, T., and Kroemer, G. (2010) Molecular mechanisms of necroptosis: an ordered cellular explosion, *Nat Rev Mol Cell Biol 11*, 700-714.
194. Galluzzi, L., and Kroemer, G. (2008) Necroptosis: a specialized pathway of programmed necrosis, *Cell 135*, 1161-1163.
195. Hitomi, J., Christofferson, D. E., Ng, A., Yao, J., Degterev, A., Xavier, R. J., and Yuan, J. (2008) Identification of a molecular signaling network that regulates a cellular necrotic cell death pathway, *Cell 135*, 1311-1323.

196. Yuan, J., and Kroemer, G. (2010) Alternative cell death mechanisms in development and beyond, *Genes Dev 24*, 2592-2602.
197. Degterev, A., Huang, Z., Boyce, M., Li, Y., Jagtap, P., Mizushima, N., Cuny, G. D., Mitchison, T. J., Moskowitz, M. A., and Yuan, J. (2005) Chemical inhibitor of nonapoptotic cell death with therapeutic potential for ischemic brain injury, *Nat Chem Biol 1*, 112-119.
198. Xu, X., Chua, C. C., Zhang, M., Geng, D., Liu, C. F., Hamdy, R. C., and Chua, B. H. (2010) The role of PARP activation in glutamate-induced necroptosis in HT-22 cells, *Brain Res 1343*, 206-212.
199. Delavallee, L., Cabon, L., Galan-Malo, P., Lorenzo, H. K., and Susin, S. A. (2011) AIF-mediated caspase-independent necroptosis: a new chance for targeted therapeutics, *IUBMB Life 63*, 221-232.
200. Cabon, L., Galan-Malo, P., Bouharrour, A., Delavallee, L., Brunelle-Navas, M. N., Lorenzo, H. K., Gross, A., and Susin, S. A. (2012) BID regulates AIF-mediated caspase-independent necroptosis by promoting BAX activation, *Cell Death Differ 19*, 245-256.
201. Hong, S. J., Dawson, T. M., and Dawson, V. L. (2004) Nuclear and mitochondrial conversations in cell death: PARP-1 and AIF signaling, *Trends Pharmacol Sci 25*, 259-264.
202. Ferraris, D. V. (2010) Evolution of poly(ADP-ribose) polymerase-1 (PARP-1) inhibitors. From concept to clinic, *J Med Chem 53*, 4561-4584.
203. Farmer, H., McCabe, N., Lord, C. J., Tutt, A. N., Johnson, D. A., Richardson, T. B., Santarosa, M., Dillon, K. J., Hickson, I., Knights, C., Martin, N. M., Jackson, S. P., Smith, G. C., and Ashworth, A. (2005) Targeting the DNA repair defect in BRCA mutant cells as a therapeutic strategy, *Nature 434*, 917-921.
204. Shah, R. G., Ghodgaonkar, M. M., Affar el, B., and Shah, G. M. (2005) DNA vector-based RNAi approach for stable depletion of poly(ADP-ribose) polymerase-1, *Biochem Biophys Res Commun 331*, 167-174.
205. Nusinow, D. A., Hernandez-Munoz, I., Fazzio, T. G., Shah, G. M., Kraus, W. L., and Panning, B. (2007) Poly(ADP-ribose) polymerase 1 is inhibited by a histone H2A variant, MacroH2A, and contributes to silencing of the inactive X chromosome, *J Biol Chem 282*, 12851-12859.
206. Tentori, L., Muzi, A., Dorio, A. S., Bultrini, S., Mazzon, E., Lacal, P. M., Shah, G. M., Zhang, J., Navarra, P., Nocentini, G., Cuzzocrea, S., and Graziani, G. (2008) Stable depletion of poly (ADP-ribose) polymerase-1 reduces in vivo melanoma growth and increases chemosensitivity, *Eur J Cancer 44*, 1302-1314.
207. Matsumura, Y., and Ananthaswamy, H. N. (2004) Toxic effects of ultraviolet radiation on the skin, *Toxicol Appl Pharmacol 195*, 298-308.
208. Cleaver, J. E., and Crowley, E. (2002) UV damage, DNA repair and skin carcinogenesis, *Front Biosci 7*, d1024-1043.
209. Vodenicharov, M. D., and, and Shah, G. M. (2005) Nuclear and non-nuclear signals leading to UV-induced apoptosis., in *From DNA photolesions to mutations, skin cancer and cell death.*, pp 247-267, New York: RSC Elsevier.
210. Zhao, H., and Piwnica-Worms, H. (2001) ATR-mediated checkpoint pathways regulate phosphorylation and activation of human Chk1, *Mol Cell Biol 21*, 4129-4139.

211. Fuchs, S. Y., Adler, V., Pincus, M. R., and Ronai, Z. (1998) MEKK1/JNK signaling stabilizes and activates p53, *Proc Natl Acad Sci U S A 95*, 10541-10546.
212. Huang, C., Ma, W. Y., Maxiner, A., Sun, Y., and Dong, Z. (1999) p38 kinase mediates UV-induced phosphorylation of p53 protein at serine 389, *J Biol Chem 274*, 12229-12235.
213. Meek, D. W. (2009) Tumour suppression by p53: a role for the DNA damage response?, *Nat Rev Cancer 9*, 714-723.
214. Slee, E. A., O'Connor, D. J., and Lu, X. (2004) To die or not to die: how does p53 decide?, *Oncogene 23*, 2809-2818.
215. Meek, D. W. (2004) The p53 response to DNA damage, *DNA Repair (Amst) 3*, 1049-1056.
216. Muthusamy, V., and Piva, T. J. (2010) The UV response of the skin: a review of the MAPK, NFkappaB and TNFalpha signal transduction pathways, *Arch Dermatol Res 302*, 5-17.
217. Gupta, M., Gupta, S. K., Hoffman, B., and Liebermann, D. A. (2006) Gadd45a and Gadd45b protect hematopoietic cells from UV-induced apoptosis via distinct signaling pathways, including p38 activation and JNK inhibition, *J Biol Chem 281*, 17552-17558.
218. Peus, D., Vasa, R. A., Beyerle, A., Meves, A., Krautmacher, C., and Pittelkow, M. R. (1999) UVB activates ERK1/2 and p38 signaling pathways via reactive oxygen species in cultured keratinocytes, *J Invest Dermatol 112*, 751-756.
219. Ming, M., Han, W., Maddox, J., Soltani, K., Shea, C. R., Freeman, D. M., and He, Y. Y. (2010) UVB-induced ERK/AKT-dependent PTEN suppression promotes survival of epidermal keratinocytes, *Oncogene 29*, 492-502.
220. Denning, M. F., Wang, Y., Tibudan, S., Alkan, S., Nickoloff, B. J., and Qin, J. Z. (2002) Caspase activation and disruption of mitochondrial membrane potential during UV radiation-induced apoptosis of human keratinocytes requires activation of protein kinase C, *Cell Death Differ 9*, 40-52.
221. Kulms, D., and Schwarz, T. (2000) Molecular mechanisms of UV-induced apoptosis, *Photodermatol Photoimmunol Photomed 16*, 195-201.
222. Flohr, C., Burkle, A., Radicella, J. P., and Epe, B. (2003) Poly(ADP-ribosyl)ation accelerates DNA repair in a pathway dependent on Cockayne syndrome B protein, *Nucleic Acids Res 31*, 5332-5337.
223. Thorslund, T., von Kobbe, C., Harrigan, J. A., Indig, F. E., Christiansen, M., Stevnsner, T., and Bohr, V. A. (2005) Cooperation of the Cockayne syndrome group B protein and poly(ADP-ribose) polymerase 1 in the response to oxidative stress, *Mol Cell Biol 25*, 7625-7636.
224. Farkas, B., Magyarlaki, M., Csete, B., Nemeth, J., Rabloczky, G., Bernath, S., Literati Nagy, P., and Sumegi, B. (2002) Reduction of acute photodamage in skin by topical application of a novel PARP inhibitor, *Biochem Pharmacol 63*, 921-932.
225. Mi, Y., Thomas, S. D., Xu, X., Casson, L. K., Miller, D. M., and Bates, P. J. (2003) Apoptosis in leukemia cells is accompanied by alterations in the levels and localization of nucleolin, *J Biol Chem 278*, 8572-8579.
226. Brind'Amour, J. (2005) Role of poly(ADP-ribose) polymerase-1 (PARP-1) in cellular response to UVB in SKH-1 mice epidermis, in *Mémoire de maîtrise*, p 125, Université Laval, Québec.

227. Fire, A., Xu, S., Montgomery, M. K., Kostas, S. A., Driver, S. E., and Mello, C. C. (1998) Potent and specific genetic interference by double-stranded RNA in Caenorhabditis elegans, *Nature 391*, 806-811.
228. Hamilton, A. J., and Baulcombe, D. C. (1999) A species of small antisense RNA in posttranscriptional gene silencing in plants, *Science 286*, 950-952.
229. Hammond, S. M., Bernstein, E., Beach, D., and Hannon, G. J. (2000) An RNA-directed nuclease mediates post-transcriptional gene silencing in Drosophila cells, *Nature 404*, 293-296.
230. Zamore, P. D., Tuschl, T., Sharp, P. A., and Bartel, D. P. (2000) RNAi: double-stranded RNA directs the ATP-dependent cleavage of mRNA at 21 to 23 nucleotide intervals, *Cell 101*, 25-33.
231. Tuschl, T., Zamore, P. D., Lehmann, R., Bartel, D. P., and Sharp, P. A. (1999) Targeted mRNA degradation by double-stranded RNA in vitro, *Genes Dev 13*, 3191-3197.
232. Lee, R. C., Feinbaum, R. L., and Ambros, V. (1993) The C. elegans heterochronic gene lin-4 encodes small RNAs with antisense complementarity to lin-14, *Cell 75*, 843-854.
233. Reinhart, B. J., Slack, F. J., Basson, M., Pasquinelli, A. E., Bettinger, J. C., Rougvie, A. E., Horvitz, H. R., and Ruvkun, G. (2000) The 21-nucleotide let-7 RNA regulates developmental timing in Caenorhabditis elegans, *Nature 403*, 901-906.
234. Ambros, V., Bartel, B., Bartel, D. P., Burge, C. B., Carrington, J. C., Chen, X., Dreyfuss, G., Eddy, S. R., Griffiths-Jones, S., Marshall, M., Matzke, M., Ruvkun, G., and Tuschl, T. (2003) A uniform system for microRNA annotation, *RNA 9*, 277-279.
235. Elbashir, S. M., Harborth, J., Lendeckel, W., Yalcin, A., Weber, K., and Tuschl, T. (2001) Duplexes of 21-nucleotide RNAs mediate RNA interference in cultured mammalian cells, *Nature 411*, 494-498.
236. Du, T., and Zamore, P. D. (2005) microPrimer: the biogenesis and function of microRNA, *Development 132*, 4645-4652.
237. Bernstein, E., Caudy, A. A., Hammond, S. M., and Hannon, G. J. (2001) Role for a bidentate ribonuclease in the initiation step of RNA interference, *Nature 409*, 363-366.
238. Hammond, S. M. (2005) Dicing and slicing: the core machinery of the RNA interference pathway, *FEBS Lett 579*, 5822-5829.
239. Davidson, B. L., and McCray, P. B., Jr. (2011) Current prospects for RNA interference-based therapies, *Nat Rev Genet 12*, 329-340.
240. Kim, D. H., Behlke, M. A., Rose, S. D., Chang, M. S., Choi, S., and Rossi, J. J. (2005) Synthetic dsRNA Dicer substrates enhance RNAi potency and efficacy, *Nat Biotechnol 23*, 222-226.
241. Shi, Y. (2003) Mammalian RNAi for the masses, *Trends Genet 19*, 9-12.
242. Caplen, N. J., Parrish, S., Imani, F., Fire, A., and Morgan, R. A. (2001) Specific inhibition of gene expression by small double-stranded RNAs in invertebrate and vertebrate systems, *Proc Natl Acad Sci U S A 98*, 9742-9747.
243. Elbashir, S. M., Martinez, J., Patkaniowska, A., Lendeckel, W., and Tuschl, T. (2001) Functional anatomy of siRNAs for mediating efficient RNAi in Drosophila melanogaster embryo lysate, *EMBO J 20*, 6877-6888.

244. Rose, S. D., Kim, D. H., Amarzguioui, M., Heidel, J. D., Collingwood, M. A., Davis, M. E., Rossi, J. J., and Behlke, M. A. (2005) Functional polarity is introduced by Dicer processing of short substrate RNAs, *Nucleic Acids Res 33*, 4140-4156.
245. Kurreck, J. (2009) RNA interference: from basic research to therapeutic applications, *Angew Chem Int Ed Engl 48*, 1378-1398.
246. Sui, G., Soohoo, C., Affar el, B., Gay, F., Shi, Y., and Forrester, W. C. (2002) A DNA vector-based RNAi technology to suppress gene expression in mammalian cells, *Proc Natl Acad Sci U S A 99*, 5515-5520.
247. Paddison, P. J., and Hannon, G. J. (2002) RNA interference: the new somatic cell genetics?, *Cancer Cell 2*, 17-23.
248. Paddison, P. J., Caudy, A. A., Bernstein, E., Hannon, G. J., and Conklin, D. S. (2002) Short hairpin RNAs (shRNAs) induce sequence-specific silencing in mammalian cells, *Genes Dev 16*, 948-958.
249. Brummelkamp, T. R., Bernards, R., and Agami, R. (2002) A system for stable expression of short interfering RNAs in mammalian cells, *Science 296*, 550-553.
250. Siolas, D., Lerner, C., Burchard, J., Ge, W., Linsley, P. S., Paddison, P. J., Hannon, G. J., and Cleary, M. A. (2005) Synthetic shRNAs as potent RNAi triggers, *Nat Biotechnol 23*, 227-231.
251. Elbashir, S. M., Lendeckel, W., and Tuschl, T. (2001) RNA interference is mediated by 21- and 22-nucleotide RNAs, *Genes Dev 15*, 188-200.
252. Kawamata, T., and Tomari, Y. (2010) Making RISC, *Trends Biochem Sci 35*, 368-376.
253. Chakravarthy, S., Sternberg, S. H., Kellenberger, C. A., and Doudna, J. A. (2010) Substrate-specific kinetics of Dicer-catalyzed RNA processing, *J Mol Biol 404*, 392-402.
254. Zhang, H., Kolb, F. A., Jaskiewicz, L., Westhof, E., and Filipowicz, W. (2004) Single processing center models for human Dicer and bacterial RNase III, *Cell 118*, 57-68.
255. Macrae, I. J., Zhou, K., Li, F., Repic, A., Brooks, A. N., Cande, W. Z., Adams, P. D., and Doudna, J. A. (2006) Structural basis for double-stranded RNA processing by Dicer, *Science 311*, 195-198.
256. Lee, Y., Hur, I., Park, S. Y., Kim, Y. K., Suh, M. R., and Kim, V. N. (2006) The role of PACT in the RNA silencing pathway, *EMBO J 25*, 522-532.
257. Haase, A. D., Jaskiewicz, L., Zhang, H., Laine, S., Sack, R., Gatignol, A., and Filipowicz, W. (2005) TRBP, a regulator of cellular PKR and HIV-1 virus expression, interacts with Dicer and functions in RNA silencing, *EMBO Rep 6*, 961-967.
258. Chendrimada, T. P., Gregory, R. I., Kumaraswamy, E., Norman, J., Cooch, N., Nishikura, K., and Shiekhattar, R. (2005) TRBP recruits the Dicer complex to Ago2 for microRNA processing and gene silencing, *Nature 436*, 740-744.
259. Montgomery, M. K., Xu, S., and Fire, A. (1998) RNA as a target of double-stranded RNA-mediated genetic interference in Caenorhabditis elegans, *Proc Natl Acad Sci U S A 95*, 15502-15507.
260. Pratt, A. J., and MacRae, I. J. (2009) The RNA-induced silencing complex: a versatile gene-silencing machine, *J Biol Chem 284*, 17897-17901.

261. Hammond, S. M., Boettcher, S., Caudy, A. A., Kobayashi, R., and Hannon, G. J. (2001) Argonaute2, a link between genetic and biochemical analyses of RNAi, *Science 293*, 1146-1150.
262. Rivas, F. V., Tolia, N. H., Song, J. J., Aragon, J. P., Liu, J., Hannon, G. J., and Joshua-Tor, L. (2005) Purified Argonaute2 and an siRNA form recombinant human RISC, *Nat Struct Mol Biol 12*, 340-349.
263. Miyoshi, K., Tsukumo, H., Nagami, T., Siomi, H., and Siomi, M. C. (2005) Slicer function of Drosophila Argonautes and its involvement in RISC formation, *Genes Dev 19*, 2837-2848.
264. Tolia, N. H., and Joshua-Tor, L. (2007) Slicer and the argonautes, *Nat Chem Biol 3*, 36-43.
265. Hutvagner, G., and Simard, M. J. (2008) Argonaute proteins: key players in RNA silencing, *Nat Rev Mol Cell Biol 9*, 22-32.
266. Song, J. J., Liu, J., Tolia, N. H., Schneiderman, J., Smith, S. K., Martienssen, R. A., Hannon, G. J., and Joshua-Tor, L. (2003) The crystal structure of the Argonaute2 PAZ domain reveals an RNA binding motif in RNAi effector complexes, *Nat Struct Biol 10*, 1026-1032.
267. Ma, J. B., Ye, K., and Patel, D. J. (2004) Structural basis for overhang-specific small interfering RNA recognition by the PAZ domain, *Nature 429*, 318-322.
268. Ma, J. B., Yuan, Y. R., Meister, G., Pei, Y., Tuschl, T., and Patel, D. J. (2005) Structural basis for 5'-end-specific recognition of guide RNA by the A. fulgidus Piwi protein, *Nature 434*, 666-670.
269. Frank, F., Sonenberg, N., and Nagar, B. (2010) Structural basis for 5'-nucleotide base-specific recognition of guide RNA by human AGO2, *Nature 465*, 818-822.
270. Song, J. J., Smith, S. K., Hannon, G. J., and Joshua-Tor, L. (2004) Crystal structure of Argonaute and its implications for RISC slicer activity, *Science 305*, 1434-1437.
271. Liu, J., Carmell, M. A., Rivas, F. V., Marsden, C. G., Thomson, J. M., Song, J. J., Hammond, S. M., Joshua-Tor, L., and Hannon, G. J. (2004) Argonaute2 is the catalytic engine of mammalian RNAi, *Science 305*, 1437-1441.
272. Meister, G., Landthaler, M., Patkaniowska, A., Dorsett, Y., Teng, G., and Tuschl, T. (2004) Human Argonaute2 mediates RNA cleavage targeted by miRNAs and siRNAs, *Mol Cell 15*, 185-197.
273. Wang, Y., Juranek, S., Li, H., Sheng, G., Wardle, G. S., Tuschl, T., and Patel, D. J. (2009) Nucleation, propagation and cleavage of target RNAs in Ago silencing complexes, *Nature 461*, 754-761.
274. Collins, R. E., and Cheng, X. (2006) Structural and biochemical advances in mammalian RNAi, *J Cell Biochem 99*, 1251-1266.
275. Schwarz, D. S., Hutvagner, G., Du, T., Xu, Z., Aronin, N., and Zamore, P. D. (2003) Asymmetry in the assembly of the RNAi enzyme complex, *Cell 115*, 199-208.
276. Sakurai, K., Amarzguioui, M., Kim, D. H., Alluin, J., Heale, B., Song, M. S., Gatignol, A., Behlke, M. A., and Rossi, J. J. (2011) A role for human Dicer in pre-RISC loading of siRNAs, *Nucleic Acids Res 39*, 1510-1525.
277. Gregory, R. I., Chendrimada, T. P., Cooch, N., and Shiekhattar, R. (2005) Human RISC couples microRNA biogenesis and posttranscriptional gene silencing, *Cell 123*, 631-640.

278. MacRae, I. J., Ma, E., Zhou, M., Robinson, C. V., and Doudna, J. A. (2008) In vitro reconstitution of the human RISC-loading complex, *Proc Natl Acad Sci U S A 105*, 512-517.
279. Matranga, C., Tomari, Y., Shin, C., Bartel, D. P., and Zamore, P. D. (2005) Passenger-strand cleavage facilitates assembly of siRNA into Ago2-containing RNAi enzyme complexes, *Cell 123*, 607-620.
280. Rand, T. A., Petersen, S., Du, F., and Wang, X. (2005) Argonaute2 cleaves the anti-guide strand of siRNA during RISC activation, *Cell 123*, 621-629.
281. Leuschner, P. J., Ameres, S. L., Kueng, S., and Martinez, J. (2006) Cleavage of the siRNA passenger strand during RISC assembly in human cells, *EMBO Rep 7*, 314-320.
282. Liu, Y., Ye, X., Jiang, F., Liang, C., Chen, D., Peng, J., Kinch, L. N., Grishin, N. V., and Liu, Q. (2009) C3PO, an endoribonuclease that promotes RNAi by facilitating RISC activation, *Science 325*, 750-753.
283. Maiti, M., Lee, H. C., and Liu, Y. (2007) QIP, a putative exonuclease, interacts with the Neurospora Argonaute protein and facilitates conversion of duplex siRNA into single strands, *Genes Dev 21*, 590-600.
284. Parker, J. S., Roe, S. M., and Barford, D. (2005) Structural insights into mRNA recognition from a PIWI domain-siRNA guide complex, *Nature 434*, 663-666.
285. Rana, T. M. (2007) Illuminating the silence: understanding the structure and function of small RNAs, *Nat Rev Mol Cell Biol 8*, 23-36.
286. Doench, J. G., and Sharp, P. A. (2004) Specificity of microRNA target selection in translational repression, *Genes Dev 18*, 504-511.
287. Martinez, J., and Tuschl, T. (2004) RISC is a 5' phosphomonoester-producing RNA endonuclease, *Genes Dev 18*, 975-980.
288. Schwarz, D. S., Tomari, Y., and Zamore, P. D. (2004) The RNA-induced silencing complex is a Mg2+-dependent endonuclease, *Curr Biol 14*, 787-791.
289. Chu, C. Y., and Rana, T. M. (2007) Small RNAs: regulators and guardians of the genome, *J Cell Physiol 213*, 412-419.
290. Hutvagner, G., and Zamore, P. D. (2002) A microRNA in a multiple-turnover RNAi enzyme complex, *Science 297*, 2056-2060.
291. Forstemann, K., Horwich, M. D., Wee, L., Tomari, Y., and Zamore, P. D. (2007) Drosophila microRNAs are sorted into functionally distinct argonaute complexes after production by dicer-1, *Cell 130*, 287-297.
292. Robu, M., Shah, R. G., Petitclerc, N., Brind'amour, J., Kandan-Kulangara, F., and Shah, G. M. (2013) Role of poly(ADP-ribose) polymerase-1 in the removal of UV-induced DNA lesions by nucleotide excision repair, *Proc Natl Acad Sci U S A 110*, 1658-1663.
293. Zhao, G., Cui, J., Zhang, J. G., Qin, Q., Chen, Q., Yin, T., Deng, S. C., Liu, Y., Liu, L., Wang, B., Tian, K., Wang, G. B., and Wang, C. Y. (2011) SIRT1 RNAi knockdown induces apoptosis and senescence, inhibits invasion and enhances chemosensitivity in pancreatic cancer cells, *Gene Ther 18*, 920-928.
294. Oikawa, Y., Matsuda, E., Nishii, T., Ishida, Y., and Kawaichi, M. (2008) Down-regulation of CIBZ, a novel substrate of caspase-3, induces apoptosis, *J Biol Chem 283*, 14242-14247.
295. Luthi, A. U., and Martin, S. J. (2007) The CASBAH: a searchable database of caspase substrates, *Cell Death Differ 14*, 641-650.

296. Zhang, M., Zhou, Y., Xie, C., Zhou, F., Chen, Y., Han, G., and Zhang, W. J. (2006) STAT6 specific shRNA inhibits proliferation and induces apoptosis in colon cancer HT-29 cells, *Cancer Lett 243*, 38-46.
297. Pop, C., and Salvesen, G. S. (2009) Human caspases: activation, specificity, and regulation, *J Biol Chem 284*, 21777-21781.
298. Germain, M., Affar, E. B., D'Amours, D., Dixit, V. M., Salvesen, G. S., and Poirier, G. G. (1999) Cleavage of automodified poly(ADP-ribose) polymerase during apoptosis. Evidence for involvement of caspase-7, *J Biol Chem 274*, 28379-28384.
299. D'Amours, D., Sallmann, F. R., Dixit, V. M., and Poirier, G. G. (2001) Gain-of-function of poly(ADP-ribose) polymerase-1 upon cleavage by apoptotic proteases: implications for apoptosis, *J Cell Sci 114*, 3771-3778.
300. Yung, T. M., and Satoh, M. S. (2001) Functional competition between poly(ADP-ribose) polymerase and its 24-kDa apoptotic fragment in DNA repair and transcription, *J Biol Chem 276*, 11279-11286.
301. Erener, S., Petrilli, V., Kassner, I., Minotti, R., Castillo, R., Santoro, R., Hassa, P. O., Tschopp, J., and Hottiger, M. O. (2012) Inflammasome-activated caspase 7 cleaves PARP1 to enhance the expression of a subset of NF-kappaB target genes, *Mol Cell 46*, 200-211.
302. Petrilli, V., Herceg, Z., Hassa, P. O., Patel, N. S., Di Paola, R., Cortes, U., Dugo, L., Filipe, H. M., Thiemermann, C., Hottiger, M. O., Cuzzocrea, S., and Wang, Z. Q. (2004) Noncleavable poly(ADP-ribose) polymerase-1 regulates the inflammation response in mice, *J Clin Invest 114*, 1072-1081.
303. Ma, E., MacRae, I. J., Kirsch, J. F., and Doudna, J. A. (2008) Autoinhibition of human dicer by its internal helicase domain, *J Mol Biol 380*, 237-243.
304. Gong, M., Chen, Y., Senturia, R., Ulgherait, M., Faller, M., and Guo, F. (2012) Caspases cleave and inhibit the microRNA processing protein DiGeorge Critical Region 8, *Protein Sci 21*, 797-808.
305. Cheloufi, S., Dos Santos, C. O., Chong, M. M., and Hannon, G. J. (2010) A dicer-independent miRNA biogenesis pathway that requires Ago catalysis, *Nature 465*, 584-589.
306. Lee, Y. S., Nakahara, K., Pham, J. W., Kim, K., He, Z., Sontheimer, E. J., and Carthew, R. W. (2004) Distinct roles for Drosophila Dicer-1 and Dicer-2 in the siRNA/miRNA silencing pathways, *Cell 117*, 69-81.
307. Bernstein, E., Kim, S. Y., Carmell, M. A., Murchison, E. P., Alcorn, H., Li, M. Z., Mills, A. A., Elledge, S. J., Anderson, K. V., and Hannon, G. J. (2003) Dicer is essential for mouse development, *Nat Genet 35*, 215-217.
308. Nakagawa, A., Shi, Y., Kage-Nakadai, E., Mitani, S., and Xue, D (2010) Caspase-dependent conversion of Dicer ribonuclease into a death-promoting deoxyribonuclease, *Science 328*, 327-334.

Annex 1: Approaches to detect PARP-1 activation in vivo, in situ and in vitro

Methods in molecular biology (2011) 780, 3-34

A1.1 Résumé en français

Une détection précise et sensible de l'activation catalytique de la poly(ADP-ribose) polymérase-1 (PARP-1) est requise dans une large variété d'échantillons car cette activité joue un rôle dans de nombreuses réponses cellulaires aux dommages à l'ADN, allant de la réparation de l'ADN à la mort cellulaire, en passant par des fonctions d'entretien comme la transcription. Étant donné que le gène *PARP-1* est exprimé de façon constitutive, son activation n'est pas supposée provenir de l'augmentation de l'expression de son ARNm ou de sa protéine mais en démontrant qu'elle est bien la conséquence de la réaction catalytique qui résulte en la consommation du substrat nicotinamide adénine dinucléotide (NAD^+) et la formation de trois produits : le polymère d'ADP-ribose (pADPr ou PAR), le nicotinamide et des protons. Nous décrivons ici différentes approches communément utilisées dans notre laboratoire pour la détection de l'activation de PARP-1 *in vivo* (dans les cellules, tissus et tumeurs), *in situ* et *in vitro* grâce à l'évaluation de la formation de pADPr, la déplétion du substrat NAD ou la formation de protons résultant en une acidification intracellulaire rapide et réversible. Il est important de noter que même si certains autres membres de la famille PARP peuvent effectuer la même réaction catalytique, la plupart de ces essais reflète en grande partie l'activation de PARP-1 dans une vaste majorité des circonstances expérimentales et plus spécifiquement dans les réponses aux dommages à l'ADN. Cependant, si nécessaire, l'action spécifique de PARP-1 devrait être confirmée par l'utilisation d'approches impliquant un « knockout » ou un « knockdown » par interférence de l'ARN de PARP-1.

A1.2 Book Chapter

Approaches to detect PARP-1 activation *in vivo, in situ* and *in vitro*

Girish M Shah[*], Febitha Kandan-Kulangara[#], Alicia Montoni[#], Rashmi G. Shah[#], Julie Brind'Amour[1], Momchil D. Vodenicharov[2] and El Bachir Affar[3]

Laboratory for Skin Cancer Research, CHUL (CHUQ) Hospital Research Centre of Laval University, Faculty of Medicine, Laval University, Québec (QC) Canada G1V 4G2

Running Header: Approaches to detect PARP-1 activation

*Corresponding Author:
Girish M. Shah, PhD,
Tel: 418-656-4141 /ext 48259 e-mail: girish.shah@crchul.ulaval.ca

# Denotes equal contribution of these three authors for this manuscript.
[1]Present address: University of British Columbia, Terry Fox Laboratory, Vancouver (BC) Canada V5Z 1L3.
[2]Present address: University of Sherbrooke, Department of Biology, Faculty of Medicine, Sherbrooke (QC) Canada J1K 2R1.
[3]Present address: University of Montreal, Department of Medicine, Hospital Maisonneuve-Rosemont Research Centre, Montreal (QC), Canada H1T 2M4.

A1.3 ABSTRACT

An accurate and sensitive detection of catalytic activation of poly(ADP-ribose) polymerase-1 (PARP-1) is required to be performed in a wide variety of samples because this activity plays a role in various cellular responses to DNA damage ranging from DNA repair to cell death, as well as in housekeeping functions such as transcription. Since *PARP-1* gene is expressed constitutively, its activation cannot be surmised from increased expression of its mRNA or protein but by demonstrating the consequences of its catalytic reaction which results in consumption of the substrate nicotinamide adenine dinucleotide (NAD^+) and formation of three products, namely polymer of ADP-ribose (pADPr or PAR), nicotinamide and protons. Here we describe various approaches commonly used in our laboratory for detection of PARP-1 activation *in vivo* (cells, tissues and tumors), *in situ* and *in vitro* via assessment of formation of pADPr, depletion of the substrate NAD or formation of protons resulting in rapid and reversible intracellular acidification. It is important to note that although some other members of the PARP family can carry out the same catalytic reaction, many of these assays largely reflect PARP-1 activation in a vast majority of the experimental circumstances and more specifically in DNA damage responses. However, if required, PARP-1-specific action should be confirmed by use of PARP-1 knockout or RNAi-mediated knockdown approaches.

Keywords: poly(ADP-ribose) polymerase-1 (PARP-1); NAD; poly(ADP-ribose) or pADPr or PAR; DNA damage; pADPr formed *in situ* (PARIS); Western Blotting; immunocytology; immunohistology, NAD cycling assay; intracellular acidification; PARP-1 activation assay *in vitro*; activity-Western blot

A1.4 INTRODUCTION

Among the earliest known responses of higher eukaryotic cells to DNA damage is catalytic activation of PARP-1, which splits the substrate NAD^+ to produce ADP-ribose, nicotinamide and proton ***(1, 2)***. The activated PARP-1 strings together multiple ADP-ribose units to make a polymer of ADP-ribose (pADPr or PAR), which is known to bind to and modify physiological properties of key cellular proteins, including PARP-1 itself ***(3)***. Thus, PARP-1 activation can be demonstrated by analyzing different consequences of this reaction. The detection of pADPr or pADPr-modified proteins is the most widely used approach to demonstrate PARP-1 activation, whereas depletion of the substrate NAD and formation of protons, i.e., a rapid and reversible intracellular acidification are occasionally used as ancillary proofs for activation of PARP-1 ***(1)***. We will review principal techniques used for demonstration of pADPr or pADPr-modified proteins *in vivo*, i.e., in cells, tissues and tumors by Western blot (section 3.1) or immunocytological and immunohistological methods (section 3.2). We will describe PARIS method to demonstrate the presence of activated PARP-1 by its capacity to form pADPr *in situ* from biotinylated NAD (section 3.3). We will describe methods to assess depletion of NAD levels in the cells or tissues (section 3.4) and intracellular acidification in cells (section 3.5). We will conclude with PARP-1 activation assay *in vitro* (section 3.6) followed by activity-Western blot technique to detect activation of PARP-1 immobilized on a nitrocellulose membrane (section 3.7). In a majority of circumstances involving DNA damage to higher eukaryotic cells, these assays will reflect activation of PARP-1 in the cells, however, it is preferable to confirm that these changes are not caused by other PARPs or other enzymes (*see* **Note 1**) through use of PARP-1-knockout/knockdown approaches or PARP-inhibitors, as shown earlier ***(1, 4, 5)***.

A1.5 MATERIALS

A1.5.1 Cultured cells and mice: GM-U6 human skin fibroblasts (Coriell, ref. ***(5)***, αMEM), human carcinoid neuroendocrine BON cells (gift of Dr Hopfner, ref. ***(6)***, DMEM-F12), mouse embryonic fibroblasts (MEFs, ref. ***(1)***, DMEM high glucose), Molt3 cells (ATCC, RPMI-1640) and HeLa (ATCC, DMEM high glucose) are cultured at 37°C in 5% CO_2 in a humidified incubator in specified media supplemented with 10% fetal bovine serum (FBS) and 1X Pen-Strep (50 units/mL penicillin and 50 µg/mL streptomycin, Gibco). All media were purchased from Gibco and all chemicals mentioned here and elsewhere in this text were from Sigma, unless otherwise specified.

SKH-1 hairless female mice (Charles River) and *PARP-1*$^{+/+}$ 129S1-SVImJ female mice (Jackson) are used for studies with UV-irradiation of skin. BALB/c nude female mice (Charles River) are injected with carcinoid cells to develop orthotopic liver tumors.

A1.5.2 PARP-1-activating DNA damage to cells, mice or tumors: In each of the protocols, cells or mice are subjected to one of the following DNA damaging treatments.

(i) UVC irradiation of cells: Cells are irradiated with UVC as described earlier ***(7)***. For global irradiation, cells are exposed to 30 J/m^2 UVC under a thin layer of dyeless serum-free medium or PBS using Spectrolinker XL-1500 fitted with UVC (BLE-1T155, peak 254 nm) fluorescent tubes or Spectroline portable model EF-140 fitted with 254 nm UVC tubes (Spectronics Corporation). For local irradiation with UVC, cells under a thin layer of PBS were exposed to 100 J/m^2 UVC through a 5 µm isopore membrane (Millipore).

(ii) Positive control for PARP-1 activation in cells: Two DNA damaging treatments that activate PARP-1 in a wide variety of cell lines are used as positive controls, namely 100-300 µM H_2O_2 or 100 µM *N*-methyl-*N'*-Nitro-*N*-Nitrosoguanidine (MNNG) (*see* **Note 2)**.

(iii) UVB irradiation of mice: The dorsal skin surface of unrestrained SKH-1 hairless mice or shaved *PARP-1*$^{+/+}$ mice are exposed to 1,600 J/m^2 UVB filtered through 0.0127 cm thick Kodacel K6805 cellulose triacetate films (Eastman Kodak) to block contaminating UVC wavelengths.

(iv) Streptozotocin treatment of carcinoid liver tumors: Female BALB/c nude mice bearing liver tumors are intraperitoneally injected with 0.9% saline or 100 mg/kg of streptozotocin (STZ). After 15 or 60 min, euthanize the mice with CO_2 under anesthesia, remove the tumor samples and quickly freeze in liquid N_2 for storage at -80°C.

A1.5.3 Western blot to detect pADPr-modified proteins

i) SDS-Polyacrylamide Gel Electrophoresis (SDS-PAGE)

1. Tris buffers: 1.5 M Tris-HCl, pH 8.8 (for separating gel), 1.0 M Tris-HCl, pH 6.8 (for stacking gel). Filter the buffers through 0.45 μm filters and store at 4°C.
2. 30% Acrylamide: bisacrylamide (37.5:1, 2.6 %C, Bio-Rad). Store at 4°C.
3. N,N,N',N'-Tetramethylethylenediamine (TEMED). Store at ambient temperature.
4. 10% (w/v) Sodium dodecyl sulphate (SDS) in filtered distilled water (dH_2O). Store at ambient temperature.
5. 10% (w/v) Ammonium persulfate solution (APS) in dH_2O. Prepare fresh for the day or prepare large batch and store small aliquots at -20°C. Avoid repeated freeze-thaw cycles.
6. Dual color and Broad Range SDS-PAGE protein molecular weight markers from Bio-Rad. Store at -20°C.
7. Running buffer (5X): 125 mM Tris, 960 mM glycine, 0.5% (w/v) SDS. Dilute 200 mL of 5X running buffer with 800 mL dH_2O to make 1X and store both 5X and 1X at ambient temperature.
8. Hybond-C nitrocellulose membrane from GE Healthcare Life Sciences.
9. Whatman chromatography filter paper (3MM Chr, Schleicher & Schuell, Fisher Scientific).
10. 10X Transfer buffer: 250 mM Tris, 1.92 M glycine. Dilute 400 mL of 10X transfer buffer with 2.8 L distilled water and 800 mL methanol to make 1X (25 mM Tris, 192 mM glycine, 20% (v/v) methanol). Store 10X buffer at ambient temperature and 1X at 4°C.
11. Ponceau S: 0.1% (w/v) in 5% (v/v) acetic acid.
12. Urea-SDS sample buffer: 62.5 mM Tris-HCl, pH 6.8, 6 M urea (deionized using AG-X8 resin, Bio-Rad), 10% (v/v) glycerol, 2% (w/v) SDS, 0.00125% (w/v) bromophenol blue and freshly added 5% (v/v) β-mercaptoethanol (β-ME). Prepare solution without β-ME and store at ambient temperature.

13. Bio-Rad Protein Assay reagent for Bradford. Dilute to 22% in dH_2O and store at 4°C.

ii) Western Blotting

1. 10X Phosphate buffer saline (PBS): 1.37 M NaCl, 27 mM KCl, 20 mM KH_2PO_4 and 100 mM Na_2HPO_4. To make 1X PBS (pH 7.4) dilute 100 mL of 10X with 900 mL dH_2O.
2. PBS-T: PBS containing 0.1% (v/v) Tween-20. For 1 L PBS-T, add 100 mL of 10X PBS, 1 mL of Tween-20, complete with dH_2O to 1 L.
3. Blocking buffer (PBS-MT): 5% (w/v) nonfat dry milk in PBS-T.
4. Primary antibody: Anti-pADPr monoclonal (10H, 1:500 in PBS-MT) is purified from hybridoma supernatant of 10H cells (Riken BRC, ref. ***(8)***). 10H antibody is also available from commercial sources. Anti-pADPr polyclonal (LP96-10, 1:10,000) is from Aparptosis Inc. Most primary antibody solutions can be used repeatedly over weeks or months after addition of Na-azide to 1mM final concentration and storage at 4°C up to few weeks or stored frozen for months at -20°C.
5. Secondary antibody: Anti-mouse or anti-rabbit IgG conjugated to horseradish peroxidase (1:2,500 in PBS-MT) from Jackson ImmunoResearch. Prepare just before use.
6. Detection: Enhanced chemiluminescence (Immobilon Western, Millipore) and detection films BioMax XAR (Kodak) or Fuji Medical X-ray (Fujifilm).
7. Stripping buffer: Prepare 62.5 mM Tris-HCl, pH 6.8, 2% (w/v) SDS and store at ambient temperature. Just prior to use, add β-ME 6 µL/mL of above solution.

A1.5.4 Immunocytological methods to detect pADPr in cells

Filter dH_2O and PBS through 0.45 µm filter.

1. Three options for fixation and permeabilization are:

a) 70:30 (v/v) Methanol/acetone, stored at -20°C

b) Formaldehyde-methanol:

(i) 1% Formaldehyde (w/v): Dissolve 1 g of paraformaldehyde in 80 mL of dH_2O and add 1 mL of 1 M NaOH. Heat at 65°C to dissolve the paraformaldehyde. Add 10 mL of 10X PBS and allow the mixture to cool to ambient temperature. Adjust the pH to 7.4 using ~1 mL of

1 M HCl. Adjust the volume to 100 mL and filter through 0.45 µm filter. Use fresh or store aliquots at -20°C, which are stable for several months (avoid freeze-thaw cycles).

(ii) Methanol (Fisher Scientific), store at -20°C.

c) 10% Trichloroacetic acid (TCA) in PBS, store at 4°C.

2. Blocking solution: 1% or 5% (w/v) bovine serum albumin (BSA) in PBS containing 0.1% (v/v) Triton X-100 with 1X pen-strep and 1 mM sodium azide.

3. Rinsing buffers: PBS pH 7.4 and PBS containing 0.1% (v/v) Triton X-100

4. Primary antibody: 10H hybridoma supernatant (1:50) in blocking solution.

5. Secondary antibody: Dilute Alexa fluorophore-conjugated secondary antibody (1:500, Molecular Probes) in PBS containing 0.1% Triton X-100 and 1% or 5% BSA.

6. 4',6-Diamidino-2-phenylindole (DAPI): Make DAPI in PBS at 5 mg/mL and keep at 4°C in dark. Prepare 250 ng/mL working solution in PBS before use.

7. Anti-fade 0.1% p-phenylenediamine (PPD) mounting solution (protect from light): To make 10 mL solution, dissolve 0.01 g of PPD in 1 mL of 10X PBS and mix with 4 mL of glycerol. In another tube, mix 2.5 mL glycerol and 2.5 mL of 40 mM potassium phosphate buffer, pH 8.5. Add buffered glycerol to PPD tube, mix well, aliquot in dark or foil-covered tubes and store at -20°C.

A1.5.5 Immunohistological methods to detect pADPr in tissues

Filter dH_2O and PBS through 0.45 µm filter.

1. 10% TCA in PBS and keep at 4°C.

2. Ethanol solutions: 70 and 90 and 100% ethanol, diluted in water as required.

3. 4% (w/v) Formaldehyde: Prepare exactly as described in step 1b of section 2.4, except start with 4 g paraformaldehyde.

4. Antigen retrieval solution (0.01 M Na-Citrate buffer pH 6.0): For 500 mL, add 9.0 mL of 0.1 M Citric acid and 41.0 mL of 0.1 M Na-Citrate (dihydrate) to 400 mL of distilled water, adjust the pH to 6.0 with 5 N NaOH and make the final volume to 500 mL. Filter through 0.45 µm filter.

5. 3% H_2O_2 in methanol (fresh): For 100 mL, add 10 mL of 30% H_2O_2 to 90 mL of methanol.

6. Blocking solution: PBS containing 10% (v/v) goat serum and 0.01% (v/v) Tween-20.

7. Primary antibody 10H (1:25 in blocking solution) and peroxidase conjugated anti-mouse secondary antibody (1:200 in blocking solution).
8. 3, 3'-Diaminobenzidine (DAB) solution (fresh): Prepare enough for fresh use. Dissolve 20 mg DAB in 100 mL of 1X PBS; to it add 10 µL of 30% H_2O_2 just before use.
9. Harris modified hematoxylin solution Sigma-HHS-16 containing 7 g/L hematoxylin.
10. Toluene (Fisher Scientific).
11. Permount mounting medium (Fisher Scientific).

A1.5.6 PARIS method

1. Biotinylated NAD: 6-biotin-17-nicotinamide adenine dinucleotide (Trevigen 4670-500-01). Stock 250 µM in dH_2O. Store aliquots at -80°C and avoid repeated freeze-thaw cycles.
2. Non-tagged NAD: 50 mM in dH_2O. Store aliquots at -20°C and avoid repeated freeze-thaw cycles.
3. PARIS buffer: 56 mM HEPES pH 7.5, 28 mM KCl, 28 mM NaCl, 2 mM $MgCl_2$. Store at 4°C.
4. PARIS buffer with 100 µM digitonin (fresh): Prepare 16 mM stock digitonin in DMSO. Just before use, dilute it to 3 mM working solution in PARIS buffer and add 3.3 µL of this working solution to 100 µL of PARIS buffer and keep at 4°C until use.
5. 1% (w/v) Formaldehyde in PBS, prepare as described in step 1b of section 2.4.
6. 0.5% H_2O_2 in methanol: Add 1.67 mL of 30% H_2O_2 in 98.33 mL methanol.
7. Blocking solution: 5% (w/v) BSA and 0.1% (v/v) Triton X-100 in PBS.
8. Streptavidin-peroxidase polymer ultrasensitive: 1 mg/mL in 0.01 M sodium phosphate buffer pH 7.4, 0.15 M NaCl, 50% (v/v) glycerol.
9. Chromogen (prepare fresh): Cobalt-enhanced nickel-DAB (3,3'-Diaminobenzidine tetrahydrochloride). Just prior to use, dissolve one tablet each of SigmaFast DAB/Cobalt and urea hydrogen peroxide in 5 mL dH_2O.
10. Permount mounting medium (Fisher Scientific).
11. Rinsing buffers: PBS pH 7.4 and PBS containing 0.1% (v/v) Triton X-100.

A1.5.7 NAD^+ extraction and measurement

1. Perchloric acid (PCA): 0.5 and 1 N.

2. 1 N KOH-0.33 M potassium phosphate buffer, pH 7.5 and 2 N KOH-0.33 M potassium phosphate buffer, pH 7.5. To prepare these solutions, use stocks of 8 N KOH and 1 M potassium phosphate buffer, pH 7.5.

3. β-Nicotinamide adenine dinucleotide (NAD) standard solutions: Prepare 50 mM stock in dH_2O, and dilute to 50 µM to verify the concentration at 260 nm (ε^{mM} =18). Prepare 400 nM working solution in water based on verified concentration of NAD. Store in 500 µL aliquots at -20°C. Avoid freeze-thaw cycles.

4. NAD-premix solution: 0.48 M bicine, pH 7.8, 20 mM EDTA, 4 mg/mL BSA, 2 mM 3-[4,5-dimethylthiazol-2-yl]-2,5-diphenyltetrazolium bromide (MTT, light sensitive), 2.4 M ethanol. To prepare 100 mL of the above solution, mix 40 mL of 1.2 M bicine pH 7.8, 4 mL of 0.5 M EDTA, 4 mL of 100 mg/mL BSA, 20 mL of 10 mM MTT, 24 mL of 10 M ethanol, and 8 mL of water. Store in 5 mL aliquots in foil covered or dark tubes at -20°C.

5. Alcohol dehydrogenase (ADH): 1 mg/mL in 0.1 M bicine, pH 7.8. Prepare fresh for the day.

6. 40 mM Phenazine ethosulphate (PES, light sensitive) in water. Prepare fresh for the day.

A1.5.8 Intracellular pH

1. 2′,7′-bis-(2-carboxyethyl)-5(and-6)-carboxyfluorescein, acetoxymethyl ester (BCECF AM, Molecular Probes): dissolve in DMSO at 1 mg/mL, store in aliquots at -20°C.

2. HBSS solution (100 mL): 10 mM HEPES pH 7.4, 134 mM NaCl, 4 mM KCl, 1.2 mM NaH_2PO_4, 1.2 mM $MgSO_4$, 11 mM D-glucose, 2 mM $CaCl_2$. Make the volume to about 90 mL with water before the pH adjustment. Adjust pH to 7.4 with NaOH and make up the volume to 100 mL. Sterilize by filtration through 0.22 µm filter and store at 4°C.

3. High potassium calibration buffers:

Common stock buffer (1 L): 140 mM KCl, 1 mM $MgCl_2$, 2 mM $CaCl_2$, 5 mM D-glucose. Make up the volume to 1 L with dH_2O.

Acidifying buffer: To 500 mL of common stock buffer, add 2-[N-morpholino] ethanesulfonic acid (MES) to 20 mM final concentration. Filter through 0.45 µm filter and keep at 4°C.

Alkalinizing solution: To 500 mL of common stock buffer, add Tris base to 20 mM final concentration. Filter through 0.45 µm filter and keep at 4°C.

Calibration buffers: For accurate pH measurements, bring acidifying and alkalinizing solutions to ambient temperature. Prepare four calibration buffers at pH 7.4, 7.1, 6.8 and 6.4. For each calibration buffer, take 10 mL of any one of the above solutions (acid or alkaline) in a beaker and add the other with constant stirring on the magnetic stirrer till the desired pH is achieved. Store the calibration buffers at 4°C.

4. Nigericin: 1 mg/mL in ethanol in a glass vial (nigericin binds to plastic) and store at -20°C.

A1.5.9 PARP-1 activation in vitro

i) PARP-1 activation assay reagents

1. PARP-1 assay common cocktail: The total assay volume of 140 µL consists of 100 µL of cocktail containing all the common items and remaining 40 µL is for other variable reagents, such as DNA, histones and PARP-1. Prepare a common assay cocktail sufficient in volume for all the samples and controls in a given batch to ensure consistency of results. Each assay must be conducted at least in duplicate. Each 100 µL of common assay cocktail contains 140 mM Tris-HCl pH 8.0, 14 mM $MgCl_2$, 2.1 mM DL-dithiothreitol (DTT), 14% (v/v) glycerol, 280 µM NAD, and if required 0.5 µCi ^{32}P-adenylate NAD (Perkin Elmer, NEG023). Mix and distribute 100 µL in each glass assay tube.

2. Activated DNA: Prepare 0.5 mg/mL of commercial activated DNA or damaged DNA from your experiment. Store at -20°C. Add 10 µL per assay.

3. Histones: 1 mg/mL. Store at -20°C. Add 10 µL per assay.

4. Purified PARP-1: Use hydroxyapatite-purified PARP-1 available from many commercial sources. Avoid using 3-aminobenzamide column or DNA cellulose column purified PARP-1 for this assay. The PARP-1 used in this study is from Aparptosis Inc. Dilute PARP-1 to 30 U/mL in PARP-1 dilution buffer (100 mM Tris-HCl, pH 8.0, 19 mM $MgCl_2$, 10% (v/v)

glycerol and 1.5 mM DTT). Store at -80°C and during removal of aliquots of enzyme for assay, thaw rapidly and quickly refreeze the tube at -80°C.

5. BSA: 10 mg/mL in dH_2O. Store at -20°C.

6. TCA solutions: Prepare 50% TCA in dH_2O. Prepare 25% TCA in dH_2O containing 20 mM Na-pyrophosphate ($Na_4P_2O_7$: 1M: 26.59g/100 mL). Store at 4°C.

7. Ethanol: 100% (4°C).

8. Ether: 100% (4°C).

9. Whatman GF/C glass microfiber 25 mm filter discs.

ii) pADPr-purification reagents

1. Stock 100% TCA. Store at 4°C.

2. 1M KOH-50 mM EDTA. Store at 4°C.

3. AAGE9 buffer: 250 mM ammonium acetate (NH_4OAc) pH 9.0, 6 M guanidine hydrochloride, 10 mM EDTA. Keep at ambient temperature.

4. Dihydroxyboronyl Bio-Rex (DHBB) affinity resin: Preparation of DHBB affinity resin is based on the protocol described earlier ***(9)***.

i) In a 1 L beaker, soak 25 g of Bio-Rex 70 resin (200-400 mesh) for 30 min in 100 mL 0.25 M NH_4OAc, pH 5.0. Monitor the pH with pH-paper and adjust the pH to 5.0 with concentrated acetic acid.

ii) Under the fume-hood and with constant stirring, add 2.5 g of 1-ethyl-3-(3-dimethylaminopropyl)carbodiimide and stir the resin for 15 min.

iii) Add 2.5 g m-aminophenylboronic acid, dissolved in 15 mL of water, to the resin suspension. Adjust the pH to 5.0 if necessary and allow the reaction to occur in the dark at ambient temperature overnight with gentle stirring.

iv) Filter the resin slurry through Whatman 1 filter placed in a Buchner funnel attached to vacuum line.

v) Wash the resin by passage of 1 L each of water, solution A (0.1 M NH_4OAc, 1 M ammonium chloride (NH_4Cl), pH 4.5), solution B (0.1 M ammonium bicarbonate (NH_4HCO_3), 1 M NH_4Cl, pH 9.0), 500 mL of water, and finally 100 mL of solution C (6 M guanidine-hydrochloride, 50 mM 3-[N-morpholino]propanesulfonic acid (MOPS), 10 mM EDTA, pH 6.0).

vi) Suspend the resin (1:1) to a final volume of 50 mL with solution C and store at 4°C in dark bottles.

5. 1 M NH_4HCO_3, pH 9.0. Store at 4°C.

6. 10 mM HCl. Store at ambient temperature.

A1.5.10 Activity-Western blot

1. Renaturation buffer: 50 mM Tris-HCl pH 8.0, 100 mM NaCl, 1 mM DTT, 0.3% (v/v) Tween-20. Add 1 mM DTT just before use.

2. 20 mM Zinc-acetate in dH_2O. Prepare fresh and keep at 4°C until use.

3. 1 mg/mL Activated DNA in dH_2O. Store at -20°C.

4. 1 M $MgCl_2$. Store at ambient temperature.

5. 50 mM NAD. Store at -20°C. Avoid freeze-thaw cycles.

6. SDS-wash buffer: 50 mM Tris-HCl pH 8, 100 mM NaCl, 1 mM DTT and 2% (w/v) SDS.

A1.6 METHODS

A1.6.1 Western blot to detect pADPr-modified proteins in cells or tissues

This is a relatively simple and most commonly used method to demonstrate activation of PARP-1 by visualization of pADPr-modified proteins in a Western blot of the whole cell/tissue extract probed with anti-pADPr antibody (**Fig. A1.1**). Several common features of these blots are listed here. It is known that PARP-1 is a major acceptor of pADPr chains after DNA damage. Therefore, although many proteins are targeted for pADPr-modification, the predominant signal in majority of the blots is seen from 110-250 kDa, which is also the region in which purified PARP-1 gives a strong signal after automodification in an *in vitro* reaction ***(1)***, suggesting that cellular signal may also be largely composed of automodified PARP-1. Since proteins are modified by pADPr-chains of different lengths, the signal for even a single target protein, such as PARP-1 modified by pADPr generally appears as a smear above the size of the original protein, rather than a single well-defined band of modified protein. Finally, since pADPr-formation and its subsequent degradation by poly(ADP-ribose) glycohydrolase (PARG) is rapid, one needs to ascertain the time of peak pADPr accumulation by analyzing samples harvested from 15 seconds to 4 h, depending on the type of DNA damage and the cell type ***(1, 7, 10)***. Two important technical issues for preparation of the samples are: (i) samples prepared in commonly used RIPA buffer are not as efficient in extracting PARP-1 as the urea-SDS sample buffer mentioned here; and (ii) samples must be processed rapidly after harvesting to prevent degradation of pADPr by PARG.

<u>A) Preparation of cell or tissue lysate for Western blot</u>

Treat cells or animals to PARP-1 activating treatment, as described in section 2.2.

(i) Lysate preparation from cells: Follow step 1a for adherent cells or step 1b for non-adherent cells.

1a. For adherent cells, place the culture dishes on ice, aspirate the medium and wash the cells once in cold PBS. Using 0.5 to 0.75 mL of PBS, scrape the cells and collect in 1.7 mL tubes. Scrape again in similar volume of PBS, pool the cells and proceed to step 2.

Alternatively, cells can be washed in cold PBS and scrapped directly in the minimal volume of urea-SDS sample buffer to proceed to step 4.

1b. For non-adherent cells, spin smaller volume samples (<1.5 mL) in a micro-centrifuge at 4,500*g* for 5 min at 4°C, whereas spin larger volume samples in centrifuge with swing-out bucket rotor at 1,000*g* for 5 min at 4°C. Aspirate supernatant and suspend the cells in 1 mL of cold PBS, transfer the contents to a 1.7 mL tube. Proceed to step 2.

2. Spin in a micro-centrifuge at 4,500*g* for 5 min at 4°C.

3. Remove the supernatant and suspend the cells at a concentration of 10^5 cells /10 μL of urea-SDS sample buffer. Add the sample buffer along the side of the tube to collect all the cells, which might have settled along the length of the tube. Spin briefly in a mini/micro-centrifuge to collect the sample.

4. Cool the samples on ice and sonicate with a microprobe at 45% amplitude for a 15-20 sec at ambient temperature to shear the DNA. If required, repeat the sonication step after cooling the samples on ice for 2-5 min. Spin at 15,000*g* for 1 min at 4°C. The sonicated suspension should be easy to pipet with a fine bore tip. Samples can be stored before or after sonication at -20°C.

(ii) Lysate preparation from tissue or tumors: For preparing lysate from tissue, either use fresh tissue rapidly after harvesting (step 1a) or freeze small pieces in liquid N_2 and store at -80°C (step 1b).

1a. If starting with fresh tissue, cut it into small pieces and homogenize at 4°C using Dounce homogenizer in the urea-SDS sample buffer described above. For samples of whole skin or epidermis, use polytron homogenizer with a probe containing knives (Polytron PT 3100 and probe/aggregate Kinematica PT-DA 3005/2EC).

1b. For the frozen tissue pieces, crush them to a fine powder in liquid N_2 using chilled mortar and pestle, transfer the powder to chilled 1.7 mL tubes on dry ice. Add a suitable volume of urea-SDS sample buffer and transfer to 4°C.

2. Sonicate with a microprobe at 45% amplitude at 4°C for five bursts of 20 sec, each separated by an interval of 5 to 10 min to allow cooling and settling of foam.

3. Spin at 15,000*g* for 10 min at 4°C and remove the clear uniform tissue lysate to a new tube while carefully avoiding the floating fat layer and the pelleted debris. This step

prevents streaking at higher molecular weights in the Western blots. Store the samples at -20°C.

B) Protein estimation

The samples for Western blot are equalized either for cell number or for protein content.

1. To measure protein concentration, precipitate 1-5 µL aliquot of the cell extract with 10% TCA in dH_2O on ice for at least 30 min (can be overnight). For tissues extracts with unknown cell count or weight of tissue, use 1 µL aliquot for precipitation.
2. Spin at 15,000*g* for 5 min at 4°C and discard the supernatant.
3. Wash the pellet with 1 mL of 100% ethanol. Remove the supernatant carefully as the pellet tends to dislodge very easily. Dry the pellet at ambient temperature.
4. Dissolve the pellet in suitable volume of 0.25 N NaOH-0.025% Triton X-100. For cells, anticipate 1 mg protein/10^7 cells and dissolve the pellet at a concentration of 50-100 µg/mL. For tissue extract, dissolve the pellet in 100 µL.
5. For standard graph, use commercially available 1 mg/mL BSA. Prepare series of dilutions from 0-150 µg/mL in 0.25 N NaOH-0.025% Triton X-100.
6. Assess the protein concentration in 10 µL of standard BSA solutions or cell-derived samples, by mixing with 190 µL diluted Bradford reagent in 96 well plates. For tissues, start with 5 and 10 µL aliquots in the assay and adjust the dilution or volume according to the initial read-out to fall within the linear range of the assay.
7. Read the plate in microplate reader at 595 nm after 5-10 min. The color is stable up to 1h.

C) Sample preparation, SDS-PAGE electrophoresis, transfer and blotting

Sample preparation: Prepare aliquots of each sample representing 1-2 x 10^5 cells or 20-30 µg of protein. Just before loading the sample on gel, heat at 65°C for 15 min or at 95°C for 5 min, briefly spin in micro-centrifuge and load on the gel.

The following instructions assume the use of Mini-PROTEAN Tetra cell system and Mini Trans-blot cell from Bio-Rad. The glass plates for the gels are scrubbed clean with detergent and rinsed extensively with distilled water, cleaned with 100% ethanol and scrub-dried.

1. For one 1.0 mm 8% SDS-PAGE separating gel, prepare 5 mL solution containing 2.3 mL H_2O, 1.3 mL 30% acrylamide, 1.3 mL 1.5 M Tris-HCl pH 8.8, 50 µL of 10% SDS, 50 µL of 10% APS and 3 µL of TEMED. Pour ~4.5 mL of the solution, leaving ~2 cm space from the top of small plate for the stacking gel. Overlay with 300 µL H_2O and leave the gel to polymerize for 30-45 min.

2. Pour off the water from the gel and remove the residual water gently with a Whatman paper.

3. Prepare 2 mL of the stacking gel solution by mixing 1.4 mL H_2O, 330 µL of 30% acrylamide, 250 µL of 1.0 M Tris-HCl pH 6.8, 20 µL of 10% SDS, 20 µL of 10% APS and 2 µL of TEMED (*see* **Note 3**).

4. Pour the stacking gel solution between the glass plates and insert a comb. Let it polymerize for at least 15 min.

5. After the stacking gel polymerizes, remove the comb and wash the wells with water. Alternately, the polymerized gel along with the comb in place can be covered in moist paper-towels, wrapped in saran-wrap and stored at 4°C for up to 2 weeks. Take care that the gel does not become dry during storage.

6. Mount the gel onto the SDS-PAGE electrophoresis chamber containing running buffer.

7. Load protein molecular weight markers and samples on SDS–PAGE wells and run at constant voltage (100 to 200 V) until the dye front of the samples reaches the bottom of the gel.

8. Transfer the proteins onto nitrocellulose membrane in a Transblot cell containing transfer buffer at 4°C, stirring constantly and electrophorese at 100 V for 1.5 h or at 35 V overnight.

9. After the transfer is complete, stain the membrane with Ponceau-S to identify and mark the molecular weights.

All the following steps are carried out on a rocking platform.

10. Block the membrane for a minimum of 1 h in PBS-MT prior to immunoprobing with anti-pADPr antibody (10H at 1:500 or LP96-10 at 1:10,000 diluted in PBS-MT) overnight at 4°C

(*see* **Note 4**).

Following steps are at ambient temperature.

11. Wash the membrane 6 x 10 min with PBS-T.

12. Incubate the membrane for 30 min in secondary antibody solution (1:2,500 in PBS-MT).

13. Wash the membrane 6 x 10 min with PBS-T followed by similar washes in PBS.

14. Reveal the blot with the chemiluminescence reagent prepared according to manufacturer's instructions. Detect the signal on X-ray film or ChemiGenius 2 BioImaging System (SynGene) using GeneSnap 6.0 software.

Fig. A1.1 demonstrates that DNA damage induced by variety of agents in different cells and tissues results in an appearance of a unique smear of pADPr-modified proteins in the 110-250 kDa zone.

D) Stripping and reprobing of blots

Membranes can be repeatedly probed with different antibodies by erasing the blot after each immunoprobing. Few antibodies such as 10H give best results with virgin blot, but other antibodies such as monoclonal anti-PARP-1 C-2-10 or anti-β-Actin can be used on a blot that has been erased up to three times.

1. Wash the revealed membrane in PBS 3 x 5 min at ambient temperature.

2. Incubate the blot in 10-15 mL (or sufficient volume to cover the blot) of stripping buffer with freshly added β-ME (6 μL/mL) at 65°C for 30 min in a closed container.

3. Wash the blot 5 x 5 min with PBS. Erased membrane can be reprobed immediately or stored at 4°C in saran-wrap.

A1.6.2 Immunocytological or immunohistological detection of pADPr formed in cells or tissues

This method is most commonly used for intracellular visualization of the pADPr at the time of harvesting. This method also allows co-localization of pADPr with other cellular proteins in sub-nuclear foci. In the protocols described here, the final step for detection of pADPr is through use of fluorescent-tagged secondary antibody, but it can be exchanged for DAB staining.

A) Immunocytological detection of pADPr or pADPr-modified proteins in cells

1. Grow cells in appropriate medium on ethanol-sterilized 25 mm (dia.) glass coverslips in 35-mm dishes.

2. Treat the cells at 70-80% confluence with DNA-damaging agent as described in section 2.2, and harvest at different time points.

3. Place the dish with coverslip on ice, aspirate the medium, wash 2 x 2 mL with cold PBS.

4. Fixation methods: There are several methods to fix and permeabilize the cells. The choice of method is largely dictated by its compatibility with the immunodetection of other antigens that are being probed along with pADPr. Following are three fixation methods used in our studies. *(a) Methanol:acetone fixation:* Incubate the cells in 2 mL of methanol: acetone (70:30) for 30 min at -20°C and proceed to step 5. *(b) Formaldehyde-methanol fixation* (**Fig A1.2A**): Incubate the cells in 2 mL of 1% formaldehyde for 10 min at ambient temperature, wash 3 x 2 mL with cold PBS, quench formaldehyde by 2 x 5 min with 2 mL 0.1M NH_4Cl in PBS, wash 3 x 2 mL with PBS, permeabilize the cells by incubating with 2 mL 100% methanol for 10 min at -20°C and proceed to step 5. *(c) TCA-ethanol fixation* (**Fig A1.2B**): Incubate the cells in 2 mL of 10% TCA for 15 min at 4°C, wash successively for 3 min each at 4°C with chilled 70, 90 and100 % ethanol and proceed to step 5.

5. Wash 5 x 2 mL with cold PBS and block in PBS containing 1 or 5% BSA for 1 h at ambient temperature or for longer periods at 4°C.

6. Remove the blocking solution and invert the coverslip over 40 µL of anti-pADPr 10H (1:50) antibody layered on parafilm. Incubate for 2 h at ambient temperature or overnight at 4°C in a humidified chamber.

7. Transfer the coverslips back to the dishes and wash 3 x 5 min with cold PBS-Triton.

8. From this step onwards all reactions should be done in dark to avoid fluorochrome quenching. Invert the coverslips over 40 µL of fluorophore (e.g., FITC)-conjugated secondary antibody (1:500) layered on parafilm. Incubate for 45 min at ambient temperature.

9. Transfer the coverslips back to the dishes, wash 3 x 5 min with PBS-Triton. Wash once with PBS and add DAPI solution in PBS for 5 min to stain the DNA and identify the nuclei.

10. Wash 2 x 2 mL with filtered water and air-dry the coverslips in dark.

11. Mount the coverslip on a microscopic slide (cell-side down) over 30 µL of mounting medium containing anti-fade. Remove air-bubbles in the mounting medium by giving gentle pressure on the coverslip and dab the excess medium with absorbent paper. Seal the edges with two coats of nail polish. The slides can be viewed immediately or stored in dark at -80°C for weeks.

12. View the slides at 40 to 63X objectives using a Zeiss Axiovert 200 fluorescence microscope. As an example, in the nuclei stained blue with DAPI, staining for pADPr can be seen in the formaldehyde-methanol fixed cells (**Fig. A1.2A**) or in TCA-ethanol fixed cells (**Fig. A1.2B**).

B) Immunohistological detection of PAR or PAR-modified proteins in tissues

Following protocol describes detection of PAR in mouse skin exposed to DNA damaging UV radiation. It can be applied to other tissues after suitable modifications.

1. Remove tissue of interest, such as dorsal skin, as rapidly as possible from euthanized animals. Spread the skin (epidermis side-down) on a glass plate kept over crushed dry ice, scrape the sub-dermal fat layer and make small 1-2 mm wide and 5-10 mm long sections. For other tissues, make small (<5 mm thick and about 1 cm long) pieces of tissue. Place the pieces in a histocassette between two filter papers.

2. Soak the cassette in 10% TCA for 1 h at 4ºC.

3. Transfer the cassettes to successive baths of 70, 90 and 100 ethanol at 4ºC for 1 h each.

4. Transfer the cassettes to fixative bath of 4% formaldehyde and incubate overnight at ambient temperature. Keep the cassettes in the same bath but at 4ºC for a minimum of 24 h prior to processing for paraffin embedding and subsequent preparation of slides with 5 µm sections. The slides can be stored at ambient temperature indefinitely.

All the following steps are at ambient temperature, unless specified otherwise.

5. For detection of pADPr, deparaffinize the section by immersing the slides for 5 min each in 3 serial baths of 100% toluene. Prior to toluene treatment, slides may be heated to 60ºC on a hot plate, and excess melted paraffin around the tissue section removed using absorbent paper.

6. Rehydrate in successive baths of ethanol (100-90-70%) for 5 min each.

7. Block endogenous peroxidase in methanol containing 3% H_2O_2 for 10 min.

8. Retrieve the antigen by boiling the slides for 15 min in 0.01M Na-citrate buffer, pH 6.0. This step can be performed in a microwave oven, for example 20% power in a 700Watt-microwave. Let stand to cool to ambient temperature

9. Block non-specific binding with PBS containing 10% goat serum and 0.01% Tween-20 for 1 h.

10. Incubate with ~50 µL of primary antibody (1:25 in blocking buffer) at 4°C overnight in a humidified chamber.

Perform all the wash steps on a rocking platform.

11. Wash the slides 3 x 2 min with PBS and once with blocking buffer.

12. Incubate with peroxidase linked anti-mouse secondary antibody (1:200 in blocking buffer) for 3 h.

13. Wash 5 x 5 min with PBS. Incubate the slides in 0.2 mg DAB/mL PBS from 3-5 min. Wash quickly in a PBS bath, then 10 min in tap water.

14. Counter-stain with Harris modified hematoxylin for 15 seconds, rinse with tap water for 2 min.

15. Dehydrate in successive baths of ethanol (70-90-100%) before mounting with Permount medium and cover with a coverslip making sure there is no air bubble trapped. Leave it overnight to dry.

16. View the slides with 40X objectives in a Zeiss Axiovert 200 microscope. In UV-exposed epidermis from SKH-1 mouse, pADPr formation can be visualized by brown signal in the nuclei in a background of blue counterstained cells (**Fig. A1.2C**).

A1.6.3 PARIS method to detect tagged pADPr formed *in situ*

Unlike the methods described earlier in section 3.2 which detect the steady state levels of pADPr, i.e., a net result of synthesis and degradation of pADPr at the time of harvesting, PARIS method provides a snapshot of PARP-1 molecules that are active at the time of harvesting. This is achieved by allowing the cells to synthesize pADPr *in situ* after harvesting but in the presence of tagged or radiolabeled NAD that has been introduced in the cells. Since NAD does not enter intact cells, all of these methods involve a permeabilization step with agents such as digitonin. The new pADPr synthesized *in situ* in this assay would carry the tag from the newly introduced tagged NAD and thus it can be

distinguished from the previously existing pADPr in the cell formed prior to harvesting from endogenous NAD.

The earlier versions of this method used radiolabeled (^{32}P) NAD and detection of proteins modified by radiolabeled pADPr ***(11)***. Subsequently, this method using radiolabeled NAD was applied to sections of the brain of animals and was dubbed as PARIS, i.e., polymer of ADP-ribose formed *in situ* ***(12)***. More recently, the radiolabeled NAD was replaced by biotinylated NAD that was shown to work very well with cells and tissue sections ***(13, 14)***. In view of the convenience of the biotinylated NAD over radiolabeled NAD, we describe here a detailed protocol for PARIS method using biotinylated NAD for cultured cells, and it can be readily modified to use with fresh frozen tissue sections.

PARIS method to detect biotinylated pADPr formed in situ in cultured cells

1. Grow cells in appropriate medium on 25 mm ethanol-sterilized coverslips in 35-mm dishes or 4-chamber tissue culture treated glass slides (BD Falcon).
2. DNA damaging treatment with H_2O_2, as described in section 2.2 can be performed either at this stage before permeabilization or after permeabilization in step 6, depending on the experimental question that is being addressed.

Unless specified, all the subsequent steps are at ambient temperature.

3. Wash the cells in 2 mL of cold PARIS buffer without digitonin.
4. Transfer the coverslips to a small boat made from aluminium foil and incubate with 100 µL of PARIS buffer containing 100 µM digitonin for 30 min at 4°C.
5. Remove the buffer to a 700 µL microtube, add biotinylated NAD to a final concentration of 25 µM and "non-tagged" NAD to 75 µM. In the samples without biotinylated NAD, add 100 µM non-tagged NAD. Transfer it back to the cells on the coverslip. Incubate for 10 min at 37°C. Go to step 7 if DNA damaging treatment was carried out in step 2.
6. If DNA damaging treatment was not carried out in step 2, remove the NAD containing buffer in the same microtube, add the DNA damaging agent in the tube, mix and transfer it back to the cells on the coverslip. Incubate for 10 min at 37°C.

7. After a quick rinse in cold PBS, transfer the coverslips to the dishes and fix the cells in 1% formaldehyde for 10 min.
8. Wash 3 x 5 min with cold PBS.
9. Block the endogenous peroxidase by incubation for 15 min in 0.5% H_2O_2 in methanol.
10. Wash 3 x 5 min with cold PBS.
11. Block non-specific binding with blocking solution for 1 h.
12. Incubate with streptavidin-peroxidase (1:100) in PBS containing 0.1% Triton X-100 for 1 h.
13. Develop the slide in freshly prepared cobalt blue DAB reagent for 15-20 min until cells turn blue. If using regular DAB reagent that gives brown color, do not exceed 5-10 min to avoid high background color.
14. Wash rapidly once in cold PBS.
15. Rinse twice in dH_2O, air-dry and mount the coverslips with Permount.
16. View the slides using Axiovert 200 microscope and software AxioVision 4.7 (Zeiss) at 40 or 63X objectives. The strong nuclear signal for biotinylated NAD can be seen in H_2O_2-exposed cells that contained biotinylated pADPr derived from biotinylated NAD (**Fig. 3**).

A1.6.4 Quantification of NAD levels in cells or tissues to assess PARP-1 activation

A measurement of the extent of lowering of the substrate NAD in cells or tissues in response to DNA damage provides a fair representation of activation of PARP-1. An example of the use of this method to support demonstration of PARP-1 activation can be seen in **Fig. A1.4.** Molt 3 cells treated with 10 or 100 μM MNNG show different extent of formation of pADPr-modified proteins (**Fig. A1.4A**) and corresponding depletion in cellular NAD and consequent ATP levels (**Fig. A1.4B**) ***(1)***.

Since PARP-1 uses the oxidized form of NAD, i.e., NAD^+, and since acids can readily extract oxidized form of NAD, the protocol described below for extraction of NAD is a simplified version of our previously described protocol ***(9)***. This is followed by a very convenient and rapid micro-assay for NAD by cycling method using alcohol

dehydrogenase ***(9)***. It should be noted that different samples should be equalized for protein content or cell number for assessing differences in NAD content.

For almost all the studies with cultured cells and most studies with organs or tumors from experimental animals, this simple protocol showing decreased NAD levels is a sufficient measure of PARP-1 activation. However, in case of blood and tissue samples from patients or in some animal protocols where uneven yield or poor quality of material could be a factor for accurate assay of NAD alone, it is advisable to carry out analysis of niacin number, which is a ratio of (NAD/NADPx100), because while NADP remains fairly stable, NAD levels can change due to activity of PARP-1 or due to other factors such as deficiency of niacin, as we have shown earlier for niacin deficient carcinoid patients ***(15)***. The protocol for both NAD and NADP in oxidized and reduced form is required in these procedure that has been briefly described earlier ***(15)***. Here, we focus on the simple acid extraction of oxidized form of NAD and micro-cycling assay of NAD.

A) Extraction of NAD from cells or tissues by PCA

1. Treat cells/animals with DNA-damaging agent to induce pADPr synthesis.

2a. For adherent cells, wash the cells with PBS at 4°C and scrape them in PBS (1-10 mL). Collect the cells in a 15 mL tube on ice.

2b. For suspension cells, collect the cells in appropriate size tube, and spin at 1,000*g* for 10 min at 4°C in a swing-out rotor. Remove the medium, and suspend the cell pellet in cold PBS.

3. Spin the cell suspension at 1,000*g* for 10 min at 4°C and discard the supernatant.

4. Add 2 mL of 0.5 N PCA and vortex to disperse the pellet. Keep on ice for 15 min. Proceed to step 6.

5. In case of tissues such as liver, tumor or skin, grind the pieces of frozen tissues to a powder in liquid N_2, using mortar and pestle. Suspend the powder in 5 mL of 1 N PCA and homogenize at 4°C at high speed in a Polytron homogenizer. Leave the tissue homogenate on ice for 30 min.

6. Collect the acid supernatant of the cells or the tissue after centrifugation at 1,000*g* for 10 min at 4°C in a swing out rotor. Proceed with supernatant to step 7. Only for tissue samples with unknown cell number, dissolve the acid-insoluble pellet obtained here in 500-1,000 µL NaOH-Triton for protein estimation as mentioned in section 3.1.2.
7. Neutralize the acid supernatant from cells with 1 mL of 1 N KOH-0.33 M potassium phosphate buffer, pH 7.5 or the tissue-derived supernatant with 2.5 mL of 2 N KOH-0.33 M potassium phosphate buffer, pH 7.5. Using pH papers, verify and adjust the pH with acid or alkali to around 7.5. Keep on ice for 30 min. Keep a record of the total volume of the extract for calculation of the NAD concentration, expressed as moles per 10^6 cells or per mg protein.
8. Remove the $KClO_4$ precipitate formed by spinning at 2,000*g* for 15 min at 4°C.
9. Aliquot and store the supernatant at -20°C until NAD determination by microassay.

B) Micro-assay for NAD in acid extract from tissues or cells

Carry out the assay in a 96-well flat bottom assay plate (e.g., Falcon 3912), in the dark at 30°C in a dry-air oven.
1. Just before the assay, make a NAD-assay mix by mixing 5 parts of the NAD pre-mix solution with 1 part of ADH and 1 part of PES. Keep it on ice, protected from light.
2. In a total volume of 150 µL, take 0-20 pmol standard NAD or an aliquot of sample, make it to 100 µL with water and mix with 50 µL of freshly prepared NAD mix. The final concentration of reagents in total 150 µL solution are: 0.114 M Bicine, pH 7.8, 0.57 M ethanol, 4.8 mM EDTA-Na_4, 1 mg/mL BSA, 0.48 mM MTT, 1.9 mM PES and 48 µg/mL ADH.
3. Incubate the plate in the dark at 30°C for 30 min and monitor the absorbance at 595 nm in a microplate reader.

A1.6.5 Intracellular acidification as a measure of protons released by activated PARP-1

The release of protons from NAD is one of the consequences of catalytic activity of PARP-1; therefore, extensive activation of PARP-1 in response to high levels of DNA

damage would be expected to result in a release of large number of protons in a short period of time, causing a transient drop in intracellular pH (pHi) until the cells are able to neutralize or export the excess protons. We previously reported that PARP-1 activity was responsible for rapid intracellular acidification to the extent of 0.5-0.6 pH units in cells exposed to 100 μM MNNG (**Fig. A1.4C**), and that this acidification was indeed due to action of PARP-1 because inhibition or absence of PARP-1 abolished the acidification ***(1)***. Therefore, an assessment of intracellular acidification by measuring pHi after DNA damage can serve as an ancillary measure of PARP-1 activation. The protocol for measuring pHi was described very briefly in our earlier work ***(1)***; here we provide a detailed protocol.

The assay rests on the use of pH sensitive fluorescent probe BCECF, which is introduced in the cells in its cell permeable ester-form. Once inside the cell, cellular esterases remove the ester group trapping the probe inside the cells; thus permitting monitoring of pHi by flow cytometry using a pair of pH-sensitive (525 nm) and pH-insensitive (640 nm) emission wavelengths after excitation at a higher energy wavelength (488 nm). The ratio 525/640 increases with increased pHi. We have shown that this protocol works equally well for non-adherent cells (e.g. Molt 3 or HL-60) or for adherent cells, such as *PARP-1*$^{+/+}$ or *PARP-1*$^{-/-}$ MEF ***(1)***.

Standard curve and measurement of pH in experimental samples: In the studies involving measurement of pHi up to 1 h after DNA damage, load the BCECF dye in the cells as described below prior to treatment with DNA damaging agent. For measuring pHi at longer time interval after DNA damage, treat the cells under normal culture conditions, and begin the procedure of loading with BCECF 15 min prior to desired time-point. Note that each pH measurement requires 500,000 cells; hence calculate the total number of cells required for the experimental conditions and standard curve, and load the cells in one batch with BCECF as described below.

1a. For suspension cells, spin the cells at 1,000*g* for 10 min at ambient temperature. Discard the medium, wash the cells with PBS and suspend in serum-free medium at a concentration of 1 x 10^6/mL.

1b. For adherent cells, aspirate the medium, wash with PBS and add serum-free medium.

2. Add 2 µL BCECF/mL (stock 1 mg/mL) and incubate at 37°C for 15 min. Mix intermittently.

3. Collect the cells (by trypsinization in case of attached cells), and divide them in aliquots of 500,000 cells each for the standard curve and the experimental conditions in 1.7 mL tubes.

4. Centrifuge at 4,500*g* for 5 min. Discard the supernatant. The pellet of cells will appear yellow due to the BCECF incorporation.

5. Suspend the cells at 1 x 10^6 cells/mL of HBSS (experimental cells) or high potassium standard pH buffers (pH 6.4, 6.8, 7.1 or 7.4) and transfer the cells for standard pH buffer to glass tubes.

6. To the cells for standard curve, add nigericin at a final concentration of 2 µg/mL and leave them at ambient temperature. Read the pH between 20-60 min after the addition of nigericin.

7. Meanwhile, treat the cells in HBSS with DNA damaging agent for desired time as described in section 2.2.

8. Measure the emission fluorescence for the standard curve and the experimental conditions.

9. Plot a standard pHi versus absorbance graph from the mean absorbance values obtained for the standard buffers v/s the pH in the buffers.

10. Calculate the pHi of the experimental sample using the standard graph. The pHi of control cells is normally between 7.2-7.4.

A1.6.6 PARP-1 activation *in vitro*

PARP-1 activation *in vitro* is a classical enzymological activity assay in which PARP-1, activated in the presence of damaged DNA and NAD, forms pADPr chains that modify PARP-1 itself and other proteins such as histones added in the assay. This assay has acquired applications well beyond the original purpose of assaying activity of the enzyme.

It is used for monitoring purification process for PARP-1, identification of novel PARP-1 activating DNA structures, preparation of radiolabeled or non-isotopic pADPr for identification of various pADPr-binding proteins and for assays of pADPr-digesting enzyme PARG. The core assay described below is the basic enzyme-activation assay, which has been derived from different assays described earlier ***(1, 7, 9)***. Note that different components of this core assay can be omitted, altered in amounts or replaced by alternate materials depending on the desired end-use of the assay (*see* **Note 5)**.

A) PARP-1 activation assay

In a glass tube containing 100 µL of PARP-assay common cocktail add 10 µL each of DNA (5 µg) and histones (10 µg) (*see* **Note 6**). Warm the reaction mixture at 30°C for 2 min and add 20 µL (0.6 U) of purified PARP-1. Gently mix and incubate at 30°C for 20-60 min, as required for the desired end-point of the assay. Together the final 140 µL assay mixture contains 100 mM Tris-HCl pH 8.0, 10 mM $MgCl_2$, 1.5 mM DTT, 10% glycerol, 5 µg activated DNA, 10 µg histones, 200 µM NAD, and if required 0.5 µCi ^{32}P-adenylate NAD and 0.6 U of PARP-1. During this reaction, activated PARP-1 modifies itself (automodification) and histones with pADPr. At the end of PARP-1 activation reaction, process the sample by any one of the following methods that is suitable for desired aim of the assay.

(i) To determine the capacity of a given DNA-structure or damaged DNA to activate PARP-1, use radiolabeled NAD and replace activated DNA and histones with the experimental DNA. Remove an aliquot of assay mixture at various time during the assay, mix with 4 volumes of urea-SDS sample buffer for SDS-PAGE (section 2.3). Since PARP-1 reaction occurs very quickly, for zero minute-sample, add gel-loading buffer prior to addition of PARP-1. Resolve the sample on 8% SDS-PAGE to separate free NAD from pADPr-modified PARP-1. Dry the gel and detect by autoradiography. As an example, see the capacity of UVB-irradiated closed circular DNA to activate PARP-1 in this assay (**Fig. A1.5A**).

(ii) To quantify PARP-1 activation in the above assay, terminate the assay by addition of 50 µL BSA (10 mg/mL) and 100 µL of 50% TCA, and keep on ice for 30 min. Dilute with 500 µL of 25% TCA containing 20 mM Na-pyrophosphate and filter through Whatman GF/C filters using vacuum filter holder assembly for 25 mm discs (Millipore). Wash the filters 2 x 5 mL with ice-cold 25% TCA containing 20 mM Na-pyrophosphate, twice with 5 mL ethanol and once with ether. Dry the filters at ambient temperature and measure ^{32}P-pADPr retained on the filter by scintillation counting. As an example, this assay reveals that radiolabeled pADPr formed in the presence of UV-induced DNA damage or activated DNA is more than in the presence of undamaged DNA (**Fig. A1.5B**).

(iii) If the assay is conducted with non-isotopic NAD, mix an aliquot of the reaction mixture with urea-SDS sample buffer for SDS-PAGE and process for immunoblotting with anti-pADPr and anti-PARP-1 antibodies, as described in section 3.1. **Fig. A1.5C** demonstrates capacity of UVB-irradiated DNA to activate PARP-1 using non-isotopic NAD.

B) Purification of pADPr from PARP-1 activation assay *in vitro*

To prepare radiolabeled or unlabeled pADPr, carry out the reaction on a larger scale (e.g., 900 µL) with or without radiolabeled NAD in 1.7 mL tubes and proceed as follows.

1. Terminate the reaction by adding 1/3 volume of ice-cold 100% TCA, precipitate the pADPr-attached to proteins on ice for 1 h.
2. Spin at 15,000*g* for 10 min at 4°C. Remove traces of acid by washing with cold ethanol and ether.
3, Dissolve the pellet in 1 mL of 1 M KOH, 50 mM EDTA at 60°C for 1 h.
4. Mix with 9 mL of AAGE9 buffer, and adjust the pH to 9.0 with HCl.
5. Process the sample for boronate affinity purification of pADPr, as per the method derived from earlier studies ***(16, 17)***. In brief, prepare a DHBB resin column by pouring 1 mL DHBB suspension (0.5 mL resin) into a 10 mL econocolumn. Equilibrate the column by washes with 5 mL of AAGE9 buffer, 5 mL water, and 10 mL AAGE9. Pass the alkali digest of PARP-1 activation assay prepared in step 3, through the column to capture all the pADPr. Wash with 25 mL of AAGE9 buffer and then with 10 mL of 1 M NH_4HCO_3, pH 9.0. Elute pADPr with 4 x 1 mL of 10 mM HCl or dH_2O (37°C) into a silanized tube. The

concentration of non-isotopic pADPr (measured as monomer concentration) can be estimated by absorbance at 258 nm (ε^{mM}= 13.5), whereas radiolabeled pADPr can be quantified by scintillation counting.

6. Store the pADPr eluate at 4°C or at -20°C (for a longer time) until further analysis.

A1.6.7 Activity-Western blot method to detect PARP-1 activation on nitrocellulose membrane

This is a very sensitive and commonly used method to demonstrate catalytic activity of PARP-1 and its 89-kDa apoptotic fragment ***(18)*** or to confirm the extent of downregulation of pADPr-forming capacity of the cells that are depleted of PARP-1 by RNAi ***(4)*** (**Fig. A1.6**). The original method developed by de Murcia's group required use of radiolabeled NAD ***(19)***, which we modified for use with non-isotopic NAD ***(18)***. In brief, this technique involves running a conventional Western blot of the cell or tissue extract or purified PARP-1, catalytic activation of the enzyme that is immobilized on the membrane, followed by immunodetection of pADPr-modified PARP-1 using 10H antibody. Following are the key steps of the procedure:

1. Prepare the cell or tissue lysates or proteins and resolve the samples on SDS-PAGE as described in section 3.1. Use only the pre-stained molecular weight markers, because staining with a dye under acidic condition to reveal these markers is not compatible with the active state of PARP-1.

2. Soak the acrylamide gel for 1 h at 37°C in 50 mL of electrophoresis running buffer containing 5% (v/v) freshly added β-ME.

3. Electrophoretically transfer the proteins at 4°C (100 V for 1 h) to nitrocellulose membrane.

All the subsequent steps are carried out on a rocking platform at ambient temperature.

4. *Renaturation of PARP-1:* Incubate the membrane for 1 h in 20 mL renaturation buffer containing 2 μg/mL activated DNA, 20 μM Zn (II) acetate and 2 mM $MgCl_2$.

5. *Activation of PARP-1.* Start the enzymatic reaction by incubating the membrane for 1 h with fresh 20 mL of renaturation buffer containing activated DNA, Zn^{2+} and Mg^{2+} along with 100 μM NAD.

6. Remove free NAD by 4 x 15 min washes with 15 mL of renaturation buffer without any additives.
7. Remove all non-covalently linked pADPr or non-specific background by 4 x 15 min washes with 25 mL SDS-wash buffer.
8. Proceed with blocking step, reactions with primary and secondary antibody followed by revelation exactly as described for Western blot in section 3.1.
9. Equal gel-loading for different samples can be controlled after immunoprobing either by staining with Sypro-Ruby or by immunoprobing for β-actin.

The activity-Western blot technique is very useful in determining the effectiveness of PARP-1 knockdown by RNAi ***(4, 5)***. The extent of knockdown must be sufficient to prevent any significant synthesis of pADPr in activity-Western blot, as shown in **Fig. A1.6**. This is crucial to demonstrate in RNAi models, because small residual amount of PARP-1 can form significant amount of pADPr to have physiological consequences.

A1.7 NOTES

1. Role of other cellular factors that can cause changes in the parameters used for assessment of PARP-1 activation: There are 18 members of PARP-1 family ***(3)*** and therefore the assay parameters described in this article could theoretically arise due to activity of PARPs other than PARP-1. However, most of these other PARPs cannot make pADPr, although they do generate mono-ADP-ribose. Moreover, of the two PARPs (PARP-1 and 2) that can respond to DNA damage, PARP-1 makes overwhelmingly large proportion of the pADPr after DNA damage ***(3)***. Therefore, in a vast majority of experimental models using eukaryotic cells and DNA damaging conditions, the changes in these parameters will largely reflect PARP-1 activation. Using PARP-1 knockout or knockdown (RNAi) models, we have often confirmed that the formation of pADPr after DNA damage is mainly due to activation of PARP-1 ***(1, 4, 5)***. Similarly, roles of other NAD-consuming enzymes in causing drop in NAD levels or other proton releasing or exporting enzymes in causing intracellular acidification should be carefully excluded by use of PARP-1 knockout, knockdown or inhibitor approaches ***(1)***.

2. Positive and negative controls for immunocytochemistry: For pADPr-containing positive controls, treat cells with 100-300 μM H_2O_2 for 10 min in PBS or serum-free medium or with 100 μM MNNG for 25 min in the medium with or without serum. Freshly dilute H_2O_2 (30% w/w) solution to 100-300 mM working stock solution in cold PBS. Freshly prepare 100 mM MNNG stock solution in DMSO and protect from light. For negative controls, prepare samples treated with solvents. It is also useful to prepare samples reacted only with secondary antibody.

3. Multiple of SDS-PAGE gels: For making multiple Tris-glycine SDS-PAGE gels, an easy-to-use chart for gel-volumes is available from electrophoresis equipment suppliers such as Bio-Rad or it can be obtained from reference manuals ***(20)***.

4. Issues related to probing with antibodies for Western blot: To save on the volume of primary antibody required for probing, use hybridization bottles and rotate them in hybridization chamber or Labquake-rotisserie (Thermolyne) placed at 4°C. In addition, as many as three blots can be probed simultaneously in the boxes or hybridization bottles with

the same quantity of antibody solution by separating each membrane with nylon mesh (Boekel Scientific).

5. Variation in PARP-activation assay components: Different components of this assay can be omitted, altered in amounts or replaced by other materials depending on the purpose of carrying out this assay ***(9)***. The unlabeled NAD can still be used if immunodetection with anti-pADPr antibody serves the purpose. In contrast, radiolabeled NAD provides advantages of sensitivity and easy quantification of PARP-1 activity. There are two options for radiolabeled NAD: (i) ^{32}P-adenylate NAD is cheaper and will produce polymer with a greater specific activity; (ii) the ^{14}C-NAD will produce polymer with a very long half-life, but more importantly the radiolabel will stay during digestion of pADPr for more detailed analyses ***(9)***. Histone should be excluded from the reaction if very long pADPr (>300-mer) are to be synthesized and extracted after the reaction or if it is required that all pADPr are attached only to PARP-1. Finally, activated DNA in the assay can be replaced by any other type of DNA whose capacity to activate PARP-1 is to be tested in this assay.

6. pADPr handling in silanized plastics: The pADPr tends to be sticky and its concentration decreases upon storage in normal plastic tubes. Hence silanize all plastic tubes or columns that come in direct contact with free pADPr. Conduct PARP-1 activation assay that ends with TCA precipitation in glass tubes.

A1.8 ACKNOWLEDGEMENT

We thank M. Miwa (Japan) for the permission to obtain the 10H hybridoma clone from Riken BRC Cell Bank. The writing of this review and some of the experimental work was supported by an operating grant to GMS from the Natural Sciences and Engineering Research Council of Canada (155257-06). Some of the experimental work described here was supported by the operating grants to GMS from the Canadian Institutes of Health Research (MOP-89964) and the Canadian Cancer Society Research Institute (NCIC-16407). GMS was partially supported by the FRSQ-senior research scientist award and FKK was recipient of the doctoral scholarship award from the Natural Sciences and Engineering Research Council of Canada.

A1.9 REFERENCES

1. Affar EB, Shah RG, Dallaire A-K, Castonguay V, Shah GM. (2002) Role of poly(ADP-ribose) polymerase in rapid intracellular acidification induced by alkylating DNA damage, *Proc. Natl. Acad. Sci. USA* ***99***, 245-250.

2. Amé JC, Jacobson EL, Jacobson MK. (2000) ADP-ribose polymer metabolism, in *From DNA damage and stress signalling to cell death: Poly ADP-ribosylation reactions* (de Murcia, G., and Shall, S., Eds.), pp 1-34, Oxford University Press, New York.

3. Rouleau M, Patel A, Hendzel MJ, Kaufmann SH, Poirier GG. (2010) PARP inhibition: PARP1 and beyond, *Nat Rev Cancer* ***10***, 293-301.

4. Shah RG, Ghodgaonkar MM, Affar EB, Shah GM. (2005) DNA vector-based RNAi approach for stable depletion of poly(ADP-ribose) polymerase-1, *Biochem Biophys Res Commun* ***331***, 167-174.

5. Ghodgaonkar MM, Zacal NJ, Kassam SN, Rainbow AJ, Shah GM. (2008) Depletion of poly(ADP-ribose)polymerase-1 reduces host cell reactivation for UV-treated adenovirus in human dermal fibroblasts, *DNA Repair (Amst)* ***7***, 617-632.

6. Hopfner M, Sutter AP, Beck NI, Barthel B, Maaser K, Jockers-Scherubl MC, Zeitz M, Scherubl H. (2002) Meta-iodobenzylguanidine induces growth inhibition and apoptosis of neuroendocrine gastrointestinal tumor cells, *Int J Cancer* ***101***, 210-216.

7. Vodenicharov MD, Ghodgaonkar MM, Halappanavar SS, Shah RG, Shah GM. (2005) Mechanism of early biphasic activation of poly(ADP-ribose) polymerase-1 in response to ultraviolet B radiation, *J Cell Sci* ***118***, 589-599.

8. Kawamitsu H, Hoshino H, Okada H, Miwa M, Momoi H, Sugimura T. (1984) Monoclonal antibodies to poly(adenosine diphosphate ribose) recognize different structures, *Biochemistry* ***23***, 3771-3777.

9. Shah GM, Poirier D, Duchaine C, Brochu G, Desnoyers S, Lagueux J, Verreault A, Hoflack JC, Kirkland JB, Poirier GG. (1995) Methods for biochemical study of poly(ADP-ribose) metabolism in vitro and in vivo, *Anal. Biochem.* ***227***, 1-13.

10. Halappanavar SS, Le Rhun Y, Mounir S, Martins M, Huot J, Earnshaw WC, Shah GM. (1999) Survival and proliferation of cells expressing caspase-uncleavable poly(ADP-ribose) polymerase in response to death-inducing DNA damage by an alkylating agent., *J. Biol. Chem.* ***274***, 37097-37104.

11. Scovassi AI, Mariani C, Negroni M, Negri C, Bertazzoni U. (1993) ADP-ribosylation of nonhistone proteins in HeLa cells: modification of DNA topoisomerase II, *Exp-Cell-Res* ***206***, 177-181.

12. Pieper AA, Brat DJ, Krug DK, Watkins CC, Gupta A, Blackshaw S, Verma A, Wang ZQ, Snyder SH. (1999) Poly(ADP-ribose) polymerase-deficient mice are protected from streptozotocin-induced diabetes, *Proc. Natl. Acad. Sci. USA* ***96***, 3059-3064.

13. Bakondi E, Bai P, Szabo EE, Hunyadi J, Gergely P, Szabo C, Virag L. (2002) Detection of poly(ADP-ribose) polymerase activation in oxidatively stressed cells and tissues using biotinylated NAD substrate, *J Histochem Cytochem* ***50***, 91-98.

14. Zhou Y, Liang S, Williams LR. (2002) Markers of poly (ADP-ribose) polymerase activity as correlates of DNA damage, *Methods Mol Biol* ***203***, 247-255.

15. Shah GM, Shah RG, Veillette H, Kirkland JB, Pasieka JL, Warner RRP. (2005) Biochemical assessment of niacin deficiency among carcinoid cancer patients, *Am. J. Gastroenterol* ***100***, 2307-2314.

16. Alvarez-Gonzalez R, Jacobson MK. (1987) Characterization of polymers of adenosine diphosphate ribose generated in vitro and in vivo, *Biochemistry* ***26***, 3218-3224.

17. Jacobson MK, Payne DM, Alvarez-Gonzalez R, Juarez-Salinas H, Sims JL, Jacobson EL. (1984) Determination of in vivo levels of polymeric and monomeric ADP-ribose by fluorescence methods, *Methods Enzymol* ***106***, 483-494.

18. Shah GM, Kaufmann SH, Poirier GG. (1995) Detection of poly(ADP-ribose) polymerase and its apoptosis-specific fragment by a nonisotopic activity-Western blot technique, *Anal. Biochem.* ***232***, 251-254.

19. Simonin F, Briand JP, Muller S, de Murcia G. (1991) Detection of poly(ADP-ribose) polymerase in crude extracts by activity-blot, *Anal. Biochem.* ***195***, 226-231.

20. Sambrooke J, Russel DW (2001) *Molecular Cloning: A Laboratory Manual*, Vol. **3**, 3 ed., Cold Sprong Harbor Laboratory Press, New York.

A1.10 Legends to the figures

Fig. A1.1. Western blot detection of pADPr-modified proteins in cells, tissues and tumors. Formation of pADPr-modified proteins in response to DNA damaging agents was examined by Western blot with anti-pADPr 10H antibody in four different types of samples: (A) Carcinoid neuroendocrine BON cells were treated with 100 μM Temozolomide (TMZ) for 30 min; (B) Epidermis of PARP-$1^{+/+}$ mice was harvested 5 min after exposure to 1,600 J/m^2 UVB; (C) Epidermis of hairless SKH-1 mice was harvested at 5 or 15 min after exposure to 1,600 J/m^2 UVB; (D) Carcinoid neuroendocrine tumor in nude mouse liver was removed after intraperitoneal exposure to 100 mg/kg streptozotocin (STZ) for 15 or 60 min. Together all four panels clearly demonstrate that in response to DNA damage, all types of samples from cells to skin or tumors demonstrate a consistent smear from 110-250 kDa region representing pADPr-modified proteins. The size of these bands does signify that automodified PARP-1 is the major contributor to this band. The entire lanes of all the gels are shown here to reveal that many other bands can be seen in the immunoblots of samples, indicating presence of other acceptors of pADPr.

Fig. A1.2. Immunocytological and immunohistological detection of pADPr in cultured cells or tissues. (A) Immunocytological detection of pADPr in nuclei of human skin fibroblasts GM-U6 cells ten minutes after exposure to 30 J/m^2 UVC. DAPI stain for DNA was used for revealing nuclei. The cells were fixed with formaldehyde-methanol fixation protocol. The punctate signal for pADPr is seen in the nucleus. (B) Immunocytological co-localization of cyclobutane pyrimidine dimers (CPD) and pADPr in PARP-$1^{+/+}$ mouse embryonic fibroblasts at 15 seconds after localized irradiation to 100 J/m^2 through UVC-opaque isopore membranes containing irregularly dispersed 5 μm holes. The merged panel with yellow color reveals co-localization of CPD and pADPr signals, confirming formation of pADPr at the site of CPD. The samples were fixed with TCA-protocol, which permits simultaneous immunodetection of CPD and pADPr. (C) Immunohistological detection of pADPr in epidermis of SKH-1 mouse skin 15 min after exposure to 1,600 J/m^2 of UVB. The sample was fixed by TCA-protocol and reveals almost exclusive formation of pADPr

in epidermal layer, which is compatible with the extent of penetration of UVB in the layers of the skin.

Fig. A1.3. PARIS method for detection of pADPr formed *in situ* with biotinylated NAD in cells. HeLa cells were permeabilized to incorporate specified NAD and treated (or not) with 300 μM H_2O_2 for 10 min. In the cells loaded with biotinylated NAD, H_2O_2-treatment induced a strong blue nuclear signal for biotinylated pADPr formed *in situ*, whereas the signal was very weak for untreated cells. For cells with non-tagged NAD, both control and treated cells did not show any significant nuclear signal.

Fig. A1.4. MNNG-induced pADPr-formation, NAD-depletion and intracellular acidification in Molt 3 cells. (A) pADPr-immunoblot. Molt 3 cells were treated with 10 or 100 μM MNNG for given time and immunoblotted with anti-polymer polyclonal antibody LP96-10. (B) NAD and ATP depletion. Samples of Molt 3 cells, treated with 10 or 100 μM MNNG as above, were analyzed for NAD (○) or ATP (□). Results (Mean ± SD) were obtained from 4 experiments, each in triplicate. (C) Time course of acidification. Molt 3 cells were treated with 10 (◇) or 100 (■) μM MNNG, and changes in pH were monitored by BCECF method up to 7 h. Results (Mean ± SD) were obtained from 4 experiments, each in triplicate (reproduced from **ref.** ***(1)*** with the permission from National Academy of Sciences USA, copyright 2002).

Fig. A1.5. PARP-1 activation *in vitro* by UVB-irradiated closed circular plasmid DNA. (A) PARP-1 activation *in vitro* with UVB-irradiated plasmid. Purified PARP-1 was activated with control or UVB (3.2 kJ/m^2) treated circular plasmid DNA in the presence of ^{32}P-NAD and 200 μM non-isotopic NAD. Aliquots were resolved on SDS-PAGE prior to autoradiography. (B) Quantification of PARP-1 activation in the *in vitro* assays. PARP-1 was reacted with two plasmids, as described above, along with activated, i.e., extensively nicked DNA. Reaction was terminated at 30 min and ^{32}P-pADPr-modified PARP-1 was TCA-precipitated and counted. (C) *In vitro* PARP-1 activation assay with non-isotopic NAD. *In vitro* PARP-1 activation assay with control and UVB-irradiated plasmid DNA was carried out with 200 μM non-isotopic NAD for 60 min. The unmodified PARP-1 and pADPr-modified PARP-1 were detected by immunoblotting with antibodies specific for PARP-1 (C-2-10, 1:10,000, Aparptosis) and pADPr. Note that extensively automodified

PARP-1 is not detectable by anti-PARP-1 antibody, possibly due to masking of its epitope by pADPr (lanes 2 and 4) (reproduced from **ref.** ***(7)*** with permission from The Company of Biologists, copyright 2005).

Fig. A1.6. Activity-Western Blot for PARP-1 activation on membrane. Stable depletion of PARP-1 was achieved in *PARP-1*$^{+/+}$ MEF by transfection with SiP14 DNA vector. The PARP-1-replete pBS-U6 clones are controls. The extent of PARP-1 depletion in SiP14 clone 3 was compared with control pBS-U6 clone, parental *PARP-1*$^{+/+}$ and *PARP-1*$^{-/-}$ MEF by Western blotting for PARP-1 (C-2-10) (top panel). The activity-Western blot of these samples confirmed significantly reduced presence of automodified PARP-1 in SiP clone (middle panel). Membrane was stained with Sypro-Ruby (bottom panel) as a loading control (reproduced from ref. ***(4)*** with permission from Elsevier Press, copyright 2005).

A1.11 Figures

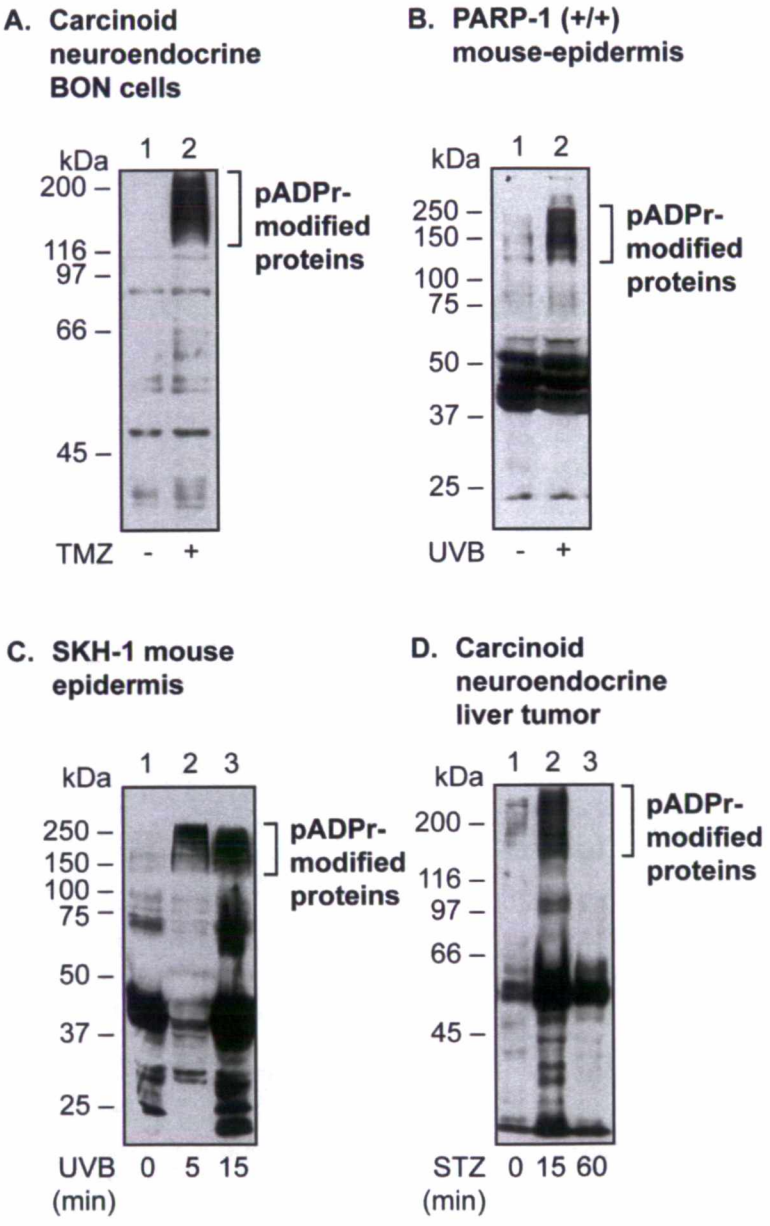

Figure A1.1: Western blot detection of pADPr-modified proteins in cells, tissues and tumors

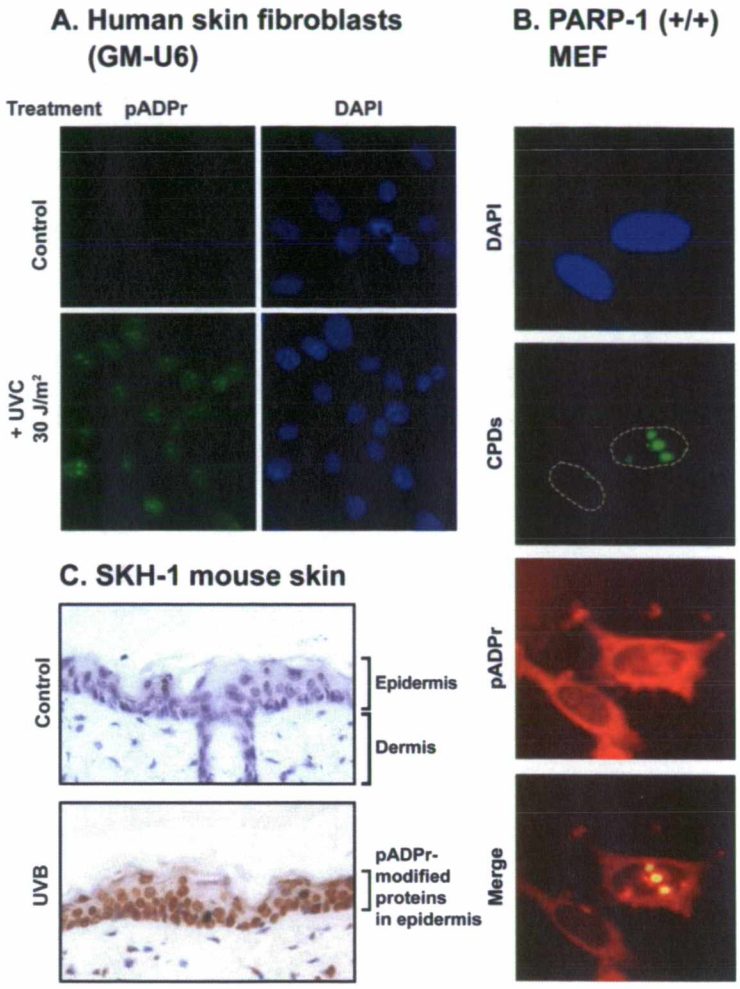

Figure A1.2: Immunocytological and immunohistological detection of pADPr in cultured cells or tissues

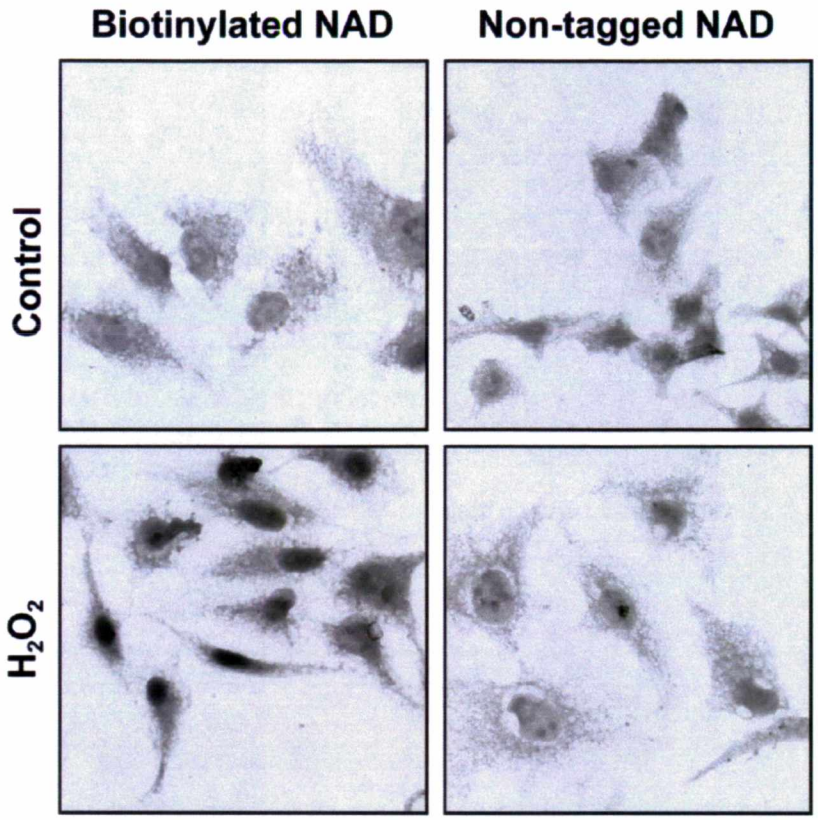

Figure A1.3: PARIS method for detection of pADPr formed *in situ* with biotinylated NAD in cells.

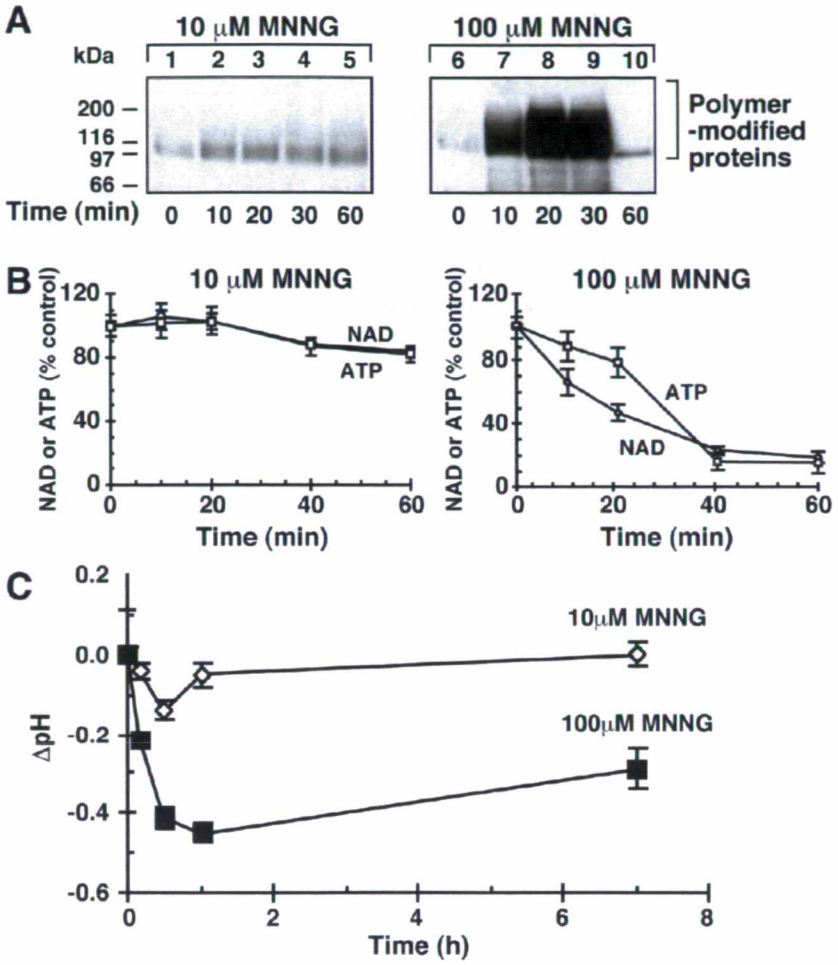

Figure A1.4: MNNG-induced pADPr-formation, NAD-depletion and intracellular acidification in Molt 3 cells

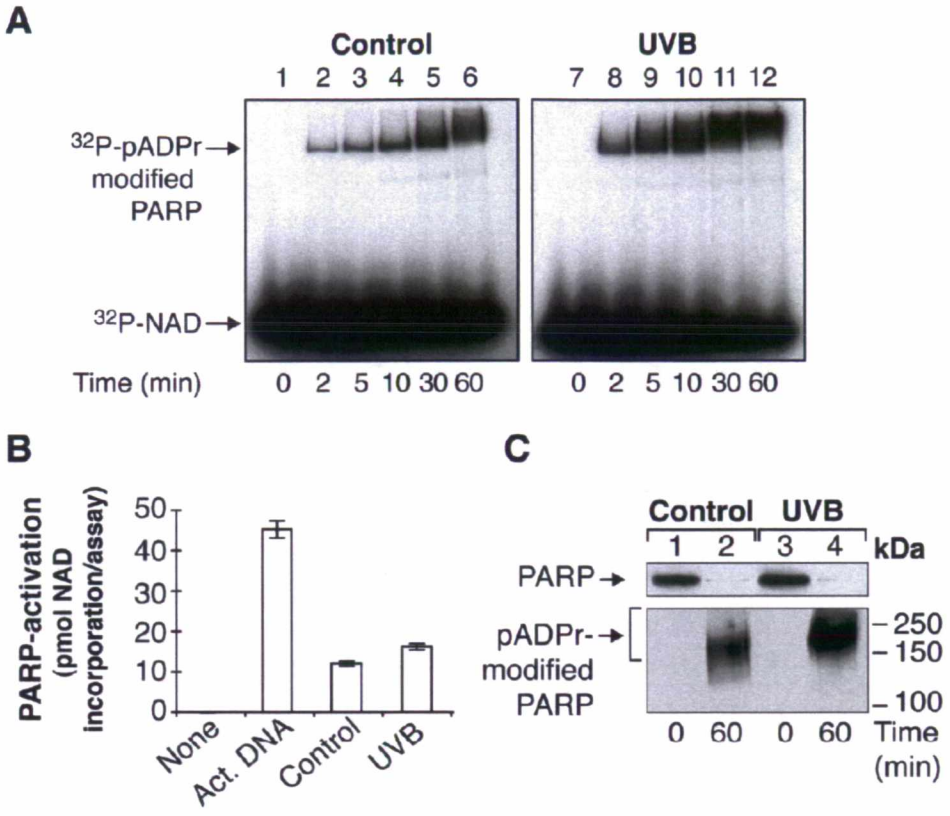

Figure A1.5: PARP-1 activation *in vitro* by UVB-irradiated closed circular plasmid DNA

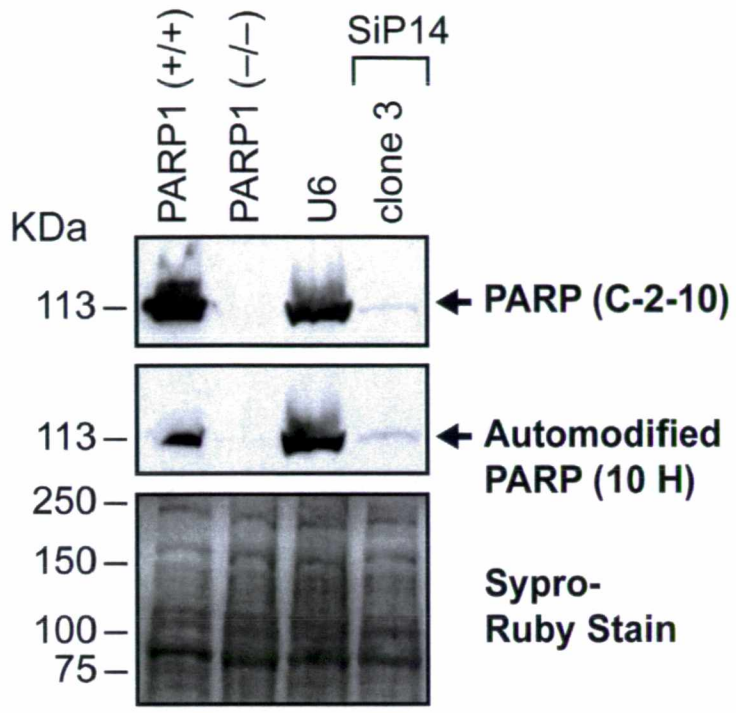

Figure A1.6: Activity-Western Blot for PARP-1 activation on membrane